Modelling of Power Electronics Controllers for Harmonic Analysis in Power Systems

by

Manuel Madrigal Martínez

A thesis submitted to the Department of Electronics and Electrical Engineering

of The University of Glasgow for the degree of

Doctor of Philosophy

December 2001

Glasgow, Scotland, U.K.

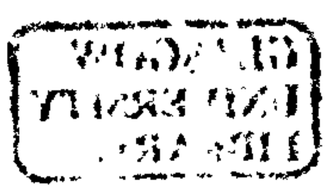

To my parents

Marcelino and Adelaida

... and to all those who believe that education is not a title, but a fertile land for a better life.

Abstract

Recent advances of high power, self-commutated devices have given rise to a new generation of power electronics controllers, opening many future applications in power flow control and power quality enhancement in electrical power systems. One of these applications is related to voltage source converters based on pulse width modulation control, a technology that enables a fast, smooth and versatile response of the converters over a wide range of operating characteristics. These power electronics controllers are being used at the transmission and distribution voltage levels in the form of static synchronous compensators, dynamic voltage restorers, unified power flow controllers, and HVDC stations based on voltage source converters. It may be argued that once the technology develops further and self-commutated devices with lower conduction losses become available, the deployment of such power systems controllers will take place in earnest. Nevertheless, from the system viewpoint, there are still several questions in the operation, modelling and analysis of these controllers which need to be addressed, since harmonic instabilities and resonance problems within the system may a rise as a result of unexpected interactions.

The research work presented in this thesis is concerned with the modelling of this new generation of power electronics controllers with a view to conduct comprehensive power systems harmonic analyses. An issue of paramount importance in this research is the representation of the self-commutated valves used by the controllers addressed in this work. Such a representation is based on switching functions that enable the realization of flexible and comprehensive harmonic models. Modularity is another key issue of great importance in this research, and the model of the voltage source converter is used as the basic building block with which to assemble harmonic models of actual power systems controllers. In this research the complex Fourier series in the form of operational matrices was used to derive the harmonic models.

Also, a novel methodology is presented in this thesis for conducting transient analysis of electric networks containing non-linearities and power electronic components. The methodology is termed the extended harmonic domain. This method is based on the use of time-dependent Fourier series, operational matrices, state-space representation and averaging methods. With this method, state-space equations for linear circuit, non-linear circuits, and power electronics controllers models are obtained. The state variables are the harmonic coefficients of $x(t)$ instead of $x(t)$ itself. The solution of the state-space equations gives the dynamic response

of the harmonic coefficients of $x(t)$.

Moreover, a new harmonic power flow methodology, based on the instantaneous power flow balance concept, the harmonic domain, and Newton–Raphson method, is developed and explained in the thesis. This method is based on the instantaneous power balance as opposed to the active and reactive power balance, followed by traditional harmonic power flow methods. The power system and the power electronics controllers are modelled entirely in the harmonic domain.

Acknowledgements

I wish to express my gratitude to Dr. Enrique Acha for his excellent supervision and friendship throughout my research project. I am indebted to him for giving me the opportunity to contribute in a publication, which gave me a great sense of achievement.

I would like to thank the Consejo Nacional de Ciencia y Tecnología, Mexico, and the Instituto Tecnológico de Morelia, Mexico, for their financial assistance to carry out my Ph.D. studies at the University of Glasgow.

Many thanks to my examiners, Dr. I. Arisan Erinmez, Professor John Arnold and Professor John Barker for their valuable suggestions to my research work.

I am sincerely thankful to John Parle, Olimpo Anaya, Kee Han Chan and Cindy Goh for walking and laughing with me throughout this unforgettable journey of my life. I also wish to thank my friends from the department and the University, especially those from the Power Systems Group for their friendship.

I am grateful to Jesús Rico for his unconditional friendship and important contribution to this work. I am indebted to my brother Marcelino Madrigal and friend Lino Coria for being important part of all my achievements. Thanks to my colleagues from the P.G.I.I.E. and D.I.E at the Instituto Tecnológico de Morelia, for their support during my stay in Glasgow.

Finally,... I will miss the excellent weekends with my friends in the rain and cloudy skies of Glasgow!.

Contents

List of Figures

List of Tables

Abbreviations

AC	alternating current
CSC	current source converter
DC	direct current
DVR	dynamic voltage restorer
EHD	extended harmonic domain
FACTS	flexible AC transmission systems
FFT	fast Fourier transform
GTO	gate turn off thyristor
HD	harmonic domain
HVDC	high voltage direct current transmission
HVDC-VSC	HVDC station based on voltage source converters
IGBT	insulated gate bipolar transistor
IPF	instantaneous power flow
LTI	linear time invariant
LTP	linear time periodic
PCC	point of common coupling
PF	power factor
PI	proportional plus integral
PWM	pulse width modulation
RMS	root mean square

STATCOM	static synchronous compensator
TCR	thyristor-controlled reactor
TCSC	thyristor-controlled series compensator
THD	total harmonic distortion
UPFC	unified power flow controller
VSC	voltage source converter
VZC	voltage zero crossing
WFFT	windowed fast Fourier transform
p.u.	per unit
Th	Thévenin
s	seconds
ms	milliseconds
H	Henries
mH	millihenries
F	Farads
μF	microfarads
V	volts
A	amperes
h	harmonic order
t	time
k	iteration counter
j	$\sqrt{-1}$
e	exponential
γ	wave propagation
Z_c	characteristic impedance

R'	series resistance in Ω/km
L'	series inductance in H/km
C'	shunt capacitance in F/km
G'	shunt suceptance in S/km
ω_0	angular frequency in rad/s equal to $2\pi f_0 = 2\pi/T_0$
T_0	period
f_0	fundamental frequency
ω	continuous angular frequency
δ_{VSC}	VSC internal voltage angle
P_f^i	active power at fundamental frequency injected into node i
Q_f^i	reactive power at fundamental frequency injected into node i
V_{-1}^i	voltage harmonic of order -1 at node i
α	thyristor firing angle
m	modulation factor
ϕ_m	modulation shift angle
$\mathbf{D}(jh\omega_0)$	operational matrix of differentiation
$\mathbf{P}_s$	DC to AC transformation matrix
$\mathbf{Q}_s$	AC to DC transformation matrix
$\mathbf{U}_I$	identity matrix
$\mathbf{Z}_e$	equivalent external impedance

In this thesis, unless otherwise stated, bold face type represents matrix quantities, e.g. $\mathbf{P}_s$, $\mathbf{X}$, $\mathbf{p}_s(t)$. Upper case letters represent frequency domain quantities, e.g. S_h, $X_h(t)$, $\mathbf{Q}_s$. Lower case letters represent time domain quantities, e.g. $v(t)$, $s_{ab}(t)$, $\mathbf{q}_s(t)$.

1. Introduction

1.1. Foreword

Deregulation of electricity markets [1], open access transmission between countries [2], customers' demands for improved power quality services [3], and increasing environmental demands to use cleaner technology and renewable energy [4], have brought about news challenges on the design, planning and operation of transmission and distribution systems. One of the challenges is to enhance the capability, controllability and reliability of electric systems, where great progress in this direction may be obtained by using flexible AC transmission systems (FACTS), Custom Power controllers and high voltage direct current (HVDC) transmission systems [5].

FACTS [6] is the term used to denote a whole family of concepts and controllers for improved operation and a more flexible use of power systems. Some of these controllers have today reached maturity in both concept and application. FACTS controllers utilise power electronic technology based on advanced switching devices, to enable a fast and smooth operation of the power controller.

The gate turn off thyristors (GTOs) and insulated gate bipolar transistors (IGBTs) are good examples of advanced switching devices which can handle high power, operate at high switching frequencies and have gate "turn-off" capabilities. Devices with such characteristics together with advances in pulse width modulation (PWM) control, have enabled the construction of voltage source converters (VSC) and their use in electricity distribution and transmission networks. This has provided the motivation for conducting research and development of power electronic controllers suitable for network-wide studies.

The applications of VSCs on distribution systems can be found under the titles of Custom Power [7] and HVDC transmission systems based on VSC technology [5] so called HVDC-VSC stations. Although HVDC-VSC stations may not form part of Custom Power, they share with it the use of PWM voltage source converter technology.

One of the current challenges facing power engineers and research groups is the study and characterisation of FACTS, Custom Power, and HVDC-VSC stations and their interaction with transmission and distribution networks. Some of the power research areas directly involved with these technologies are: Power flow, optimal power flow, transient stability, power quality, renewable energy, and harmonic analysis. Power flow and optimal power flow have received

considerable research attention [8][9]. Also, many papers related to transient stability can be found in the open literature. As far as power quality and renewable energy issues are concerned, Custom Power and HVDC-VSC stations have been studied from the technology application viewpoint. Despite the fact that these new technologies inevitably generate harmonic frequencies, very little work has been conducted on harmonic analysis. One possible reason is that low order harmonic frequencies are not generated by PWM converters, and it may be argued that the high harmonic frequencies, generated by them, should not cause major problems in the distribution and transmission system if a fixed high-frequency harmonic filter is used [10]. However, a more careful analysis of the operation of fixed harmonic filters and these electronics-based controllers indicate that they might interact with elements of the transmission and distribution system such as power generators, transformers, capacitor banks and other switching stations. Clearly, such interactions are undesirable since they may cause stability problems, overvoltages, frequency oscillations, harmonic instabilities and, in general, abnormal device operation [11].

1.2. Modelling and Analysis

The study and design of a physical system can be carried out using empirical methods, but when the system becomes too complicated or too expensive to be experimented with, analytical methods become indispensable. The analytical study of physical systems may seem to consist of four parts: modelling considerations, development of the mathematical description, analysis, and design. In order to develop a suitable model of a physical system, a thorough understanding of the physical system and its operational range is essential.

Once a model is found for a physical system, the next step is to develop a mathematical description, by applying various physical laws and mathematical methods to describe the system. For example, applying Kirchhoff's voltage and current laws, Fourier analysis. The equations that describe systems may assume many forms; they may be linear equations, non-linear equations, time-varying equations, difference equations, diffential equations, or others. Depending on the purpose of the model, one form of equation may be preferable over another to describe the same system. For example, the following equation $Y_{TCR} = (\sigma - \sin\sigma)/\pi\omega_0 L$ is used to represent a specific power electronic controller in power flow studies, and the matrix equation $\mathbf{Y}_{TCR} = \frac{1}{L}\mathbf{D}^{-1}(\mathrm{j}h\omega_0)\mathbf{S}$ may be used to represent the same controller but for harmonic studies. Hence, a system may have many different mathematical descriptions, just as a physical system may have many different models.

Once the model of the system is obtained, the next step in the study involves quantitative and/or qualitative analysis. In the quantitative analysis, we are interested in exact responses of systems due to the applications of certain input signals. In the qualitative analysis, we are interested in the general properties of the system, such as stability, controllability, and observability.

An important aspect of this thesis concerns the modelling and quantitative analysis of volt-

age source converters using GTOs or IGBTs switches, for harmonic power systems studies. Since the intention is to study the system level response of these converters, there is a well established engineering justification to simplify the GTOs and IGBTs representations as much as practicable and, hence, their turn-on and turn-off electric capabilities, are represented in this research by ideal electric switches. The rationale behind this simplification is that GTOs and IGBTs turn-on and turn-off times are in the order of $1-5\,\mu s$, which is a very short time period compared to $200\,\mu s$ the period of the 100th harmonic, which is one of the higher harmonic frequencies of interest for harmonic power systems analysis.

1.3. Power Electronics Controllers and Harmonic Analysis

An outline of the most important power electronics controllers from the harmonic analysis viewpoint is presented below.

SVC: The static VAR compensator (SVC) is a controller based on high power thyristor technology. It is a static shunt reactive power compensator. In the first half of the 1970s the SVC became a well-established compensator in high power networks. Since then, there has been a great increase in its number of applications. A SVC system typically comprises a transformer, linear reactors and/or capacitors controlled by antiparallel thyristor valves [12]. The harmonics generated by the SVC are well known [13] but interaction with other non-linearities such as transformers undergoing saturation or other power electronics controllers requires more thorough studies.

TCSC: The thyristor-controlled series compensator (TCSC) is used as a series compensator for active power flow control, damping of power oscillations and mitigations of subsynchronous resonance. A TCSC comprises a series capacitor in parallel with a thyristor-controlled reactor (TCR) and a metal-oxide varistor for over-voltage protection.

The TCSC provides active power flow control with very little delay, leading to much improved system damping and stability margins for the compensated transmission circuit [14][15]. In steady-state operation the harmonic currents generated by the TCR are trapped inside the TCSC due to the low impedance of the capacitor compared to the network equivalent impedance, producing considerable voltage distortion in the TCSC capacitor [16] but very few harmonic currents flow into the electric systems. In the 500 kV Slatt TCSC system [17] for capacitive operation mode, the total harmonic distortion (THD) of the line current had a maximum value of 1.4%. Similarly for the 230 kV Kayenta TCSC system [18], in the capacitive operation, the maximum THD voltage in the system was less than 1.5%. Owing to the principle of operation of the TCSC and its series connection with the transmission system, TCSCs are critically exposed to harmonic voltage magnifications resulting from resonant impedance conditions. It was

reported [17] that due to small offsets in the line current, the quarter-wave-symmetry of the capacitor voltage was lost, causing the thyristor to conduct uneven currents at each half cycle. In this case, research in small-signal stability [19] has shown that the TCSC can present resonance conditions under different operating scenarios. Most of these problems relating to non-ideal operation of the TCSC have been conducted using time domain simulations, but it should be remarked that time domain simulations do not yield the level of detail necessary to study the TCSCs frequency conversion effect since they only provide the aggregated final response. A more complete model for harmonic analysis is proposed in [13] where not only the resonance point at fundamental frequency is obtained, but also at different harmonic frequencies.

STATCOM: The static synchronous compensator (STATCOM) was the first FACTS controller to use VSC technology. The STATCOM includes a DC capacitor and a coupling transformer. The converter uses GTOs or IGBTs switches, which are turned on and off by PWM control techniques. The STATCOM is used to exchange reactive and active power with the AC system [20]. Over the last few years, an increasing amount of research work addressing the STATCOM has been published in the open literature mainly in the design, operation and control of the STATCOM. Fundamentally, all these analysis techniques involve time domain simulations. Since the PWM technology does not generate low order harmonic frequencies, its harmonic contribution is commonly neglected in harmonic analysis. However, the harmonic spectrum generated by the PWM appears at high frequencies which can produce resonance problems between the transmission system and the capacitor connected in the DC side of the STATCOM. Some STATCOM models for harmonic analysis have been proposed. In [21], a STATCOM-based PWM converter is represented as a harmonic voltage source, with no explicit representation of the capacitor effect. In [22][23], a set of simplified analytical expressions were put forward with which the STATCOM currents can be calculated at both the fundamental and harmonic frequencies. A more complete model for harmonic analysis is proposed in [13] where the DC capacitor is explicitly represented.

A particular configuration of the STATCOM is the dynamic voltage restorer (DVR). The DVR is a controller used for dynamic voltage restoration purposes. The DVR makes use of a VSC controlled by PWM and a DC voltage storage unit; the DVR is connected, through a coupling transformer in series with the transmission system in order to eliminate voltage sags. Since the DVR operation takes place under transient conditions, no research for harmonic analysis in steady-state has been reported. However, during typical DVR operation of around 10 cycles from an initial disturbance, the DVR may be considered as operating in a quasi-steady-state periodic condition, therefore the steady-state harmonic interaction with the transmission system becomes only an issue of research interest. Since the DVR is a part of the UPFC, its model is explicit represented in the UPFC model.

UPFC: The unified power flow controller (UPFC) was proposed in [24]. It is composed of a STATCOM and a DVR sharing a common DC link. The UPFC is able to control the transmission line impedance, nodal voltage magnitude and active and reactive power flow in the line. The UPFC may also provide independently controllable shunt reactive power compensation. For this controller, much of the work reported has been in the general operation [25], control [26][27], stability [28], power flows and optimal power flows [29][30]. Most of the UPFC models found in the open literature are very simple and only suitable to study the fundamental frequency response, and no work on harmonic analysis has been reported. Even though the UPFC uses PWM techniques, not all harmonics generated by the UPFC are fully eliminated.

HVDC-VSC stations: Conventional HVDC transmission systems use line commutated current source converters (CSC). In these converters each valve consists of a number of thyristors connected in series. The turn-on of the thyristor is controlled by the gate signal while the turn-off occurs at the zero crossing of the AC current which is determined by the AC network voltage (i.e. line commutation), where both the sending end and the receiving end of the HVDC system absorb reactive power from the AC systems. Hence, the HVDC system requires an AC system at least at one end to have an AC voltage to commuttate. This reactive power requirement is a constraint for HVDC stations connecting a weak AC system or small island AC network [31][32].

An interesting alternative for HVDC applications is the use of VSCs, which eliminates the reactive power compensation requirements. With this characteristic, the HVDC stations based on VSC technology opens a wide range of applications [10][33][34][35][5] with the following major advantages:

- Capable to control reactive power independently of active power.
- No risk of commutation failures.
- Capacity to feed a weak AC network or a network without internal generation.
- Faster response due to the use of PWM switching frequency.

HVDC Light or HVDC Plus stations are the names given by ABB and Siemens company, respectively, to HVDC systems based on VSCs. Since its introduction to the market in 1997, some of the most interesting applications and possibilities are:

- City centre infeed.
- Multi-terminal DC grid.
- Connection of wind power parks to the main grid.
- Utilising existing rights-of-way.

It is expected that the HVDC-VSC technology will improve many of the problems faced by current transmission and distribution systems, such as renewable power interconnection with the main grid and opposition to build new transmission and distribution networks on enviromental grounds.

Other application of the HVDC-VSC stations is the back-to-back tie station, where no DC line or cable exist. The HVDC-VSC back-to-back station comprises two VSCs sharing a DC capacitor in the DC link. Besides controlling the through power flow, it can supply reactive power and provide independent dynamic voltage control at its two terminals. Only a limited amount of research is found relating to this type of station, but some important applications are already in place, e.g. the HVDC-VSC back-to-back installation at the Eagle Pass substation which connect the 138 kV transmission systems of USA and Mexico [35]. Hence, for this new HVDC-VSC technology most of the research work has been directed to applications.

1.4. Techniques for Harmonic Analysis

Time Domain: Harmonic analysis using time domain simulations has been used for many years in power systems, where voltage and current waveform distortion are analysed with the help of fast Fourier transform (FFT) techniques. One difficult task with this approach is the gathering of suitable initial condition which would enable the system to reach the steady-state condition on which the harmonic analysis would be carried out [36]. Good initial conditions are required to overcome the long period of integration time required to reach the steady-state when the system includes magnetic non-linearities and power electronics controllers. Most of the research in this area of power systems harmonics has been denoted to reinforce the initialisation facilities of software packages such as EMTP [38] and PSCAD/EMTDC [39].

Frequency Domain: The frequency domain has been used extensively in the modelling and analysis of power systems operating under harmonic distortion. Probably, the most successful frequency domain technique, for its flexibility in both modelling and analysis, has been the harmonic domain (HD) technique based on the complex Fourier series. The HD has been applied to the modelling and analysis of transmission lines, synchronous generators, transformers, and electric arcs [40][41][42][43], and using the Hartley transform similar models were obtained in [44]. Using the HD applied to switching functions, models for the TCR have been presented [45][46]. The same technique can be applied to obtain a model for the TCSC for stability and steady-state analysis. A more formal representation of the HD, using operational matrices and different transforms is given in [47]. The HD has been applied to conventional power elements and power electronics controllers based on thyristors for steady-state analysis, as explained in detail in [13]. In the present thesis, the HD is used to obtain models for power electronics controllers which use IGBTs or GTOs. Also, a significant development is that the HD is extended

to carry out dynamic harmonic analysis.

Dynamic Frequency Domain: A number of power quality studies are carried out by analysing the system harmonics as recorded from disturbance events. The analyses require time sampling techniques, following by windowing fast Fourier transform (WFFT) over the actual waveform recorded [48][49]. Even for digital simulation, time domain and discrete Fourier transform techniques are used for the analysis of the harmonics during transient events [39]. Therefore, frequency techniques are not reported in the open literature to be used for transient harmonic analysis in AC electric circuits. In this thesis, a transient harmonic technique termed extended harmonic domain (EHD) is presented. The EHD is used for harmonic modelling and analysis of linear and non-linear circuits, and power electronics controllers. The EHD is based on generalized averaging methods [51], time-dependent Fourier series, harmonic state-space for time-varying systems [52] and the HD. The EHD is a formulation based on orthogonal basis and operational matrices. In the simulation environment afforded by EHD, the coefficients of the Fourier series are the state variables. The solution process allows the computation of the time evolution of the harmonic coefficients. A similar technique termed dynamic phasors [53][54] was applied to obtain phasor-based models for AC power elements and FACTS controllers used for fault and stability studies.

1.5. Methods for Harmonic Propagation Studies in Electrical Networks

Injection method: This is the simplest and most widely used method for harmonic propagation studies in distribution and industrial networks. The simplicity of the method lies on the linear approach adopted to represent the non-linear elements, which produce harmonics. This method allows the representation of non-linear elements by a current or voltage source at different harmonic frequencies. This simplification reduces the harmonic propagation problem to the solution of a set of linear equations solved at each harmonic frequency of interest [55][13]. For high harmonic voltage distortion (>5%), this method is inaccurate since the harmonic sources are calculated assuming that the bus voltages are sinusoidal.

Harmonic power flow: The work on harmonic power flow analysis was pioneered by D. Xia and G.T. Heydt [56][57] where the conventional Newton–Raphson power flow method was reformulated to include the harmonic current flows and solved simultaneously using Newton's method. In [58], the previous method was extended to unbalanced systems and in [59] a converter model was included in the algorithm. A difficult task associated with this method is that the equations which represent each non-linear load type must be included in the formulation of the Jacobian.

In [60], a harmonic power flow method consisting of two basic parts was presented; the first part is the construction of a decoupled harmonic Norton equivalent via FFTs, and the second part performs the network solutions at the fundamental and one harmonic frequency at a time. This method requires the use of time domain simulations and the use of FFTs.

The method in [61] solves the harmonic propagation problem using a sequential method where linearisation is used to obtain the equivalent admittance of the non-linear elements. A modular approach for three-phase harmonic power flow is given in [62]. In this solution approach, three iterative process are required: The first one for the fundamental positive sequence power flow, the second one for the fundamental three-phase power flow solution, and then for the full harmonic solution.

A hybrid methodology is described in [63] for the harmonic propagation problem using the frequency domain to represent linear components and the time domain to represent non-linear and time-varying components. The method uses Poincaré acceleration to reach the steady-state solution.

A general characteristic of these methods is that linear loads are represented by linear equivalent impedances at harmonic frequencies. Also, the effect of harmonics in the power calculations are not taken into account. In this thesis a different harmonic power flow formulation is presented, this approach is based on the instantaneous power flow principle.

Instantaneous power flow: The instantaneous power balance concept, the HD, and the Newton–Raphson method as applied to power networks are suitably combined to develop the instantaneous power flow (IPF) method in this thesis. The IPF lends itself to a modular approach where all the power electronic controllers are included in the methodology. Moreover, all the conventional elements already developed in HD are incorporated with ease in this methodology. This method follows the principle of conservation of energy as applied to electrical circuits, where the instantaneous power and the active power are the only powers which possess the conservation property under harmonic distortion. The IPF is a new harmonic power flow method proposed in this thesis.

1.6. Motivation of the Research Project

Modern electrical power systems are being upgraded with a new breed of power electronics technology based on high switching frequency devices such as GTOs and IGBTs, and PWM control. This new technology is creating new and exciting challenges and opportunities at the transmission and distribution levels [10]. The current applications can be found in controllers such as the STATCOM, DVR, UPFC and HVDC-VSC stations which share the same technology base, i.e. VSCs [70][71][72][34]. Even though harmonic generation is an intrinsic characteristic of VSCs, so far no harmonic models for these controllers exist. However, it is well known

that harmonics, even at high frequencies, can produce undesirable effects at transmission and distribution networks, effects which can be predicted only with the use of suitable models. In order to provide for this timely necessity, advanced harmonic models for controllers based on VSC technology are proposed for the first time in this thesis.

Several of the restrictions that thyristor-based controllers face are eliminated with the use of VSC technology. For example, turn-on and turn-off capabilities, high switching frequency, and faster responses are key attributes of power controllers based on VSC. These and other advantages of VSC technology should provide the motivation for their widespread use in future power systems applications. Hence, new mathematical models, solution methods and analysis techniques are required to be able to study future power networks where the use of VSC-based controllers may become widespread. The research work presented in this thesis advances this timely area of electrical engineering by applying time-varying system theory and averaging methods in the modelling and harmonic analysis of VSC technology. Besides the modelling of novel power electronic controllers, the advance lies on the fact that the harmonic domain [13] has been extended to carry out dynamic analysis, opening a new avenue of research in control and design of power electronics controllers.

The incorporation of FACTS and Custom Power controllers in power systems, calls for an upgrade of the analysis tools used by power engineers in the planning and operation of their networks. Some of these tools are power flow, optimal power flow, stability and harmonic power flow analysis. Moreover, new analysis techniques and software may need to be developed afresh to study new aspects of power system phenomena which may not be properly studied with existing or even upgraded analysis tools, such is the case of harmonic power flow. In this thesis, a new methodology to solve the harmonic power flow problem is presented. This new method is termed instantaneous power flow since it is based on the instantaneous power balance of the electrical network.

1.7. Objectives of the Research Project

The main objective of the research project is to formulate suitable frames-of-reference for VSC-based power electronics controllers, which can be modelled and analysed using harmonic domain techniques for steady-state and dynamic analysis.

In order to achieve this objective, the thesis covers three main themes: 1) Modelling of power electronics controllers based on VSCs and PWM techniques for harmonic steady-state analysis, 2) Development of a frame-of-reference where power electronics controllers based on VSC and PWM techniques can be represented for harmonic dynamic analysis, and 3) Development of the instantaneous power flow method.

The research work is based on three basic premises: 1) The power electronics controllers use GTOs or IGBTs switches which have turn-on and turn-off capabilities, 2) The power elec-

tronics controllers may be analysed as linear, time-varying systems due to their turn-on and turn-off capabilities, and 3) The use of Fourier series and time-dependent Fourier series applied to linear, time-varying systems yields the exact steady-state and dynamic harmonic solution of the system. With these key points, the following objectives are achieved:

- The realization of a new and comprehensive VSC harmonic model. This model is used as the basic building block with which other power electronics controller models are assembled, namely: STATCOM, HVDC-VSC stations and the UPFC. The models obtained are for steady-state harmonic analysis of balanced and unbalanced three-phase power systems.

- The development of a new state-space based on time-dependent Fourier series. In this new state-space, the state variables are the harmonics of $x(t)$ instead of $x(t)$ itself. Models of the STATCOM and HVDC-VSC stations are obtained in this state-space for dynamic harmonic analysis of balanced and unbalanced three-phase power systems.

- The development of a harmonic power flow method based on the instantaneous power balance principle and the Newton–Raphson method. The new method is based on the harmonic domain frame-of-reference where transmission lines, generators, transformers, and power electronics controllers are well represented.

1.8. Publications

The following publications were generated during the course of the present research work.

Book:

1. E. Acha, **M. Madrigal**, *Power Systems Harmonics: Computer Modelling and Analysis*, John Wiley & Sons, Chichester, April 2001. Hardcover (382 pages), ISBN 0-471-52175-2.

Transactions papers:

1. J.J. Rico, E. Acha, **M. Madrigal**, "The Study of Inrush Current Phenomenon Using Operational Matrices", *IEEE Transactions on Power Delivery*, Vol. 16, No. 2, April 2001, pp. 231–237.

2. **M. Madrigal**, E. Acha, "Equivalent Harmonic Impedances of Thyristor Controlled Series Compensators", Submitted to *IEEE Transactions on Power Delivery*, June 1999.

3. J.J. Rico, **M. Madrigal**, E. Acha, "Dynamic Harmonic Evolution Using the Extended Harmonic Domain", Submitted to *IEEE Transactions on Power Delivery*, August 2000.

4. **M. Madrigal**, E. Acha, "UPFC Model for Harmonic Analysis", Submitted to *IEEE Transactions on Power Delivery*, December 2001.

5. A. Asensi, J.G. Mayordomo, A. Hernández, **M. Madrigal**, O. Anaya, E. Acha, "Modelling of Single-Phase PWM Converter Array for Three-Phase Voltage Regulation and Balancing in Large-Scale Power Networks", Submitted to *IEE Proceedings Generation, Transmission and Distribution*, December 2001.

Engineering letters:

1. K.H. Chan, E. Acha, **M. Madrigal**, J.A. Parle, "The Use of Direct Time-phase Domain Synchronous Generator Model in Standard EMTP-type Industrial Packages", *IEEE Power Engineering Review*, Vol. 21, No. 6, June 2001, pp. 63–65.

2. J.A. Parle, **M. Madrigal**, E. Acha, "Phase Domain Transmission Line Modelling for Harmonic Analysis", *IEEE Power Engineering Review*, Vol. 21, No. 10, October 2001, pp. 46–48.

Conference papers:

1. **M. Madrigal**, E. Acha, "Modelling of Custom Power Equipment using Harmonic Domain Techniques", Invited paper in *Proceedings of the 9th International Conference on Harmonics and Quality of Power*, Orlando Fl., October 1–4 2000, Vol. I, pp. 264–269.

2. **M. Madrigal**, O. Anaya, E. Acha, J.G. Mayordomo, R. Asensi, "Single-Phase PWM Converters for Three-Phase Reactive Power Compensation. Part I: Time Domain Studies", *Proceedings of the 9th International Conference on Harmonics and Quality of Power*, Orlando Fl., October 1–4 2000, Vol. II, pp. 541–547.

3. **M. Madrigal**, E. Acha, J.G. Mayordomo, R. Asensi, A. Hernández, "Single-Phase PWM Converters for Three-Phase Reactive Power Compensation. Part II: Frequency Domain Studies", *Proceedings of the 9th International Conference on Harmonics and Quality of Power*, Orlando Fl., October 1–4 2000, Vol. II, pp. 645–651.

4. E. Acha, O. Anaya, J. Parle, **M. Madrigal**, "Real-Time Simulation for Power Quality Disturbance Application", *Proceedings of the 9th International Conference on Harmonics and Quality of Power*, Orlando Fl., October 1–4 2000, Vol. III, pp. 763–768.

5. K.H. Chan, **M. Madrigal**, "Phase Domain Dynamic Analysis of Conventional and Advanced Static Var Compensator in Voltage Sag due to Motor Start-up", *Proceedings of the 6th IASTED International Conference on Power and Energy Systems*, Rhodes Greece, July 3–6 2001, pp. 394–400.

6. **M. Madrigal**, E. Acha, "Harmonic Modelling of Voltage Source Converters for HVDC Stations", *Proceedings of the 7th International Conference on AC and DC Power Transmission*, London, November 28–30 2001, pp. 125–131.

7. N. Garcia, **M. Madrigal**, E. Acha, "Interaction of the STATCOM and its Associated Transformer Non-linearity: Time Domain Modelling and Analysis", *Proceedings of the 7th International Conference on AC and DC Power Transmission*, London, November 28–30 2001, pp. 355–360.

8. N. Garcia, **M. Madrigal**, E. Acha, "Time Domain Modelling and Analysis of a Coupled DVR-STATCOM (UPFC) System", Accepted for the *14th Power Systems Computation Conference, PSCC-2002*, to be held on Sevilla, Spain, June 24–28 2002.

1.9. Contributions

The main contributions of the research work presented in this thesis may be summarised as follows:

- A flexible and comprehensive model of the VSC based on PWM techniques was developed. The VSC model makes explicit representation of the capacitor and the voltage ripple on the DC side. The steady-state condition is taken into account by using an iterative process in order to maintain zero DC current through the capacitor. The VSC model was obtained in the harmonic domain by using switching functions. The model is represented by a three-phase equivalent circuit, which caters for both balanced and unbalanced system conditions.

- Using the VSC model as the basic building block, models for the STATCOM, HVDC-VSC stations and the UPFC were obtained, where the DVR was modelled as a part of the UPFC.

- For the STATCOM model, a simple equation which represents the driving point equivalent impedance was obtained and used for resonance prediction analysis. The STATCOM model was compared with the results obtained by a STATCOM model implemented in PSCAD/EMTDC.

- Two HVDC-VSC configurations were obtained; the back-to-back tie and the DC cable link configurations. An explicit representation of the DC cable is used since the model is in the frequency domain. For these configurations, one VSC plays the role of the master DC voltage regulator and the other VSC plays the role of a power dispatcher. Results were compared with models implemented in PSCAD/EMTDC.

- A model for the UPFC was obtained. The UPFC model was used to determine its power control regions. Moreover, the model was also used to assess the UPFC's harmonic distortion response and resonance effects on transmission lines.

- A new state-space for dynamic harmonic analysis was developed. This new state-space is based on time-dependent Fourier series and averaging methods. The state variables are the harmonic coefficients of $x(t)$ instead of $x(t)$ itself. The solution of the state-space equations gives the dynamic response of the harmonic coefficients of $x(t)$. These harmonics are used to obtain dynamic quantities such as THD, PF, RMS values and powers. For three-phase circuits, the dynamic harmonics are used to obtain the dynamic performance of zero, positive and negative sequence quantities. This new state-space is named extended harmonic domain to indicate the fact that the harmonic domain is a particular case of this state-space.

- State-space equations for the STATCOM and HVDC stations models were obtained. The steady-state models of the STATCOM and HVDC stations give the exact initial conditions for dynamic analysis. The results show that the dynamic responses of the harmonics are very sensitive to disturbances, even for sharp impulses which are difficult to detect with time response methods.

- An instantaneous power flow method is developed. This method is based on the instantaneous power balance as opposed to the active and reactive power balance, followed by traditional harmonic power flow methods. The power system and the power electronics controllers are modelled entirely in the harmonic domain. This new method uses the Newton–Raphson method to solve the non-linear equations resulting from the electric power system constrains. The results obtained show excellent convergence characteristics.

1.10. Thesis Outline

The thesis is divided into 9 chapters as described below.

Chapter 2 explains the steady-state operation of voltage source converters. The chapter presents a general model of the VSC for harmonic analysis using harmonic domain techniques. Chapter 3 presents a STATCOM model based on VSC using the modelling and analysis carried out for the STATCOM. Chapter 4 presents models for the HVDC-VSC back-to-back and HVDC-VSC transmission system. Following the same modelling philosophy, a model for the UPFC is presented in Chapter 5. With the use of averaging methods, a new space-state for dynamic harmonic analysis is presented in Chapter 6. This state-space is refereed to as EHD and used to solve electric circuits and to define dynamic electric indices. In Chapter 7, the EHD is used to obtain the space-state equations of the STATCOM and HVDC-VSC stations. Chapter

8 presents a new method for harmonic power flow analysis, the method is based on the instantaneous power balance, harmonic domain and Newton–Raphson method. Chapter 9 gives the general conclusions of this thesis and outlines future research work.

This manuscript was prepared using LyX(version 1.1.5) document processor for LaTeX, using pslatex font size 12. The figures were drawn using Xfig (version 3.2) both running under Red Hat Linux (version 6.2). The simulations were carried out using Matlab (version 5.3) for Windows.

2. Voltage Source Converters

2.1. Introduction

VSCs using PWM control are the mainstay of modern power electronics controllers, such as STATCOM, DVR and HVDC-VSC stations [7][5]. One of the many advantages of VSCs using PWM control is that they can produce quasi-sinusoidal voltage waveforms, having almost any desired phase relationship with an existing AC system waveform, thus dictating the direction and magnitude of the active and reactive power exchanged with the AC system. In practice, the high harmonic frequencies generated by the VSC could be filtered out by high-frequency harmonic filter [10], but in practice the operation of such filters will not be perfect or they may not even be operating. Moreover, harmonic interactions between the VSC and the electric network will always take place. This interaction may produce harmonic resonances which can only be predicted with realistic models of the VSC and the electric network.

Comprehensive models for power converters have been reported in the open literature. In power systems harmonic studies, switching functions have found widespread acceptance in the modelling of converters based on thyristor [64][65][66], where the commutation period of the thyristors has been included in the switching functions. As an extension, switching functions have also been used in the modelling of converters based on GTOs or IGBTs, showing even greater adequacy than in the former application [67][68][69].

In this chapter, switching functions in the form of harmonic transfer matrices are used to model three-phase PWM VSCs for steady-state harmonic analysis. The models are given in the form of harmonic equivalent impedances. In these models, the capacitor and its effects on the AC and DC sides are taken explicitly into account. The model is derived with a view to be used as the main building block with which other power electronics controllers can be assembled, and consequently a modular approach is adopted in its development.

2.2. Principles of Operation

Power converters may be classified into two categories [8][73]: Current source converters (CSC) and voltage source converters (VSC).

2. *Voltage Source Converters*

1. In the CSC the DC current has only one polarity, and the power reversal takes place through reversal of the DC voltage polarity. This converter uses the conventional thyristor device which has only the turn-on control, and its turn-off depends on the current coming to zero as per circuit and system conditions.

2. In the VSC the DC voltage has only one polarity, and the power reversal takes place through reversal of the DC current polarity. This type of converter uses devices with turn-on and turn-off capabilities such as GTOs and IGBTs.

Basically, a VSC generates AC voltage from a DC voltage which is supported by a capacitor. In a VSC, the magnitude, the phase angle and the frequency of the output voltage can be controlled by resorting to switching control. The VSC is distinguished by the following features:

- The capacitor is across the DC side.
- The valves (GTOs or IGBTs) have gate turn-off capability. Each valve has an antiparallel fast recovery diode across it to allow current flow in either direction.
- It is assumed that the DC voltage is always present and that it is sufficiently high with respect to the AC line voltage so that the antiparallel diodes are normally reversed biased.
- The valves are triggered "on" and "off" by logic signals to their gates from the PWM control block.

In order to explain the basic principles of VSC operation, Figure 2.1 shows a single-phase full-wave VSC. The VSC consists of four valves, and a DC capacitor previously charged to provide constant DC voltage. The designated valve numbers represent their sequence of turn-on and turn-off. The DC voltage, v_d, is converted to AC line voltage, v_{ab}, with the appropriate turn-on and turn-off sequence of the valves. With devices 3 and 4 turned off, and devices 1 and 2 turned on, voltage v_{ab} becomes $+v_d$ for one half cycle, and with devices 3 and 4 turned on and devices 1 and 2 turned off, voltage v_{ab} becomes $-v_d$ for the other half cycle. The waveform of v_{ab} (frequency, magnitude and angle) depends on the switching functions that govern the devices regardless of the AC current i_{ab}. The current i_{ab} results from the interaction of the AC voltage generated by the VSC, the AC voltage and impedance of the system. For example, assume that the current i_{ab} has the waveform shown in Figure 2.1:

- From t_1 to t_2, v_{ab} is positive and i_{ab} is negative. The current flows through device 1 into the phase a, and the output of the phase b through device 2, with power flow from DC to AC side (inverter action).
- From t_2 to t_3, the current reverses, and flow through diodes 1' and 2' with power flow from AC to DC side (rectifier operation).

- From t_3 to t_4, devices 1 and 2 are turned off and devices 3 and 4 are turned on, thereby v_{ab} becomes negative while i_{ab} is still positive. The current now flows through devices 3 and 4 with power from DC to AC side (inverter action).

- From t_4 to t_5, with devices 3 and 4 still on, and 1 and 2 off, and v_{ab} negative, current i_{ab} reverses and flows through diodes 3' and 4' with power flow from AC to DC side (rectifier action).

- In t_5, the cycle starts again. Also, Figure 2.1 shows current i_d in the DC side with the positive part flowing from the AC to DC side (rectifier action), and the negative part flowing from DC to AC side (inverter action).

- Clearly the current i_d contains harmonics and a negative dc-term.

- During transient VSC operation, the dc-term of i_d is due to the charge or discharge of the capacitor (in this figure it corresponds to the discharge).

- During steady-state VSC operation, the dc-term of i_d cannot flow through the capacitor and must come from the DC system, i.e. given by I_{dc}.

2.3. Steady-state Operation of the VSC

Figure 2.2 represents a three-phase VSC. It includes a star-delta connected transformer with the impedance Z_e reffered to the primary side. The transformation ratio is considered 1:1 for the analysis.

The voltage in the DC side of the VSC is given by the voltage in the capacitor,

$$v_{\text{cap}}(t) = \frac{1}{C}\int_0^t i_{\text{cap}}(t)\mathrm{d}t + v_{\text{cap}}(0^+) \tag{2.1}$$

where the voltage $v_{\text{cap}}(0^+)$ is the voltage evaluated at $t = 0^+$ due to charging from an earlier period,

$$v_{\text{cap}}(0^+) = \frac{1}{C}\int_{-\infty}^{0^+} i_{\text{cap}}(t)\mathrm{d}t \tag{2.2}$$

For steady-state analysis the voltage $v_{\text{cap}}(0^+)$ may be assumed to be constant, meaning that the capacitor is not charging or discharging anymore. In this situation the dc-term of $i_{\text{cap}}(t)$ is zero (the capacitor is an open circuit to the DC current in steady-state). Since the dc-term of $i_{\text{cap}}(t)$ is considered to be zero, it is not possible to exchange active power, in steady-state, with the AC system.

To maintain the DC capacitor voltage, the active power supplied by the DC system has to be equal to the active power absorbed by the AC system plus the losses of the VSC, which includes

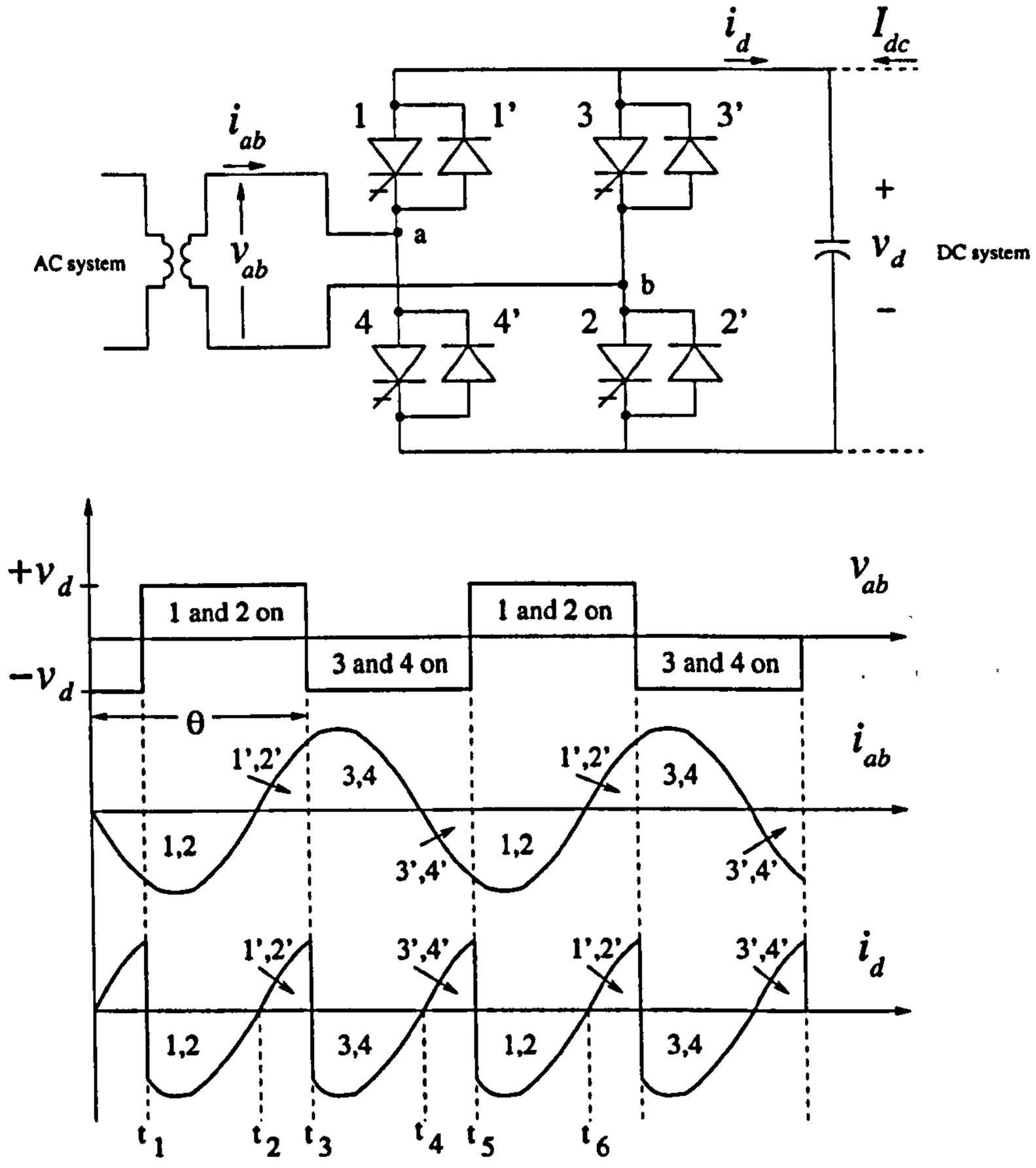

Figure 2.1.: Single-phase, full-wave VSC

the switching losses and capacitor leakage losses in the converter. If the active power is greater than the AC system demand plus the converter losses, the surplus portion will be absorbed by the VSC and, thus, cause the DC capacitor voltage to increase. If this active power is less than the AC system demand plus the converter losses, the DC capacitor voltage will decrease. In order to maintain a constant DC voltage, a PI controller may be employed to regulate the DC capacitor voltage. The basic idea of this controller is to use the error between a voltage reference and the actual DC voltage as a feedback signal. This signal is fed to a PI regulator to produce a phase angle shift, δ, of the VSC output voltage to control the active power exchanged by the converter and the AC system. Hence, it is possible to talk about a constant voltage, $v_{\text{cap}}(0^+)$, in steady-state.

In Figure 2.2, the line voltage on the AC side and on the DC side are related to each other by the following expressions,

$$v_{ab}(t) = s_{ab}(t)v_{\text{cap}}(t) \tag{2.3}$$

$$v_{bc}(t) = s_{bc}(t)v_{\text{cap}}(t) \tag{2.4}$$

$$v_{ca}(t) = s_{ca}(t)v_{\text{cap}}(t) \tag{2.5}$$

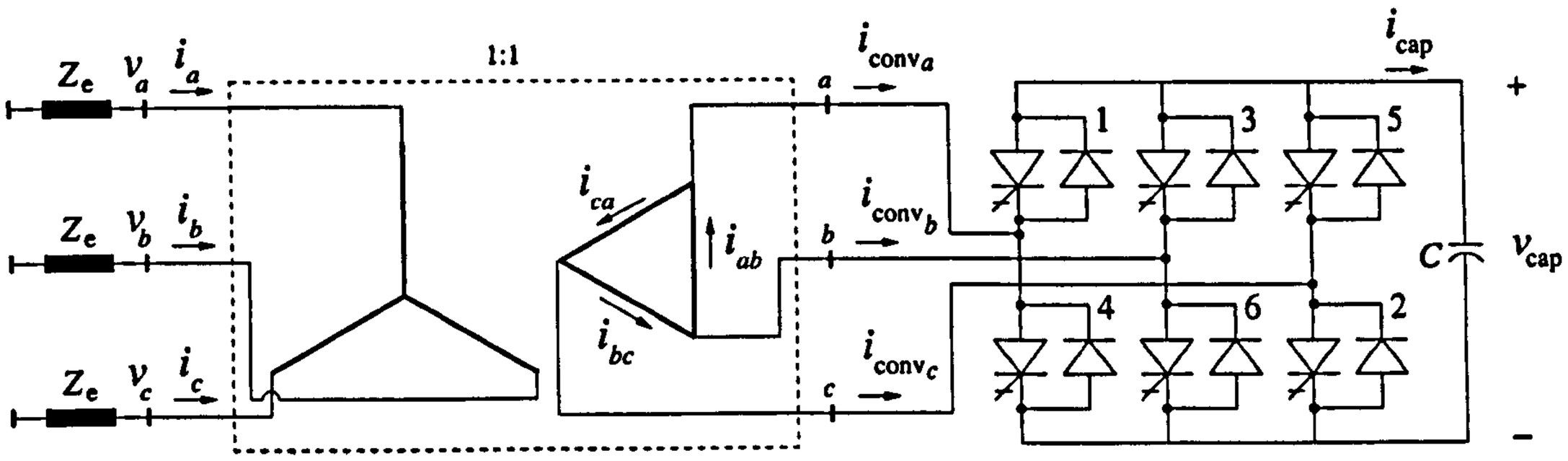

Figure 2.2.: Three-phase voltage source converter

where $s_{ab}(t)$, $s_{bc}(t)$ and $s_{ca}(t)$ are the switching functions that govern the switches 1-6, 3-2 and 5-4, respectively. Assuming lossless switches, the instantaneous power on the AC and DC side of the VSC would match with each other, i.e.

$$v_{ab}(t)i_{ab}(t) + v_{bc}(t)i_{bc}(t) + v_{ca}(t)i_{ca}(t) = v_{\text{cap}}(t)i_{\text{cap}}(t) \tag{2.6}$$

Substitution of (2.3)–(2.5) in (2.6) leads to an expression that relates the AC side and DC side currents as a function of the switching functions given by

$$i_{\text{cap}}(t) = s_{ab}(t)i_{ab}(t) + s_{bc}(t)i_{bc}(t) + s_{ca}(t)i_{ca}(t) \tag{2.7}$$

It can be seen from Figure 2.2 that the phase voltages $v_a(t)$, $v_b(t)$ and $v_c(t)$ on the primary side of the transformer, are proportional to the line voltages $v_{ab}(t)$, $v_{bc}(t)$ and $v_{ca}(t)$ on the secondary side. Also, the line currents $i_a(t)$, $i_b(t)$ and $i_c(t)$ on the primary side of the transformer, are proportional to the phase currents $i_{ab}(t)$, $i_{bc}(t)$ and $i_{ca}(t)$, respectively. The AC line currents of the converter are given by: $i_{\text{conv}_a}(t) = i_{ab}(t) - i_{ca}(t)$, $i_{\text{conv}_b}(t) = i_{bc}(t) - i_{ab}(t)$ and $i_{\text{conv}_c}(t) = i_{ca}(t) - i_{bc}(t)$.

Using a three-phase representation, and voltages and currents in the primary side of the transformer, equations (2.3)–(2.5) may be represented by

$$\mathbf{v}_{abc}(t) = \mathbf{p}_s(t)v_{\text{cap}}(t) \tag{2.8}$$

and equation (2.7) by

$$i_{\text{cap}}(t) = \mathbf{q}_s(t)\mathbf{i}_{abc}(t) \tag{2.9}$$

where the voltage and current vectors are

$$\mathbf{v}_{abc}(t) = \begin{bmatrix} v_a(t) \\ v_b(t) \\ v_c(t) \end{bmatrix} \tag{2.10}$$

and

$$\mathbf{i}_{abc}(t) = \begin{bmatrix} i_a(t) \\ i_b(t) \\ i_c(t) \end{bmatrix} \tag{2.11}$$

The transformation vectors are given by

$$\mathbf{p}_s(t) = \begin{bmatrix} s_{ab}(t) \\ s_{bc}(t) \\ s_{ca}(t) \end{bmatrix} \tag{2.12}$$

$$\mathbf{q}_s(t) = \begin{bmatrix} s_{ab}(t) & s_{bc}(t) & s_{ca}(t) \end{bmatrix} \tag{2.13}$$

The switching functions can be treated as general periodical functions where their harmonic coefficients depend on the PWM technique used in the operation of the VSC configuration.

2.4. PWM VSC Switching Functions

Pulse width modulation (PWM) is a technique which enables effective control of the harmonic content and harmonic magnitude generated by VSCs, by controlling the turn-on and turn-off of the power electronic switching devices. Although many PWM techniques exist, only two will be described in this chapter.

2.4.1. Unipolar voltage switching technique

A PWM with unipolar voltage switching is represented in Figure 2.3. In this figure v_r is the carrier signal with frequency f_r, $v_{sa} = -v_{sb}$ is the modulation signal with frequency f_s, e.g. 50 Hz, and m is a modulation factor, which corresponds to the maximum value of v_{sa}. The functions $s_a(t)$ and $s_b(t)$ are obtained by comparing v_{sa} and v_{sb} with v_r. Both switched waveforms take a value of one when $v_{sa} > |v_r|$ and $v_{sb} > |v_r|$, respectively, and zero otherwise. If the conduction of GTO number 1, in Figure 2.2, is governed by the pulses of $s_a(t)$, and the GTO number 6 by $s_b(t)$, then the output voltage $v_{ab}(t)$ is proportional to the PWM switching function $s_{ab}(t)$ i.e. $v_{ab}(t) = s_{ab}(t)v_{\text{cap}}(t)$. The voltages for the other phases are obtained in the same way. In this PWM technique the magnitude of the fundamental frequency of $s_{ab}(t)$ is the modulation factor m, and the phase angle is the modulation shift angle ϕ_m of the modulation signal v_{as}, and the harmonics of $s_{ab}(t)$ are controlled by the frequency of the carrier signal f_r.

Figure 2.4 shows the harmonic magnitudes of a switching function. This switching function was generated by a unipolar voltage switching technique with $f_r = 250$ Hz. It can be seen that

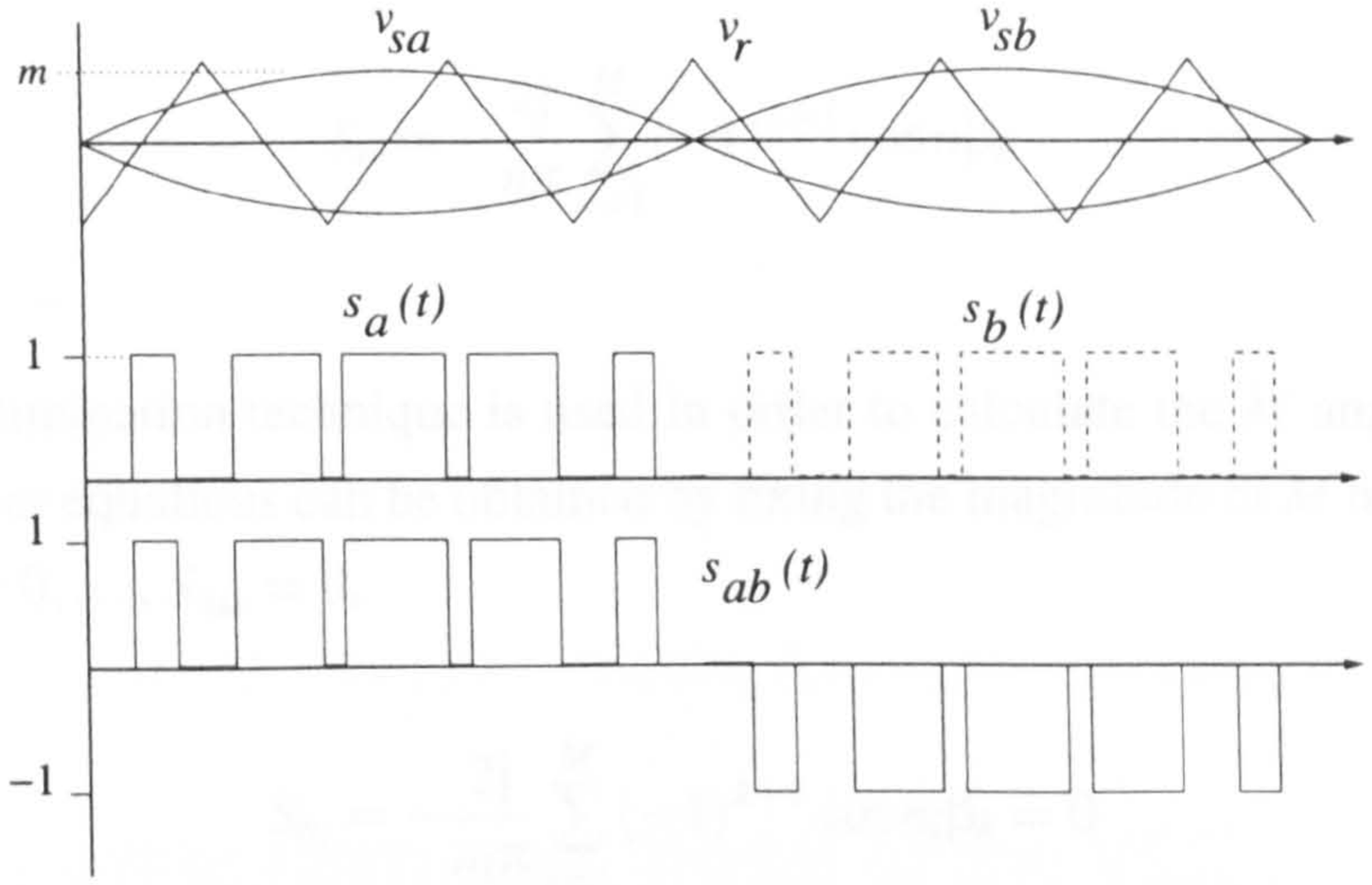

Figure 2.3.: PWM converter with unipolar voltage switching

the magnitude of the harmonics depends on the modulation factor m rather than in the phase angle of the modulation signal ϕ_m. Also, these magnitudes do not present a linear response to the modulation factor. The analytical expression for this switching function is given in Appendix A.

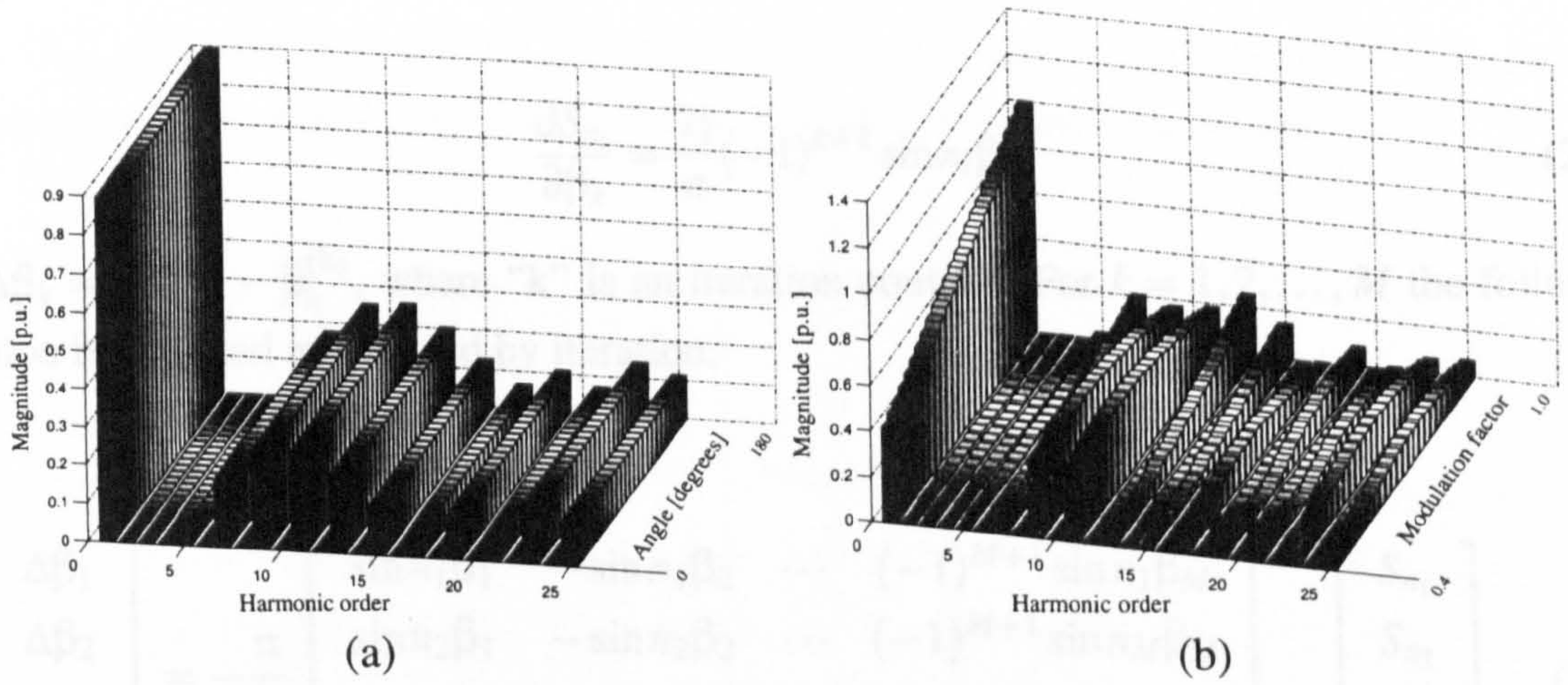

Figure 2.4.: Harmonic generated by the unipolar voltage switching technique

2.4.2. Selective harmonic elimination technique

The general switching function of Figure 2.5 is used to explain the selective harmonic elimination technique [97]. This switching function has the harmonic content given by the following Fourier series,

$$s(t) = \sum_{n=-h}^{h} S_n e^{jn\omega_0 t}$$

where

$$S_n = -\frac{2j}{n\pi}\sum_{k=1}^{M}(-1)^{k+1}\cos n\beta_k \tag{2.14}$$

for $n = 1, 3, 5, 7, \ldots$.

A harmonic elimination technique is used in order to calculate the M angles, β_s. The required M non-linear equations can be obtained by fixing the magnitude of M harmonics to zero, i.e. $S_{n_1} = 0, S_{n_2} = 0, \ldots, S_{n_M} = 0$,

$$S_{n_i} = -\frac{2j}{n_i\pi}\sum_{k=1}^{M}(-1)^{k+1}\cos n_i\beta_k = 0 \tag{2.15}$$

for $i = 1, 2, \ldots, M$, where $n_1, n_2, \ldots, n_M$ are the harmonics to be eliminated.

Solving (2.15) for the M angles, using Newton's method, the following equation is obtained,

$$\Delta\beta_k = -\left.\frac{\partial S_{n_i}}{\partial\beta_k}\right|^{-1} S_{n_i} \tag{2.16}$$

where

$$\frac{\partial S_{n_i}}{\partial\beta_k} = \frac{2j}{\pi}(-1)^{k+1}\sin n_i\beta_k \tag{2.17}$$

and $\Delta\beta_k = \beta_k^{(k+1)} - \beta_k^{(k)}$, where "k" is an iteration counter. For $k = 1, 2, \ldots, M$ the following equation is obtained and solved by iteration,

$$\begin{bmatrix} \Delta\beta_1 \\ \Delta\beta_2 \\ \vdots \\ \Delta\beta_M \end{bmatrix} = -\frac{\pi}{2j}\begin{bmatrix} \sin n_1\beta_1 & -\sin n_1\beta_2 & \cdots & (-1)^{M+1}\sin n_1\beta_M \\ \sin n_2\beta_1 & -\sin n_2\beta_2 & \cdots & (-1)^{M+1}\sin n_M\beta_M \\ \vdots & \vdots & \ddots & \vdots \\ \sin n_M\beta_1 & -\sin n_M\beta_2 & \cdots & (-1)^{M+1}\sin n_M\beta_M \end{bmatrix}^{-1}\begin{bmatrix} S_{n_1} \\ S_{n_2} \\ \vdots \\ S_{n_M} \end{bmatrix} \tag{2.18}$$

The calculated angles must satisfy the following condition: $\beta_1 < \beta_2 < \cdots < \beta_M$.

For example, to eliminate the 3rd harmonic, the calculated angle is $\beta_1 = 30°$. To eliminate harmonics 5th, 7th, 11th, 13th and 17th, the calculated angles are $\beta_1 = 11.35°, \beta_2 = 17.27°, \beta_3 = 23.81°, \beta_4 = 34.88°$ and $\beta_5 = 37.27°$.

In three-phase PWM converter applications, the switching functions for the other two phases are calculated by shifting the switching function by 120° and −120°, respectively.

A multi-pulse configuration, such as that shown in Appendix A, can be used in order to reduce the harmonic content of the switching functions.

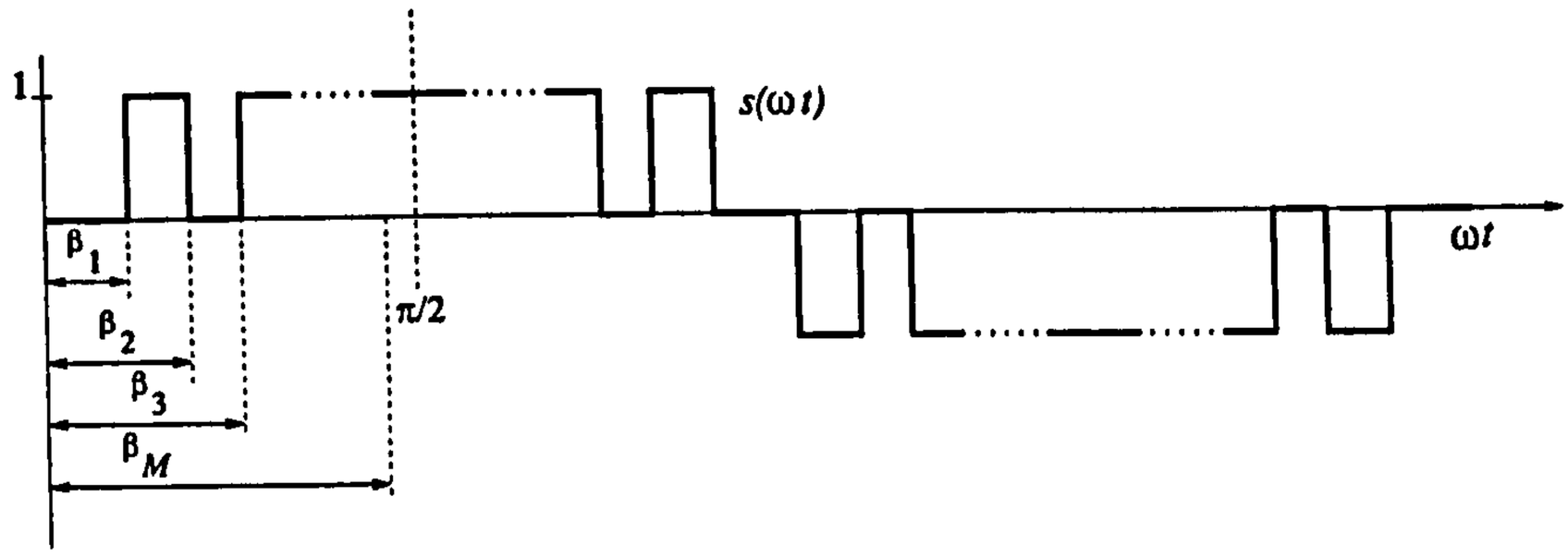

Figure 2.5.: Switching function for selective elimination

2.5. Steady-state Harmonic Model of the VSC

The steady-state model of the VSC for harmonic analysis is derived by using the HD technique explained in Appendix B.

Equation (2.1) may be expressed in HD by

$$\mathbf{V}_{cap} = \frac{1}{C}\mathbf{D}^{-1}(jh\omega_0)\mathbf{I}_{cap} + \mathbf{V}_0 \tag{2.19}$$

where $\mathbf{V}_{cap}$ is assembled with the harmonic content of $v_{cap}(t)$. Likewise, vector $\mathbf{I}_{cap}$ includes the harmonic content of $i_{cap}(t)$, and $\mathbf{V}_0$ contains only a constant dc-term, i.e.

$$\mathbf{V}_0 = \begin{bmatrix} 0 \\ \vdots \\ 0 \\ v_{cap}(0^+) \\ 0 \\ \vdots \\ 0 \end{bmatrix} \tag{2.20}$$

Equation (2.19) can be written as

$$\mathbf{V}_{cap} = \mathbf{Z}_{cap}\mathbf{I}_{cap} + \mathbf{V}_0 \tag{2.21}$$

where $\mathbf{Z}_{cap} = \frac{1}{C}\mathbf{D}^{-1}(jh\omega_0)$ represents the equivalent impedance of the capacitor on the DC side of the converter.

From (2.8), the voltage on the DC side and its relationship to the AC phase voltages may be expressed in HD as

$$\mathbf{V}_{abc} = \mathbf{P}_s\mathbf{V}_{cap} \tag{2.22}$$

Similarly, the relationship between the line currents and the DC current is given by

$$\mathbf{I}_{\text{cap}} = \mathbf{Q}_s \mathbf{I}_{abc} \tag{2.23}$$

where the transformation matrices $\mathbf{P}_s$ and $\mathbf{Q}_s$ are given by

$$\mathbf{P}_s = \begin{bmatrix} \mathbf{S}_{ab} \\ \mathbf{S}_{bc} \\ \mathbf{S}_{ca} \end{bmatrix} \tag{2.24}$$

and

$$\mathbf{Q}_s = \begin{bmatrix} \mathbf{S}_{ab} & \mathbf{S}_{bc} & \mathbf{S}_{ca} \end{bmatrix} \tag{2.25}$$

$\mathbf{S}_{ab}$, $\mathbf{S}_{bc}$ and $\mathbf{S}_{ca}$ are Toeplitz matrices of the form of equation (B.16).

Finally, the voltage and current vectors are given by

$$\mathbf{V}_{abc} = \begin{bmatrix} \mathbf{V}_a \\ \mathbf{V}_b \\ \mathbf{V}_c \end{bmatrix} \tag{2.26}$$

and

$$\mathbf{I}_{abc} = \begin{bmatrix} \mathbf{I}_a \\ \mathbf{I}_b \\ \mathbf{I}_c \end{bmatrix} \tag{2.27}$$

For the purpose of HD modelling the VSC of Figure 2.2 may be represented as in Figure 2.6 which includes an injected current in the DC side. This additional current gives the option to exchange active power between the DC and AC systems in steady-state operation.

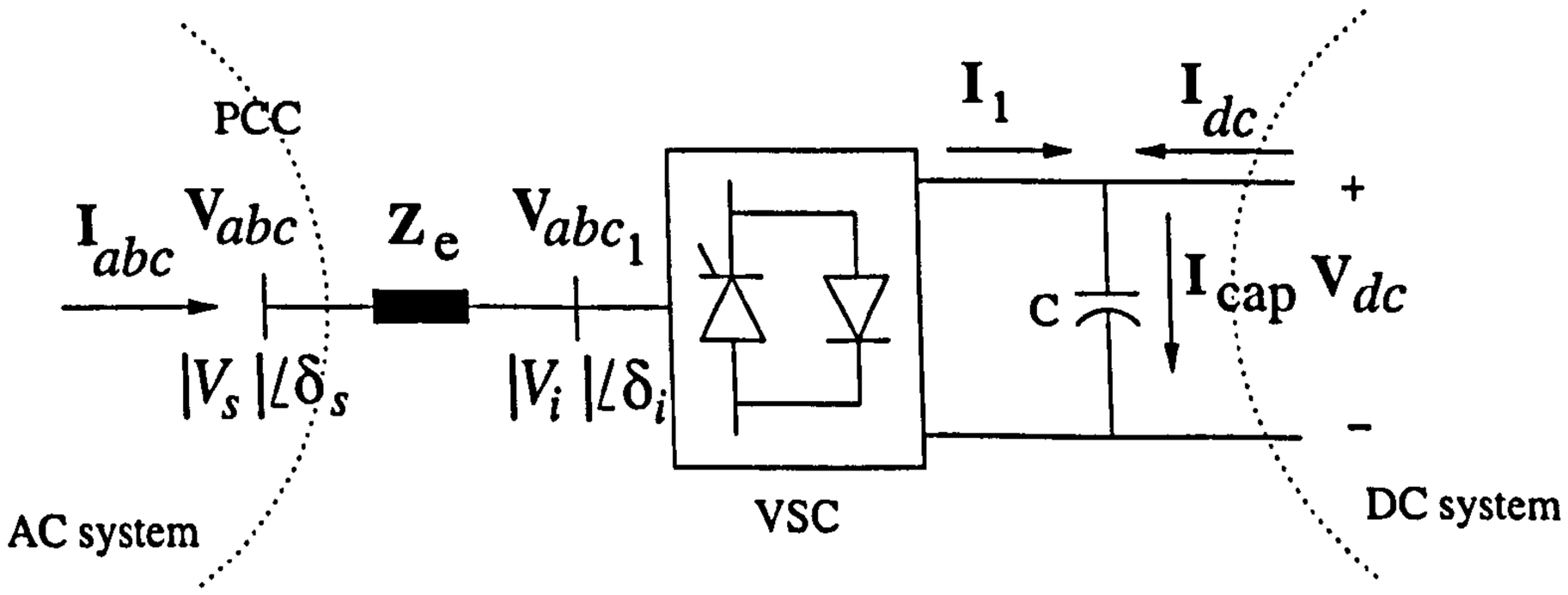

Figure 2.6.: General voltage source converter equivalent

The output voltage of the VSC (in the primary side of the transformer) is given by

$$\mathbf{V}_{abc_1} = \mathbf{P}_s \mathbf{V}_{dc} \tag{2.28}$$

The voltage in the AC system side is

$$\mathbf{V}_{abc} = \mathbf{Z}_e \mathbf{I}_{abc} + \mathbf{V}_{abc_1} \tag{2.29}$$

where $\mathbf{Z}_e = R_e \mathbf{U}_I + L_e \mathbf{D}(\mathrm{j}h\omega_0)$, R_e and L_e are the equivalent resistance and inductance of the coupling transformer. $\mathbf{U}_I$ is the identity matrix.

The current in the DC side of the VSC is given by

$$\mathbf{I}_1 = \mathbf{Q}_s \mathbf{I}_{abc} \tag{2.30}$$

and the DC side voltage,

$$\mathbf{V}_{dc} = \mathbf{Z}_{cap} \mathbf{I}_{cap} + \mathbf{V}_0 \tag{2.31}$$

with the current in the capacitor given by

$$\mathbf{I}_{cap} = \mathbf{I}_1 + \mathbf{I}_{dc} \tag{2.32}$$

Solving for $\mathbf{V}_{abc}$ and $\mathbf{V}_{dc}$ the following equation is obtained,

$$\begin{bmatrix} \mathbf{V}_{abc} \\ \mathbf{V}_{dc} \end{bmatrix} = \begin{bmatrix} \mathbf{Z}_e + \mathbf{P}_s \mathbf{Z}_{cap} \mathbf{Q}_s & \mathbf{P}_s \mathbf{Z}_{cap} \\ \mathbf{Z}_{cap} \mathbf{Q}_s & \mathbf{Z}_{cap} \end{bmatrix} \begin{bmatrix} \mathbf{I}_{abc} \\ \mathbf{I}_{dc} \end{bmatrix} + \begin{bmatrix} \mathbf{P}_s \mathbf{V}_0 \\ \mathbf{V}_0 \end{bmatrix} \tag{2.33}$$

or in a more compact form,

$$\begin{bmatrix} \mathbf{V}_{abc_T} \\ \mathbf{V}_{dc_T} \end{bmatrix} = \begin{bmatrix} \mathbf{A}_1 & \mathbf{B}_1 \\ \mathbf{C}_1 & \mathbf{D}_1 \end{bmatrix} \begin{bmatrix} \mathbf{I}_{abc} \\ \mathbf{I}_{dc} \end{bmatrix} \tag{2.34}$$

where

$$\mathbf{V}_{abc_T} = \mathbf{V}_{abc} - \mathbf{P}_s \mathbf{V}_0 \tag{2.35}$$

$$\mathbf{V}_{dc_T} = \mathbf{V}_{dc} - \mathbf{V}_0 \tag{2.36}$$

and

$$\mathbf{A}_1 = \mathbf{Z}_e + \mathbf{P}_s \mathbf{Z}_{cap} \mathbf{Q}_s \tag{2.37}$$

$$\mathbf{B}_1 = \mathbf{P}_s \mathbf{Z}_{cap} \tag{2.38}$$

$$\mathbf{C}_1 = \mathbf{Z}_{cap} \mathbf{Q}_s \tag{2.39}$$

$$\mathbf{D}_1 = \mathbf{Z}_{cap} \tag{2.40}$$

Equation (2.34) gives a two ports representation of the VSC. This VSC model is used throughout the thesis as the main block for building more complex power electronics controllers models.

2.5.1. Active and reactive power transfer

With reference to Figure 2.6, the exchange of active power between the AC and the DC system can be controlled by adjusting the phase angle difference of the converter output voltage and the voltage at the point of common coupling (PCC), i.e. $\delta_{si} = \delta_s - \delta_i$. The reactive power exchanged between the AC system and the VSC is controlled by adjusting the voltage magnitude difference across the coupling transformer, i.e. $|V_s| - |V_i|$.

The active and reactive power injected by the AC system are given by

$$\mathrm{P} \approx \frac{|V_s||V_i|}{X_e} \sin\delta_{si} \tag{2.41}$$

$$\mathrm{Q} \approx \frac{|V_s|^2}{X_e} - \frac{|V_s||V_i|}{X_e} \cos\delta_{si} \tag{2.42}$$

where X_e is the equivalent reactance of the coupling transformer.

The VSC of Figure 2.6 is used to illustrate the response of the VSC for active and reactive power exchange with the AC system. Equation (2.34) is used to obtain such a response. The following considerations and parameters are used in this analysis: The switching functions have been selected to represent a six-level VSC (as shown in Figure A.3(c) of Appendix A) with a switching frequency of 150 Hz. The PWM control uses a variable modulation factor, m, to control the output voltage magnitude. A capacitor of $500\,\mu$F with a precharged voltage of 1.5 p.u. was considered. A three-phase AC balanced voltage source of 1 p.u. with $\delta_s = 0°$ and equivalent impedance of $Z_e = 0.0133 + j0.6283\,\Omega$ at 50 Hz were used. The analysis was carried out with 15 harmonics.

Cases of active and reactive power exchanges are given below.

Active power exchange: The active power exchange was obtained by using different values of DC current injection in the range $-0.5 < I_{dc_0} < 0.5$ p.u. A constant modulation factor of $m = 0.8$ was used in this case.

Figure 2.7 shows results for phase a. Figure 2.7(a) shows the voltage and current response of the VSC for three different DC current values, i.e. $-0.5, 0.0$ and 0.5 p.u. It can be seen that the voltage $v_{dc}(t)$ maintains the same polarity, and the current $i_1(t)$ changes direction. The power balance between the AC and DC sides is achieved by adjusting the phase angle of the PWM modulation signal (equivalent to δ_i) used by the VSC which produces an output voltage

$v_{a_1}(t)$. Owing to the PWM technique used in the VSC, the ripple in $v_{dc}(t)$, and the waveform of $v_{a_1}(t)$ are almost the same for the three DC current conditions.

Figure 2.7(b) shows the behaviour of electric parameters as a function of I_{dc_0}. It can be seen that the active power is controlled by the DC current, where the maximum and minimum active power exchange is $3P = 3 \times (\pm 0.25) = \pm 0.75$ p.u. and corresponds to the DC power given by $V_{dc_0} I_{dc_0} = 1.5 \times (\pm 0.5) = \pm 0.75$ p.u. The reactive power presents the same direction (absorbed by the AC system) with an almost constant value since it has more dependence on the voltage magnitude $|V_i|$ (regulated by m) rather than on the phase angle δ_i. Owing to the presence of harmonics, a distorted power D also appears. The total harmonic distortion (THD) and the RMS value of $v_{a_1}(t)$ are almost constant, meaning that the harmonics generated by the VSC do not have a strong dependence on the voltage angle. Since the RMS of $v_{a_1}(t)$ is kept constant, the minimum apparent power corresponds to the minimum RMS value of the current $i_a(t)$, leading to a maximum THD current and minimum apparent power exchange.

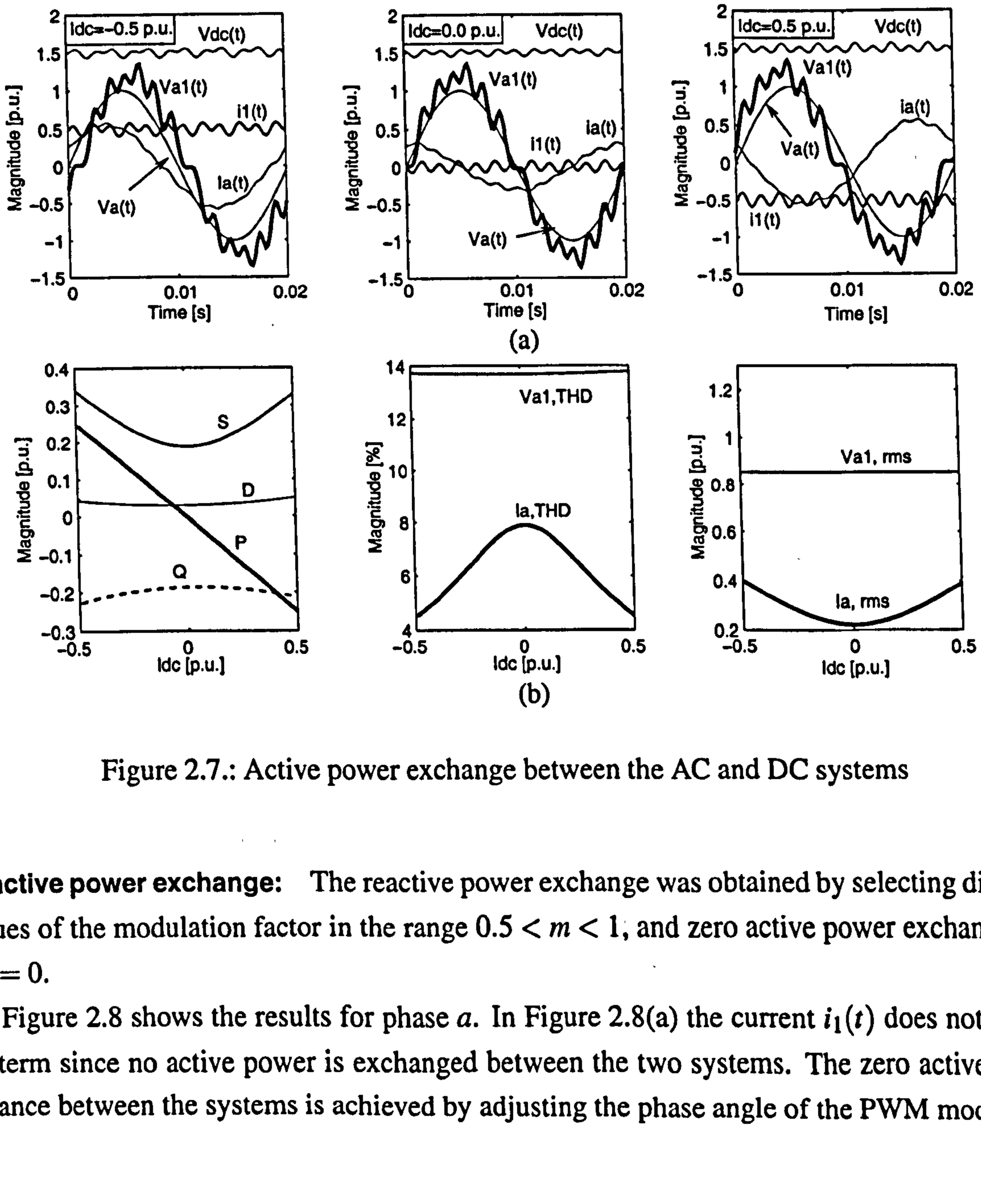

Figure 2.7.: Active power exchange between the AC and DC systems

Reactive power exchange: The reactive power exchange was obtained by selecting different values of the modulation factor in the range $0.5 < m < 1$, and zero active power exchange, i.e. $\mathbf{I}_{dc} = 0$.

Figure 2.8 shows the results for phase a. In Figure 2.8(a) the current $i_1(t)$ does not have a dc-term since no active power is exchanged between the two systems. The zero active power balance between the systems is achieved by adjusting the phase angle of the PWM modulation

signal (equivalent to δ_i) resulting in a VSC output voltage $v_{a_1}(t)$ which is in phase with $v_a(t)$. This condition gives a 90° phase shift angle of $i_a(t)$ with respect to the voltage. The $v_{dc}(t)$ ripple shows little change, but the output voltage $v_{a_1}(t)$ presents different waveforms as a result of different value of modulation factor.

Figure 2.8(b) shows some electric indices as a function of the modulation factor m. The reactive power exchange equals zero when $|V_i| = |V_s|$, a condition that occurs at $m \approx 0.665$ ($|V_i| = 0.665 \times 1.5 = 0.998$ p.u.). It should be noted that zero reactive power exchange, corresponding to minimum apparent power, results in maximum THD current. The RMS voltage presents a markedly linear response but not the THD, which indicates that the harmonics generated by the VSC are a function of the modulation factor rather than the phase angle of the modulation signal as shown in Section 2.4.

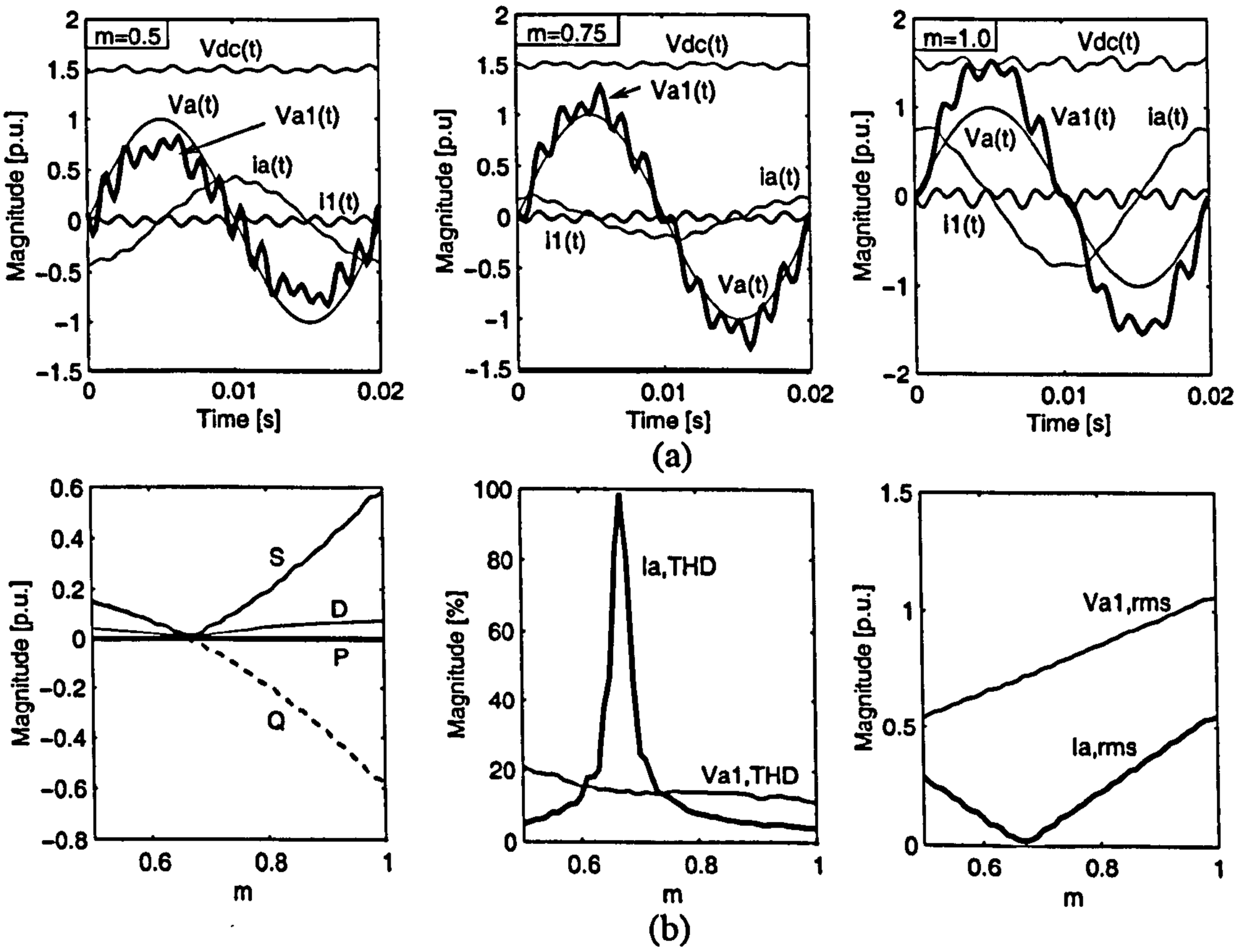

Figure 2.8.: Reactive power exchange between the AC system and the VSC

2.6. Conclusions

A flexible and comprehensive model for the periodic, steady-state operation of voltage source converters was presented in this chapter. Switching functions based on complex Fourier series are used very effectively to represent the operation of the VSC. The modelling approach applies to a wide range of VSC configurations, e.g. single-phase, multi-phase, two-level, multi-level, single-converter and multi-converter.

The model was used to show that the VSC performs very well as an effective active and reactive power controller exchanging power between an AC and a DC system. The results presented in this chapter show that the THD in the voltage output remains almost constant for active and reactive power control. This characteristic is due to the unipolar voltage switching technique used by the PWM converter, where the magnitudes of the generated harmonics have more dependence on the modulation factor than on the phase of the modulation signal.

This VSC model is used as the main building block for the models of STATCOM, HVDC-VSC stations and UPFC presented in the following chapters.

3. Static Synchronous Compensator

3.1. Introduction

The static synchronous compensator or STATCOM is a shunt connected power electronics controller which it exchanges reactive power with the AC system. The STATCOM comprises a VSC and a coupling transformer. In this chapter, a comprehensive harmonic model based on the VSC model is presented. The model takes proper account of the DC capacitor effect and comes in the form of a three-phase Thévenin equivalent expressed in HD. The harmonic impedance matrix of the Thévenin equivalent shows cross-couplings between phases and between harmonics, harmonic effects which are strongly influenced by the size of STATCOM capacitor. Results are presented which show that the STATCOM observes quite different harmonic voltage responses when it is made to operate as a reactive power generator and when it is made to operate as a reactive power absorber.

Over the last few years, an increasing amount of research work addressing the STATCOM has been published in the open literature mainly on design, operation, and control techniques of system level PWM-VSC configurations [21][71][75][76][77][78]. The study of the STATCOM has focused mainly on stability analysis [79][80][81] [82][20] and to a lesser extent on harmonic analysis. Most of the work related to harmonic analysis has been approached from the angle of VSC harmonics generation rather than the harmonic interaction with the electrical network. As a matter of fact, very little analytical work has been carried out on harmonic interaction with the network or resonance phenomena. In [83][84], analytical expressions for the STATCOM were obtained and used to explore the interaction with the network. From the modelling viewpoint, a harmonic voltage source may be used to represent the STATCOM at harmonic frequencies but this will include no explicit representation of the capacitor [21]. In [22][23], a set of simplified analytical expressions were put forward with which the STATCOM currents can be calculated at harmonics and the fundamental frequency. However, the capacitor plays a key role in STATCOM operation and a great deal of modelling flexibility is gained by having explicit access to the capacitor parameters, such as capacitor size, and DC voltage and current.

3.2. STATCOM Model

In the STATCOM, active power exchange is only possible during the charge and/or discharge of the capacitor. During normal operation the DC capacitor charges and discharges to a greater or lesser degree during the course of each cycle. However, for the purpose of steady-state operation the capacitor voltage may be assumed to take an average constant value [22], hence no active power exchange take place.

Using equation (2.33), with $\mathbf{I}_{dc} = 0$ and following the conventions stated in Figure 2.6, yields the following STATCOM equations,

$$\mathbf{V}_{abc} = \left(\mathbf{Z}_{\mathrm{e}} + \mathbf{P}_s \mathbf{Z}_{\mathrm{cap}} \mathbf{Q}_s\right) \mathbf{I}_{abc} + \mathbf{P}_s \mathbf{V}_0 \tag{3.1}$$

which may also be represented by

$$\mathbf{V}_{abc} = \left(\mathbf{Z}_{\mathrm{e}} + \mathbf{Z}_{\mathrm{Th}}\right) \mathbf{I}_{abc} + \mathbf{E}_{\mathrm{Th}} \tag{3.2}$$

where the equivalent impedance $\mathbf{Z}_{\mathrm{Th}}$, i.e. Thévenin impedance, is the impedance seen from the AC side of the VSC

$$\mathbf{Z}_{\mathrm{Th}} = \mathbf{P}_s \mathbf{Z}_{\mathrm{cap}} \mathbf{Q}_s \tag{3.3}$$

The Thévenin equivalent voltage is given by

$$\mathbf{E}_{\mathrm{Th}} = \mathbf{P}_s \mathbf{V}_0 \tag{3.4}$$

The Thévenin equivalent voltage is a constant three-phase harmonic voltage source, which represents the effect of the switching functions over the DC voltage $v_{\mathrm{cap}}(0^+)$, see equation (2.20). It should be noted that a simpler model, which corresponds to what has been reported in the open literature, arises if the capacitor effect is not explicitly represented, i.e. $\mathbf{Z}_{\mathrm{Th}} = 0$. Figure 3.1 incorporates the STATCOM equivalent circuit representation.

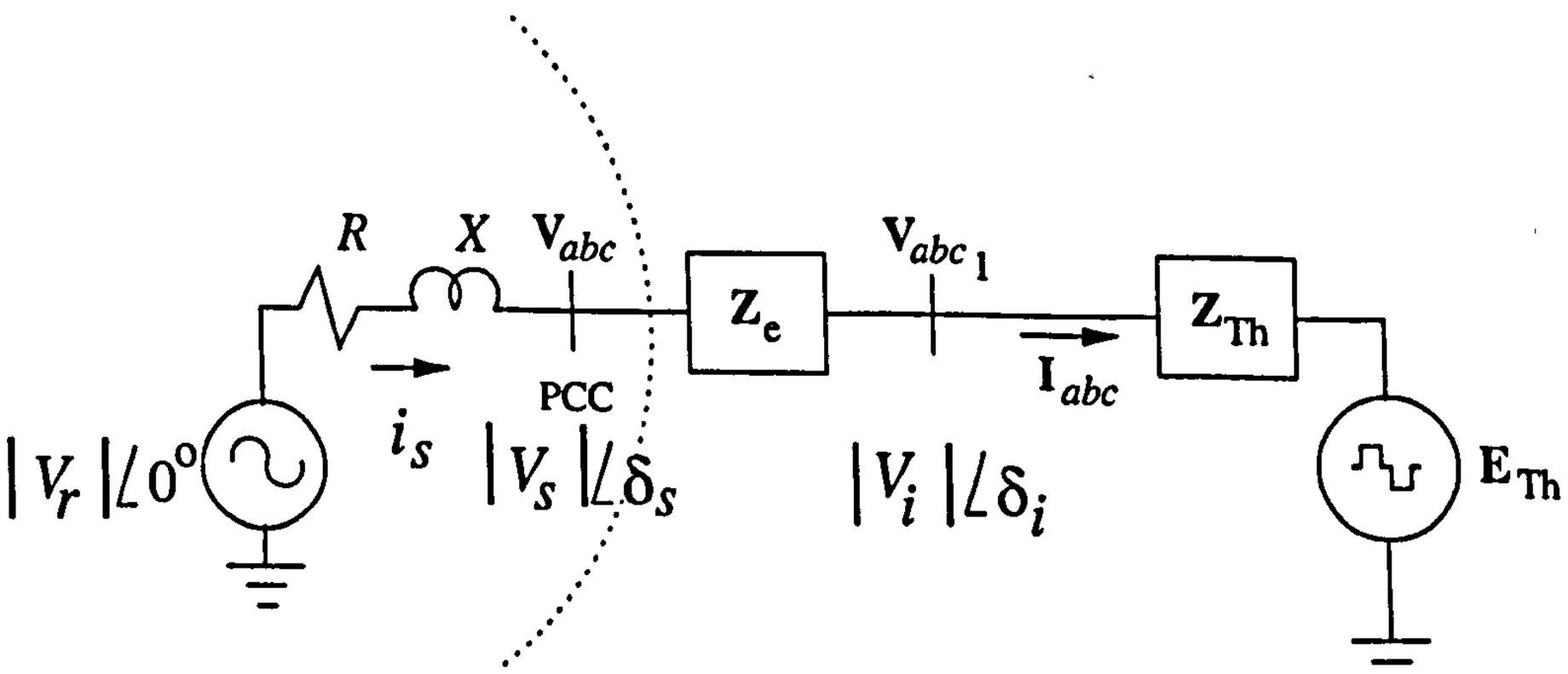

Figure 3.1.: STATCOM equivalent circuit

Since in steady-state operation, the STATCOM can only exchange reactive power, the control of the STATCOM must maintain the DC voltage, $v_{cap}(0^+)$, at a constant value. A DC constant voltage in the capacitor gives a dc-term of the current $\mathbf{I}_1$ equal to zero, i.e. $I_{1_0} = 0$.

It is important to remark that the STATCOM equivalent circuit incorporates the switching functions $s_{ab}(t)$, $s_{bc}(t)$ and $s_{ca}(t)$ according to equations (2.24) and (2.25). These switching functions may be obtained by using PWM techniques. In fact, any PWM techniques may be used in this model as long as the switching functions are amenable to a harmonic vector representation.

3.2.1. Time domain comparison results

The response of the STATCOM model is compared with that of a model implemented in PSCAD/EMTDC [39]. The following parameters were used for the test system:

Source: 115 kV line-to-line, internal RL parallel equivalent impedance with $R_g = 100\,\Omega$ and $L_g = 0.01$ H.

Transformer: $Z_e = R_e + j\omega_0 L_e\ \Omega$, $R_e = 0.1\,\Omega$ and $L_e = 0.05$ H.

VSC: Six-pulse, two-level converter with IGBTs switched by a PWM technique. A carrier frequency of 150 Hz was used.

Capacitor: $300\,\mu$F charged at 115 kV.

Simulation: 100 harmonics were used in the simulation. The result was obtained in two iterations using the iterative process described in Appendix C. For the PSCAD/EMTDC, a simulation time of 1.7 s with a time step of $20\,\mu$s was used to ensure a smooth steady-state condition. The diagram of the PSCAD/EMTDC implementation is shown in Appendix E.

Table 3.1 shows the most significant harmonic currents (in the converter side) produced by the STATCOM. The table presents a comparison between the results generated by the STATCOM model in the HD and the model in PSCAD/EMTDC. The results can be seen to match with each other, with some differences at high harmonic frequencies. These differences are the result of the simulation time, time step and FFT routine used by the PSCAD/EMTDC in order to obtain the harmonic content of the current.

Figure 3.2 shows the comparison using time domain representation. Both results match well with each other.

Figure 3.3 shows the line voltages in the PCC and in the VSC side. The results show that voltages obtained with both models are in good agreement. The effect of the capacitor is evident in the rounded sections on top and bottom of the VSC line voltage. It should be remarked that a larger capacitor will produce a flatter voltage.

Table 3.1.: Harmonic currents comparison

harmonic	HD: $\lvert I_{\text{conv}_a}\rvert$	HD: $\angle\theta°$	PSCAD: $\lvert I_{\text{conv}_a}\rvert$	PSCAD: $\angle\theta°$
1	2.9399	150.4989	2.9086	150.5459
5	0.4503	29.6973	0.4543	33.3165
7	0.0430	−33.1086	0.0468	−25.3038
11	0.0282	−153.0447	0.0262	−141.4797
13	0.0735	148.7240	0.0720	158.6975
17	0.0132	−146.5965	0.0114	−142.1273
19	0.0022	172.4591	0.0039	154.9566
23	0.0202	−153.8191	0.0217	−135.7802
25	0.0007	68.7134	0.0011	−175.2769
29	0.0068	21.8991	0.0058	45.1193
31	0.0140	−35.9797	0.0137	−13.6335

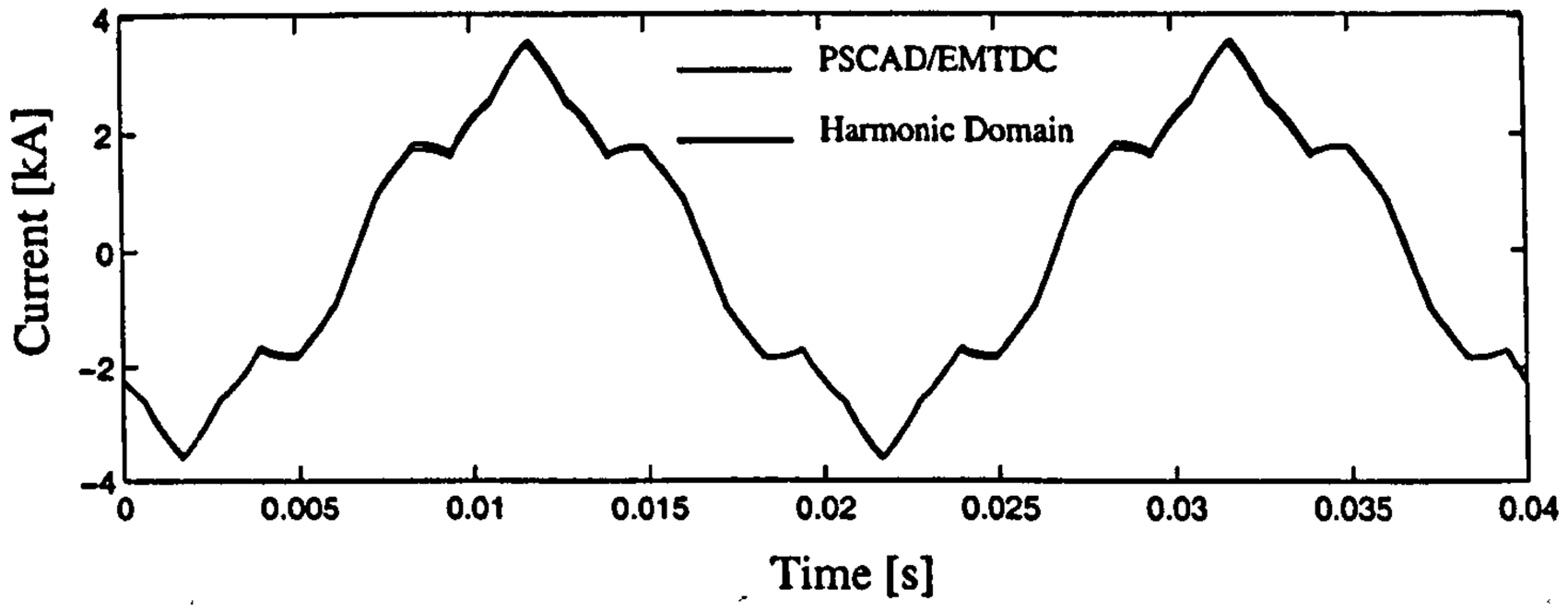

Figure 3.2.: Line current $i_{\text{conv}_a}(t)$

3.2.2. Case study: Reactive power transfer

In this section the three-phase circuit of Figure 3.1 is used to assess different reactive power conditions, with the constraint of $\delta_{is} = \delta_i - \delta_s = 0$, since no active power exchange exists. The solution uses the iterative process explained in Appendix C.

The system data is as follows: $|V_r| = 1$ p.u., $R = 0.0033\,\Omega$, $X = 0.1571\,\Omega$, $R_e = 0.01\,\Omega$ and $X_e = 0.4712\,\Omega$ at 50 Hz.

Two cases are considered below, corresponding to two different operating conditions. They represent cases when the STATCOM absorbs and supplies reactive power, respectively. To achieve such operating conditions, the following precharge DC capacitor voltage values are used: $v_{\text{cap}}(0^+) = 0.7$ p.u. and 1.2 p.u., respectively. In this case the PWM control was set to eliminate only the third harmonic giving a conduction period of 120°.

Absorbing reactive power: In this test case, a value of $v_{\text{cap}}(0^+)$ equal to 0.7 p.u. enables the STATCOM to absorb reactive power equal to 0.2836 p.u. Table 3.2 shows the harmonic magnitude of voltages of $v_s(t)$, $v_i(t)$, and current $i_s(t)$ for two STATCOM representations, namely

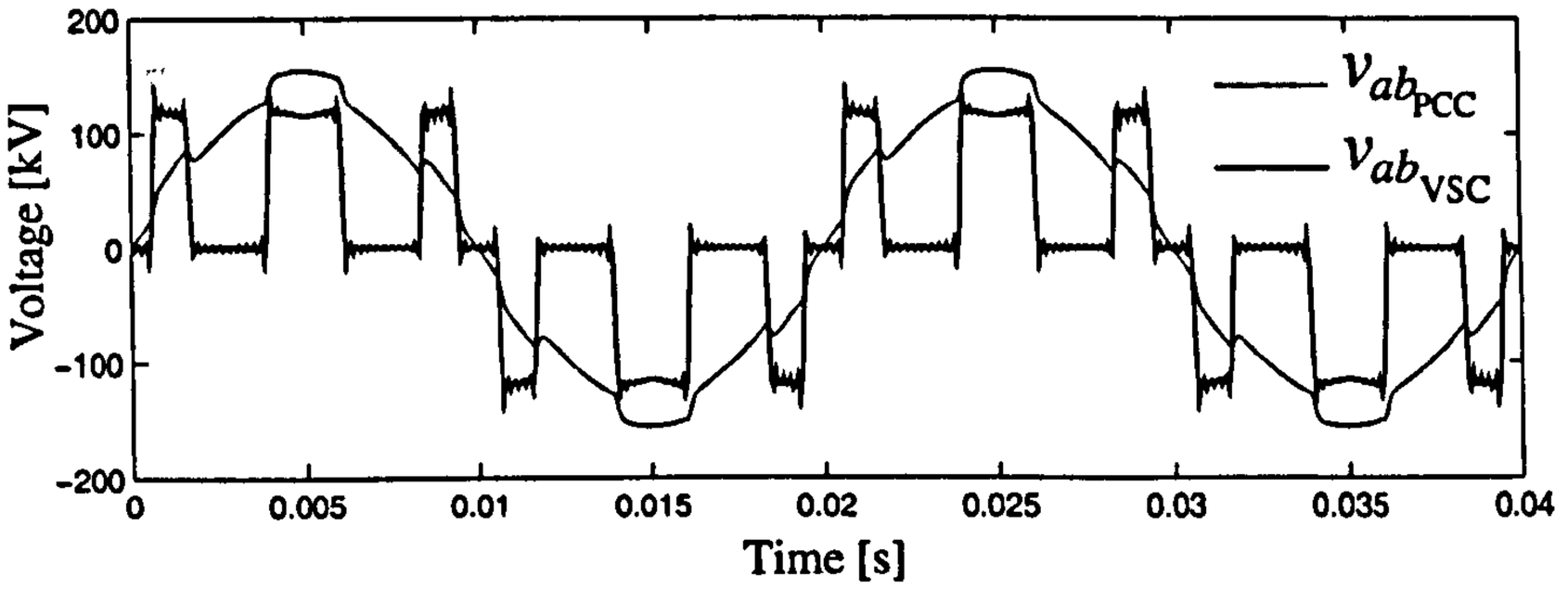

(a) Harmonic domain

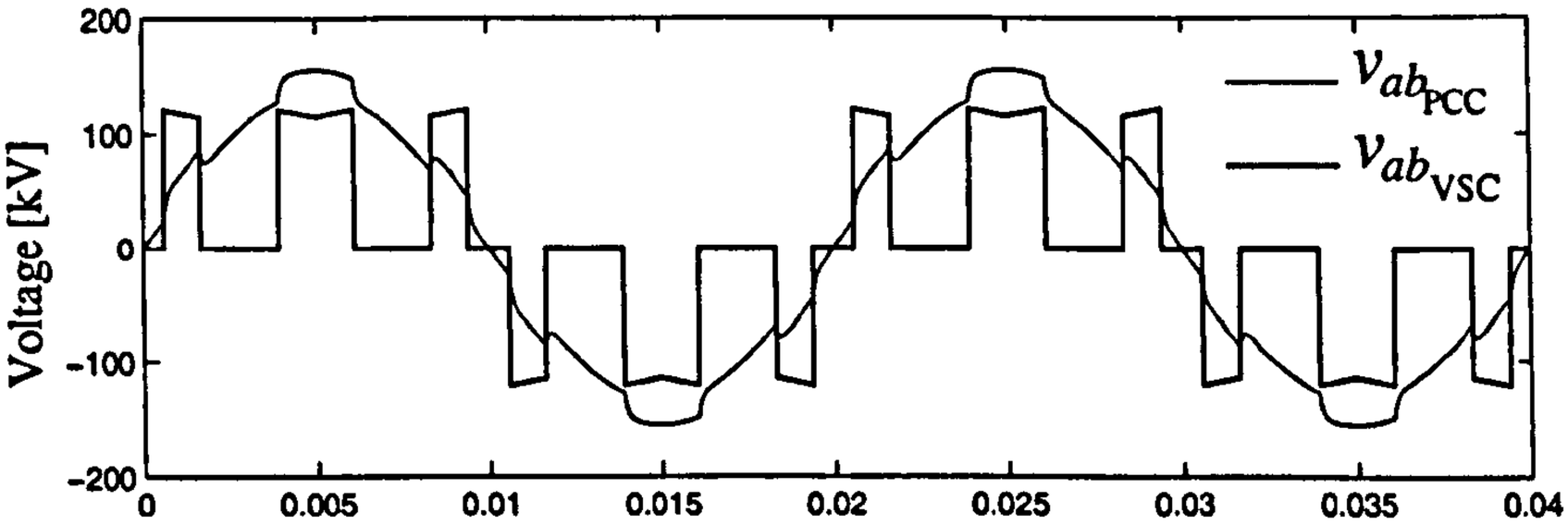

(b) PSCAD/EMTDC

Figure 3.3.: Line voltages in the PCC and in the VSC

Thévenin equivalent and voltage source. For both cases only the results for phase *a* are presented since balanced conditions were assumed to exist in this example. In the latter case, the effect of the capacitor is not explicitly represented, a fact that introduces modelling constraints and approximations. The numeric values of $v_s(t)$, $v_i(t)$, and current $i_s(t)$, given in Table 3.2 for both STATCOM representations, give a clear indication of the errors incurred when the simpler model is used. This calls for the STATCOM Thévenin impedance model to be adopted in harmonic studies. A sufficiently large number of harmonics are included, i.e. 49th, and THD values are also given. The voltage and current waveforms corresponding to this example are shown in Figure 3.4.

Supplying reactive power: Increasing the value of $v_{cap}(0^+)$ to 1.2 p.u. enables the STATCOM to supply reactive power equal to 0.7048 p.u. Table 3.3 shows similar information to that presented when the STATCOM absorbs reactive power but now for the case when the STATCOM supplies reactive power to the system. The corresponding voltage and current waveforms are shown in Figure 3.5.

By comparing Tables 3.2 and 3.3, it can seen that the STATCOM operating mode affects very significantly the harmonic magnitudes of voltage $v_s(t)$. When the capacitor effect is neglected the harmonic pattern is rather predictable but this is clearly not the case when the capacitor effect is explicitly taken into account. It is shown in Figure 3.4(a) that when the STATCOM

Table 3.2.: Harmonic content for the case when the STATCOM absorbs reactive power

h	$\lvert I_s\rvert$ with $\mathbf{Z}_{\mathrm{Th}}$	$\lvert V_s\rvert$ with $\mathbf{Z}_{\mathrm{Th}}$	$\lvert V_i\rvert$ with $\mathbf{Z}_{\mathrm{Th}}$	$\lvert I_s\rvert$ without $\mathbf{Z}_{\mathrm{Th}}$	$\lvert V_s\rvert$ without $\mathbf{Z}_{\mathrm{Th}}$	$\lvert V_i\rvert$ without $\mathbf{Z}_{\mathrm{Th}}$
1	100	100	100	100	100	100
5	8.1105	2.4970	12.2514	13.5361	4.0927	20.0000
7	10.9782	4.7317	23.2162	6.9062	2.9234	14.2857
11	2.9648	2.0081	9.8527	2.7967	1.8603	9.0909
13	2.7366	2.1905	10.7477	2.0024	1.5741	7.6923
17	1.3121	1.3734	6.7385	1.1709	1.2037	5.8824
19	1.2299	1.4388	7.0597	0.9374	1.0770	5.2632
23	0.7329	1.0378	5.0922	0.6397	0.8897	4.3478
25	0.6965	1.0722	5.2607	0.5414	0.8185	4.0000
29	0.4662	0.8325	4.0845	0.4024	0.7056	3.4483
31	0.4475	0.8541	4.1907	0.3521	0.6601	3.2258
35	0.3217	0.6932	3.4013	0.2762	0.5847	2.8571
37	0.3111	0.7087	3.4771	0.2472	0.5531	2.7027
41	0.2336	0.5897	2.8935	0.2013	0.4991	2.4390
43	0.2275	0.6025	2.9560	0.1830	0.4759	2.3256
47	0.1673	0.4841	2.3754	0.1532	0.4354	2.1277
49	0.1656	0.4997	2.4516	0.1409	0.4176	2.0408
THD	14.4089	6.8730	33.7224	15.6922	6.1422	30.0153

absorbs reactive power, the voltage waveforms at the terminals of the converter are formed of rounded sections, with the cusps pointing upside down, whereas when it generates reactive power, the cusps are more prominent and pointing upwards as shown in Figure 3.5(a). The voltage at the point of common coupling looks more sinusoidal but it still contains a large amount of harmonic distortion. The converter current is non-sinusoidal. In contrast, if the DC capacitor is not explicitly taken into account, and a DC voltage source is used instead, i.e. $\mathbf{Z}_{\mathrm{Th}} = 0$, the voltage at the terminals of the converter is given by a train of square pulses and the voltage at the point of common coupling will be largely sinusoidal, as shown in Figures 3.4(b) and 3.5(b).

3.3. STATCOM Impedance Analysis

The Thévenin equivalent of the STATCOM given by equation (3.3) may be re-written as

$$\mathbf{P}_s\mathbf{Z}_{\mathrm{cap}}\mathbf{Q}_s = \frac{1}{C}\begin{bmatrix} \mathbf{S}_{ab}\mathbf{D}^{-1}(\mathrm{j}h\omega_0)\mathbf{S}_{ab} & \mathbf{S}_{ab}\mathbf{D}^{-1}(\mathrm{j}h\omega_0)\mathbf{S}_{bc} & \mathbf{S}_{ab}\mathbf{D}^{-1}(\mathrm{j}h\omega_0)\mathbf{S}_{ca} \\ \mathbf{S}_{bc}\mathbf{D}^{-1}(\mathrm{j}h\omega_0)\mathbf{S}_{ab} & \mathbf{S}_{bc}\mathbf{D}^{-1}(\mathrm{j}h\omega_0)\mathbf{S}_{bc} & \mathbf{S}_{bc}\mathbf{D}^{-1}(\mathrm{j}h\omega_0)\mathbf{S}_{ca} \\ \mathbf{S}_{ca}\mathbf{D}^{-1}(\mathrm{j}h\omega_0)\mathbf{S}_{ab} & \mathbf{S}_{ca}\mathbf{D}^{-1}(\mathrm{j}h\omega_0)\mathbf{S}_{bc} & \mathbf{S}_{ca}\mathbf{D}^{-1}(\mathrm{j}h\omega_0)\mathbf{S}_{ca} \end{bmatrix}$$

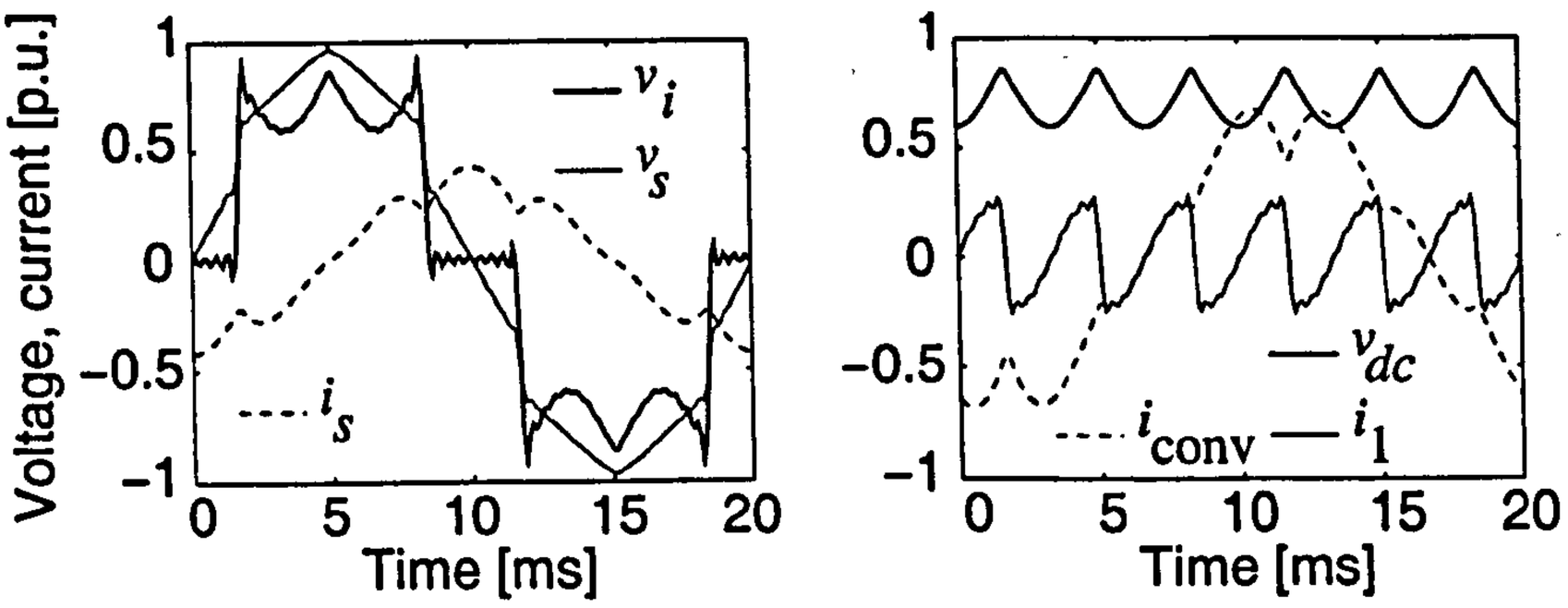

(a) Including the capacitor effect

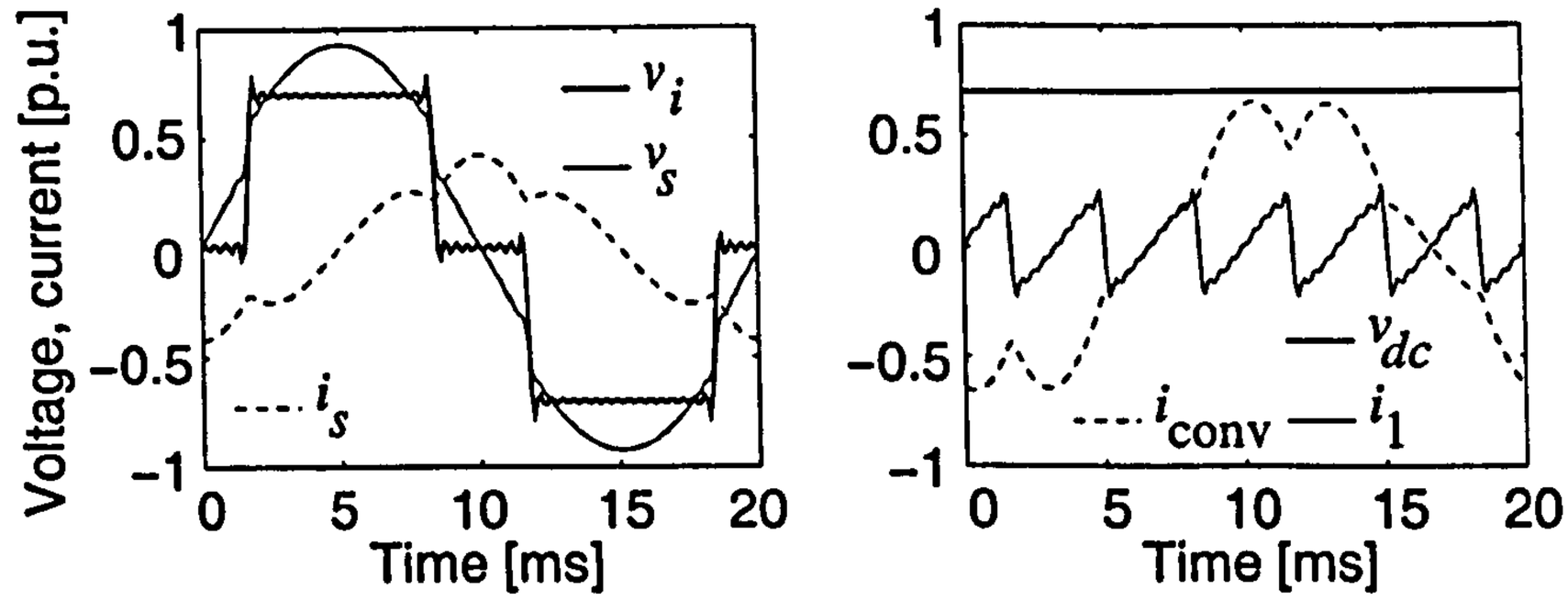

(b) Neglecting the capacitor effect

Figure 3.4.: Waveform results for the case when the STATCOM absorbs reactive power

$$= \begin{bmatrix} \mathbf{Z}_{aa} & \mathbf{Z}_{ab} & \mathbf{Z}_{ac} \\ \mathbf{Z}_{ba} & \mathbf{Z}_{bb} & \mathbf{Z}_{bc} \\ \mathbf{Z}_{ca} & \mathbf{Z}_{cb} & \mathbf{Z}_{cc} \end{bmatrix} \tag{3.5}$$

Since the structure of the transformation matrices and the differentiation matrix are known, with the help of some algebra it can be shown that the generic structure of any one of the nine submatrices, say $\mathbf{Z}_{s}$, for $h = 3$ is

$$\mathbf{Z}_{s} = \begin{bmatrix} Z_{-3,-3} & Z_{-3,-2} & Z_{-3,-1} & Z_{-3,0} & Z_{-3,1} & Z_{-3,2} & Z_{-3,3} \\ Z_{-2,-3} & Z_{-2,-2} & Z_{-2,-1} & Z_{-2,0} & Z_{-2,1} & Z_{-2,2} & Z_{-2,3} \\ Z_{-1,-3} & Z_{-1,0} & Z_{-1,-1} & Z_{-1,0} & Z_{-1,1} & Z_{-1,2} & Z_{-1,3} \\ Z_{0,-3} & Z_{0,-2} & Z_{0,-1} & Z_{0,0} & Z_{0,1} & Z_{0,2} & Z_{0,3} \\ Z_{1,-3} & Z_{1,-2} & Z_{1,-1} & Z_{1,0} & Z_{1,1} & Z_{1,2} & Z_{1,3} \\ Z_{2,-3} & Z_{2,-2} & Z_{2,-1} & Z_{2,0} & Z_{2,1} & Z_{2,2} & Z_{2,3} \\ Z_{3,-3} & Z_{3,-2} & Z_{3,-1} & Z_{3,0} & Z_{3,1} & Z_{3,2} & Z_{3,3} \end{bmatrix}$$

In turn, each element is given by

$$Z_{x,y} = \sum_{n=-h}^{h} \frac{1}{\mathrm{j}n\omega_0 C} S^{*}_{n-x} S_{n-y} \mathrm{e}^{-\mathrm{j}(n-y)\delta} \tag{3.6}$$

Table 3.3.: Harmonic content for the case when the STATCOM supplies reactive power

h	$\|I_s\|$ with $\mathbf{Z}_{\mathrm{Th}}$	$\|V_s\|$ with $\mathbf{Z}_{\mathrm{Th}}$	$\|V_i\|$ with $\mathbf{Z}_{\mathrm{Th}}$	$\|I_s\|$ without $\mathbf{Z}_{\mathrm{Th}}$	$\|V_s\|$ without $\mathbf{Z}_{\mathrm{Th}}$	$\|V_i\|$ without $\mathbf{Z}_{\mathrm{Th}}$
1	100	100	100	100	100	100
5	24.3781	9.3490	30.3995	16.3802	6.1214	20.000
7	1.3824	0.7422	2.4134	8.3573	4.3724	14.2857
11	3.0817	2.6000	2.6000	3.3844	2.7824	9.0909
13	1.0068	1.0038	3.2641	2.4231	2.3544	7.6923
17	1.1440	1.4916	4.8502	1.4170	1.8004	5.8824
19	0.5557	0.8098	2.6331	1.1344	1.6109	5.2632
23	0.5902	1.0412	3.3857	0.7741	1.3307	4.3478
25	0.3456	0.6627	2.1549	0.6552	1.2243	4.0000
29	0.3596	0.7998	2.6006	0.4869	1.0554	3.4483
31	0.2351	0.5590	1.8175	0.4261	0.9873	3.2258
35	0.2428	0.6519	2.1198	0.3343	0.8745	2.8571
37	0.1710	0.4852	1.5776	0.2991	0.8272	2.7027
41	0.1776	0.5585	1.8159	0.2436	0.7465	2.4390
43	0.1322	0.4361	1.4182	0.2215	0.7118	2.3256
47	0.1500	0.5409	1.7587	0.1854	0.6512	2.1277
49	0.1197	0.4498	1.4626	0.1706	0.6246	2.0408
THD	24.6811	10.1359	32.9581	18.9893	9.1867	30.0153

for $x, y = -h, \ldots, h$, and

$$\begin{aligned} \delta = 0 \quad & \text{for matrices } \mathbf{Z}_{aa}, \mathbf{Z}_{bb} \text{ and } \mathbf{Z}_{cc} \\ \delta = 2\pi/3 \quad & \text{for matrices } \mathbf{Z}_{ab} \text{ and } \mathbf{Z}_{bc} \\ \delta = -2\pi/3 \quad & \text{for matrix } \mathbf{Z}_{ac} \end{aligned}$$

S_s are the harmonics of the switching function $s_{ab}(t)$. Since $\mathbf{Z}_{\mathrm{Th}}$ is a Skew Hermitian matrix, the rest of the submatrices are obtained by:

$$\begin{aligned} \mathbf{Z}_{ba} &= -\mathbf{Z}_{ab}^{*} \\ \mathbf{Z}_{cb} &= -\mathbf{Z}_{bc}^{*} \\ \mathbf{Z}_{ca} &= -\mathbf{Z}_{ac}^{*} \end{aligned}$$

3.3.1. Impedance structure of $\mathbf{Z}_{\mathrm{Th}}$

The structure of $\mathbf{Z}_{\mathrm{Th}}$ depends on the switching function which represent the VSC. For example, Figure 3.6 shows the structure of $\mathbf{Z}_{\mathrm{Th}}$ for the case when the switching functions have a conduction period of 120°. The matrix structure shows that the STATCOM impedance has a very

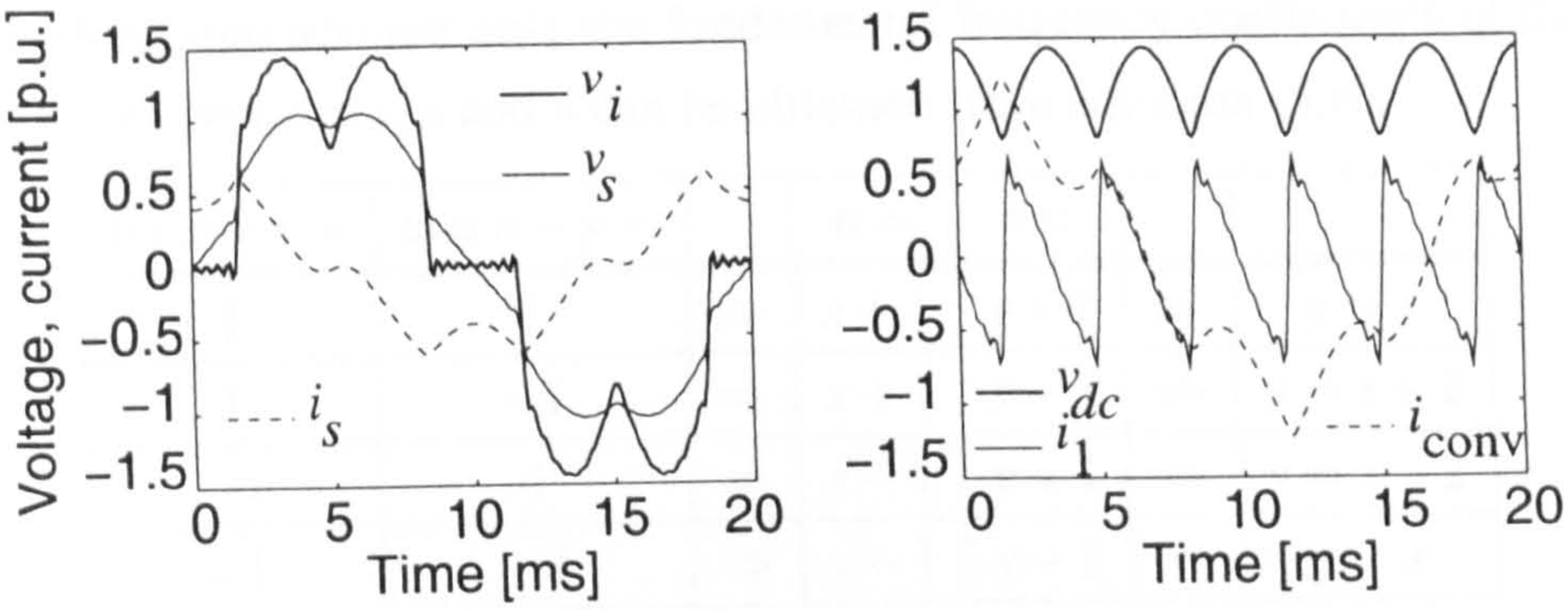

(a) Including the capacitor effect

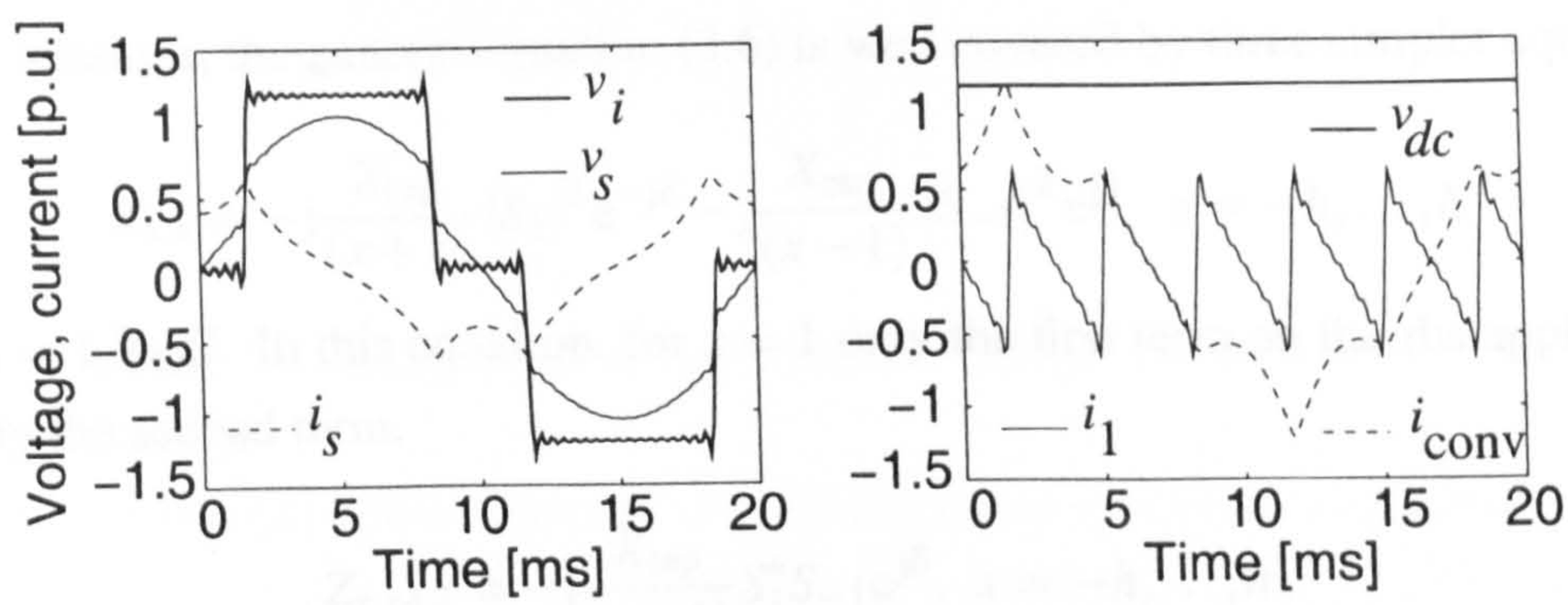

(b) Neglecting the capacitor effect

Figure 3.5.: Waveform results for the case when the STATCOM supplies reactive power

strong inter-coupling between phases and between harmonics.

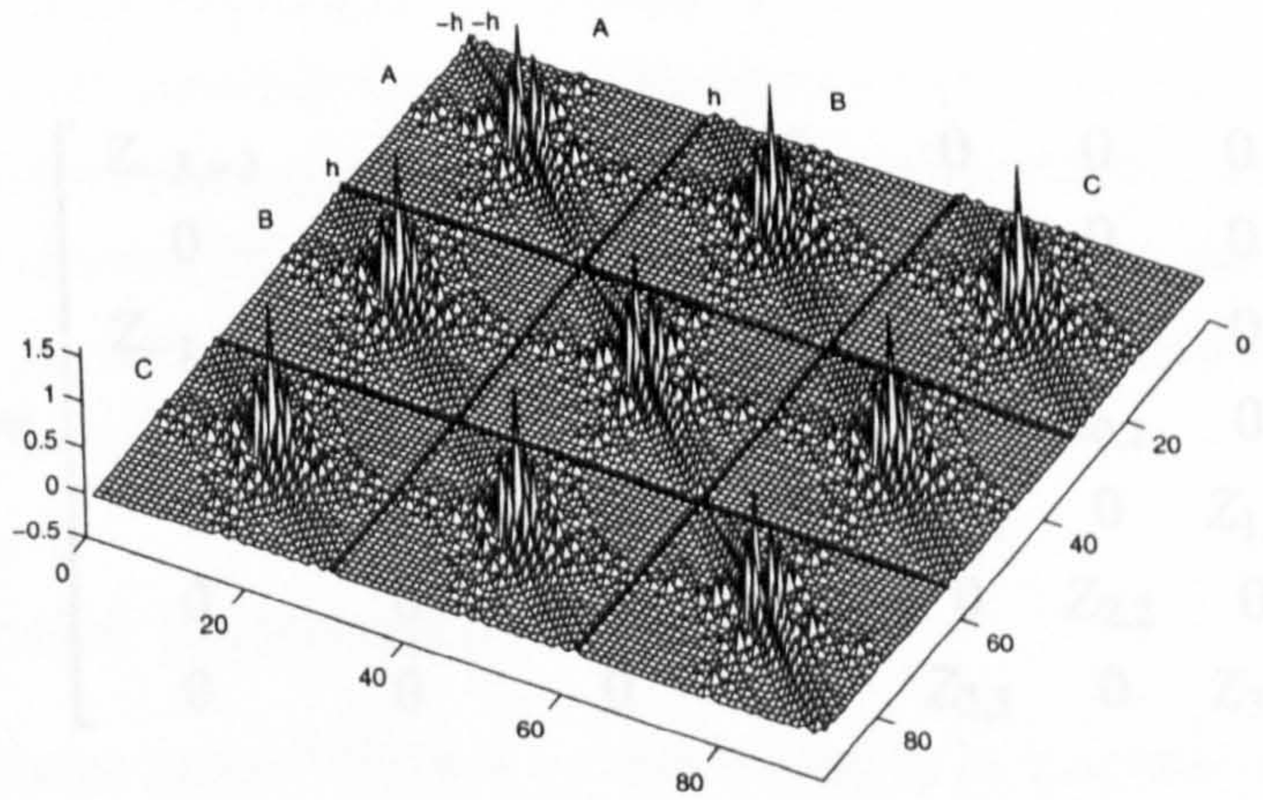

Figure 3.6.: Magnitude of $\mathbf{Z}_{\mathrm{Th}}$, for $h = 15$, $C = 1000\,\mu\mathrm{F}$ and conduction period of 120°

A very desirable condition of STATCOM operation is when the VSC does not generate significant harmonics, which may be achieved by using a very high PWM switching frequency. Assuming that this is the case and analysing equation (3.6), it may be said that the element $Z_{x,y}$ is made up mainly of the fundamental frequency of the switching functions, i.e. $S_{n-x}, S_{n-y} =$

$S_{\pm 1}$. Hence, taking into account only the fundamental frequency coefficients of the switching functions, relations between y, x and n can be obtained from equation (3.6):

for $n-x=$	and $n-y=$		$n=$	$n=$		
1	1	$\Rightarrow$	$x+1$	$y+1$	$\Rightarrow$	$y=x$
1	-1	$\Rightarrow$	$x+1$	$y-1$	$\Rightarrow$	$y=x+2$
-1	1	$\Rightarrow$	$x-1$	$y+1$	$\Rightarrow$	$y=x-2$
-1	-1	$\Rightarrow$	$x-1$	$y-1$	$\Rightarrow$	$y=x$

The elements different from zero according to the table are: $Z_{x,x}$ and $Z_{x,x\pm 2}$ for $x=-h,\ldots,h$.

Using such relations, the general equation (3.6) is well covered by three simpler equations:

$$Z_{x,x} = -\mathrm{j}\frac{X_{\mathrm{cap}}}{(x+1)}|S_1|^2\mathrm{e}^{-\mathrm{j}\delta} - \mathrm{j}\frac{X_{\mathrm{cap}}}{(x-1)}|S_{-1}|^2\mathrm{e}^{\mathrm{j}\delta},\ x=-h,\ldots,h \tag{3.7}$$

where $X_{\mathrm{cap}} = 1/\omega_0 C$. In this equation, for $x=1$ only the first term on the rhs applies, and for $x=-1$ only the second term.

$$Z_{x,x+2} = -\mathrm{j}\frac{X_{\mathrm{cap}}}{(x+1)}S_1^* S_{-1}\mathrm{e}^{\mathrm{j}\delta},\ x=-h,\ldots,h \tag{3.8}$$

For $x=-1$, $Z_{-1,1}$ is neglected since no contribution from $S_{\pm 1}$ exists.

$$Z_{x,x-2} = -\mathrm{j}\frac{X_{\mathrm{cap}}}{(x-1)}S_{-1}^* S_1\mathrm{e}^{-\mathrm{j}\delta},\ x=-h,\ldots,h \tag{3.9}$$

For $x=1$, $Z_{1,-1}$ is neglected since no contribution from $S_{\pm 1}$ exists.

The remaining elements are all zero resulting in a matrix $\mathbf{Z}_s'$ with the following banded structure,

$$\mathbf{Z}_s' = \begin{bmatrix} Z_{-3,-3} & 0 & Z_{-3,-1} & 0 & 0 & 0 & 0 \\ 0 & Z_{-2,-2} & 0 & Z_{-2,0} & 0 & 0 & 0 \\ Z_{-1,-3} & 0 & Z_{-1,-1} & 0 & 0 & 0 & 0 \\ 0 & Z_{0,-2} & 0 & Z_{0,0} & 0 & Z_{0,2} & 0 \\ 0 & 0 & 0 & 0 & Z_{1,1} & 0 & Z_{1,3} \\ 0 & 0 & 0 & Z_{2,0} & 0 & Z_{2,2} & 0 \\ 0 & 0 & 0 & 0 & Z_{3,1} & 0 & Z_{3,3} \end{bmatrix}$$

Figure 3.7 shows the structure of $\mathbf{Z}_{\mathrm{Th}}$ when using a high switching frequency for the PWM. The structure shows that the dominant impedances are given by the harmonic impedances $Z_{x,x}$ and $Z_{x,x\pm 2}$ as previously demonstrated by analysis.

The impedance structure of the STATCOM shows that even under very high PWM switching frequency operation, resonance problems may still occur due to the coupling between harmonics. For example, the fundamental frequency has a coupling to the 3rd harmonic, the 5th harmonic has a coupling to the 3rd and the 7th harmonics and so on. This effect is similar to

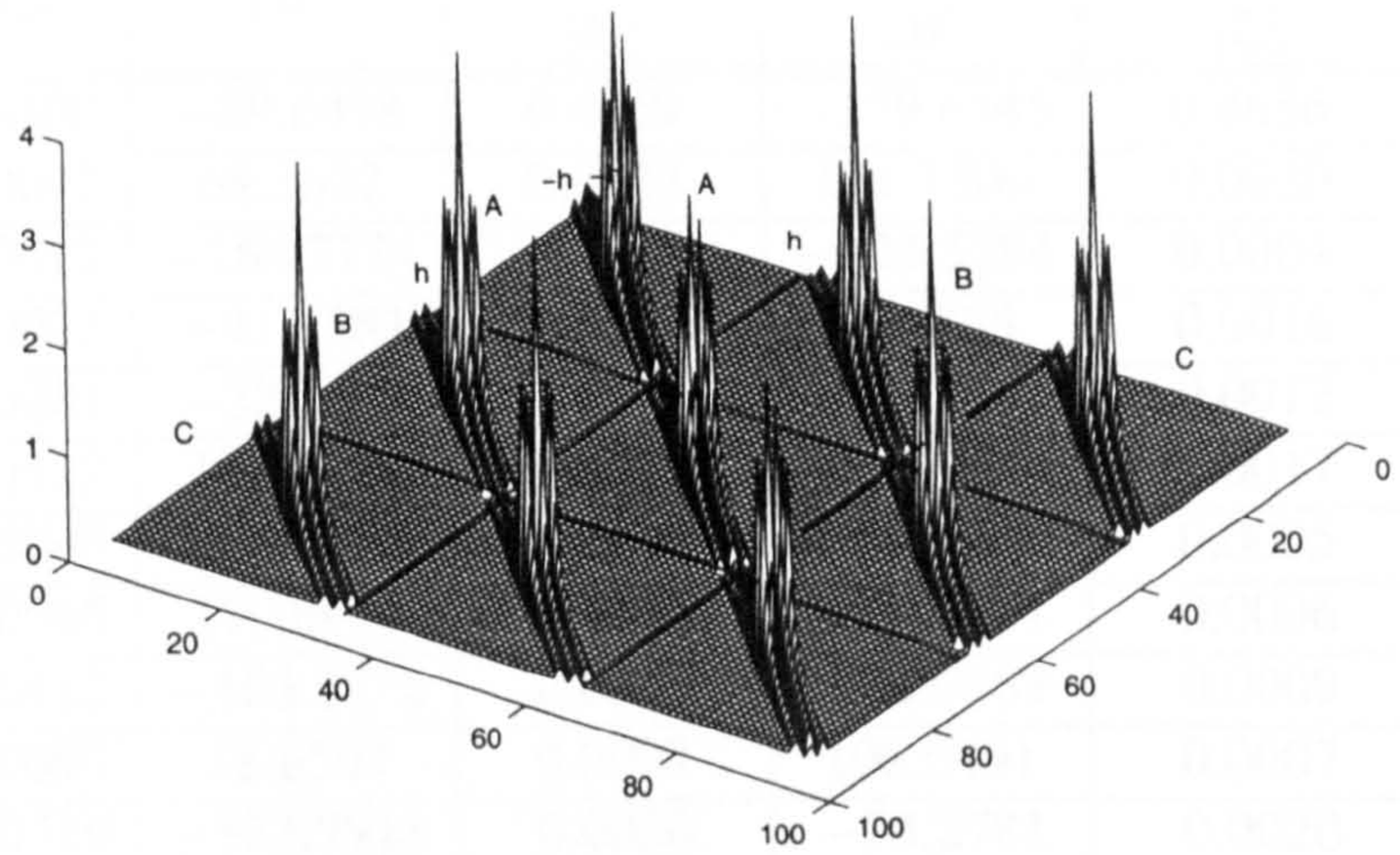

Figure 3.7.: Magnitude of $\mathbf{Z}_{\mathrm{Th}}$ with $C = 300\,\mu\mathrm{F}$ and $f_r = 1650$ Hz

the frequency conversion effect observed in the three-phase synchronous generator [43][13].

Comparison example: The STATCOM model (simplified) with $\mathbf{Z}_{\mathrm{Th}}$ calculated from (3.7)–(3.9) was compared with the the model (complete) from (3.3). The system data is as follows: $|V_r| = 1$ p.u., $R = 0.0033\,\Omega$, $X = 0.1571\,\Omega$, $R_{\mathrm{e}} = 0.01\,\Omega$ and $X_{\mathrm{e}} = 0.4712\,\Omega$ at 50 Hz. $C = 500\,\mu\mathrm{F}$ charged at 0.8316 p.u. A six-level VSC (as shown in Figure A.3), 250 Hz switching frequency, and modulation factor of 0.85 were used. The results are obtained for 50 harmonics.

Table 3.4 shows the harmonic content of the switching function used in the VSC. It can be seen that the dominant magnitude corresponds to the fundamental frequency component. The same table shows the harmonic content of the current $i_a(t)$ obtained with both STATCOM models. The results show a very good agreement even at high harmonic frequencies. Figure 3.8 shows the waveform representation of these currents. It should be remarked that the accuracy of the simplified model depends on the fundamental frequency magnitude dominant over the other harmonics of the switching function.

3.3.2. Driving point impedance of the VSC

An equivalent impedance of the VSC can be used to assess its response to a harmonic current injection coming from the AC network. To this end a driving point impedance (DPI) analysis of the VSC may be carried out as follows.

We have that the voltage response of the VSC is given by

$$\begin{bmatrix} \mathbf{V}_a \\ \mathbf{V}_b \\ \mathbf{V}_c \end{bmatrix} = \begin{bmatrix} \mathbf{Z}_{aa} & \mathbf{Z}_{ab} & \mathbf{Z}_{ac} \\ \mathbf{Z}_{ba} & \mathbf{Z}_{bb} & \mathbf{Z}_{bc} \\ \mathbf{Z}_{ca} & \mathbf{Z}_{cb} & \mathbf{Z}_{cc} \end{bmatrix} \begin{bmatrix} \mathbf{I}_a \\ \mathbf{I}_b \\ \mathbf{I}_c \end{bmatrix}$$

Table 3.4.: Harmonic contents

harmonic	$\|S_{ab}\|$	$\angle\theta°$	complete $\|I_a\|$	complete $\angle\theta°$	simplified $\|I_a\|$	simplified $\angle\theta°$
1	0.8500	−89.6438	0.4669	−179.6445	0.4656	−179.3178
3	0.0047	68.3672	0.0022	161.1300	0.0020	159.4594
5	0.0013	−164.7784	0.0015	−123.5294	0.0004	−74.4280
7	0.0073	−41.7583	0.0023	46.8875	0.0016	48.4089
9	0.0081	−32.5393	0.0012	55.1164	0.0012	57.5956
11	0.0132	131.9859	0.0012	−137.9061	0.0017	−137.8892
13	0.0049	125.7716	0.0008	−144.0297	0.0005	−144.1399
15	0.0065	170.8931	0.0006	−97.5704	0.0006	−99.0260
17	0.0112	−163.3272	0.0009	−73.9662	0.0009	−73.2504
19	0.0097	18.8567	0.0007	108.0491	0.0007	108.9179
21	0.0319	−123.9918	0.0020	−33.2781	0.0020	−33.9340
23	0.0614	−110.3304	0.0030	−20.7931	0.0036	−20.2749
25	0.0356	−105.3745	0.0024	−15.6424	0.0019	−15.3277
27	0.0642	67.6230	0.0031	157.9000	0.0031	157.6679
29	0.0462	−113.7978	0.0022	−22.6716	0.0021	−23.7543
31	0.0531	73.9026	0.0023	163.7992	0.0023	163.9406
33	0.0600	−111.3287	0.0024	−21.5271	0.0024	−21.2919
35	0.0337	61.9847	0.0010	150.7672	0.0013	152.0205
37	0.0739	70.6262	0.0029	160.6986	0.0027	160.6582
39	0.0237	51.6316	0.0008	140.2493	0.0008	141.6627
41	0.0125	66.9041	0.0004	157.9213	0.0004	156.9345
43	0.0026	56.0855	0.0001	151.4458	0.0001	146.1131
45	0.0310	47.0059	0.0009	137.8344	0.0009	137.0328
47	0.0231	36.4124	0.0006	126.6746	0.0007	126.4388
49	0.0123	−97.3687	0.0003	−4.2574	0.0003	−7.3444

Assuming the VSC to be a balanced system, then the study may be reduced to the analysis of phase a, i.e.

$$\mathbf{V}_a = \mathbf{Z}_{aa}\mathbf{I}_a + \mathbf{Z}_{ab}\mathbf{I}_b + \mathbf{Z}_{ac}\mathbf{I}_c$$

If a 1 p.u. balanced h_i harmonic current source is injected into the VSC, i.e.

$$\begin{aligned} I_{a\_h_i} &= \tfrac{1}{2} \quad I_{b\_h_i} = \tfrac{1}{2}e^{jh_i 2\pi/3} \quad I_{c\_h_i} = \tfrac{1}{2}e^{-jh_i 2\pi/3} \\ I_{a_{h_i}} &= \tfrac{1}{2} \quad I_{b_{h_i}} = \tfrac{1}{2}e^{-jh_i 2\pi/3} \quad I_{c_{h_i}} = \tfrac{1}{2}e^{jh_i 2\pi/3} \end{aligned} \tag{3.10}$$

then the $\pm m$ harmonic voltage produced by this current is given by

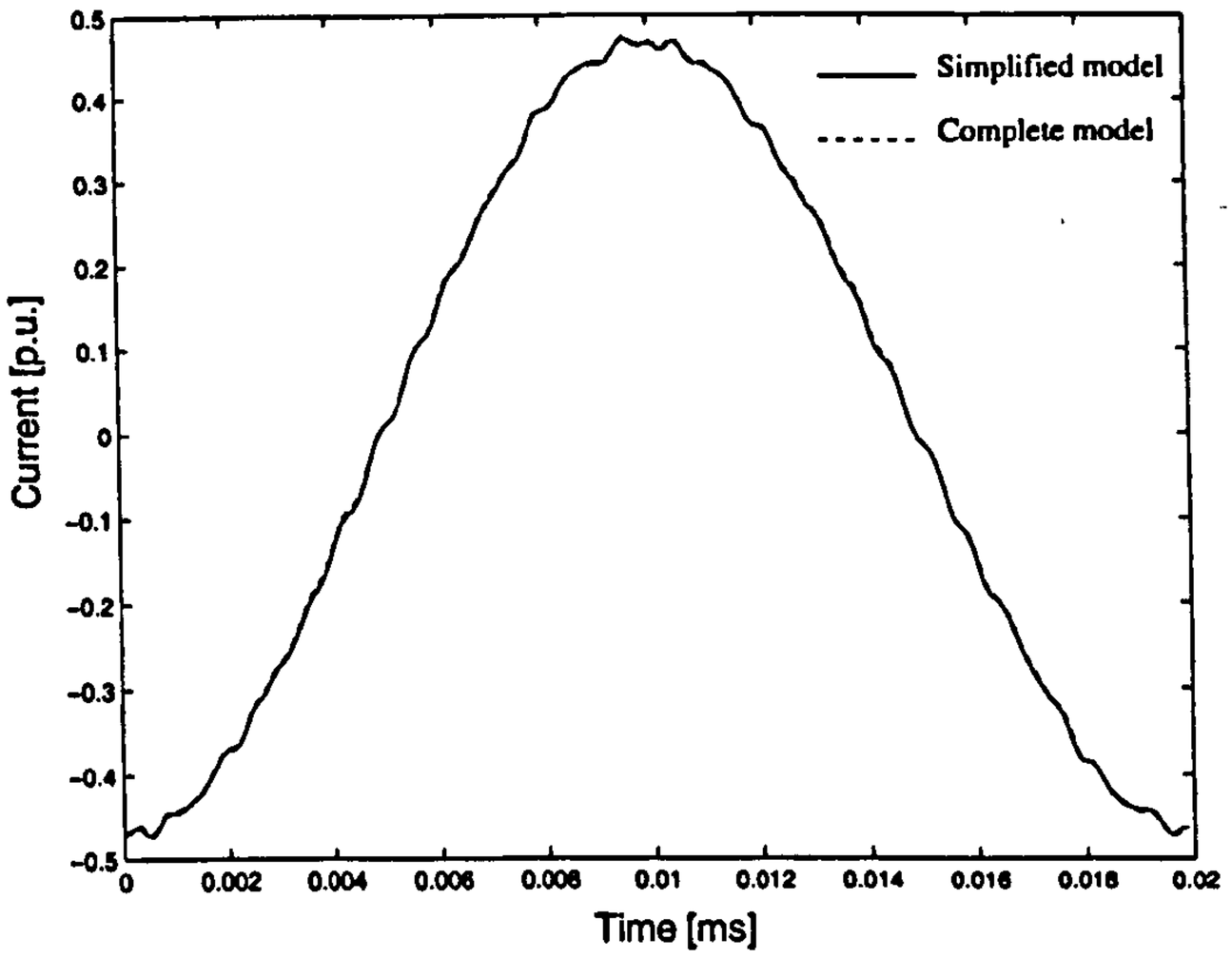

Figure 3.8.: Waveform results for the current $i_a(t)$

$$\begin{aligned} V_{a_{-m}} &= Z_{aa_{-m,-h_i}} I_{a_{-h_i}} + Z_{aa_{-m,h_i}} I_{a_{h_i}} + Z_{ab_{-m,-h_i}} I_{b_{-h_i}} + Z_{ab_{-m,h_i}} I_{b_{h_i}} \\ &\quad + Z_{ac_{-m,-h_i}} I_{c_{-h_i}} + Z_{ac_{-m,h_i}} I_{c_{h_i}} \end{aligned} \tag{3.11}$$

$$\begin{aligned} V_{a_m} &= Z_{aa_{m,-h_i}} I_{a_{-h_i}} + Z_{aa_{m,h_i}} I_{a_{h_i}} + Z_{ab_{m,-h_i}} I_{b_{-h_i}} + Z_{ab_{m,h_i}} I_{b_{h_i}} \\ &\quad + Z_{ac_{m,-h_i}} I_{c_{-h_i}} + Z_{ac_{m,h_i}} I_{c_{h_i}} \end{aligned} \tag{3.12}$$

Since $V_{a_{-m}} = V_{a_m}^*$, it is enough to calculate V_{a_m}.

From (3.6) we have that

$$Z_{aa_{m,-h_i}} = \sum_{n=-h}^{h} \frac{1}{\mathrm{j}n\omega_0 C} S_{n-m}^* S_{n+h_i}$$

$$Z_{aa_{m,h_i}} = \sum_{n=-h}^{h} \frac{1}{\mathrm{j}n\omega_0 C} S_{n-m}^* S_{n-h_i}$$

$$Z_{ab_{m,-h_i}} = \sum_{n=-h}^{h} \frac{1}{\mathrm{j}n\omega_0 C} S_{n-m}^* S_{n+h_i} \mathrm{e}^{-\mathrm{j}(n+h_i)2\pi/3}$$

$$Z_{ab_{m,h_i}} = \sum_{n=-h}^{h} \frac{1}{\mathrm{j}n\omega_0 C} S_{n-m}^* S_{n-h_i} \mathrm{e}^{-\mathrm{j}(n-h_i)2\pi/3}$$

$$Z_{ac_{m,-h_i}} = \sum_{n=-h}^{h} \frac{1}{\mathrm{j}n\omega_0 C} S_{n-m}^* S_{n+h_i} \mathrm{e}^{\mathrm{j}(n+h_i)2\pi/3}$$

$$Z_{ac_{m,h_i}} = \sum_{n=-h}^{h} \frac{1}{\mathrm{j}n\omega_0 C} S_{n-m}^* S_{n-h_i} \mathrm{e}^{\mathrm{j}(n-h_i)2\pi/3}$$

and using (3.10) in (3.12), V_{a_m} becomes

$$V_{a_m} = \frac{1}{j\omega_0 C} \sum_{n=-h}^{h} \frac{1}{n} S^*_{n-m} \left(S_{n+h_i} + S_{n-h_i}\right) \left(1/2 + \cos 2n\pi/3\right) \tag{3.13}$$

The impedance which produces the m-th harmonic voltage due to the h_i-th harmonic current is given by $Z_{m,h_i} = V_{a_m}/I_{a_{h_i}} = 2V_{a_m}$. Hence,

$$Z_{m,h_i} = \frac{1}{j\omega_0 C} \sum_{n=-h}^{h} \frac{1}{n} S^*_{n-m} \left(S_{n+h_i} + S_{n-h_i}\right) \left(1 + 2\cos 2n\pi/3\right) \tag{3.14}$$

Equation (3.14) gives the DPI of the VSC, which corresponds to a given harmonic current injected into the VSC.

For a high switching frequency, equation (3.14) can be reduced to the impedances $Z_{h_i \pm 2, h_i}$ and Z_{h_i,h_i}. Impedance Z_{h_i,h_i} is given by

$$Z_{h_i,h_i} = \frac{2|S_1|^2}{j\left(h_i^2 - 1\right)\omega_0 C} \left(h_i - h_i \cos 2h_i\pi/3 + \sqrt{3}\sin 2h_i\pi/3\right), \quad h_i > 1 \tag{3.15}$$

where Z_{h_i,h_i} is zero for $h_i = 3, 6, 9, \ldots$.

Moreover, equation (3.15) can be used to represent the STATCOM for resonance prediction analysis as follows

$$Z_{\text{STATCOM}}(h_i) = jh_i X_e + 2Z_{h_i,h_i} \tag{3.16}$$

where X_e is the impedance of the coupling transformer.

3.3.3. Case study: Resonance analysis

The analysis of resonances in the STATCOM is carried out with a STATCOM connected to a balance three-phase voltage source of 1 p.u. The coupling transformer is represented by an impedance $X_e = j1.0$ p.u. The VSC is selected to produce an almost sinusoidal voltage at the output by using a multi-module PWM converter (Appendix A), with 5 converters per phase. The switching frequency is 450 Hz, and the modulation factor is 0.9.

The simulations were carried out with 25 harmonics and different values of the capacitance, $1 - 150\,\mu$F at steps of $1\,\mu$F, and maintaining the DC voltage at 1 p.u. The results and analysis are shown below.

Figure 3.9 shows the THD in the STATCOM for different values of the capacitor. The results show resonance points for the following capacitor values: $7\,\mu$F, $12\,\mu$F, $27\,\mu$F and $110\,\mu$F. Figure 3.10 shows that these resonant points are related to given harmonics which are summarised as follows:

$7\,\mu$F: 23th, 25th

12 μF: 17th, 19th

27 μF: 11th, 13th and

110 μF: 5th, 7th.

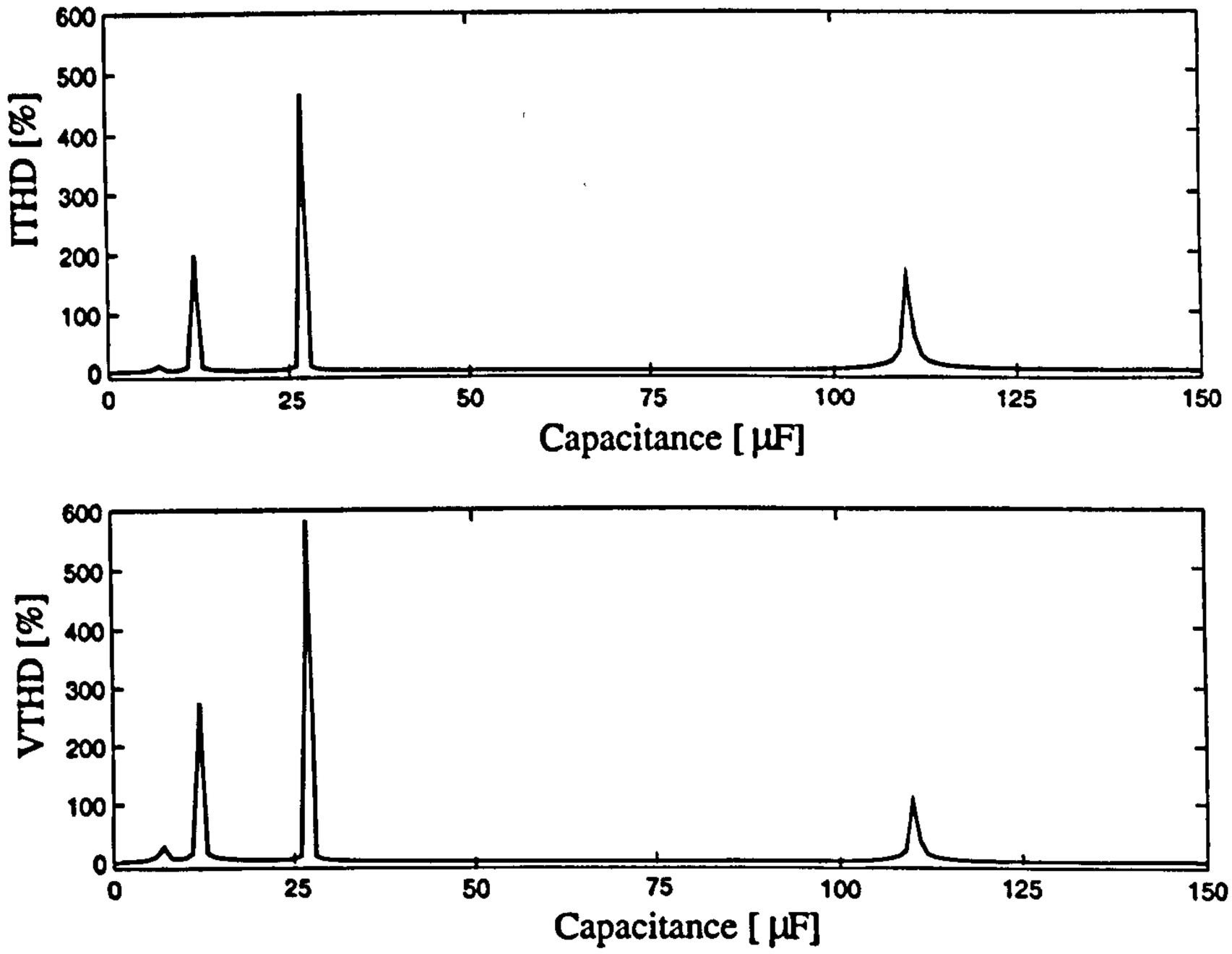

Figure 3.9.: THD at the point of coupling between the transformer and the VSC

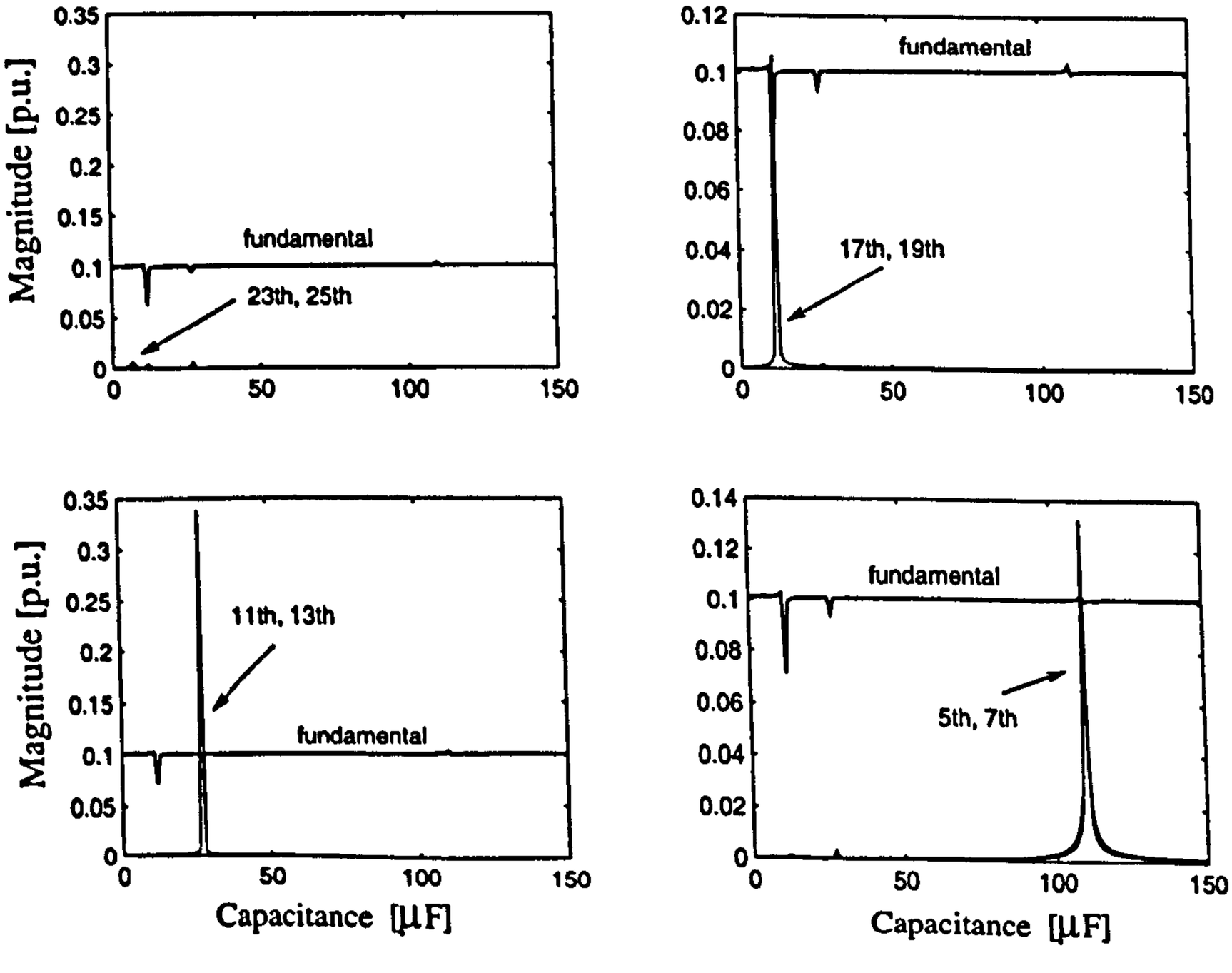

Figure 3.10.: Magnitude of the current harmonics in the STATCOM

Figure 3.11 shows the phase a of the STATCOM impedance and STATCOM admittance matrix structures (contours) for two values of the capacitor, $12\,\mu$F and $50\,\mu$F. The impedance structures look quite similar for both values of capacitors, but the admittance structures do not. Analysing the admittance structure for $12\,\mu$F, it can be seen that harmonic cross-couplings of the fundamental frequency with the 17th and 19th harmonic do exist. This suggests that resonant peaks at the 17th and 19th harmonic may be excited by the voltage source at fundamental frequency. This resonance prediction confirms the previous results.

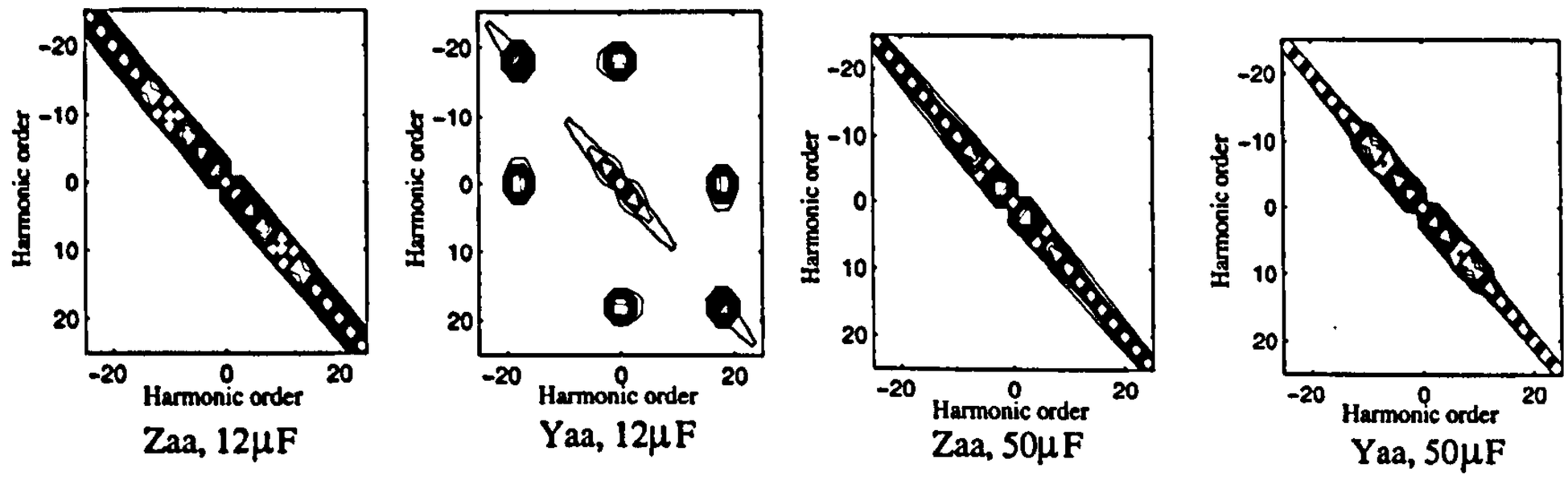

Figure 3.11.: Top view of the impedances and admittances of the STATCOM's phase a

Equation (3.16) may be used to predict the resonance frequencies for different values of the capacitor. This prediction is shown in Figure 3.12, where only odd harmonics are show. In this figure there are four points where $2Z_{h_i,h_i}$ presents the same impedance that $h_i X_e$ meaning a series resonance. Particularly, these points are: 1) resonance with the 23th and 25th harmonic for $C = 7\,\mu$F, 2) resonance with the 17th and 19th harmonic for $C = 12\,\mu$F, 3) resonance with the 11th and 13th harmonic for $C = 27\,\mu$F, 4) resonance with the 5th and 7th harmonic for $C = 110\,\mu$F. These resonance points correspond to the previous values obtained from simulation results.

3.4. Conclusions

In this chapter a steady-state model for the STATCOM in HD was developed by resorting to the VSC model presented in Chapter 2. The response of the STATCOM model is in very good agreement with the results obtained from the PSCAD/EMTDC time domain-based software. The results shown that for harmonic analysis, an implicit representation of the capacitor in the STATCOM model should be used instead of the more contrived harmonic voltage source model proposed elsewhere.

It has been shown that the equivalent impedance of the STATCOM presents high harmonic cross-couplings. Also, analytical equations have been developed to show that the harmonic cross-coupling in the STATCOM impedance obey an intrinsic frequency conversion effects present in the VSC even for cases of very high PWM switching frequencies.

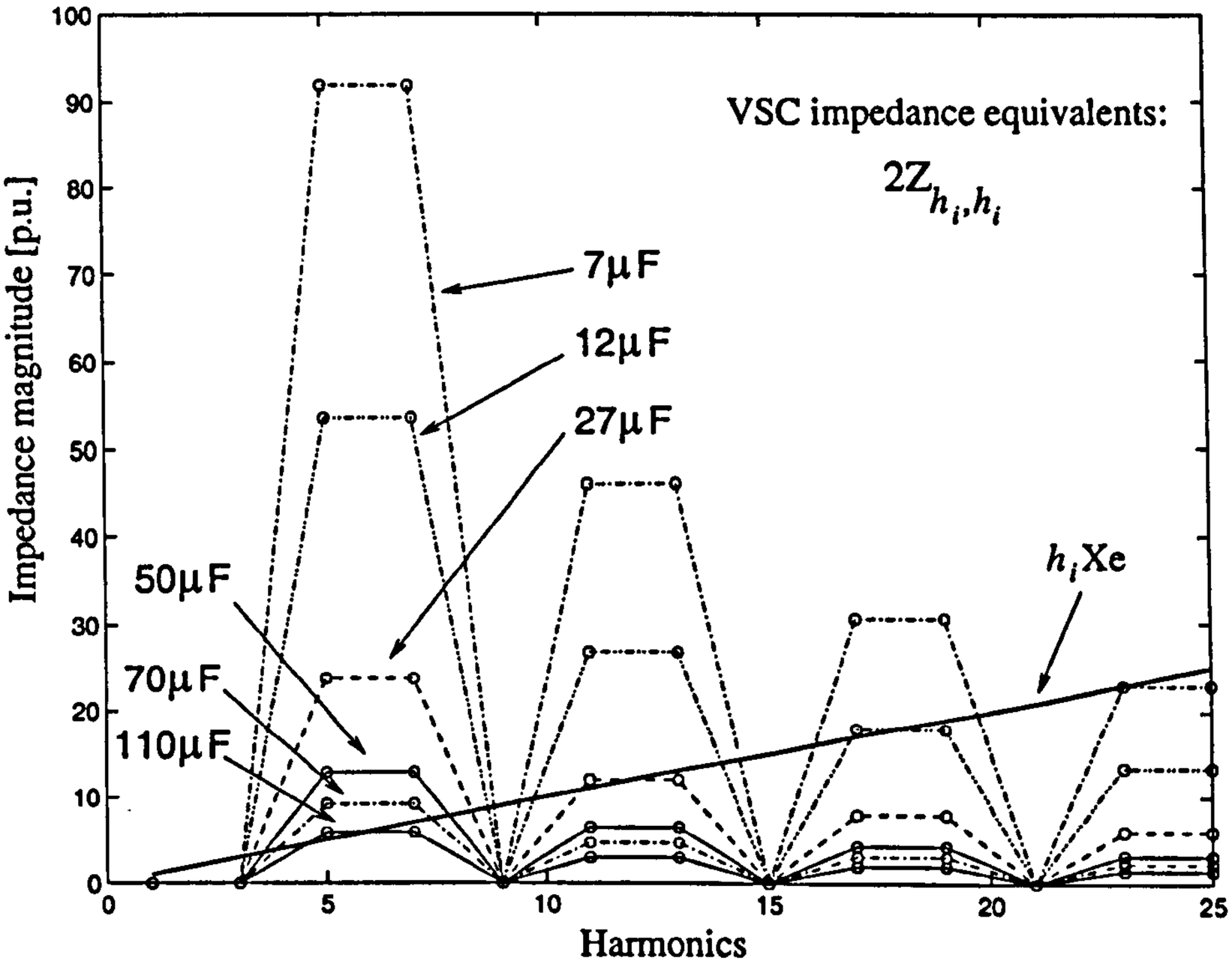

Figure 3.12.: Driving point impedance of the VSC and the impedance of the coupling transformer

A simple and comprehensive equation which represent the DPI of the VSC was also obtained, this equation may be used to predict series resonances between the VSC and the rest of the system.

4. HVDC-VSC Stations

4.1. Introduction

In this chapter, new harmonic domain models for HVDC stations based on voltage source converter (VSC) technology are presented. The models are derived in the harmonic domain, and represented by an equivalent harmonic impedance. The HVDC-VSC station models are for the HVDC-VSC back-to-back and the HVDC-VSC transmission system. The modelling philosophy follows a modular approach, which is based on the connection of two VSCs sharing a common DC link. The harmonic models are comprehensive and include cross-coupling between harmonics, capacitor effect, DC voltage ripple, exact cable model, and unbalanced conditions in both the converters and the AC system. These models are suitable for harmonic propagation, resonance analysis, and analysis at fundamental frequency. The HVDC-VSC harmonic models presented in this chapter are based on the very practical assumption that one VSC operates as a "master DC voltage regulator" and the other VSC operates as a "power dispatcher".

Results obtained with the proposed models show a very good agreament with those obtained using PSCAD/EMTDC simulations. Also, a resonance analysis in the HVDC-VSC transmission system is presented in this chapter.

4.2. HVDC-VSC Technology

Rapid development in the field of power electronics devices with turn off capability such as GTO and IGBT, makes VSCs more and more attractive for HVDC transmission systems. This innovative technology provides substantial technical and economical advantages for different applications compared to conventional HVDC transmission systems based on thyristor technology [31][32].

The HVDC stations based on VSC can be found under the names of HVDC Light (ABB product) or HVDC Plus (Power link universal systems, Siemens product). In this thesis it is named HVDC-VSC. The HVDC-VSC has a power rating in the range 7–600 MW and DC voltage in the range 10–141 kV. In contrast, conventional HVDC systems are available in the power range 100–3000 MW and DC voltages up to 600 kV.

HVDC-VSC is a very recent HVDC technology [88][89]. The HVDC-VSC stations use IGBTs and operate with a high PWM switching frequency in order to have fast control of both active and reactive power. It is reported that on 10th March 1997 power was transmitted on the world's first HVDC-VSC transmission system between Hellsjön and Grängerg in central Sweden. The Gotland HVDC-VSC, rated at 50 MW, links a wind power park on the southern tip of the Swedish island of Gotland to the city of Visby some 70 km away. The station transmits at ±80 kV using underground cables and it runs in parallel with an existing AC line. An HVDC-VSC transmission system rated at 180 MVA, ±80 kV and 65 km underground cables, was commissioned to connect the Queensland and New South Wales grids between Terranora and Mullumbimby in Australia. Also, an HVDC-VSC back-to-back tie was installed at the Eagle Pass substation in Texas, and features a 36 MW HVDC back-to-back converter connected to an existing 138 kV AC overhead line between the USA and Piedras Negras, Mexico [35].

The vendors of this technology argue that HVDC-VSC stations make it economically feasible to connect small-scale, renewable power generation plants to the main AC grid. Similarly, remote locations such as islands, mining districts, and drilling platforms can be supplied with power from the main grid via a HVDC-VSC station, thereby eliminating the need for inefficient, polluting, local generation such as diesel units. The voltage, frequency, and active and reactive power can be controlled precisely and independently from each other.

Thus far, most of the available literature on HVDC-VSC stations relates to the all-important issues of operation, construction and commissioning. Theoretical studies of PWM control schemes and bridge topology have also received attention [90][91][92]. The following applications of HVDC-VSC stations are discussed in [35]:

- Systems interconnection using an HVDC-VSC back-to-back tie.
- Grid-connection of offshore wind farms.
- Grid-connection of otherwise autonomous systems such as islands and oil platforms.
- City centre infeed.

Two HVDC-VSC configurations are researched in this thesis from the mathematical modelling viewpoint. These configurations are the HVDC-VSC back-to-back tie and HVDC-VSC transmission system.

4.3. HVDC-VSC Back-to-back Model

In its most basic form, the HVDC-VSC back-to-back comprises two equal VSCs which share a common capacitor on the DC side. From the modelling viewpoint, the HVDC-VSC back-to-back can be represented as shown in Figure 4.1.

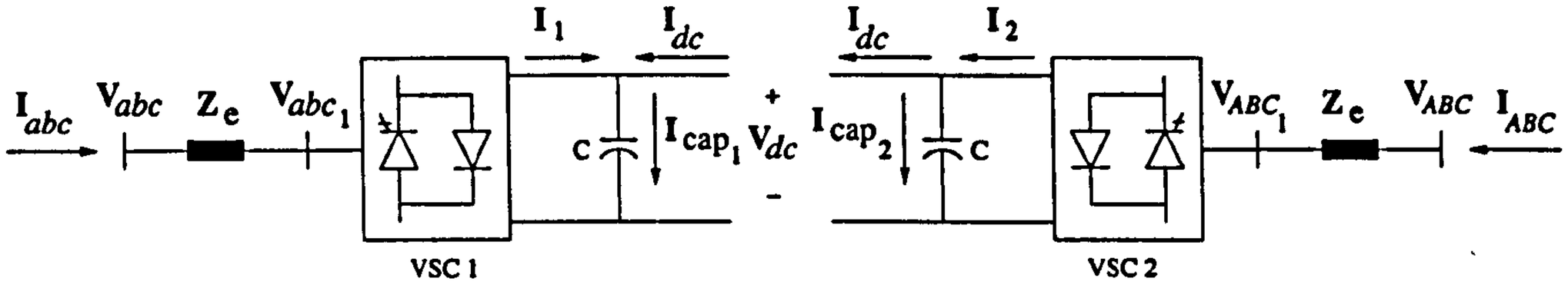

Figure 4.1.: HVDC-VSC back-to-back

The model of the HVDC-VSC back-to-back, using the result in equation (2.34), may be obtained as follows:

For VSC 1:

$$\begin{bmatrix} \mathbf{V}_{abc_T} \\ \mathbf{V}_{dc_T} \end{bmatrix} = \begin{bmatrix} \mathbf{A}_1 & \mathbf{B}_1 \\ \mathbf{C}_1 & \mathbf{D}_1 \end{bmatrix} \begin{bmatrix} \mathbf{I}_{abc} \\ \mathbf{I}_{dc} \end{bmatrix} \tag{4.1}$$

and for VSC 2:

$$\begin{bmatrix} \mathbf{V}_{ABC_T} \\ \mathbf{V}_{dc_T} \end{bmatrix} = \begin{bmatrix} \mathbf{A}_2 & \mathbf{B}_2 \\ \mathbf{C}_2 & \mathbf{D}_2 \end{bmatrix} \begin{bmatrix} \mathbf{I}_{ABC} \\ -\mathbf{I}_{dc} \end{bmatrix} \tag{4.2}$$

Combining equations (4.1) and (4.2), the following equivalent for the HVDC-VSC back-to-back station is obtained,

$$\begin{bmatrix} \mathbf{V}_{abc_T} \\ \mathbf{V}_{ABC_T} \end{bmatrix} = \begin{bmatrix} \mathbf{A}_{12} & \mathbf{B}_{12} \\ \mathbf{C}_{12} & \mathbf{D}_{12} \end{bmatrix} \begin{bmatrix} \mathbf{I}_{abc} \\ \mathbf{I}_{ABC} \end{bmatrix} \tag{4.3}$$

where

$$\mathbf{V}_{abc_T} = \mathbf{V}_{abc} - \mathbf{P}_{s_1}\mathbf{V}_0 \tag{4.4}$$

$$\mathbf{V}_{ABC_T} = \mathbf{V}_{ABC} - \mathbf{P}_{s_2}\mathbf{V}_0 \tag{4.5}$$

and

$$\begin{aligned} \mathbf{A}_{12} &= \mathbf{A}_1 - \mathbf{B}_1(\mathbf{D}_1 + \mathbf{D}_2)^{-1}\mathbf{C}_1 \\ &= \mathbf{Z}_e + \frac{1}{2}\mathbf{P}_{s_1}\mathbf{Z}_{cap}\mathbf{Q}_{s_1} \end{aligned} \tag{4.6}$$

$$\begin{aligned} \mathbf{B}_{12} &= \mathbf{B}_1(\mathbf{D}_1 + \mathbf{D}_2)^{-1}\mathbf{C}_2 \\ &= \frac{1}{2}\mathbf{P}_{s_1}\mathbf{Z}_{cap}\mathbf{Q}_{s_2} \end{aligned} \tag{4.7}$$

$$\begin{aligned} \mathbf{C}_{12} &= \mathbf{B}_2(\mathbf{D}_1 + \mathbf{D}_2)^{-1}\mathbf{C}_1 \\ &= \frac{1}{2}\mathbf{P}_{s_2}\mathbf{Z}_{cap}\mathbf{Q}_{s_1} \end{aligned} \tag{4.8}$$

$$\begin{aligned} \mathbf{D}_{12} &= \mathbf{A}_2 - \mathbf{B}_2 (\mathbf{D}_1 + \mathbf{D}_2)^{-1} \mathbf{C}_2 \\ &= \mathbf{Z}_e + \frac{1}{2} \mathbf{P}_{s_2} \mathbf{Z}_{cap} \mathbf{Q}_{s_2} \end{aligned} \tag{4.9}$$

If only one capacitor is used, then the model for the HVDC-VSC back-to-back station is arrived at and represented as shown in Figure 4.2,

$$\begin{bmatrix} \mathbf{V}_{abc_T} \\ \mathbf{V}_{ABC_T} \end{bmatrix} = \begin{bmatrix} \mathbf{Z}_e + \mathbf{P}_{s_1} \mathbf{Z}_{cap} \mathbf{Q}_{s_1} & \mathbf{P}_{s_1} \mathbf{Z}_{cap} \mathbf{Q}_{s_2} \\ \mathbf{P}_{s_2} \mathbf{Z}_{cap} \mathbf{Q}_{s_1} & \mathbf{Z}_e + \mathbf{P}_{s_2} \mathbf{Z}_{cap} \mathbf{Q}_{s_2} \end{bmatrix} \begin{bmatrix} \mathbf{I}_{abc} \\ \mathbf{I}_{ABC} \end{bmatrix} \tag{4.10}$$

Equation (4.10) can be interpreted as the equation of two STATCOM equivalents with a coupling between them given by the impedances $\mathbf{P}_{s_1} \mathbf{Z}_{cap} \mathbf{Q}_{s_2}$ and $\mathbf{P}_{s_2} \mathbf{Z}_{cap} \mathbf{Q}_{s_1}$. Hence, the ability of the DC link to operate as two individual STATCOMs depends very much on the characteristics of the mutual-impedances.

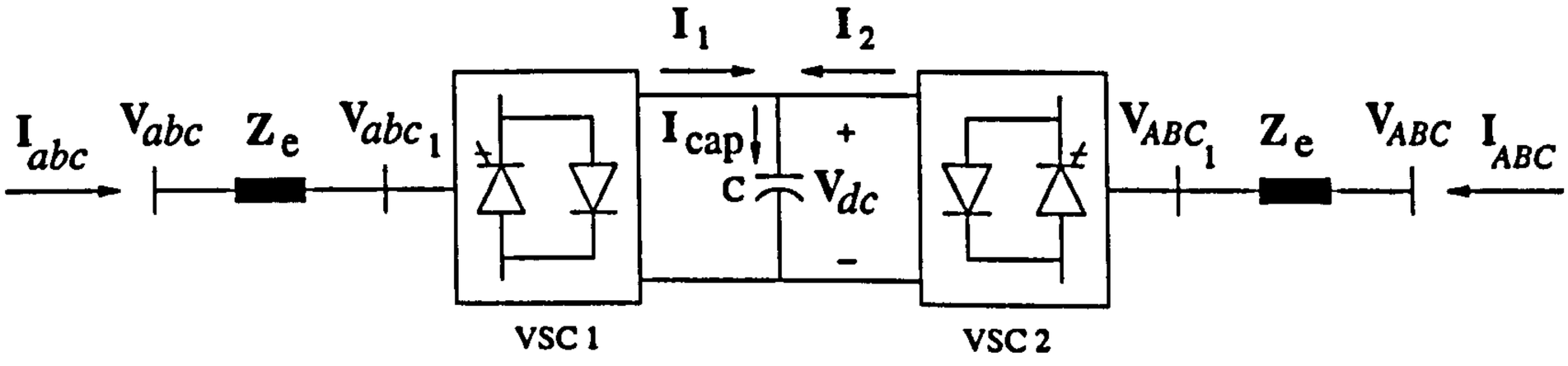

Figure 4.2.: HVDC-VSC back-to-back station

4.3.1. Control considerations

Since the HVDC-VSC back-to-back is built with two VSCs, reactive power may be exchanged with both AC systems in a similar fashion as with the STATCOM, with the only major difference that active power can also be exchanged between the two systems. The active power flow during steady-state operation is achieved when no DC current flows in the capacitor. In order to achieve such an operation, one VSC is selected to act as a "power dispatcher" and the second VSC as a "master DC voltage regulator" [33].

Power dispatcher: The function of the power dispatcher is to supply a pre-specified active power P_{spd}, which may take either positive or negative values and it is supplied by the power dispatcher in a rectifier or inverter mode. In this case, VSC 2 is selected to be the power dispatcher and the active power, P_{vsc_2}, is measured and compared against the reference value P_{spd}. The error,

$$\varepsilon = P_{spd} - P_{vsc_2}$$

is used as a negative feedback signal to increase or decrease the output voltage angle δ_{vsc_2} of the converter by means of the PWM control until the error is minimised.

Master DC voltage regulator: The function of the master DC voltage regulator is to maintain the DC voltage at a pre-selected constant value. Since VSC 2 was selected as power dispatcher then VSC 1 is the master DC voltage regulator.

The dc-term of $\mathbf{V}_{dc}$, i.e. V_{dc_0}, is measured and compared against the voltage reference V_{ref}. The voltage error,

$$\varepsilon = V_{\text{ref}} - V_{dc_0}$$

is used as a command in a negative feedback loop to adjust the voltage angle δ_{vsc_1} by means of a PWM control to minimise the error. A constant DC link voltage in steady-state is obtained when the sum of dc-terms of the currents $i_1(t)$ and $i_2(t)$ become equal to zero, i.e. zero dc-term current in the capacitor,

$$I_{1_0} + I_{2_0} = 0$$

This means that δ_{vsc_1} is adjusted until the power from the AC system satisfies the power demanded by the power dispatcher.

4.3.2. Time domain comparison results

The HVDC-VSC back-to-back model was compared with the steady-state response of a model implemented in PSCAD/EMTDC [39]. The following system parameters were used for the case study:

Source: 115 kV line to line, internal RL parallel equivalent impedance with $R_g = 100\,\Omega$ and $L_g = 0.01$ H.

Transformer: An equivalent series impedance: $R_e = 0.1\,\Omega$ and $L_e = 0.05$ H.

VSCs: Six-pulse converter with IGBTs switched by the PWM technique described in Appendix A. The carrier frequency is 1650 Hz.

Capacitor: $300\,\mu$F.

VSC 1: Selected as the master DC voltage regulator to charge the capacitor at 115 kV.

VSC 2: Selected as the power dispatcher to supply 300 MW.

Simulation: 50 harmonics were used, obtaining the solution in two iterations using the iterative process described in Appendix C. The phase angle for the power dispatcher was fixed at $\delta_{\text{vsc}_2} = 39.97°$, which is an angle previously obtained using PSCAD/EMTDC simulations. For the PSCAD/EMTDC result, a simulation time of 4 s with a time step of $20\,\mu$s are used in order to obtain a suitable steady-state condition. The

PSCAD/EMTDC model uses two controls, one for the master DC voltage regulator and the other for the power dispatcher. The diagram of the HVDC-VSC back-to-back station is shown in Appendix E.

Figure 4.3 shows the line currents for the phase *a* in the converter side. The results show that both models produce very similar results.

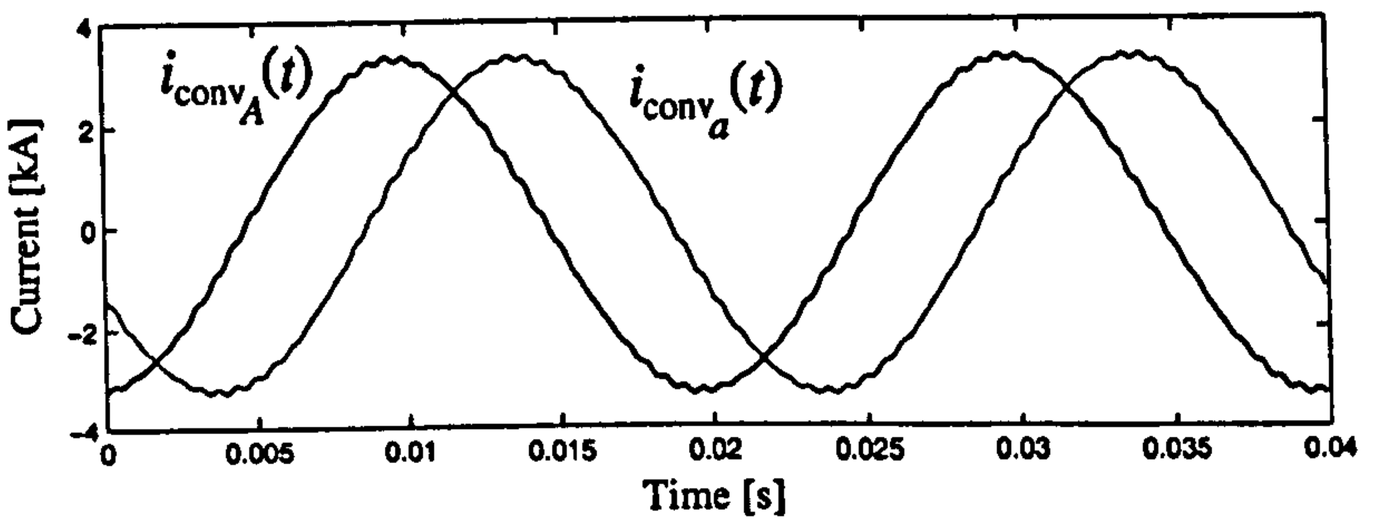

(a) Using harmonic domain

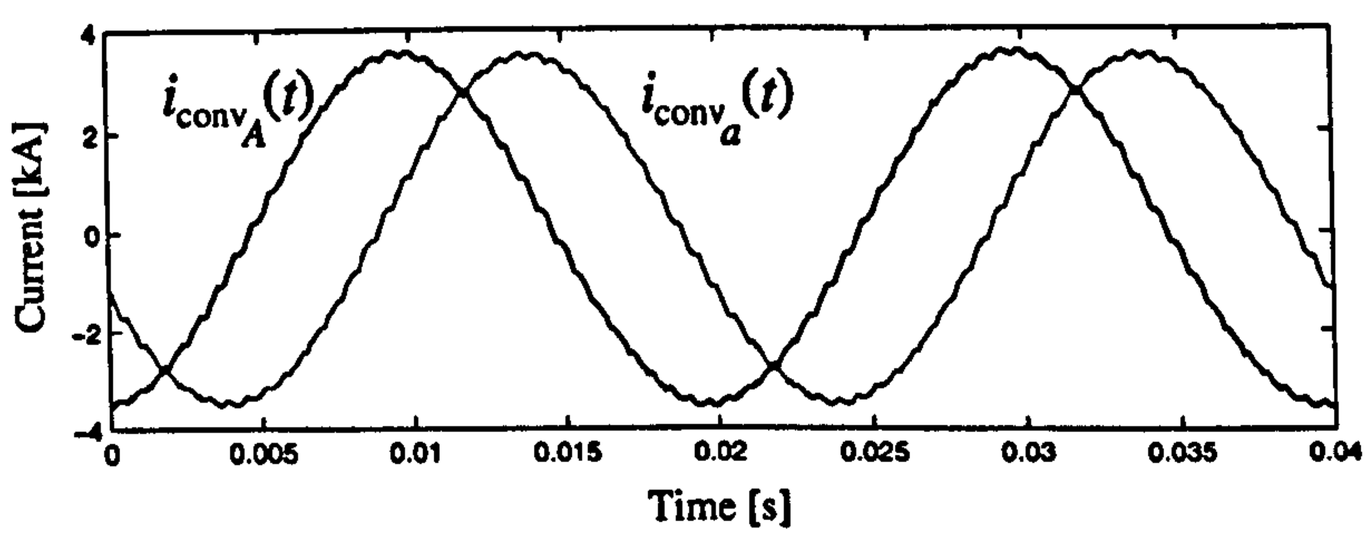

(b) Using PSCAD/EMTDC

Figure 4.3.: Current responses for the HVDC-VSC back-to-back

4.3.3. Active power transfer

Figure 4.4 shows the response of the HVDC-VSC back-to-back under different values of phase angle δ_{vsc_2} and AC equivalent impedance. As previously stated, VSC 1 is the master DC voltage regulator. The active power shown in this figure corresponds to the input power at the terminal of the power dispatcher. The simulations were carried out for the following range of angles $-90° \leq \delta_{vsc_2} \leq 90°$, and equal AC voltage sources with constant magnitude and zero phase angle.

The following key points are observed from these results:

- On the right of the figures, the curves are limited by the maximum angle value δ_{vsc_1} that can maintain constant DC voltage (loss of convergence in the method).
- Active power transfer observes a similar pattern as that observed by the voltage angle control in AC generation stations.

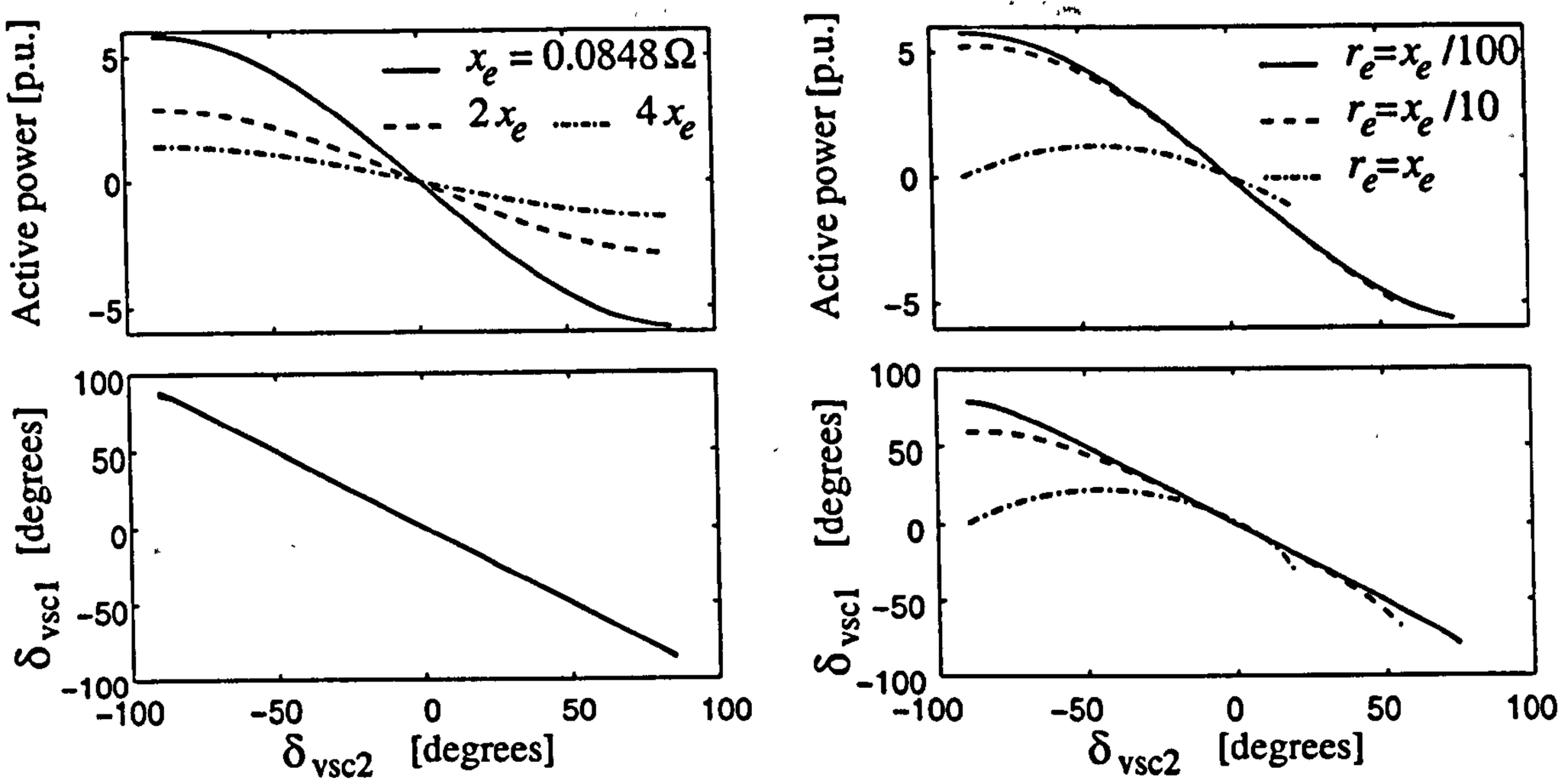

(a) $r_e = 0.0001\Omega$ (b) $x_e = 0.0848\Omega$

Figure 4.4.: HVDC-VSC back-to-back responses

- Active power reversal is achieved by changing the voltage angle from negative to a positive value.

For the "lossless" case ($r_e = 0.0001\,\Omega$) and different values of x_e, the following is noticed:

- As x_e increases, the AC transmission capability weakens, with the maximum power transfer defined by the extreme points in the curves.

- The active power follows a symmetrical response from positive to negative voltage angles.

- The relationship between the angles δ_{vsc_2} and δ_{vsc_1} is linear.

For the case when $x_e = 0.0848\,\Omega$ and the value of r_e is varied, the following key points are observed:

- As r_e increases, the AC transmission losses increase, and the maximum power transfer is defined by the extreme points in the curves or by the point where the curve reaches its maximum value.

- The active power follows a non-symmetrical response due to the losses, from negative to positive voltage angles.

- The relationship between the angles δ_{vsc_2} and δ_{vsc_1} is non-linear due to the losses.

4.4. HVDC-VSC Transmission System Model

In order to extend the HVDC-VSC back-to-back model to become the HVDC-VSC full transmission model, it is necessary to add the DC cable between the two VSCs. Figure 4.5 shows the connection of one end of the cable to one of the converters.

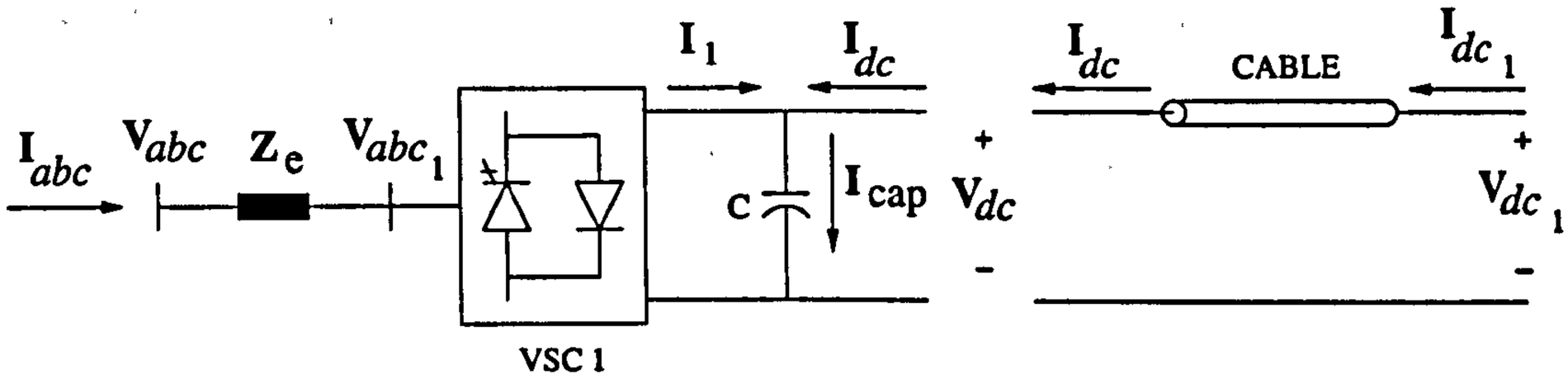

Figure 4.5.: VSC with a cable in the DC side

The equations that describe the system of Figure 4.5 are given below. The VSC 1 is represented by

$$\begin{bmatrix} \mathbf{V}_{abc_T} \\ \mathbf{V}_{dc_T} \end{bmatrix} = \begin{bmatrix} \mathbf{A}_1 & \mathbf{B}_1 \\ \mathbf{C}_1 & \mathbf{D}_1 \end{bmatrix} \begin{bmatrix} \mathbf{I}_{abc} \\ \mathbf{I}_{dc} \end{bmatrix} \tag{4.11}$$

where $\mathbf{V}_{dc_T} = \mathbf{V}_{dc} - \mathbf{V}_{0_1}$, $\mathbf{V}_{abc_T} = \mathbf{V}_{abc} - \mathbf{P}_{s_1}\mathbf{V}_{0_1}$.

The exact model, in steady-state, for the cable is

$$\begin{bmatrix} \mathbf{V}_{dc} \\ \mathbf{I}_{dc} \end{bmatrix} = \begin{bmatrix} \mathbf{A}_c & \mathbf{B}_c \\ \mathbf{C}_c & \mathbf{D}_c \end{bmatrix} \begin{bmatrix} \mathbf{V}_{dc_1} \\ \mathbf{I}_{dc_1} \end{bmatrix} \tag{4.12}$$

with

$$\mathbf{A}_c = \cosh(\gamma l/2) \tag{4.13}$$

$$\mathbf{B}_c = Z_c \sinh(\gamma l/2) \tag{4.14}$$

$$\mathbf{C}_c = \frac{1}{Z_c}\sinh(\gamma l/2) \tag{4.15}$$

$$\mathbf{D}_c = \cosh(\gamma l/2) \tag{4.16}$$

where γ and Z_c are the wave propagation and characteristic impedance of the cable, respectively, and l is the total length of the cable in km. At harmonic frequencies, the wave propagation is given by

$$\gamma = \sqrt{(R' + j\omega_0 h L')\,(G' + j\omega_0 h C')} \tag{4.17}$$

and the characteristic impedance by

$$Z_c = \sqrt{(R' + j\omega_0 hL') / (G' + j\omega_0 hC')} \tag{4.18}$$

where R' in Ω/km, L' in H/km, G' in S/km and C' in F/km are the distributed series resistance, series inductance, shunt conductance and shunt capacitance of the cable, respectively. It should be mentioned that the frequency domain representation permits the use of an exact model of the cable; something which is achieved with difficulty when time domain representations are used. For instance, it is quite common to represent the cable by using one π−section per km [111].

Combining equations (4.11) and (4.12) leads to the following equation,

$$\begin{bmatrix} \mathbf{V}_{abc_T} \\ \mathbf{V}_{dc_1} \end{bmatrix} = \begin{bmatrix} \mathbf{A}_{1c} & \mathbf{B}_{1c} \\ \mathbf{C}_{1c} & \mathbf{D}_{1c} \end{bmatrix} \begin{bmatrix} \mathbf{I}_{abc} \\ \mathbf{I}_{dc_1} \end{bmatrix} \tag{4.19}$$

where

$$\mathbf{A}_{1c} = \left(\mathbf{A}_1 - \mathbf{B}_1\mathbf{D}_1^{-1}\mathbf{C}_1\right) + \mathbf{B}_1\mathbf{D}_1^{-1}\mathbf{A}_c\left(\mathbf{D}_1^{-1}\mathbf{A}_c + \mathbf{C}_c\right)^{-1}\mathbf{D}_1^{-1}\mathbf{C}_1 \tag{4.20}$$

$$\mathbf{B}_{1c} = \left(\mathbf{B}_1\mathbf{D}_1^{-1}\mathbf{A}_c\right)\left(\mathbf{D}_1^{-1}\mathbf{A}_c + \mathbf{C}_c\right)^{-1}\left(\mathbf{D}_c + \mathbf{D}_1^{-1}\mathbf{B}_c\right) - \mathbf{B}_1\mathbf{D}_1^{-1}\mathbf{B}_c \tag{4.21}$$

$$\mathbf{C}_{1c} = \left(\mathbf{D}_1^{-1}\mathbf{A}_c + \mathbf{C}_c\right)^{-1}\mathbf{D}_1^{-1}\mathbf{C}_1 \tag{4.22}$$

$$\mathbf{D}_{1c} = \left(\mathbf{D}_1^{-1}\mathbf{A}_c + \mathbf{C}_c\right)^{-1}\left(\mathbf{D}_c + \mathbf{D}_1^{-1}\mathbf{B}_c\right) \tag{4.23}$$

The HVDC-VSC transmission system now can be obtained by using two similar equivalents circuits, as shown in Figure 4.6. The equation for the second converter is

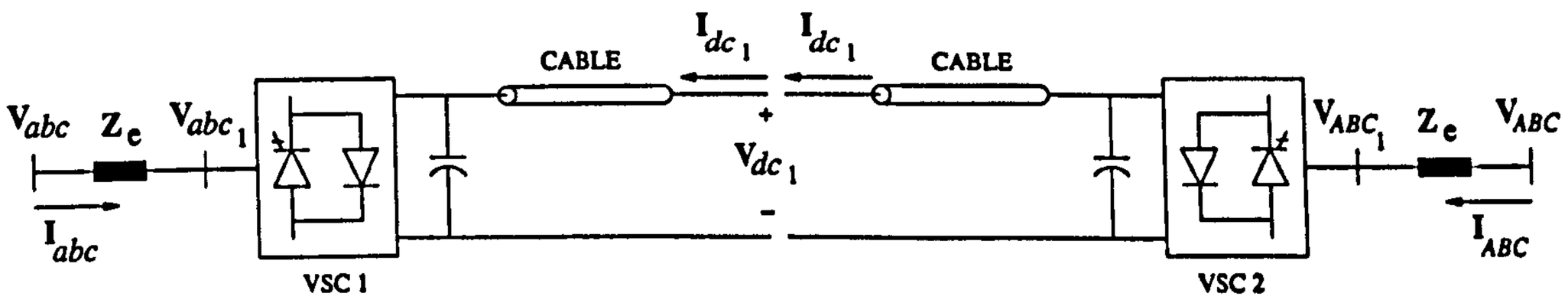

Figure 4.6.: HVDC-VSC transmission system

$$\begin{bmatrix} \mathbf{V}_{ABC_T} \\ \mathbf{V}_{dc_1} \end{bmatrix} = \begin{bmatrix} \mathbf{A}_{2c} & \mathbf{B}_{2c} \\ \mathbf{C}_{2c} & \mathbf{D}_{2c} \end{bmatrix} \begin{bmatrix} \mathbf{I}_{ABC} \\ -\mathbf{I}_{dc_1} \end{bmatrix} \tag{4.24}$$

From (4.19) and (4.24) the equivalent for the HVDC-VSC transmission system may be obtained:

$$\begin{bmatrix} \mathbf{V}_{abc_T} \\ \mathbf{V}_{ABC_T} \end{bmatrix} = \begin{bmatrix} \mathbf{A}_{1c2} & \mathbf{B}_{1c2} \\ \mathbf{C}_{1c2} & \mathbf{D}_{1c2} \end{bmatrix} \begin{bmatrix} \mathbf{I}_{abc} \\ \mathbf{I}_{ABC} \end{bmatrix} \tag{4.25}$$

where

$$\mathbf{V}_{abc_T} = \mathbf{V}_{abc} - \mathbf{P}_{s_1}\mathbf{V}_{0_1} \tag{4.26}$$

$$\mathbf{V}_{ABC_T} = \mathbf{V}_{ABC} - \mathbf{P}_{s_2}\mathbf{V}_{0_2} \tag{4.27}$$

$$\begin{aligned}
\mathbf{A}_{1c2} &= \mathbf{A}_{1c} - \mathbf{B}_{1c}\left(\mathbf{D}_{1c}+\mathbf{D}_{2c}\right)^{-1}\mathbf{C}_{1c} \\
&= \mathbf{Z}_e + \frac{1}{2}\mathbf{P}_{s_1}\mathbf{A}_c\left(\mathbf{Y}_{cap}\mathbf{A}_c+\mathbf{C}_c\right)^{-1}\mathbf{Q}_{s_1} \\
&\quad + \frac{1}{2}\mathbf{P}_{s_1}\mathbf{B}_c\left(\mathbf{D}_c+\mathbf{Y}_{cap}\mathbf{B}_c\right)^{-1}\mathbf{Q}_{s_1}
\end{aligned} \tag{4.28}$$

$$\begin{aligned}
\mathbf{B}_{1c2} &= \mathbf{B}_{1c}\left(\mathbf{D}_{1c}+\mathbf{D}_{2c}\right)^{-1}\mathbf{C}_{2c} \\
&= \frac{1}{2}\mathbf{P}_{s_1}\mathbf{A}_c\left(\mathbf{Y}_{cap}\mathbf{A}_c+\mathbf{C}_c\right)^{-1}\mathbf{Q}_{s_2} \\
&\quad - \frac{1}{2}\mathbf{P}_{s_1}\mathbf{B}_c\left(\mathbf{D}_c+\mathbf{Y}_{cap}\mathbf{B}_c\right)^{-1}\mathbf{Q}_{s_2}
\end{aligned} \tag{4.29}$$

$$\begin{aligned}
\mathbf{C}_{1c2} &= \mathbf{B}_{2c}\left(\mathbf{D}_{1c}+\mathbf{D}_{2c}\right)^{-1}\mathbf{C}_{1c} \\
&= \frac{1}{2}\mathbf{P}_{s_2}\mathbf{A}_c\left(\mathbf{Y}_{cap}\mathbf{A}_c+\mathbf{C}_c\right)^{-1}\mathbf{Q}_{s_1} \\
&\quad - \frac{1}{2}\mathbf{P}_{s_2}\mathbf{B}_c\left(\mathbf{D}_c+\mathbf{Y}_{cap}\mathbf{B}_c\right)^{-1}\mathbf{Q}_{s_1}
\end{aligned} \tag{4.30}$$

$$\begin{aligned}
\mathbf{D}_{1c2} &= \mathbf{A}_{2c} - \mathbf{B}_{2c}\left(\mathbf{D}_{1c}+\mathbf{D}_{2c}\right)^{-1}\mathbf{C}_{2c} \\
&= \mathbf{Z}_e + \frac{1}{2}\mathbf{P}_{s_2}\mathbf{A}_c\left(\mathbf{Y}_{cap}\mathbf{A}_c+\mathbf{C}_c\right)^{-1}\mathbf{Q}_{s_2} \\
&\quad + \frac{1}{2}\mathbf{P}_{s_2}\mathbf{B}_c\left(\mathbf{D}_c+\mathbf{Y}_{cap}\mathbf{B}_c\right)^{-1}\mathbf{Q}_{s_2}
\end{aligned} \tag{4.31}$$

where $\mathbf{Y}_{cap} = \mathbf{Z}_{cap}^{-1}$.

Figure 4.7 shows the final HVDC-VSC transmission system model.

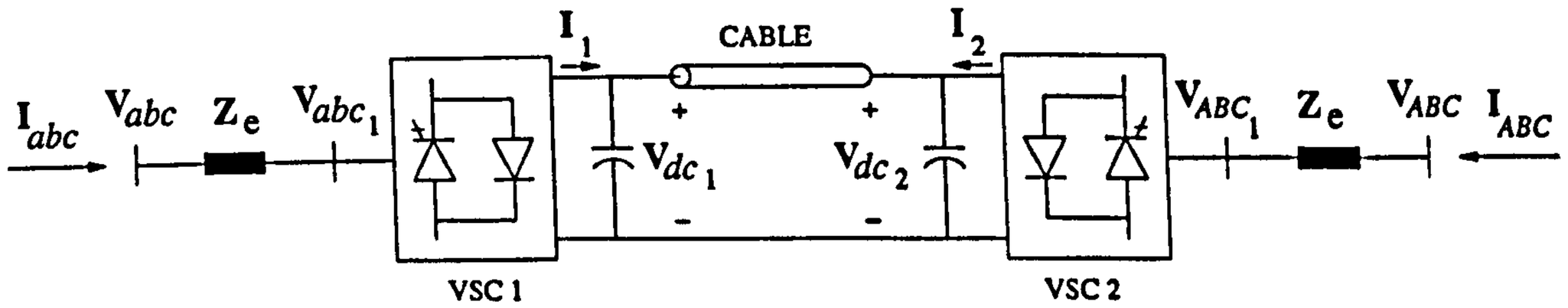

Figure 4.7.: HVDC-VSC transmission system

4.4.1. Control consideration

The VSCs of the HVDC-VSC transmission system may be assumed to have the same control rules as the VSCs for the HVDC-VSC back-to-back, i.e. VSC 1 is the master DC voltage regulator and VSC 2 is the power dispatcher. The only difference between these two configurations

is that in the HVDC-VSC transmission system, the dc-term voltage in the capacitor of VSC 2 is given by $V_{dc2_0} = V_{dc1_0} - R_{\text{cable}} I_{1_0}$. Also, the power losses in the cable can be obtained from $R_{\text{cable}} I_{1_0}^2$.

4.4.2. Time domain comparison results

The HVDC-VSC model response is compared against the steady-state response of a model implemented in PSCAD/EMTDC [39]. The system has the following parameters:

Sources: 115 kV line to line, RL parallel equivalent impedance with $R_g = 100\,\Omega$ and $L_g = 0.01$ H.

VSC 1: An equivalent series impedance for the AC system including the transformer: $R_{eq} = 0.1\,\Omega$ and $L_{eq} = 0.05$ H, and a DC capacitor of $150\,\mu$F. VSC 1 is selected to be the master DC voltage regulator to charge the capacitor at 115 kV.

VSC 2: An equivalent series impedance for the AC system including the transformer: $R_{eq} = 0.2\,\Omega$ and $L_{eq} = 0.1$ H, and a DC capacitor of $150\,\mu$F. VSC 2 is selected to be the power dispatcher to supply 200 MW.

Cable: A 100 km cable with $R' = 0.0679\,\Omega$/km, $L' = 2.4217$ mH/km and $C' = 0.4764\,\mu$F/km was used. These distributed parameters correspond to the cable shown in Appendix E and used in the PSCAD/EMTDC simulation.

Simulation: 50 harmonics were used in this study and convergence is achieved in 6 iterations using the iterative scheme described in Appendix C. The phase angle for the power dispatcher is fixed at $\delta_{vsc_2} = 47.08°$, which is the angle obtained from the PSCAD/EMTDC simulation. For the PSCAD/EMTDC simulation a time of 3 s, with a time step of $20\,\mu$s is used to obtain a suitable steady-state result. The PSCAD/EMTDC model uses two controls, one for the master DC voltage regulator and the other for the power dispatcher. The diagram of the HVDC-VSC transmission system is shown in Appendix E. The final results are: $\delta_{vsc_1} = -21.15°$ and $-23.56°$ for the PSCAD/EMTDC and HD models, respectively. The dc-term of the DC voltage V_{0_2} are: 129.8 kV and 125.1 kV for the PSCAD/EMTDC and HD results, respectively. And power dispatched of 198 MW and 186 MW for the PSCAD/EMTDC and HD, respectivey. Although both cables have the same distributed parameters, these differences are due mainly to the cable model used by the PSCAD/EMTDC.

Figure 4.8 shows the line currents in the converter side obtained with both models. These results compare very well with each other.

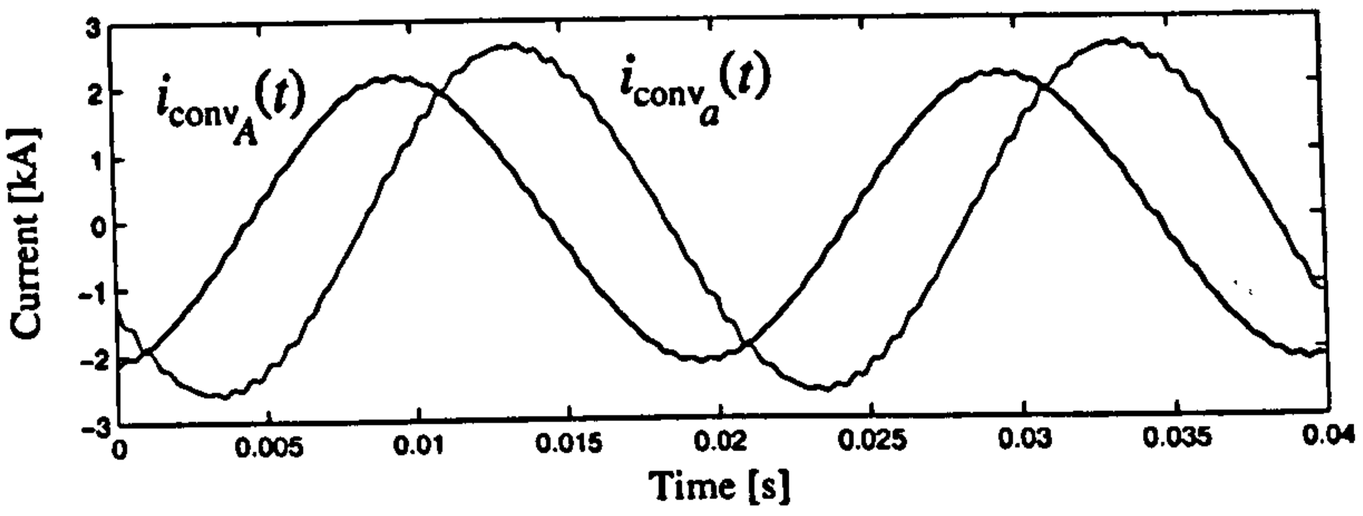

(a) Using harmonic domain

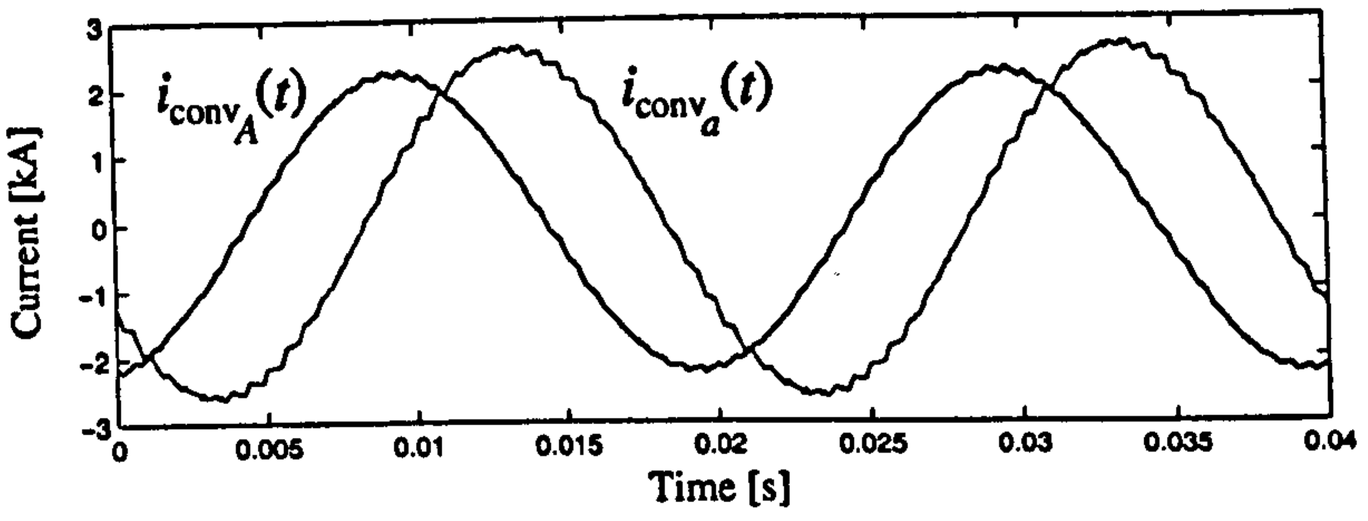

(b) Using PSCAD/EMTDC

Figure 4.8.: Currents response of the HVDC-VSC transmission system

4.4.3. Case study : Resonance analysis

An HVDC-VSC transmission system with the following parameters is used:

AC voltage sources: 115 kV line to line, RL parallel equivalent impedance with $R_g = 1\,\Omega$ and $L_g = 0.03$ H.

Transformers: Equivalent series impedance $R_e = 0.30\,\Omega$ and $L_e = 0.15$ H.

VSCs: Two-level VSC with a switching frequency of 250 Hz and modulation factor of 0.85. VSC 1 is selected to be the master DC voltage regulator to maintain the DC link at 115 kV. VSC 2 is selected to be the power dispatcher with the phase angle fixed at $-45°$. Capacitors: $50\,\mu$F.

Cable: $R' = 0.068$ Ω/km, $L' = 2.422$ mH/km, $C' = 0.476$ μF/km and $G' = 0.030$ μS/km. Different lengths of the cable are used. 15 harmonics are used in the study.

Figure 4.9 shows the impedance response as seen from the sending-end of the arrangement capacitor-cable-capacitor. Figure 4.9(a) uses a logarithmic scale in the impedance magnitude in order to identified resonance points. It is clear to see, in this figure, the resonance pattern that the arrangment presents at different frequencies for different cable lengths. In order to identify these resonance points, Figure 4.9(b) shows a contour view of Figure 4.9(a). This figure shows that, for example, resonances at the 6th harmonic exist for cable lengths of 5 km and 54 km. Also, for cable lengths of 27 km, 52 km and 76 km resonances will appear at the 12th harmonic.

Figures 4.10 and 4.11 show the response of the system for different lengths of cable. Figure 4.10 shows the injected power by each AC voltage source. It can be seen that the active power flows from the AC source *ABC* to the AC source *abc*. The total loss in the system is given by $P_{losses} = P_a + P_A$. These results show that resonance points occur at cable lengths of 5, 27, 54 and 76 km.

The results in Figure 4.11 show that the current $\mathbf{I}_1$ (DC side) contains the 6th and 12th harmonics, which interact with the DC system producing resonances for 5 km and 54 km long cables. It should be remarked that these resonances were previously predicted by inspecting the DC side impedance responses in Figure 4.9. Resonances in the DC side interact with the AC side currents producing resonance at other harmonic frequencies, as can be seen in the harmonic content of current $\mathbf{I}_a$. Resonances at other frequencies also exist and are due to the cross-coupling between harmonics in the equivalent impedance of the converters.

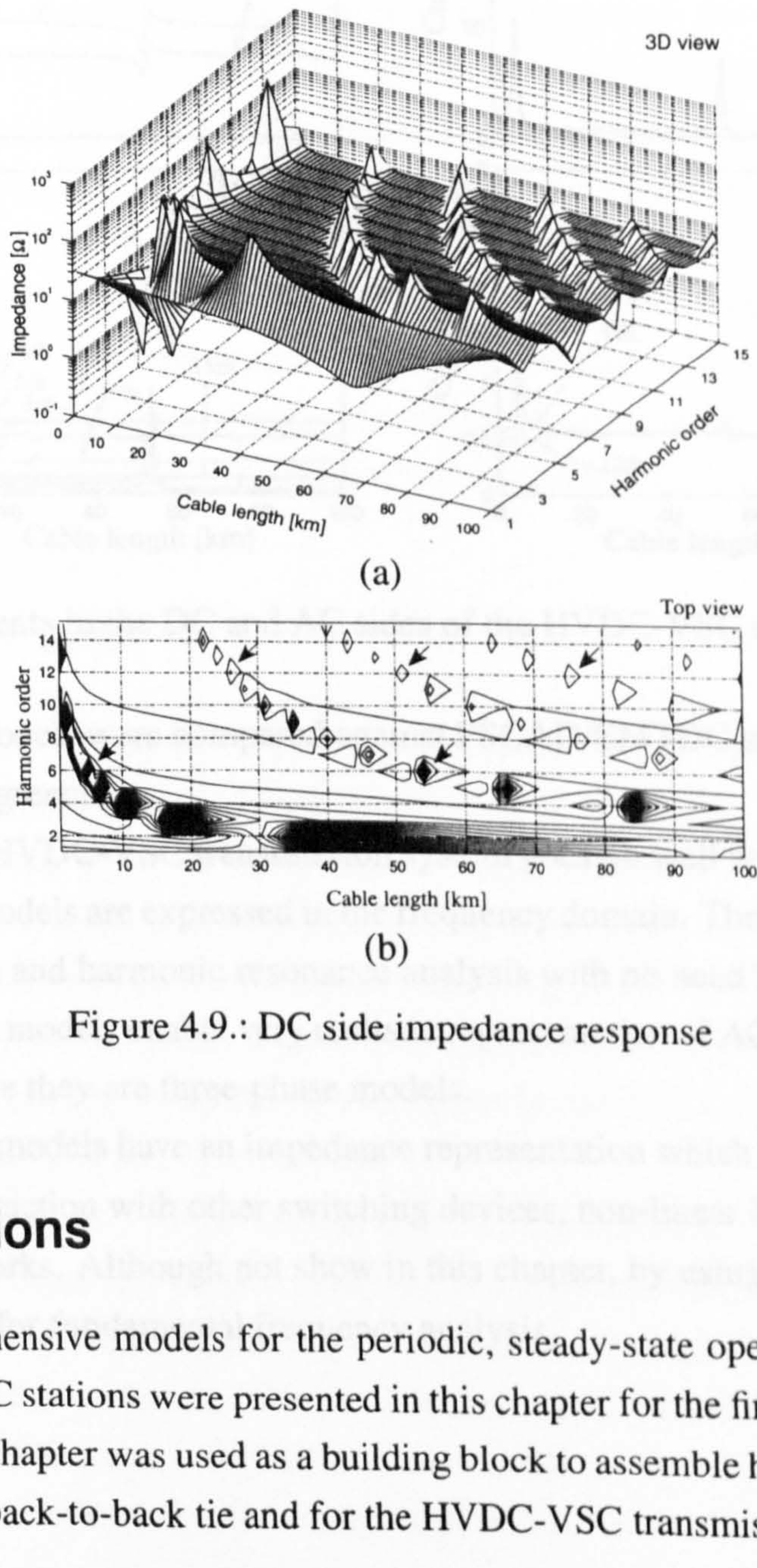

Figure 4.9.: DC side impedance response

4.5. Conclusions

Flexible and comprehensive models for the periodic, steady-state operation and harmonic response of HVDC-VSC stations were presented in this chapter for the first time. The VSC model obtained in previous chapter was used as a building block to assemble harmonic domain models for the HVDC-VSC back-to-back tie and for the HVDC-VSC transmission system. The results

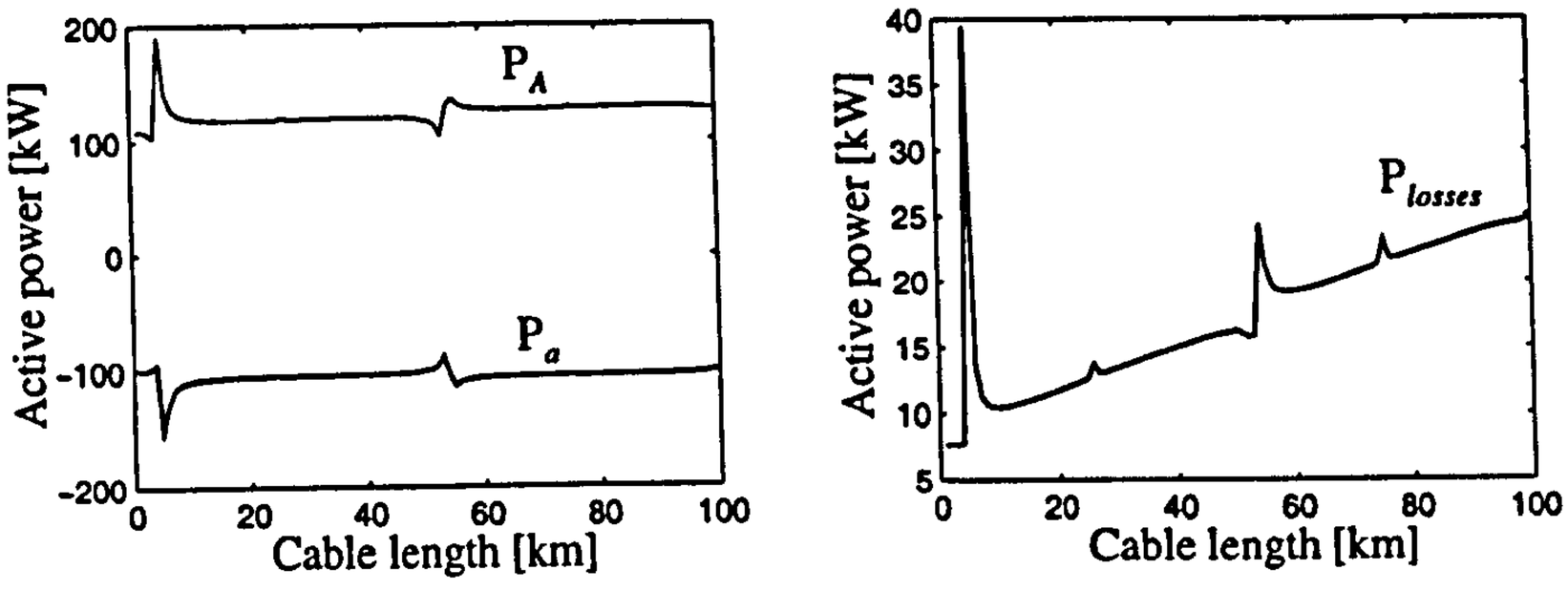

Figure 4.10.: Powers in the AC sides of the HVDC-VSC transmission system

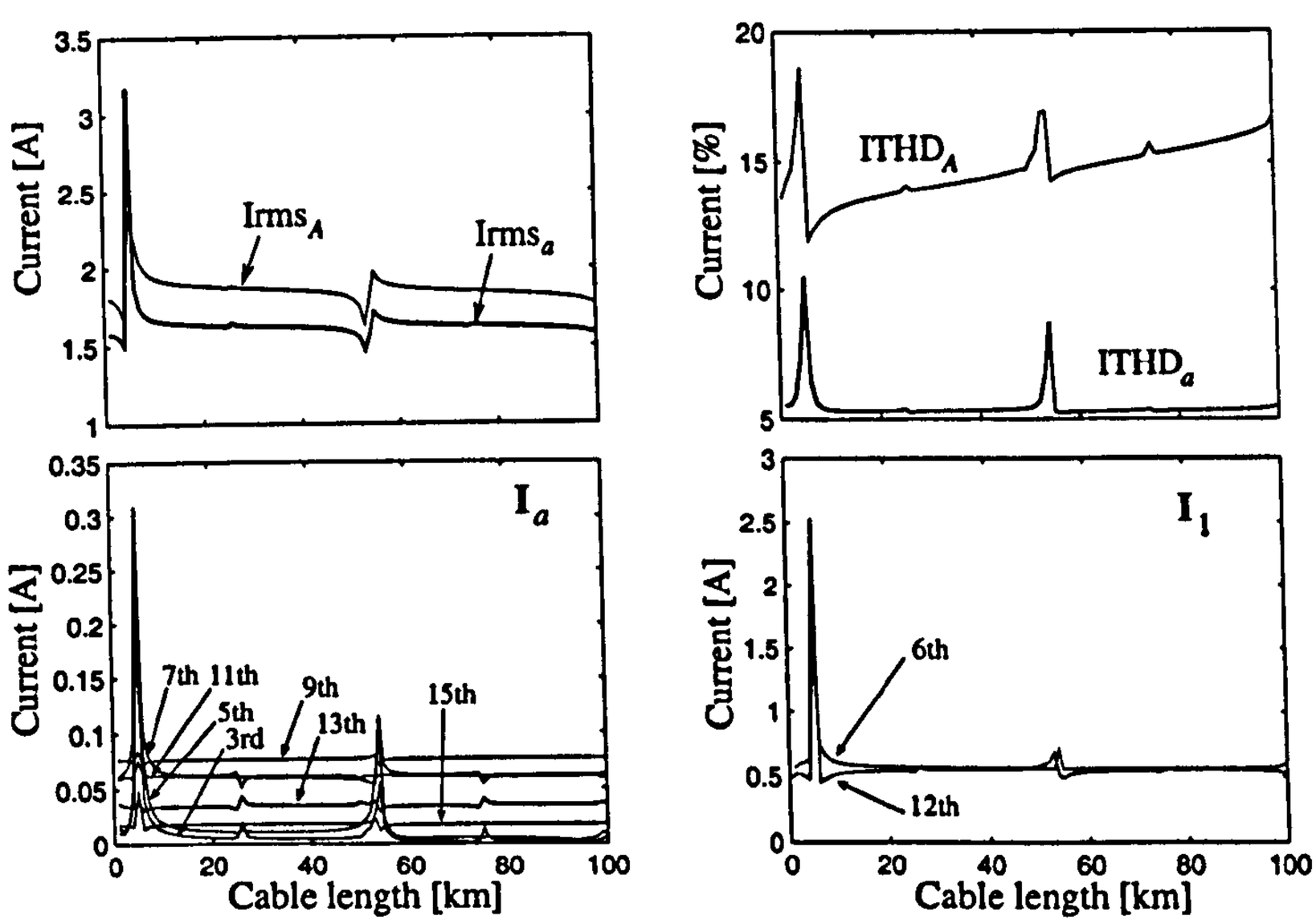

Figure 4.11.: Currents in the DC and AC sides of the HVDC-VSC transmission system

obtained with these models were compared against PSCAD/EMTDC simulations, and they are shown to be in good agreement.

The model of the HVDC-VSC transmission system goes on well with an accurate model of the cable since both models are expressed in the frequency domain. The models may be used for harmonic propagation and harmonic resonance analysis with no need to resort to time domain simulations. Also, the models enable very realistic representation of AC system imbalances and firing imbalances since they are three-phase models.

The HVDC-VSC models have an impedance representation which may be used in the analysis of harmonic interaction with other switching devices, non-linear loads, transmission lines, or transmission networks. Although not show in this chapter, by using $h = 1$ gives a simplified HVDC-VSC models for fundamental frequency analysis.

5. Unified Power Flow Controller

5.1. Introduction

A novel harmonic model for the unified power flow controller (UPFC) is presented in this chapter. The proposed model incorporates all the basic operating characteristics that existing fundamental frequency UPFC models offer, such as the active and reactive power control regions. However, the harmonic model offers additional information such as harmonic distortion regions. The UPFC model is given in a form of an equivalent impedance which is connected to the AC system to perform harmonic propagation and resonance prediction analysis. By building on the modular approach adopted in this thesis, the UPFC model is obtained as a particular connection of the HVDC-VSC back-to-back with the AC transmission system. The UPFC model is used to study the harmonic interaction with transmission lines. It is also shown that a simplified UPFC harmonic model does not give such harmonic interaction with transmission lines.

5.2. UPFC Concept

The unified power flow controller (UPFC), one of the most advanced power systems controllers ever built, was proposed by Laszlo Gyugyi in 1991 [112]. The UPFC was devised to provide very stringent control and dynamic compensation requirements in AC transmission systems. Within the framework of traditional power transmission concepts, the UPFC is able to control, simultaneously or selectively, all the parameters affecting power flow in the transmission line, such as voltage magnitude and phase angle and line impedance. This unique capability is signified by the adjective "unified" in its name. Alternatively, the UPFC can independently control both active and reactive power flow in the line.

The UPFC comprises two VSCs coupled to a DC link capacitor, one VSC is connected in parallel with the AC system and the other is connected in series with the AC system. The UPFC active and reactive power characteristic is governed by the coordinated response of the voltages generated by the parallel and series VSCs. The first UPFC installation in the world, with a total rating of $\pm$320 MVA, was commissioned in 1998 at the Inez Substation of the American Electric Power (AEP) in Kentucky, for voltage support and power flow control [71].

The basic principles of UPFC operation are well known [8][9], with most of the research work having been focused on dynamic analysis [113][114][115][116][117][118][119], power flow [120][121][122][123][124][125] and optimal power flow analysis [126][127]. In [128] the authors show how the use of multi-converter modules based on GTOs or IGBTs and sinusoidal PWM strategy may be used to build a UPFC with high power ratings. In [129] a control strategy is used to show that the UPFC can be used as a harmonic insulator from non-linear loads. Research work addressing the voltage waveforms generated by the UPFC is minimum and mainly based on time domain simulation. An exhaustive search indicates that so far no work related to UPFC harmonic modelling and analysis has been reported in the open literature. In this chapter a UPFC model for harmonic analysis in presented.

5.3. UPFC Model

The UPFC has a similar configuration to the HVDC-VSC back-to-back station, with the only major difference that one of the VSCs is connected in series with the AC system, as shown in Figure 5.1. The VSC 2 provides the main function of the UPFC by injecting a voltage $v_{pq}(t)$ in series with the line (which is connected at node R) via a series coupling transformer. This injected voltage acts, essentially, as an AC voltage series source with a magnitude V_{pq} and phase angle ρ. The basic function of VSC 1 is to supply or absorb the active power demanded or injected by VSC 2 by controlling the common DC link voltage.

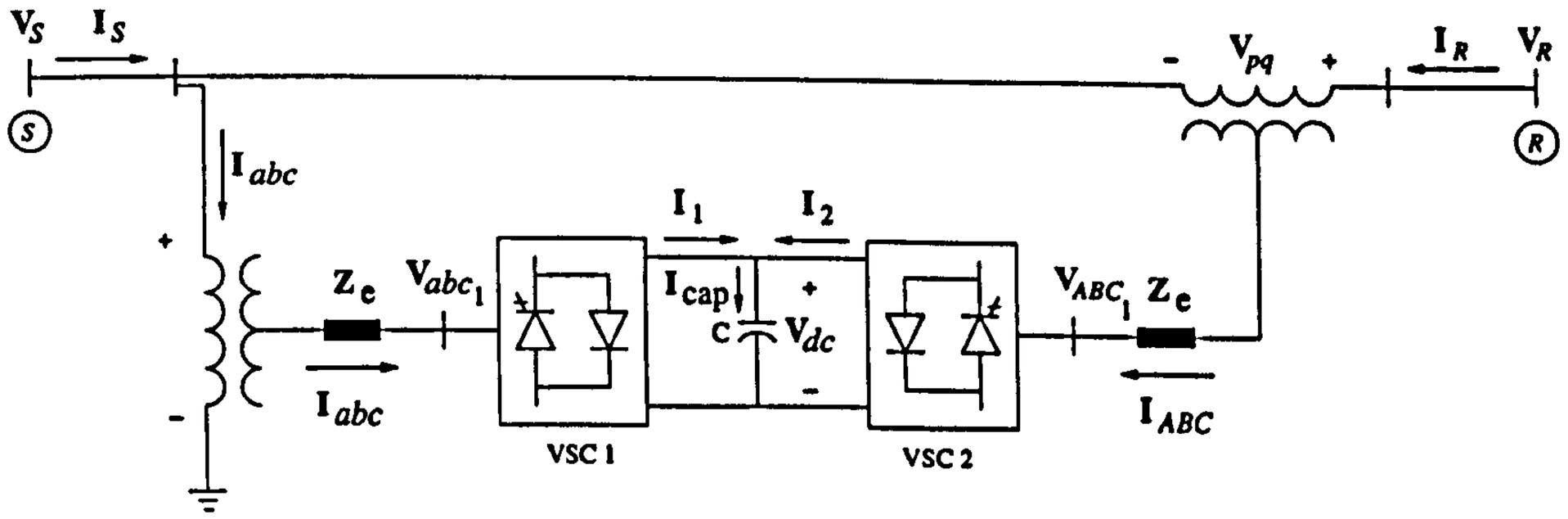

Figure 5.1.: Unified power flow controller scheme

The equations that represent the UPFC of Figure 5.1 are derived from the back-to-back arrangement shown in Figure 4.2. Hence, the derivation is started from equation (4.3):

$$\begin{bmatrix} \mathbf{V}_{abc} \\ \mathbf{V}_{ABC} \end{bmatrix} = \begin{bmatrix} \mathbf{A}_{12} & \mathbf{B}_{12} \\ \mathbf{C}_{12} & \mathbf{D}_{12} \end{bmatrix} \begin{bmatrix} \mathbf{I}_{abc} \\ \mathbf{I}_{ABC} \end{bmatrix} + \begin{bmatrix} \mathbf{P}_{s_1} \\ \mathbf{P}_{s_2} \end{bmatrix} \mathbf{V}_0 \tag{5.1}$$

The following boundary constraints exist from the UPFC scheme,

$$\mathbf{I}_{abc} = \mathbf{I}_S + \mathbf{I}_R$$

$$\mathbf{I}_{ABC} = \mathbf{I}_R$$

and, equation (5.1) becomes,

$$\begin{bmatrix} \mathbf{V}_{abc} \\ \mathbf{V}_{ABC} \end{bmatrix} = \begin{bmatrix} \mathbf{A}_{12} & (\mathbf{A}_{12}+\mathbf{B}_{12}) \\ \mathbf{C}_{12} & (\mathbf{C}_{12}+\mathbf{D}_{12}) \end{bmatrix} \begin{bmatrix} \mathbf{I}_S \\ \mathbf{I}_R \end{bmatrix} + \begin{bmatrix} \mathbf{P}_{s_1} \\ \mathbf{P}_{s_2} \end{bmatrix} \mathbf{V}_0 \tag{5.2}$$

Also, from the scheme,

$$\mathbf{V}_{abc} = \mathbf{V}_S$$
$$\mathbf{V}_{ABC} = \mathbf{V}_R - \mathbf{V}_S$$

and equation (5.2) becomes,

$$\begin{bmatrix} \mathbf{V}_S \\ \mathbf{V}_R \end{bmatrix} = \begin{bmatrix} \mathbf{A}_{12} & (\mathbf{A}_{12}+\mathbf{B}_{12}) \\ (\mathbf{A}_{12}+\mathbf{C}_{12}) & (\mathbf{A}_{12}+\mathbf{B}_{12})+(\mathbf{C}_{12}+\mathbf{D}_{12}) \end{bmatrix} \begin{bmatrix} \mathbf{I}_S \\ \mathbf{I}_R \end{bmatrix} + \begin{bmatrix} \mathbf{P}_{s_1} \\ \mathbf{P}_{s_1}+\mathbf{P}_{s_2} \end{bmatrix} \mathbf{V}_0 \tag{5.3}$$

Developing (5.3), the final UPFC model is arrived at,

$$\begin{bmatrix} \mathbf{V}_{S_T} \\ \mathbf{V}_{R_T} \end{bmatrix} = \begin{bmatrix} \mathbf{Z}_e+\mathbf{P}_{s_1}\mathbf{Z}_{cap}\mathbf{Q}_{s_1} & \mathbf{Z}_e+\mathbf{P}_{s_1}\mathbf{Z}_{cap}(\mathbf{Q}_{s_1}+\mathbf{Q}_{s_2}) \\ \mathbf{Z}_e+(\mathbf{P}_{s_1}+\mathbf{P}_{s_2})\mathbf{Z}_{cap}\mathbf{Q}_{s_1} & 2\mathbf{Z}_e+(\mathbf{P}_{s_1}+\mathbf{P}_{s_2})\mathbf{Z}_{cap}(\mathbf{Q}_{s_1}+\mathbf{Q}_{s_2}) \end{bmatrix} \times \begin{bmatrix} \mathbf{I}_S \\ \mathbf{I}_R \end{bmatrix} \tag{5.4}$$

where

$$\mathbf{V}_{S_T} = \mathbf{V}_S - \mathbf{P}_{s_1}\mathbf{V}_0 \tag{5.5}$$

$$\mathbf{V}_{R_T} = \mathbf{V}_R - (\mathbf{P}_{s_1}+\mathbf{P}_{s_2})\mathbf{V}_0 \tag{5.6}$$

It should be noticed from the UPFC scheme that the currents in the DC side are related to the AC currents as follow

$$\mathbf{I}_1 = \mathbf{Q}_{s_1}(\mathbf{I}_S+\mathbf{I}_R)$$
$$\mathbf{I}_2 = \mathbf{Q}_{s_2}\mathbf{I}_R$$

5.4. Response of the UPFC Model

The capability of the UPFC to control active and reactive power flow in the transmission line is given by a family of P-Q control circular regions defined by the transmission angle δ ($0° \leq \delta \leq 90°$), the magnitude of V_{pq} and its phase angle ρ ($0° \leq \rho \leq 360°$). These P-Q regions are well explained in [8]. In this section, the P-Q regions are reproduced using the proposed UPFC model. It should be noted that this model is more general in the sense that it produces harmonic information.

The system of Figure 5.2 was used to show the response of the UPFC. The following data is used in the analysis:

Sources: Ideal voltages sources, $V_S = 1\angle 0°$ p.u., $V_R = 1\angle -\delta$ p.u.

Transmission system: Reactance $X = 1\,\Omega$.

Transformers: Equivalent series reactance: $X_e = 0.01\,\Omega$.

VSCs: Multi-module PWM converter (Appendix A), with 3 converters connected in cascade, and a carrier frequency of 250 Hz. Modulation factor of 0.95.

Capacitor: $3\,\mu$F charged at 0.5263 p.u. in order to have $V_{pq} = 0.5\angle\rho$ p.u. in the VSC 2 output.

Simulation: 15 harmonics were used, and the angles were varied in the range, $0° \leq \delta \leq 90°$ and $0° \leq \rho \leq 360°$. The results are shown only for phase *a*. It should be noted that the angle ρ corresponds to the output voltage angle of VSC 2, where the steady-state condition of the UPFC corresponds to the steady-state condition in the capacitor, determined by using the iterative scheme shown in Appendix C.

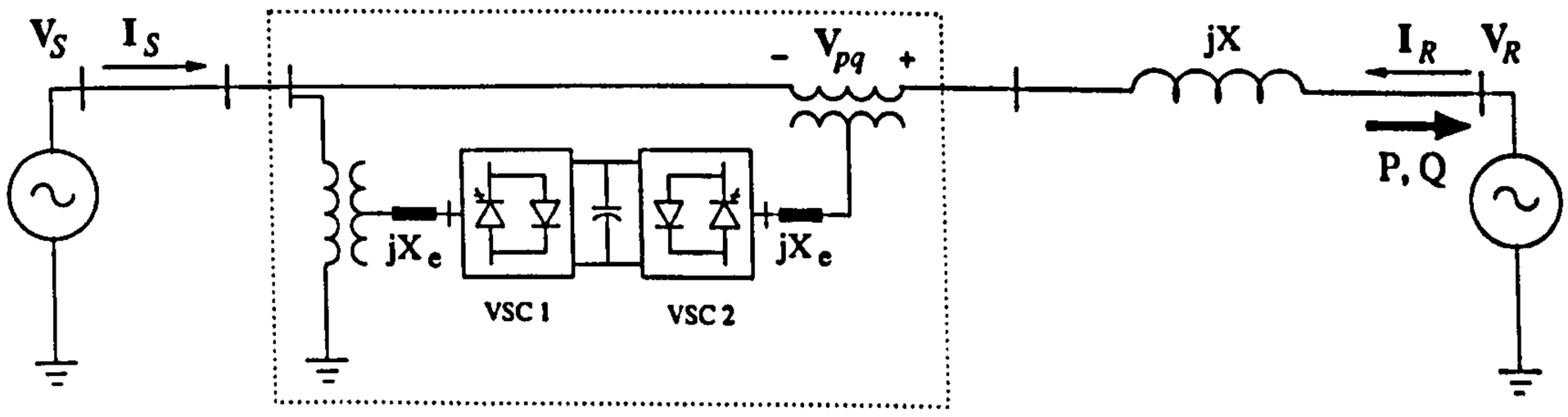

Figure 5.2.: Transmission system with an UPFC

Figure 5.3 shows the UPFC power control regions at fundamental frequency. This result illustrates very clearly the capability of the UPFC to control active and reactive power. This point is well described in [8] and the results presented are in good agreement with the response of the proposed model.

Figure 5.4 show the harmonic distortion at the sending-end of the UPFC. It can be seen that the THD voltage is higher when $\rho = 180°$. This effect is due to the fact that the sending-end

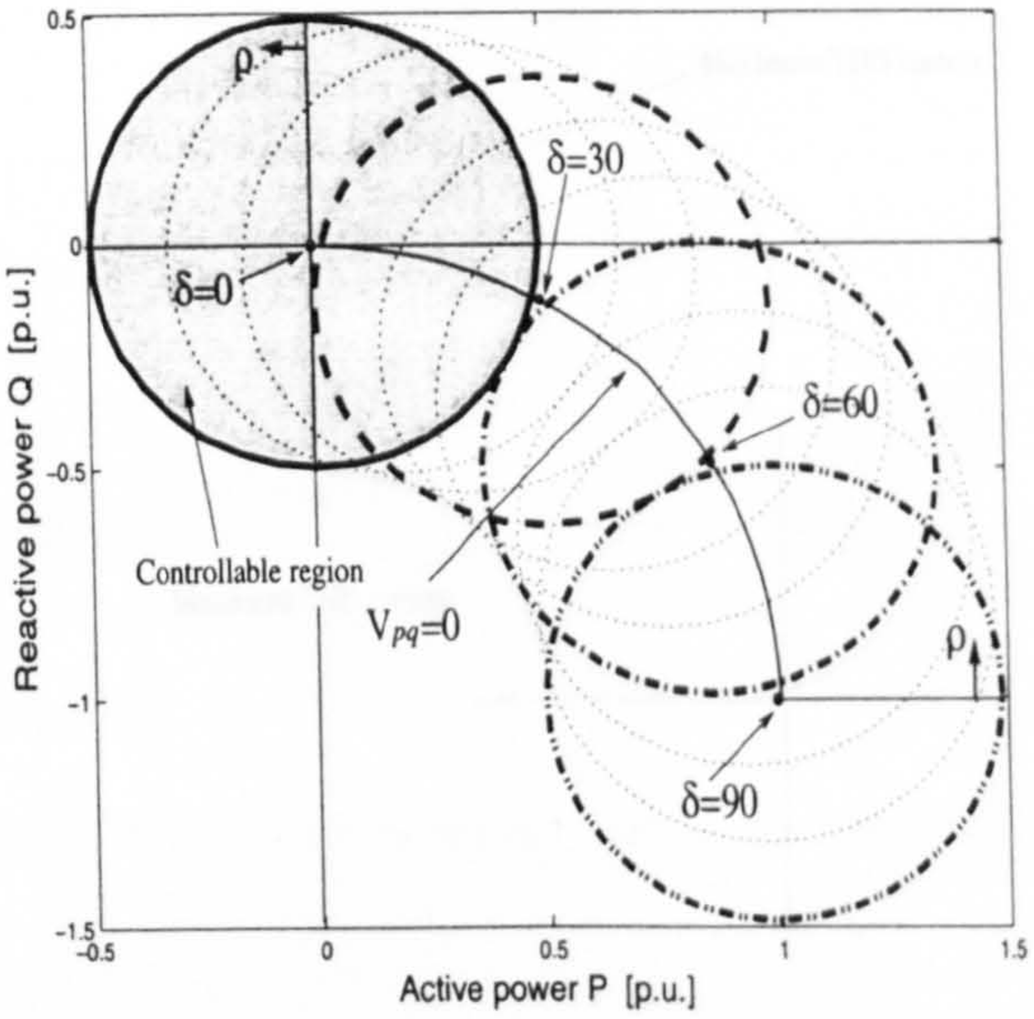

Figure 5.3.: Control region at the receiving-end of the reactance X

voltage $v_s(t) + v_{pq}(t)$ at fundamental frequency is minimum when V_{pq} is shifted by $\rho = 180°$ with respect to V_s. The maximum THD voltage may be expressed in a maximum THD voltage region as shown in Figure 5.5. In contrast, the THD current in Figure 5.4(b) shows its maximum THD at the co-ordinate ($\delta = 30°$, $\rho = 110°$) which corresponds to the operating point when transferred apparent power is minimum ($P \approx 0$, $Q \approx 0$), also shown in Figure 5.5.

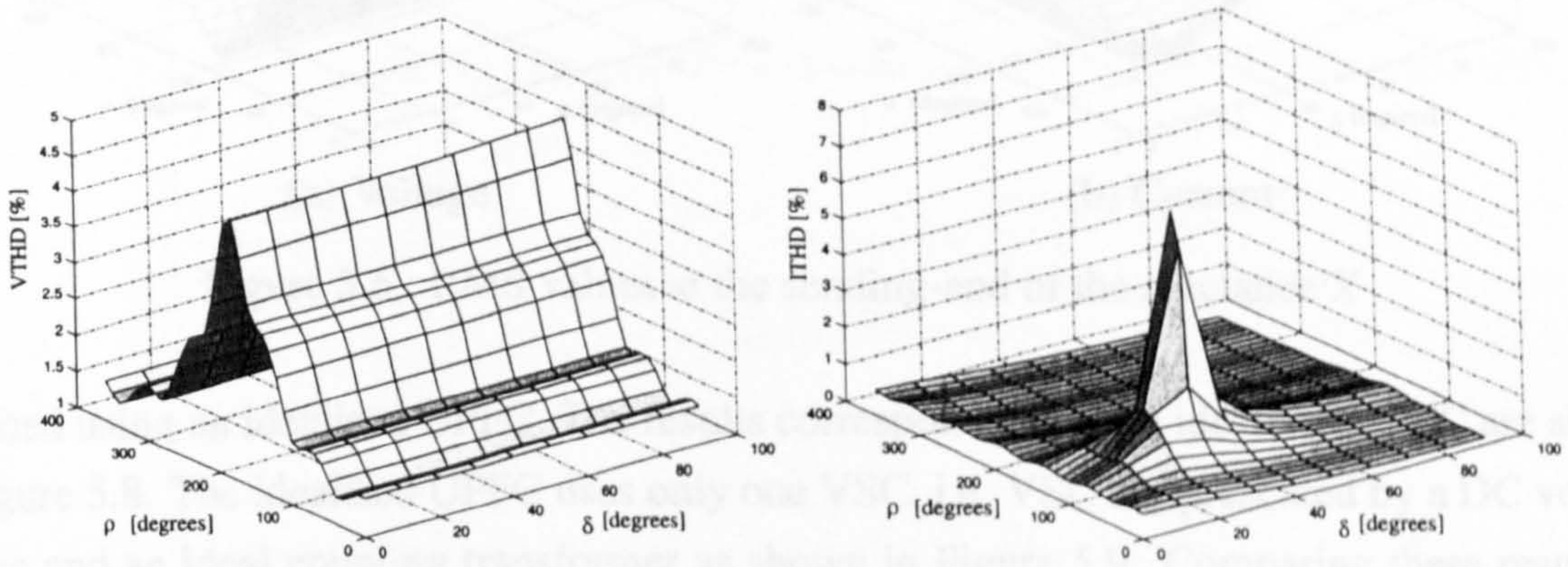

(a) Voltage (b) Current

Figure 5.4.: THD at the sending-end of the reactance X

Figure 5.6 shows the RMS values, where the minimum values correspond to the maximum THD values.

To assess the UPFC under more realistic conditions, the transmission reactance is substituted by a 10 km transmission line with the following parameters: $R' = 0.04\,\Omega$/km, $L' = 1.20$ mH/km, $C' = 8.40\,\mu$F/km and $G' = 0.03\,\mu$S/km.

Figure 5.7 shows the harmonic response at the sending-end of the transmission line. The results show the impact that the transmission line has over the UPFC's harmonic behaviour, exemplified here by the voltage and current THDs. These results are not as smooth as those

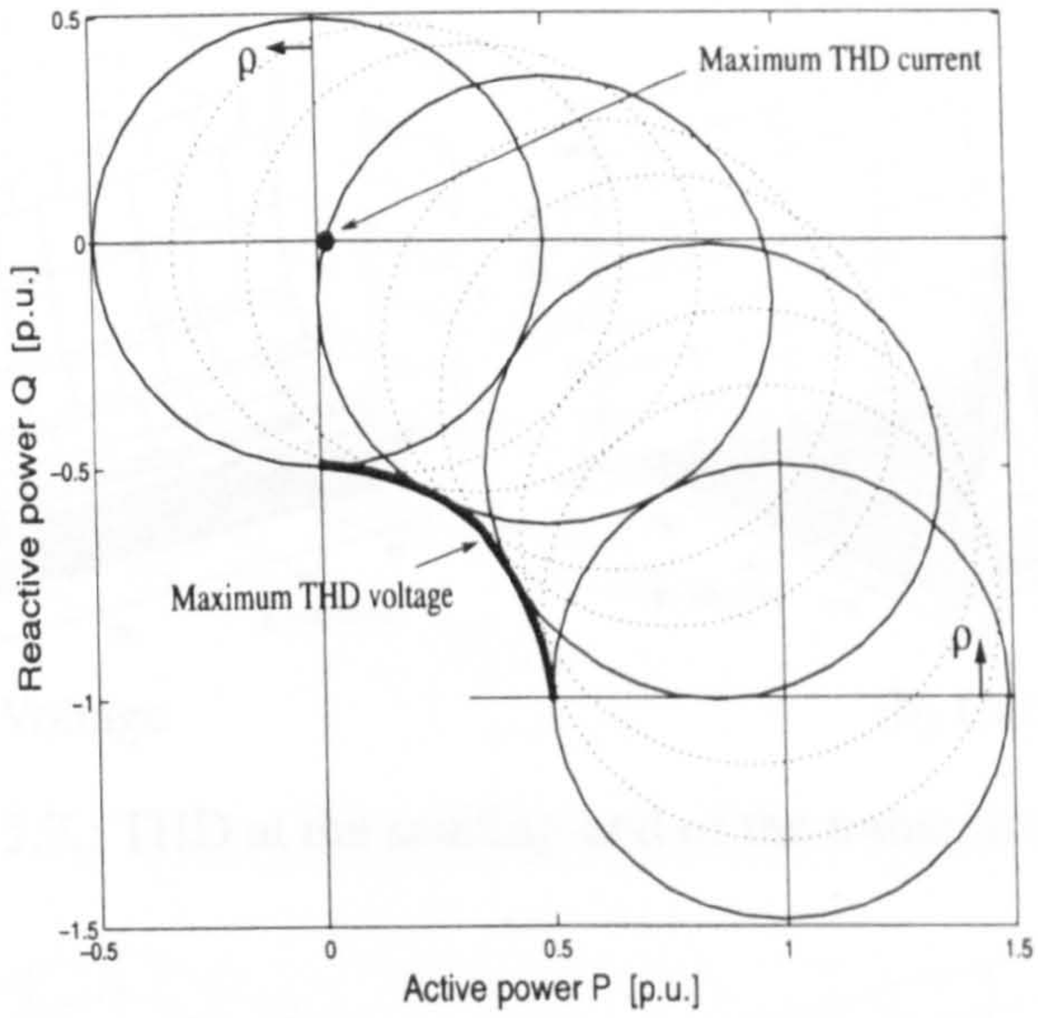

Figure 5.5.: THD regions at the sending-end of the reactance X

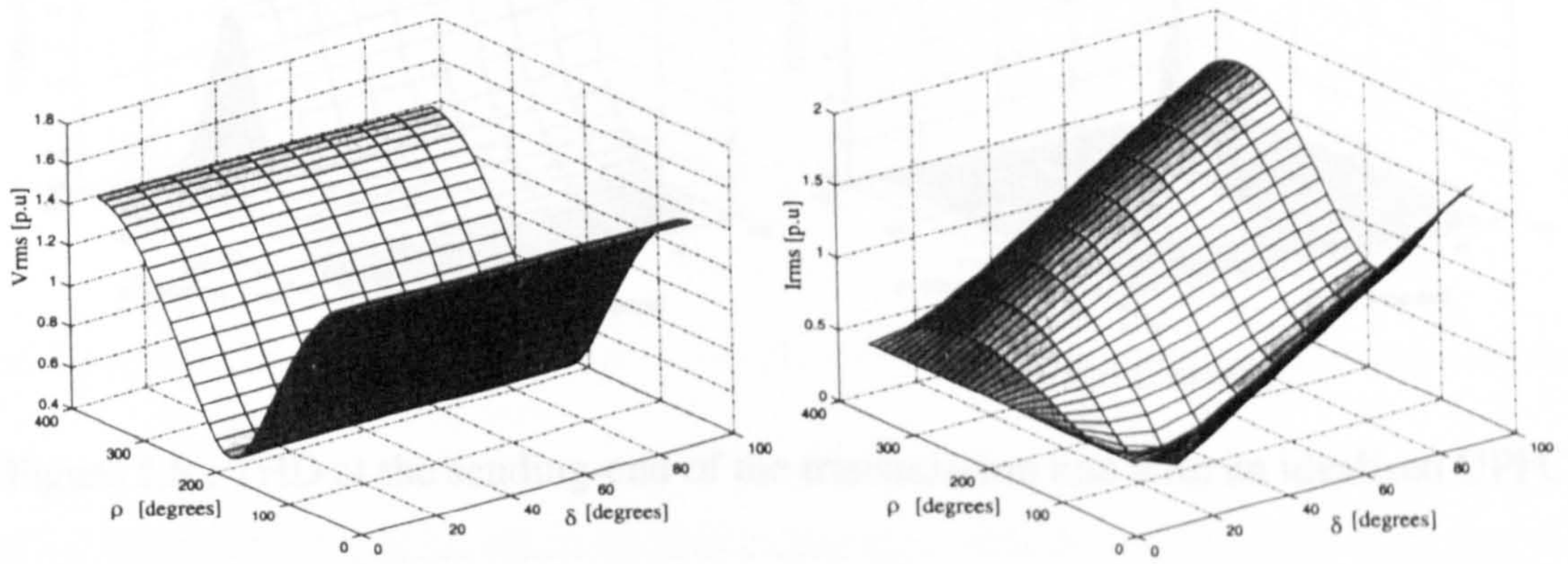

(a) Voltage (b) Current

Figure 5.6.: RMS values at the sending-end of the reactance X

obtained using an idealised UPFC. The results corresponding to the idealised UPFC are shown in Figure 5.8. The idealised UPFC uses only one VSC, i.e. VSC 2 represented by a DC voltage source and an ideal coupling transformer as shown in Figure 5.9. Comparing these results, it can be seen that the effect of VSC 1 and the DC capacitor, which interact with the transmission line, increase the THD in both voltage and current.

5.4.1. Case study: Resonance analysis

As discussed, the interaction between the UPFC and the transmission line may produce voltage and current resonances. In order to gain further insight into resonance build up in UPFC-transmission line systems, the following study was conducted.

Figure 5.10 shows the contours of the resonance points of the transmission line as a function of line length and harmonic frequencies. For a 17 km long transmission line, resonance points appears at the 18th, 23th, 29th, 35th and 41th harmonic frequencies.

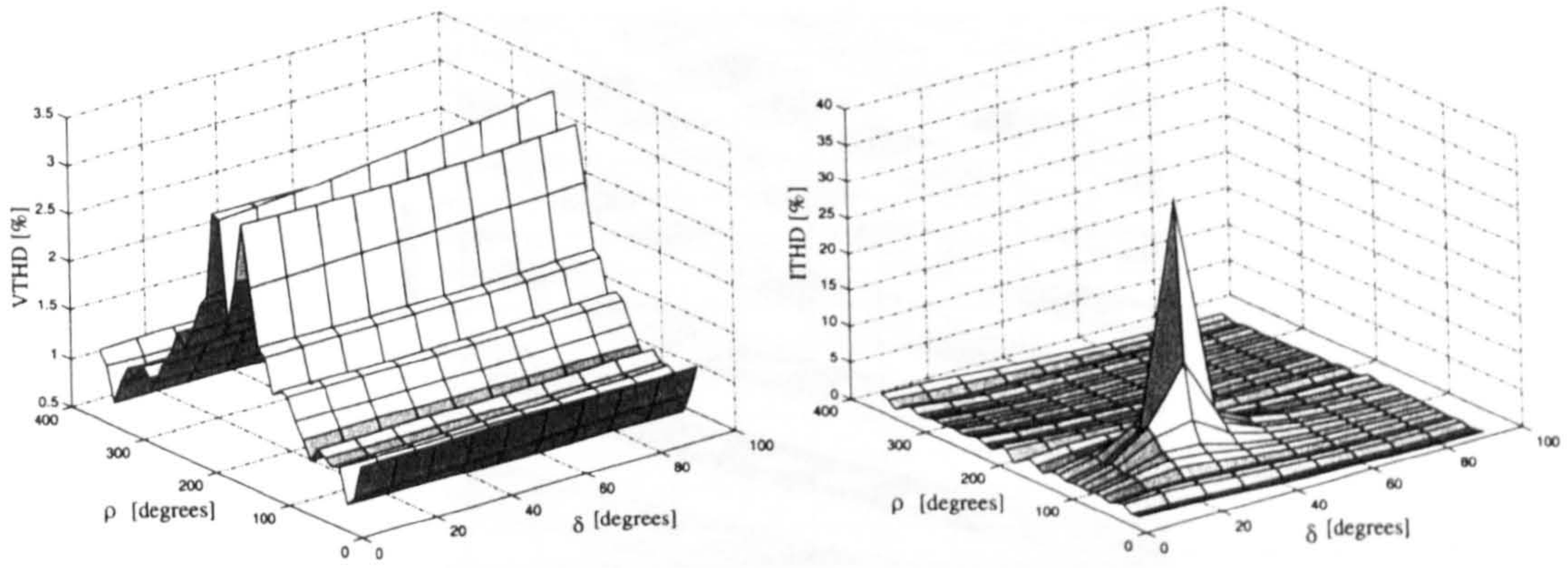

(a) Voltage (b) Current

Figure 5.7.: THD at the sending-end of the transmission line

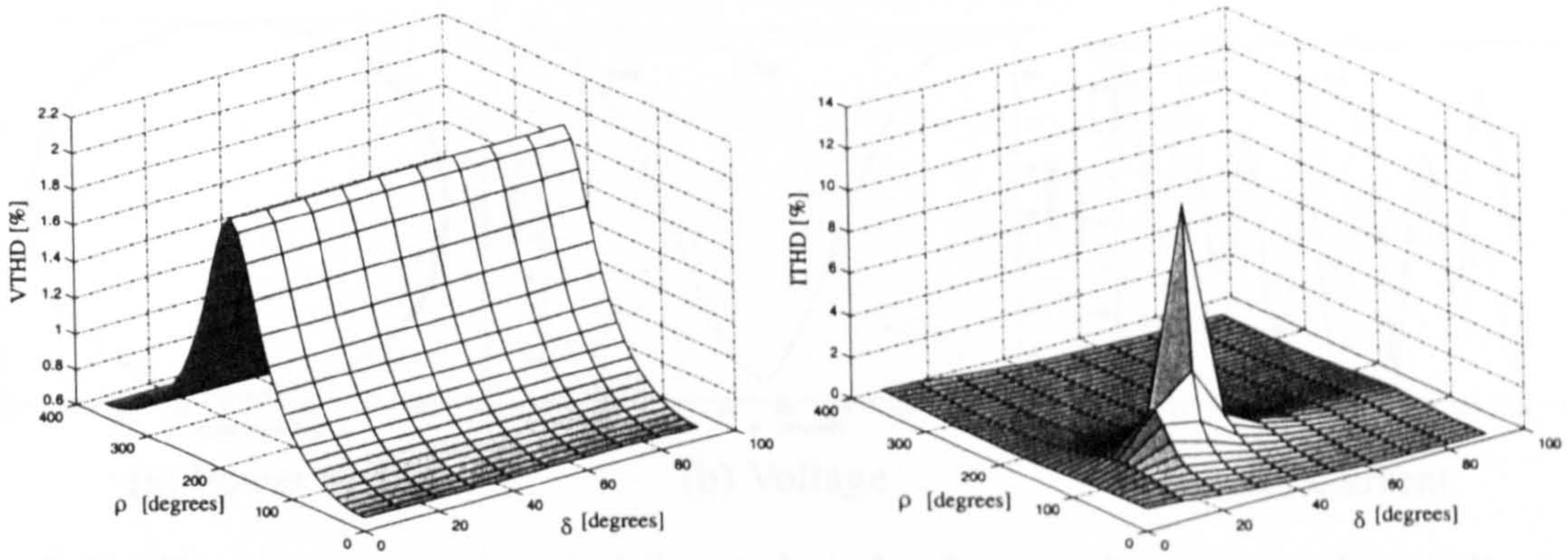

(a) Voltage (b) Current

Figure 5.8.: THD at the sending-end of the transmission line with an idealised UPFC

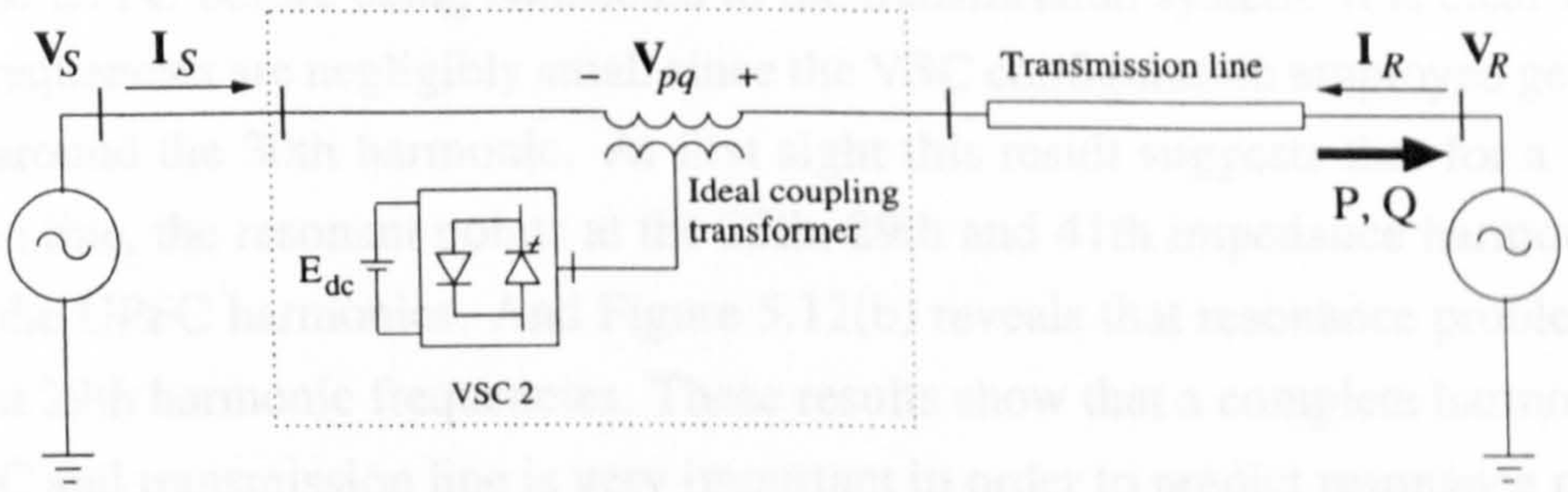

Figure 5.9.: Idealised UPFC scheme

Figure 5.11(a) shows the power region at the receiving-end of the transmission system using $\delta = 0°$. 50 harmonics were used in the study and a 17 km transmission line. The response is the expected one.

Figure 5.11(b) and (c) show the RMS and THD values for the voltage and current at the receiving-end of the transmission line. The RMS voltage gives the expected results, but the THD is very high due to a resonance effect. In the RMS and THD current is clear that a resonance condition exist in the system.

Figure 5.12 shows a fuller analysis of the results. Figure 5.12(a) shows the harmonic gen-

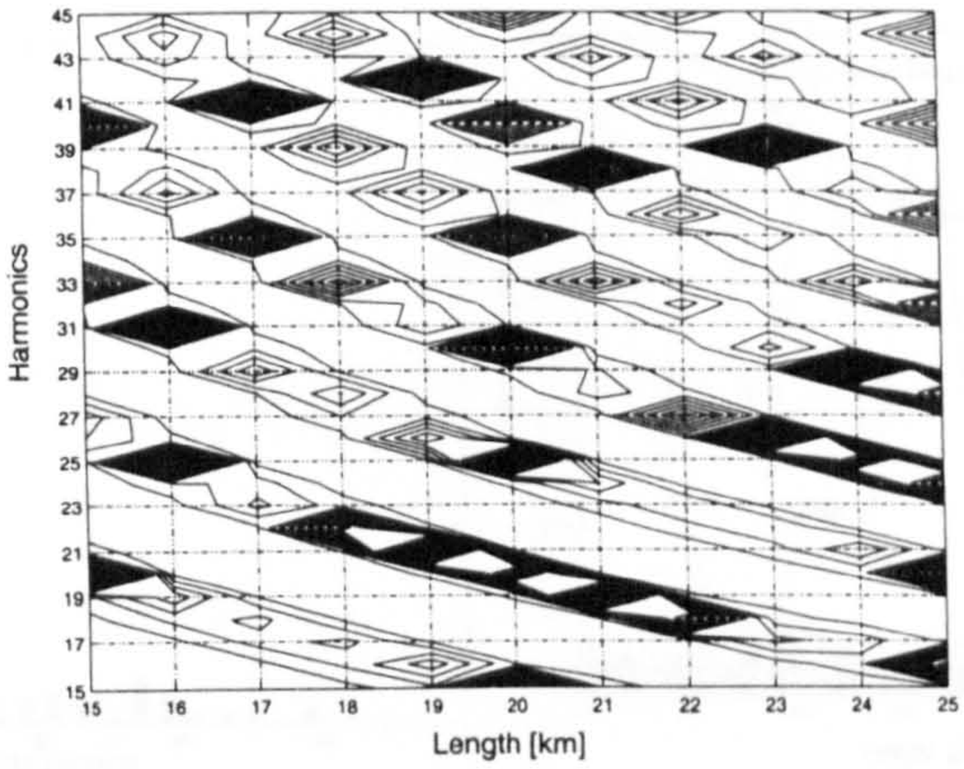

Figure 5.10.: Transmission line impedance response contours

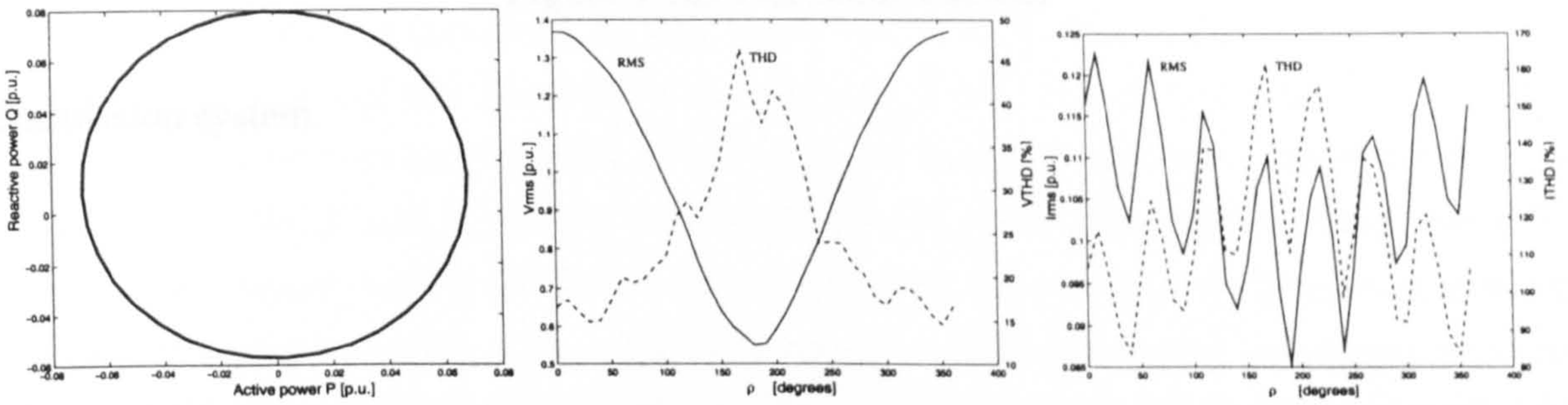

(a) Power region (b) Voltage (c) Current

Figure 5.11.: Power region at the receiving-end, and voltage and current at the sending-end of the transmission line

erated by the UPFC before being connected to the transmission system. It is clear that the low harmonic frequencies are negligibly small since the VSC configuration employed generates harmonics of around the 30th harmonic. At first sight this result suggests that for a 17 km long transmission line, the resonant points at the 23th, 29th and 41th impedance harmonics may be excited by the UPFC harmonics. And Figure 5.12(b) reveals that resonance problems occur at the 23th and 29th harmonic frequencies. These results show that a complete harmonic analysis of the UPFC and transmission line is very important in order to predict resonance problems.

5.5. Conclusions

The UPFC model for harmonic analysis was presented in this chapter. The UPFC model was derived as a particular connection of an HVDC-VSC back-to-back with the transmission system. It has been shown that the high harmonic frequencies generated by the VSCs can excite the resonance impedances of the transmission line connected at the terminals of the UPFC. Also, it was shown that a simplified UPFC model, given by a constant AC harmonic source connected in series with the transmission system, is not appropriate for harmonic interaction studies between the transmission system and the UPFC, since the capacitor in the DC link interacts with the

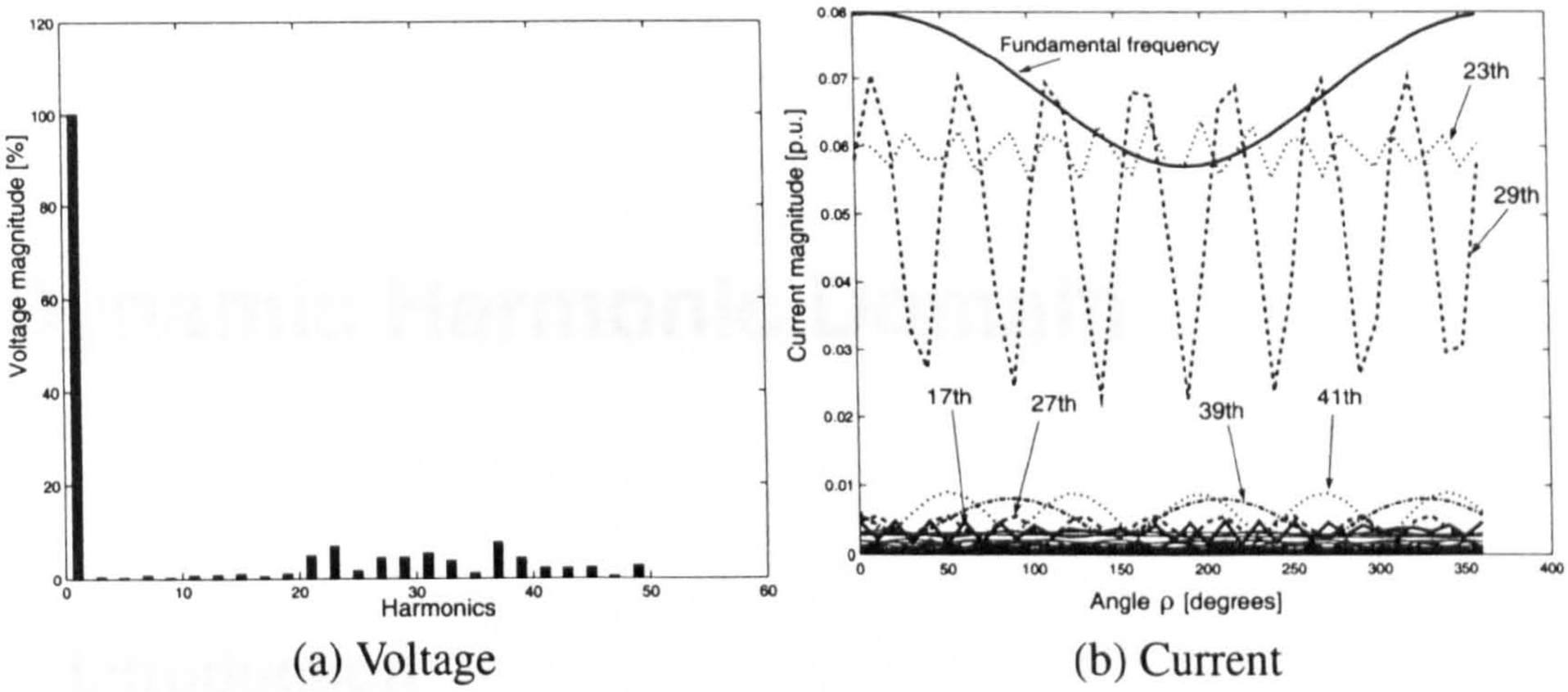

(a) Voltage (b) Current

Figure 5.12.: Harmonic content

transmission system.

6. Dynamic Harmonic Domain

6.1. Introduction

A novel methodology is presented in this chapter for conducting transient analysis of electric networks containing non-linearities and switching plant components. The methodology is termed the extended harmonic domain (EHD) as it may be seen as an extension of the harmonic domain (HD) method used for steady-state analysis in the previous chapters of this thesis. It is shown in the chapter that the EHD is a natural approach for conducting dynamic and steady-state studies of the evolution of harmonics in power circuits containing non-linear and time-varying components. It is also shown that the EHD provides a suitable basis for extending the well-known steady-state power quality indices to the transient range.

The EHD is a formulation based on orthogonal bases and operational matrices. The new approach leads to an alternative state-space. In this simulation environment the coefficients of the orthogonal basis are the state variables. The solution process allows for the computation of the time evolution of the harmonic coefficients, in a manner that is akin to a window of incremental length sliding over the actual waveform. One salient characteristic of the EHD method is that linear time periodic (LTP) systems are easily reduced to linear time invariant (LTI) systems, opening the door for the use of a wide range of tools and methods readily available for the solution of LTP systems.

6.2. Approximation of Operators

The main idea behind the approximation of operators is that a function $x(\tau)$, can be approximated in the interval $[t, t+T_0]$, to an arbitrary accuracy, by the time-dependent Fourier series [51][52],

$$x(\tau) = \sum_{n=-\infty}^{\infty} X_n(t) e^{jn\omega_0\tau} \tag{6.1}$$

where $\omega_0 = 2\pi/T_0$, $\tau \in [t, t+T_0]$, and T_0 is the period of time under consideration. The coefficients in $X_n(t)$ are a function of time since the period T_0 under consideration slides over the actual waveform. Each coefficient $X_n(t)$, is calculated by

$$X_n(t) = \frac{1}{T_0}\int_t^{t+T_0} x(\tau)e^{-jn\omega_0\tau}d\tau \tag{6.2}$$

Equation (6.2) computes the time-evolution of the harmonics as the window of length T_0 slides over the actual waveform $x(\tau)$.

6.2.1. Averaging methods

The averaging theory has shown to be an efficient method to obtain averaged models used for the analysis and control design of PWM switching DC/DC power converters [50]. A more general method called the generalized averaging method [51], has been put forward to cover some limitations that traditional state-space averaging methods present. The generalized averaging method is based on the time-dependent Fourier series expressed by equations (6.1) and (6.2). The assumption in this method is that a Fourier series expansion of a finite length segment of a circuit waveform $x(\tau)$ should be dominated by its dc-term. This means that the averaged model of the ripple is given by the dc-term of (6.1), i.e.

$$X_0(t) = \frac{1}{T_0}\int_t^{t+T_0} x(\tau)d\tau \tag{6.3}$$

where T_0 is the converter switching period. As a continuation of the work reported in [51], a multi-frequency averaging method [109] uses the dc-term and first-term of the series (6.1) increasing the accuracy of the averaging method. Most of the applications of the averaging methods can be found on DC converter applications [94]. A technique called dynamic phasors, based on the generalized averaging method, has been applied to obtain AC power elements and FACTS controllers models used for stability and fault analysis [53][54].

In this chapter, the harmonic domain (explained in Appendix B) is extended to incorporate the time-dependent Fourier series expressed by equations (6.1) and (6.2) and the state-space representation of linear, time periodic systems [52]. The new harmonic domain is termed EHD. A general characteristic of the the EHD is that it embraces the averaging methods described above, but extended to provide a dynamic, harmonic frame-of-reference where all the power electronics controller models described in this thesis can be represented, as well as the HD models described in the open literature [13].

6.3. Extended Harmonic Domain

Following a similar analysis as that described in Appendix B, if the vector of base functions $\mathbf{G}(\tau)$ is used then the function in (6.1) can be approximated as

$$x(\tau) = \mathbf{G}^T(\tau)\mathbf{X}(t) \tag{6.4}$$

where

$$\mathbf{G}(\tau) = \begin{bmatrix} e^{-jh\omega_0\tau} \\ \vdots \\ e^{-j\omega_0\tau} \\ 1 \\ e^{j\omega_0\tau} \\ \vdots \\ e^{jh\omega_0\tau} \end{bmatrix} \tag{6.5}$$

and

$$\mathbf{X}(t) = \begin{bmatrix} X_{-h}(t) \\ \vdots \\ X_{-1}(t) \\ X_0(t) \\ X_1(t) \\ \vdots \\ X_h(t) \end{bmatrix} \tag{6.6}$$

The derivative of $x(\tau)$ with respect to time is given by

$$\dot{x}(\tau) = \dot{\mathbf{G}}^T(\tau)\mathbf{X}(t) + \mathbf{G}^T(\tau)\dot{\mathbf{X}}(t)$$

where the derivative of $\mathbf{G}(\tau)$ with respect to time is given by

$$\dot{\mathbf{G}}^T(\tau) = \mathbf{G}^T(\tau)\mathbf{D}(jh\omega_0)$$

The operational matrix of differentiation $\mathbf{D}(jh\omega_0)$ has been defined in (B.11).

The product of two functions is given as

$$a(\tau)x(\tau) = \mathbf{G}^T(\tau)\mathbf{A}\mathbf{X}(t) \tag{6.7}$$

where matrix $\mathbf{A}$ has a Toeplitz structure, and it is build up with the harmonic content of $a(\tau)$,

$$\mathbf{A} = \begin{bmatrix} A_0 & A_{-1} & \cdots & A_{-h} & & & \\ A_1 & \ddots & \ddots & \ddots & \ddots & & \\ \vdots & \ddots & A_0 & A_{-1} & \ddots & \ddots & \\ A_h & \ddots & A_1 & A_0 & A_{-1} & \ddots & A_{-h} \\ & \ddots & \ddots & A_1 & A_0 & \ddots & \vdots \\ & & \ddots & \ddots & \ddots & \ddots & A_{-1} \\ & & & A_h & \cdots & A_1 & A_0 \end{bmatrix}$$

This matrix has the same structure as (B.16).

6.3.1. State-space model

In principle, the time periodic excitation and response associated with physical circuits can be expressed by the sum of a number of sinusoid terms of different harmonic frequencies. This is a property that facilitates the understanding and calculation of such circuits operating under a wide range of operating conditions. From an engineering viewpoint, it makes sense to develop numerical procedures that exploit this property.

In power electronic devices a periodic driving force causes the switching sequences to also be periodic at each operating point. This opens the possibility of switching devices being thought of as being linear between two consecutive switching times and piece-wise linear within a period, giving rise to a system that is indeed linear and time periodic.

For simplicity, consider a first-order state-space model,

$$\begin{aligned} \dot{x}(t) &= a(t)x(t) + b(t)u(t) \\ y(t) &= c(t)x(t) + d(t)u(t) \end{aligned} \tag{6.8}$$

where $a(t)$, $b(t)$, $c(t)$ and $d(t)$ have a period T_0, e.g. $a(t) = a(t+T_0)$.

The period will be assumed to be T_0 throughout. Therefore, equation (6.8) may be referred to as a LTP system.

Using the terminology described in Section 6.2, equation (6.8) is amenable to an alternative representation, which is more useful for assessing system properties,

$$\mathbf{G}^{\mathrm{T}}(t)\mathbf{D}(\mathrm{j}h\omega_0)\mathbf{X}(t) + \mathbf{G}^{\mathrm{T}}(t)\dot{\mathbf{X}}(t) = \mathbf{G}^{\mathrm{T}}(t)\mathbf{A}\mathbf{X}(t) + \mathbf{G}^{\mathrm{T}}(t)\mathbf{B}\mathbf{U} \tag{6.9}$$

$$\mathbf{G}^{\mathrm{T}}(t)\mathbf{Y}(t) = \mathbf{G}^{\mathrm{T}}(t)\mathbf{C}\mathbf{X}(t)+\mathbf{G}^{\mathrm{T}}(t)\mathbf{D}\mathbf{U}$$

Dropping the $\mathbf{G}^{\mathrm{T}}(t)$ coefficients yields a more compact state-space equation,

$$\begin{aligned}\dot{\mathbf{X}}(t) &= \{\mathbf{A}-\mathbf{D}(\mathrm{j}h\omega_0)\}\mathbf{X}(t)+\mathbf{B}\mathbf{U}\\ \mathbf{Y}(t) &= \mathbf{C}\mathbf{X}(t)+\mathbf{D}\mathbf{U}\end{aligned} \tag{6.10}$$

These equations are the core equations of the EHD methodology whose solution gives full information of the harmonic dynamic behaviour of variables $x(t)$ and $y(t)$.

Equation (6.10) is solved using a standard integration method where initial and final simulation times, t_0 and t_f, integration time step Δt and initial conditions for the state variable $\mathbf{X}(t)$ are required. Matrices **A, B, C, D** and vector **U** are constant within a time step Δt, as long as the functions $a(t)$, $b(t)$, $c(t)$, $d(t)$ and $u(t)$ do not change in magnitude and frequency in the time step. These matrices take complex entries, and the solution vectors $\mathbf{X}(t)$ and $\mathbf{Y}(t)$ are complex vectors which evolve with time, changing at every time step Δt.

6.3.2. Harmonic domain

A particular case of (6.10) is the set of equations which govern the system's steady-state solution, i.e. when $\dot{\mathbf{X}}(t) = 0$ (see Appendix B),

$$\mathbf{X} = \{\mathbf{D}(\mathrm{j}h\omega_0)-\mathbf{A}\}^{-1}\mathbf{B}\mathbf{U} \tag{6.11}$$

$$\mathbf{Y} = \mathbf{C}\mathbf{X}+\mathbf{D}\mathbf{U} \tag{6.12}$$

In steady-state applications, the matrices **A, B, C, D** and vector **U** are constant, and the solution of **X** and **Y** is carried out directly using equation (6.11). Moreover, a very useful characteristic of equation (6.11) is that it is amenable to a very powerful method for EHD initialisation. Equation (6.11) was also derived in [37] to obtain the steady-state solution of switching loads.

This is a very useful, inherent characteristic in EHD since initialisation methods are not straightforward to implement in time domain methodologies. For example, it has been reported [36] that no full initialisation method has yet been implemented in any of the EMTP-type programs for solving systems with switching devices and non-linear components. Instead, simple constrained solutions are used. For instance one option is to perform an approximate steady-state solution with non-linear branches disconnected or represented by linearised models. Alternatively, some EMTPs have either a "snapshot" or a "start again" feature. Using a standard EMTP solution, a snapshot is taken and saved once the system reaches the steady-state, subse-

quent runs are started using this information.

6.4. Dynamic Harmonic Evolution using EHD

The three-phase balanced circuit of Figure 6.1 is used to show how harmonics evolve with time. The voltage source has the following representation: $v_a(t) = \sin t + 1/3 \sin 3t$ V, $v_b(t) = \sin(t-120°) + 1/3 \sin 3t$ V, $v_c(t) = \sin(t+120°) + 1/3 \sin 3t$ V, with period $T_0 = 2\pi$; parameters $R = 1\,\Omega$ and $L = 1$ H; and initial currents 1, -2 and 0 A in the inductors, respectively.

In this section, a tuned filter in series with the neutral is used to separate the DC component from the 3rd harmonic when time domain simulations are carried out using PSCAD/EMTDC.

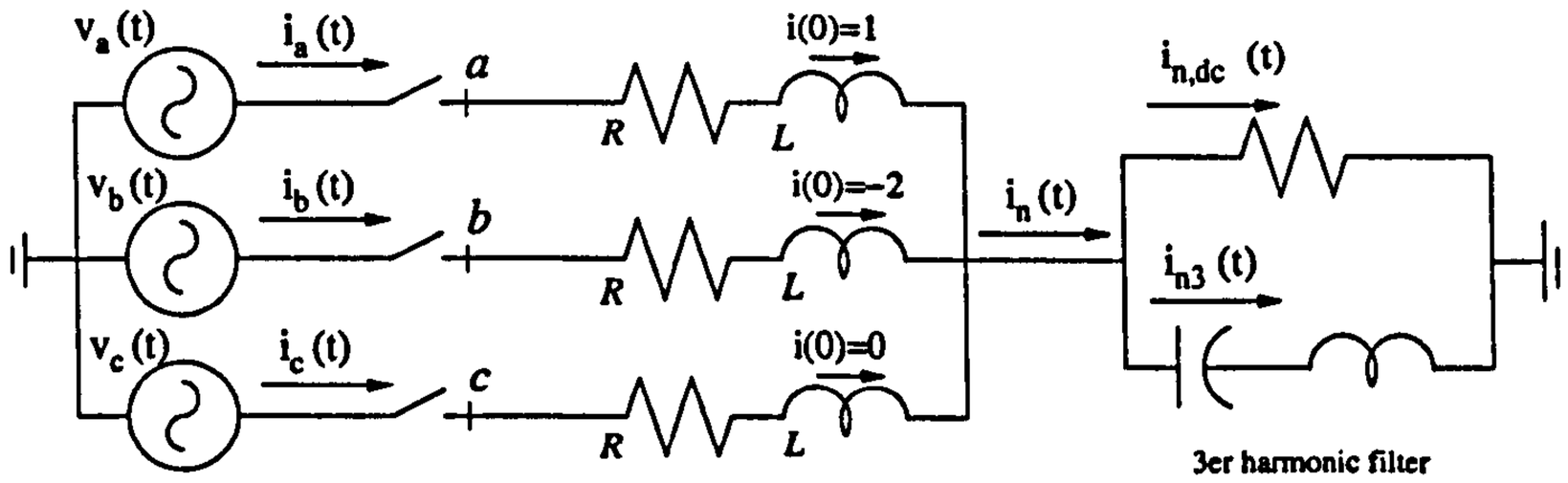

Figure 6.1.: Circuit implemented in PSCAD/EMTDC

The state-space equation that describes the circuit of Figure 6.1, with no filter, is given by,

$$\begin{bmatrix} \dot{i}_a(t) \\ \dot{i}_b(t) \\ \dot{i}_c(t) \end{bmatrix} = -\begin{bmatrix} \frac{R}{L} & 0 & 0 \\ 0 & \frac{R}{L} & 0 \\ 0 & 0 & \frac{R}{L} \end{bmatrix} \begin{bmatrix} i_a(t) \\ i_b(t) \\ i_c(t) \end{bmatrix} + \frac{1}{L} \begin{bmatrix} v_a(t) \\ v_b(t) \\ v_c(t) \end{bmatrix} \tag{6.13}$$

where the variable of interest is the ground current $i_n(t) = i_a(t) + i_b(t) + i_c(t)$.

Equation (6.13) is expressed in EHD by

$$\begin{bmatrix} \dot{\mathbf{I}}_a(t) \\ \dot{\mathbf{I}}_b(t) \\ \dot{\mathbf{I}}c(t) \end{bmatrix} = -\begin{bmatrix} \frac{R}{L}\mathbf{U}_\mathrm{I} + \mathbf{D}(\mathrm{j}h\omega_0) & 0 & 0 \\ 0 & \frac{R}{L}\mathbf{U}_\mathrm{I} + \mathbf{D}(\mathrm{j}h\omega_0) & 0 \\ 0 & 0 & \frac{R}{L}\mathbf{U}_\mathrm{I} + \mathbf{D}(\mathrm{j}h\omega_0) \end{bmatrix} \begin{bmatrix} \mathbf{I}_a(t) \\ \mathbf{I}_b(t) \\ \mathbf{I}_c(t) \end{bmatrix}$$
$$+\frac{1}{L} \begin{bmatrix} \mathbf{V}_a \\ \mathbf{V}_b \\ \mathbf{V}_c \end{bmatrix} \tag{6.14}$$

where $\mathbf{U}_\mathrm{I}$ is the identity matrix. Also in this case the variable of interest is $\mathbf{I}_n(t) = \mathbf{I}_a(t) + \mathbf{I}_b(t) + \mathbf{I}_c(t)$.

From (6.14), the vectors $\mathbf{V}_a$, $\mathbf{V}_b$, and $\mathbf{V}_c$ have values different from zero for the fundamental and third harmonic, e.g. for vector $\mathbf{V}_a$ these values are $\pm\mathrm{j}1/2$ and $\pm\mathrm{j}1/6$, respectively. The

initial conditions given to the DC currents in phase a, b and c, i.e. 1, −2 and 0, become entries in the dc-term of the vectors $\mathbf{I}_a(t)$, $\mathbf{I}_b(t)$ and $\mathbf{I}_c(t)$, respectively, i.e.

$$\mathbf{V}_a = \mathrm{j}\begin{bmatrix} 0 \\ \vdots \\ 0 \\ 1/6 \\ 0 \\ 1/2 \\ 0 \\ -1/2 \\ 0 \\ -1/6 \\ 0 \\ \vdots \\ 0 \end{bmatrix};\ \mathbf{I}_a(0) = \begin{bmatrix} 0 \\ \vdots \\ 0 \\ 0 \\ 0 \\ 0 \\ 1 \\ 0 \\ 0 \\ 0 \\ 0 \\ \vdots \\ 0 \end{bmatrix};\ \mathbf{I}_b(0) = \begin{bmatrix} 0 \\ \vdots \\ 0 \\ 0 \\ 0 \\ 0 \\ -2 \\ 0 \\ 0 \\ 0 \\ 0 \\ \vdots \\ 0 \end{bmatrix};\ \mathbf{I}_c(0) = \begin{bmatrix} 0 \\ \vdots \\ 0 \\ 0 \\ 0 \\ 0 \\ 0 \\ 0 \\ 0 \\ 0 \\ 0 \\ \vdots \\ 0 \end{bmatrix}$$

A total simulation time of 25 s with $\Delta t = 10.5$ ms and fifty harmonics were used. Figure 6.2(a) shows the harmonic dynamic behaviour of the magnitude of $\mathbf{I}_n(t)$, where only the dc-term and third harmonic appear. Figure 6.2(b) shows the angles of these harmonics and Figure 6.2(c) shows the time representation.

Figure 6.3 shows simulation results obtained with PSCAD/EMTDC. It should be noted that the time representation of the harmonics obtained with the EHD matches the currents flowing through the tuned filter.

6.4.1. EHD and WFFT comparison

The use of special filters is not the normal way to derive harmonic information from transient waveforms. Instead, windowed FFTs are used [39]. Hence, results from the EHD and a windowed FFT (WFFT) techniques are compared. A windowed technique is illustrated in Figure 6.4(a) where a sliding window of $2\pi/3$ s was used. Figure 6.4(b) shows the magnitude of the harmonics using WFFT and EHD, where the use of the WFFT technique gives rise to a dc-term, 3rd, 6th, 9th and 12th harmonic during the transient, these harmonics are a natural result of the WFFT. Whereas the result provided by the EHD technique only gives rise the dc-term and the 3rd harmonic. Figure 6.4(c) shows the phase angle of the third harmonic.

A different test case corresponds to a disturbance occurring after the neutral current reaches the steady-state. Zero initial conditions and $R = 100\,\Omega$ were selected for this example. A solid phase-to-ground short-circuit occurs in phase a at 15 s of simulation time. Figure 6.5(a) shows the dynamic behaviour of the current $i_n(t)$. For the WFFT technique a sliding window of 2π

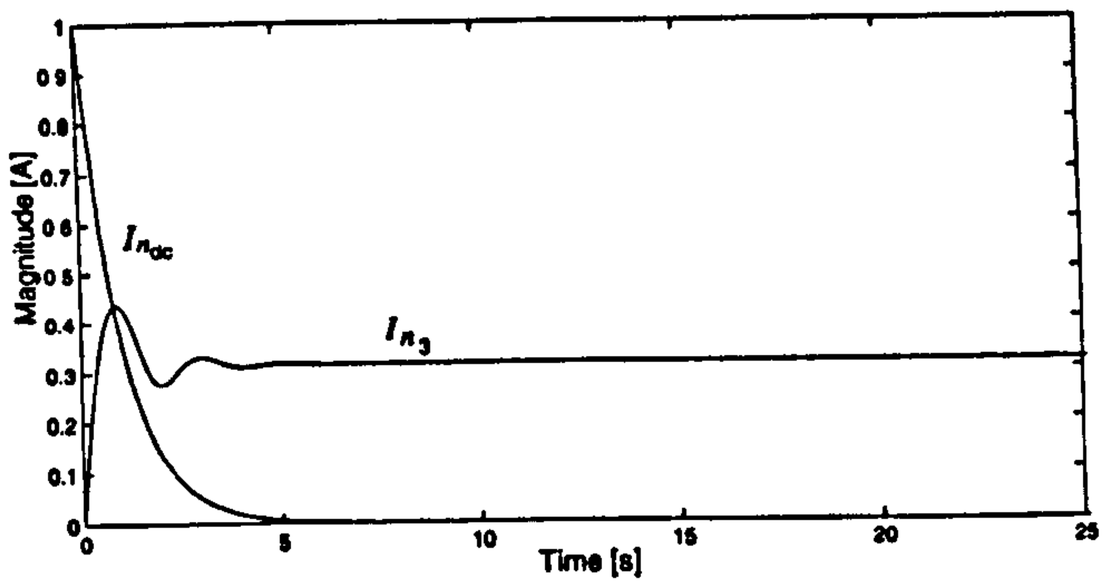

(a) Magnitude of the 3rd harmonic and dc-term

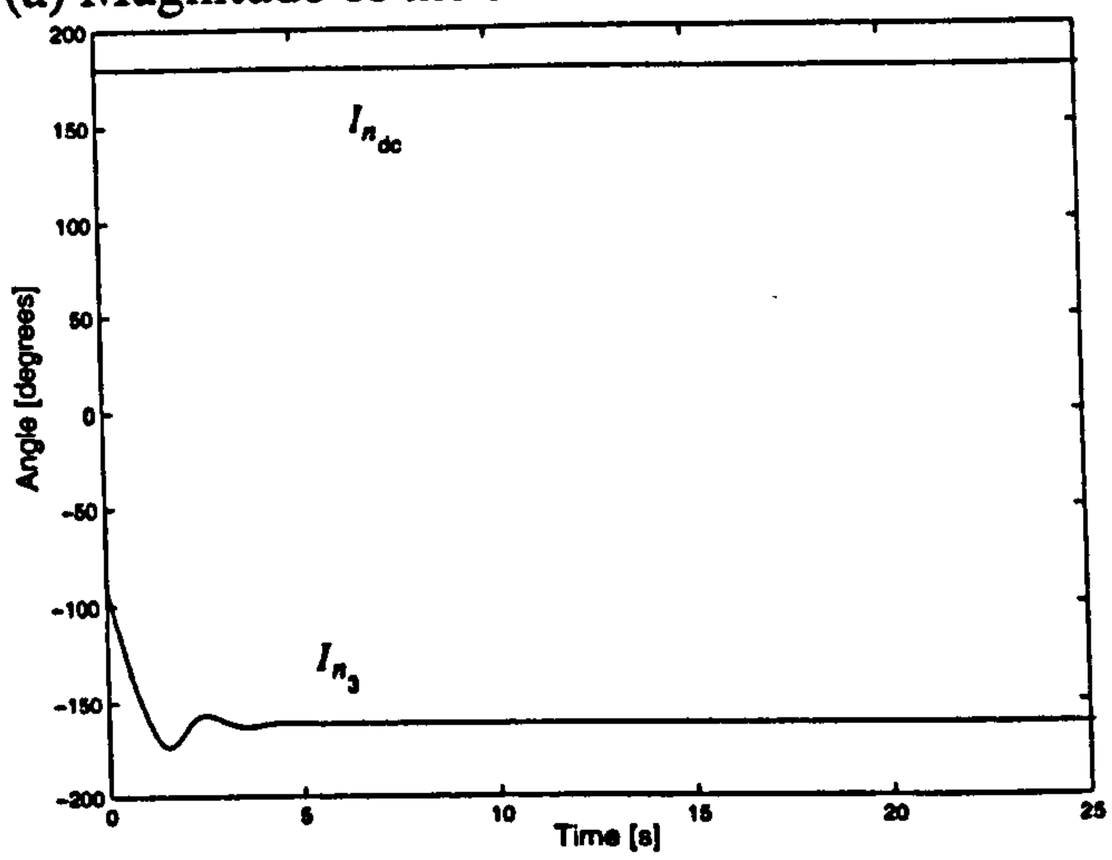

(b) Angle of the 3rd harmonic and dc-term

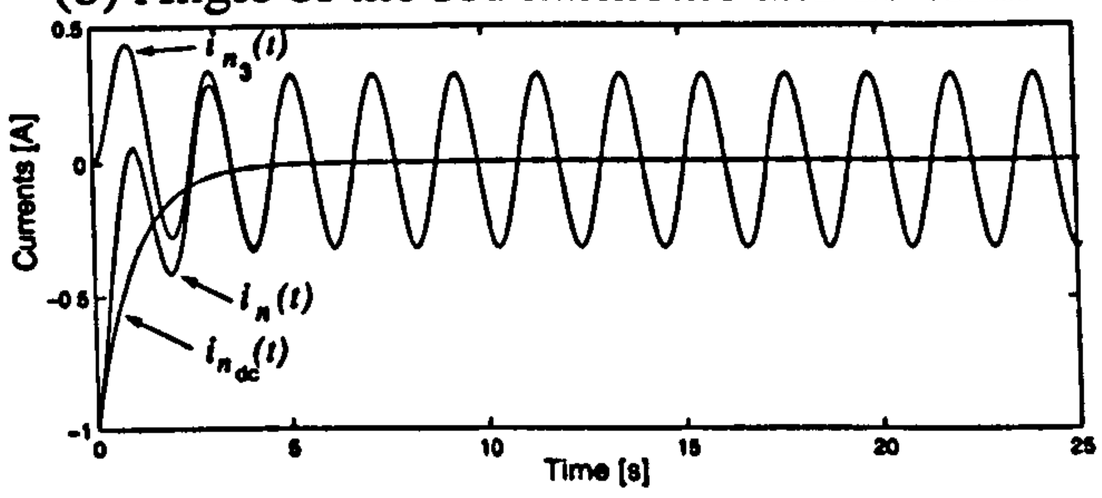

(c) Time representation

Figure 6.2.: Currents in the neutral using the EHD

s was used. The sliding window in Figure 6.5(a) is shifted to the right at each time step. The magnitude of the harmonics using the EHD and those calculated using the WFFT are shown in Figure 6.5(b). Also, Figure 6.5(c) shows the angle of the fundamental frequency and third harmonic.

It should be noted that before the disturbance takes place, i.e. steady-state, the harmonics calculated with the EHD and WFFT techniques are in agreement in both magnitude and phase angle. It should also be noted that in this case only the third harmonic exists in the current $i_n(t)$. After the disturbance takes place, using the EHD only the fundamental and third harmonic appear. It is only after the sliding window does not include the instant of time at which the transient takes place, that the results given by the two methods again match with each other. Judging by the shape of the waveform in Figure 6.5(a) it is clear that the waveform only contains

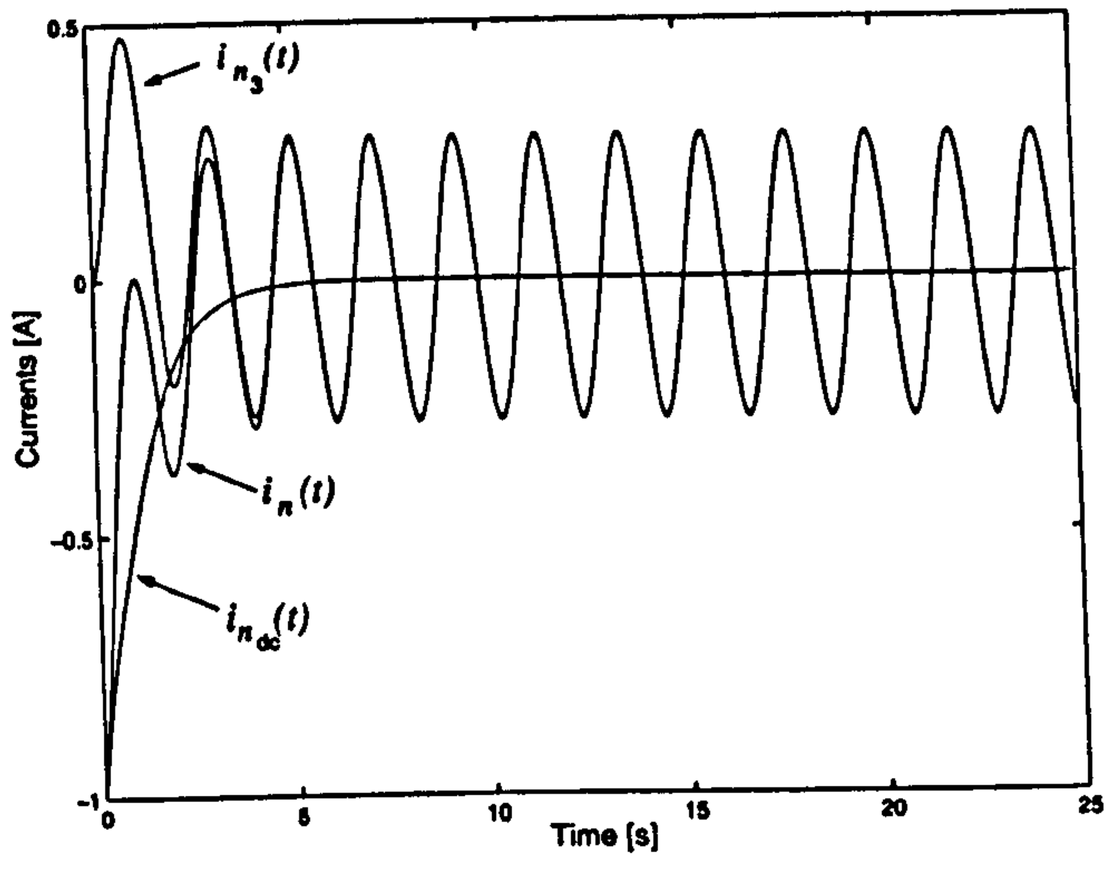

Figure 6.3.: Currents in the neutral using PSCAD/EMTDC

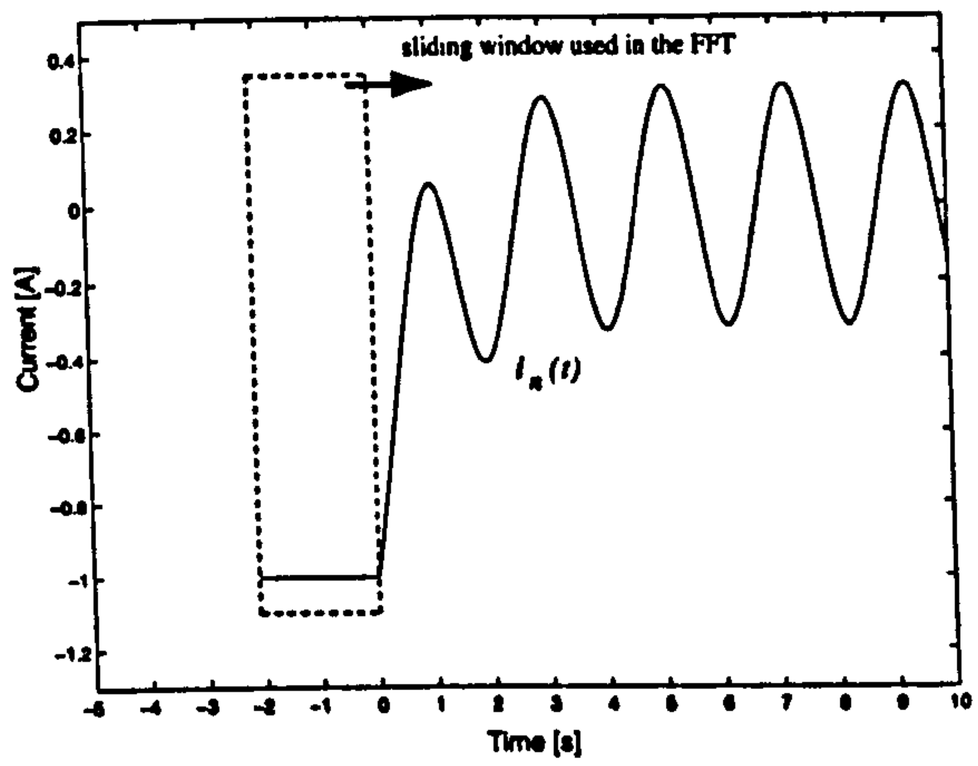

(a) Current waveform

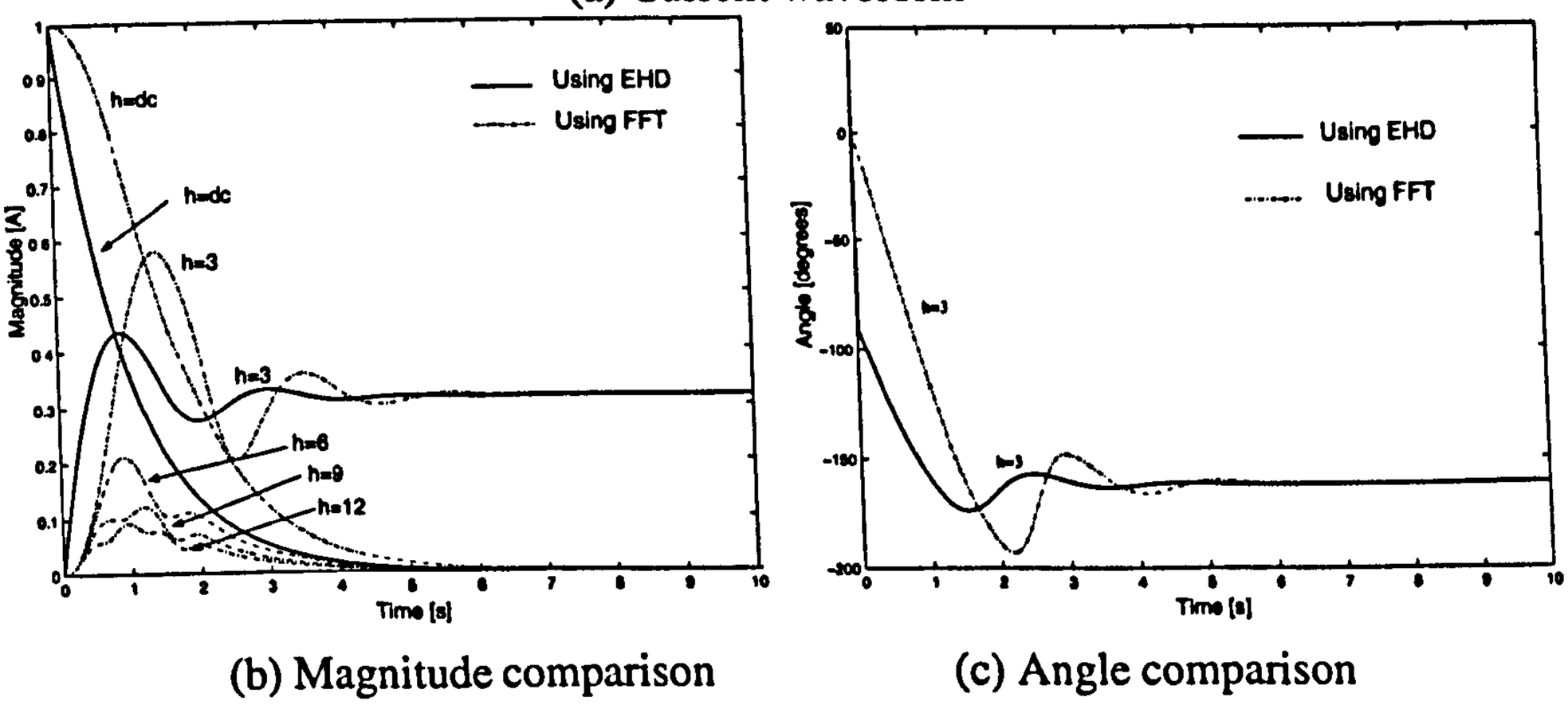

(b) Magnitude comparison (c) Angle comparison

Figure 6.4.: Comparison of the harmonics using WFFT and the EHD

the fundamental and another harmonic, which resembles the third. The EHD confirms this observation but this is not the information conveyed by the WFFT. It is likely that additional refinements in the use of the WFFT method may lead to more accurate results than the ones presented in Figure 6.5(b), but the great difficulties of doing so are well documented [48].

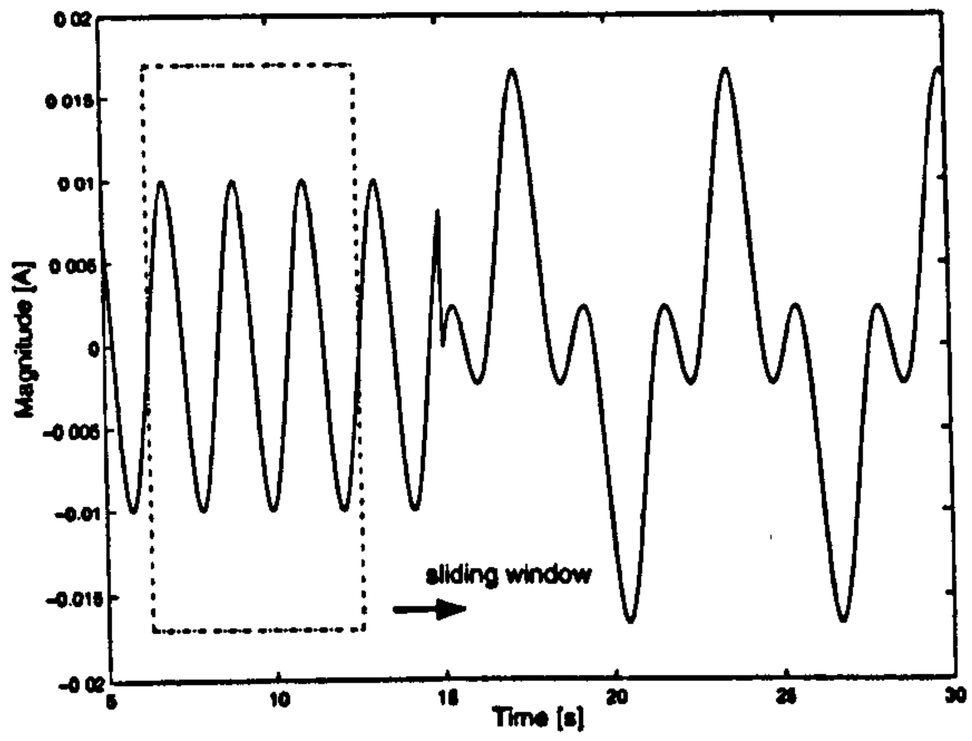

(a) Current waveform

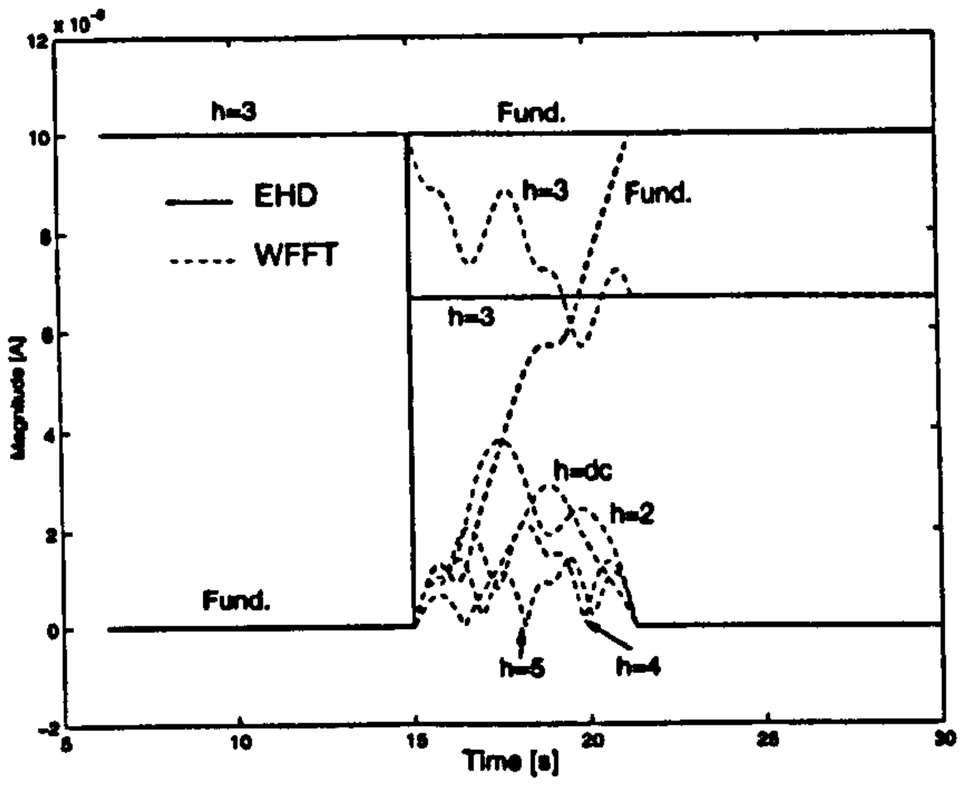

(b) Magnitude comparison

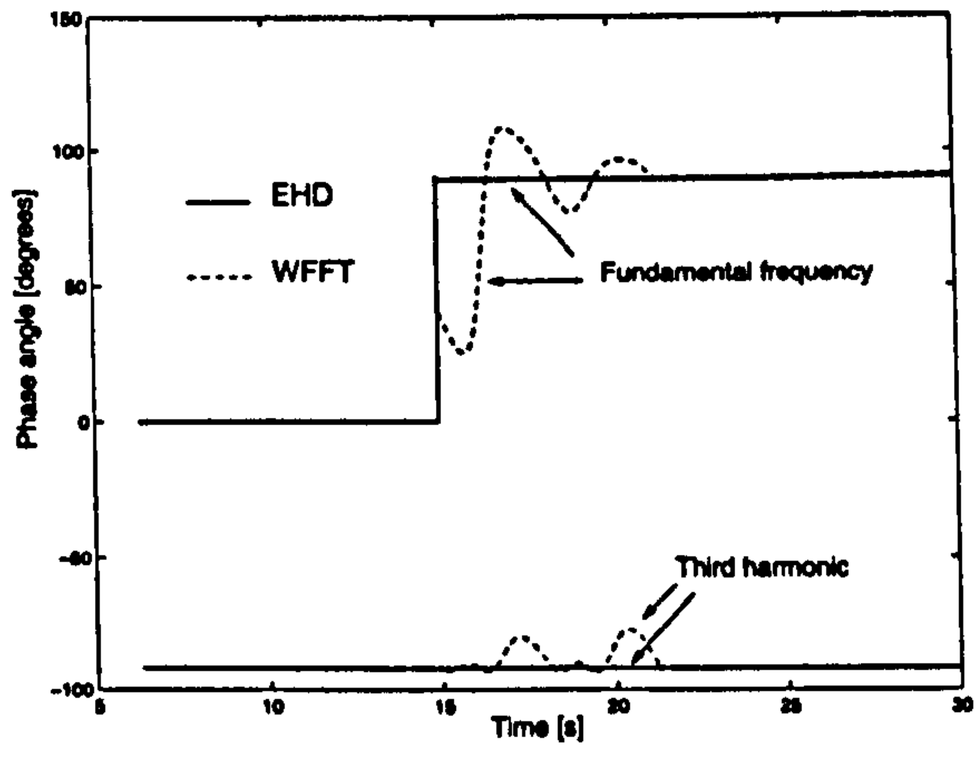

(c) Angle comparison

Figure 6.5.: Comparison of harmonics currents using WFFT and the EHD

Figure 6.5(c) shows the angles of the fundamental and 3rd harmonic currents obtained with the EHD and WFFT methods. Key observations can be derived from these results: 1) The use of the WFFT transform gives rise to a misleading harmonic spectrum, spectrum which was expected since it is an intrinsic characteristic of the windowing, 2) The fundamental and 3rd harmonic currents derived with both techniques show quite a different dynamic evolution, 3) The angle of the fundamental and 3rd harmonic current using WFFT, shows a very substantial mismatch when compared to the result obtained using the EHD method.

The EHD and the FFT methods take quite a different approach to solving the dynamic evolution of harmonics. The fundamental difference lies on the fact that the EHD is a direct method to solve dynamic systems and the FFT is not.

6.5. Evolution of Harmonics in Non-linear Circuits

As described in this chapter, the EHD may be used for dynamic harmonic analysis of linear, non-linear and time-varying systems. In this section, the EHD state-space is used to solve a non-linear system.

Figure 6.6 shows an unloaded single-phase transformer. The transformer includes the linear equivalent, and the magnetising branch. The current response of the non-linear inductance of the magnetising branch is represented by the following polynomial equation:

$$i_{\psi}(t) = a\psi(t) + b\psi^{n}(t) \tag{6.15}$$

In this type of circuits, the attenuation of the inrush current $i_{inr}(t)$ may take several seconds. Such a long period of time to reach the state-state, maybe considered to be a waste of simulation time when the purpose is to conduct a harmonic study. Moreover, it is reported that to obtain steady-state initial conditions for transient analysis of these kind of circuit is not straightforward.

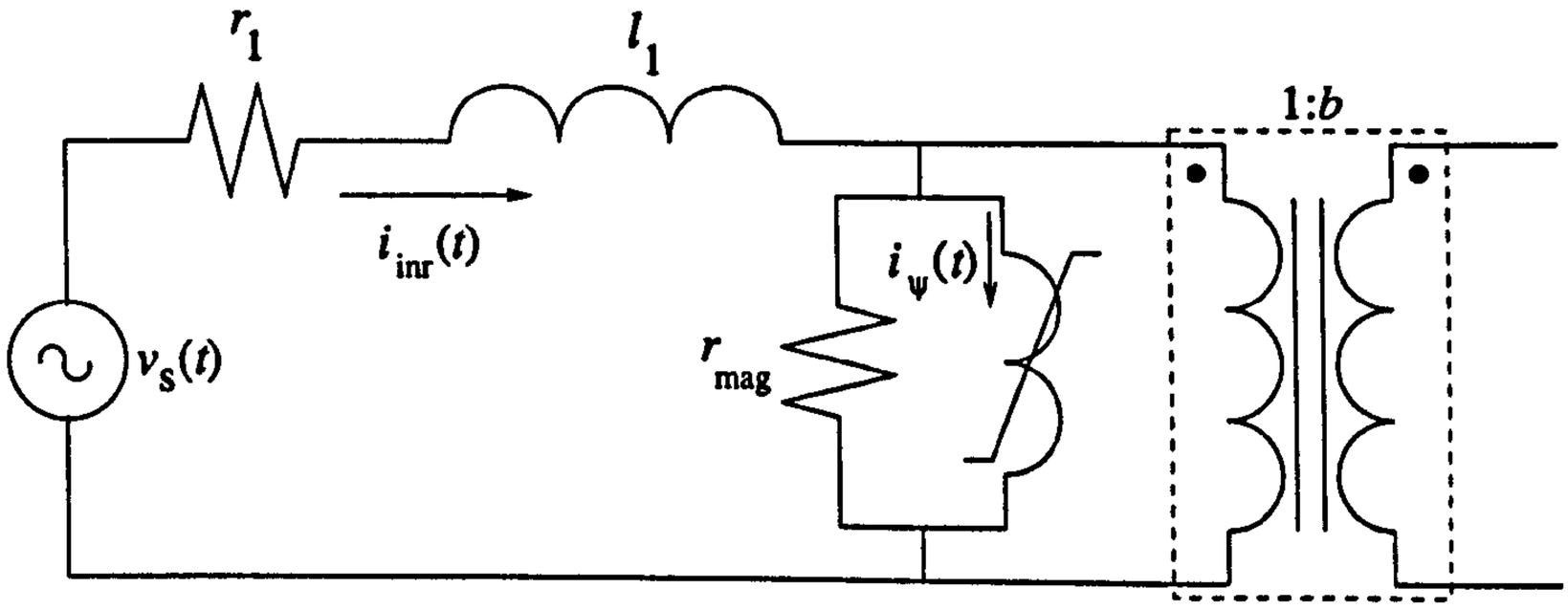

Figure 6.6.: Unloaded single-phase transformer

The state-space equation below describes the circuit:

$$\begin{bmatrix} \dot{i}_{inr}(t) \\ \dot{\psi}(t) \end{bmatrix} = \begin{bmatrix} -\frac{(r_1+r_{mag})}{l_1} & 0 \\ r_{mag} & 0 \end{bmatrix} \begin{bmatrix} i_{inr}(t) \\ \psi(t) \end{bmatrix} + \begin{bmatrix} \frac{1}{l_1} & \frac{r_{mag}}{l_1} \\ 0 & -r_{mag} \end{bmatrix} \begin{bmatrix} v_s(t) \\ i_{\psi}(t) \end{bmatrix} \tag{6.16}$$

Equation (6.16) in the EHD is given by

$$\dot{\mathbf{X}}(t) = (\mathbf{A} - \mathbf{D}_d(\mathrm{j}h\omega_0))\,\mathbf{X}(t) + \mathbf{B}\mathbf{U}(t) \tag{6.17}$$

where

$$\mathbf{X}(t) = \begin{bmatrix} \mathbf{I}_{inr}(t) \\ \Psi(t) \end{bmatrix};\ \mathbf{A} = \begin{bmatrix} -\frac{(r_1+r_{mag})}{l_1}\mathbf{U}_I & 0 \\ r_{mag}\mathbf{U}_I & 0 \end{bmatrix}$$

$$\mathbf{D}_d(\mathrm{j}h\omega_0) = \begin{bmatrix} \mathbf{D}(\mathrm{j}h\omega_0) & 0 \\ 0 & \mathbf{D}(\mathrm{j}h\omega_0) \end{bmatrix};\ \mathbf{B} = \begin{bmatrix} \frac{1}{l_1}\mathbf{U}_I & \frac{r_{mag}}{l_1}\mathbf{U}_I \\ 0 & -r_{mag}\mathbf{U}_I \end{bmatrix};\ \mathbf{U}(t) = \begin{bmatrix} \mathbf{V}_s \\ \mathbf{I}_{\psi}(t) \end{bmatrix}$$

and

$$\mathbf{I}_{\psi}(t) = a\Psi(t) + b\Psi^{n}(t)$$

$\mathbf{U_I}$ is the identity matrix.

Equation (6.17) is solved using a standard integration method where initial and final simulation times, t_0 and t_f, integration time step Δt and initial conditions for the state variable $\mathbf{X}(t)$ are specified. The harmonic vector $\mathbf{I}_\psi(t)$ is evaluated at every time step Δt.

6.5.1. Steady-state initial condition

It has been shown that HD is a very powerful technique to determine the steady-state response of non-linear systems by iteration [13].

In this case, linearising (6.15) around an operating point $\psi_e(t)$, leads to the following state equation,

$$\begin{bmatrix} \dot{i}_{inr}(t) \\ \dot{\psi}(t) \end{bmatrix} = \left(\begin{bmatrix} -\frac{(r_1+r_{mag})}{l_1} & 0 \\ r_{mag} & 0 \end{bmatrix} + \begin{bmatrix} 0 & -\frac{r_{mag}}{l_1} i'_{\psi_e}(t) \\ 0 & -r_{mag} i'_{\psi_e}(t) \end{bmatrix} \right) \begin{bmatrix} i_{inr}(t) \\ \psi(t) \end{bmatrix} + \begin{bmatrix} \frac{1}{l_1} & \frac{r_{mag}}{l_1} \\ 0 & -r_{mag} \end{bmatrix} \begin{bmatrix} v_s(t) \\ i_N(t) \end{bmatrix} \tag{6.18}$$

where

$$\begin{aligned} i_{\psi_e}(t) &= a\psi_e(t) + b\psi_e^n(t) \\ i'_{\psi_e}(t) &= a + nb\psi_e^{n-1}(t) \\ i_N(t) &= i_{\psi_e}(t) - i'_{\psi_e}(t)\psi_e(t) \end{aligned}$$

Representing equation (6.18) in EHD results in

$$\dot{\mathbf{X}}(t) = (\mathbf{A} + \mathbf{A}_{lin} - \mathbf{D}_d(jh\omega_0))\mathbf{X}(t) + \mathbf{BU} \tag{6.19}$$

where

$$\mathbf{U} = \begin{bmatrix} \mathbf{V}_s \\ \mathbf{I}_N \end{bmatrix};\ \mathbf{A}_{lin} = \begin{bmatrix} 0 & -\frac{r_{mag}}{l_1}\mathbf{I}'_{\psi_e} \\ 0 & -r_{mag}\mathbf{I}'_{\psi_e} \end{bmatrix};\ \mathbf{a} = \begin{bmatrix} \vdots \\ 0 \\ a \\ 0 \\ \vdots \end{bmatrix}$$

and

$$\mathbf{I}_{\psi_e} = a\Psi_e + b\Psi_e^n$$

$$\mathbf{I}'_{\psi_e} = \mathbf{a} + nb\Psi_e^{n-1}$$
$$\mathbf{I}_N = \mathbf{I}_{\psi_e} - \mathbf{I}'_{\psi_e}\Psi_e$$

It should be noted that $\mathbf{I}'_{\psi_e}$ in $\mathbf{A}_{lin}$ has a matrix representation.

The steady-state solution of (6.19) around the operating point $\psi_e(t)$ is obtained when $\dot{\mathbf{X}}(t) = 0$, so $\mathbf{X}$ is given by

$$\mathbf{X} = -(\mathbf{A} + \mathbf{A}_{lin} - \mathbf{D}_d(\mathrm{j}h\omega_0))^{-1}\mathbf{BU} \tag{6.20}$$

Solving equation (6.20) in an iterative process where $\mathbf{A}_{lin}$ and $\mathbf{U}$ are updated, results in the exact state-state solution for $\mathbf{X}$, this result may be used as initial condition for the state equation (6.17).

6.5.2. Case study

A dynamic harmonic analysis is carried out for the circuit of Figure 6.6, where the following parameters are used: $r_1 = 0.192\,\Omega$, $r_{mag} = 612.86\,\Omega$ and $l_1 = 0.9$ mH; and for the non-linear characteristic: $a = 0.7576$, $b = 1.03 \times 10^7$ and $n = 19$. The circuit is excited with a voltage source: $v_s(t) = 130\cos(\omega_0 t - 42.97°)$ V, and the operating frequency is $f_0 = 50$ Hz.

The case consists in the study of the circuit harmonic responses when an increase of the voltage source is applied. The disturbance is a sustained voltage $v_s(t) = 135\cos(\omega_0 t - 42.97°)$ V applied at 0.04 s after the steady-state has been reached.

In this particular circuit, it takes a very long time to reach the steady-state if a conventional integration method and not suitable initial condition are used. However, in EHD the initial condition is straightforward to obtain by using HD. Solving (6.20) by iteration, the result was obtained in 6 iterations with an error of 4.31×10^{-13} for $h = 9$. The steady-state response is given by

$$\mathbf{I}_{inr} = \begin{bmatrix} -0.0034+j0.0068 \\ 0 \\ -0.0221-j0.0131 \\ 0 \\ 0.0283-j0.0408 \\ 0 \\ 0.0583+j0.0470 \\ 0 \\ -0.0917+j0.2540 \\ 0 \\ -0.0917-j0.2540 \\ 0 \\ 0.0583-j0.0470 \\ 0 \\ 0.0283+j0.0408 \\ 0 \\ -0.0221+j0.0131 \\ 0 \\ -0.0034-j0.0068 \end{bmatrix}; \quad \Psi = \begin{bmatrix} 0 \\ 0 \\ 0 \\ 0 \\ 0 \\ 0 \\ 0-j0.0001 \\ 0 \\ -0.1408+j0.1512 \\ 0 \\ -0.1408-j0.1512 \\ 0 \\ 0+j0.0001 \\ 0 \\ 0 \\ 0 \\ 0 \\ 0 \\ 0 \end{bmatrix}$$

Using this solution as initial condition for (6.17), the inrush current shown in Figure 6.7 was obtained using $t_0 = 0$ s, $t_f = 0.2$ s, and an integration time step $\Delta t = 0.2$ ms. It is should be mentioned that the current waveform was built from the dynamic harmonics obtained from the solution of (6.17).

Analysing the current waveform, it can be seen that the initial condition was exact since no transient at the beginning of the simulation was identified.

Figure 6.8 shows a comparison between the harmonics obtained by using EHD and those obtained with WFFT over the current waveform. It is very interesting to see that during the steady-state the harmonic magnitudes and phase angles match with each other. However, during the disturbance, which is applied at 0.04 s, the harmonics obtained with EHD respond instantly to the event, and those obtained with WFFT take 0.005 s to do so. This delay is due to the fact that the waveform of the inrush current from 0.04 s to 0.045 s looks like a steady-state. From the results shown in Figure 6.8, it is clear that after the disturbance the harmonics obtained with EHD present a very clear transient state, meanwhile the harmonics obtained from WFFT present an almost steady-state condition in both magnitude and phase angle. A fact of perhaps great significance is the very different results given by the two techniques concerning the time evolution of harmonics.

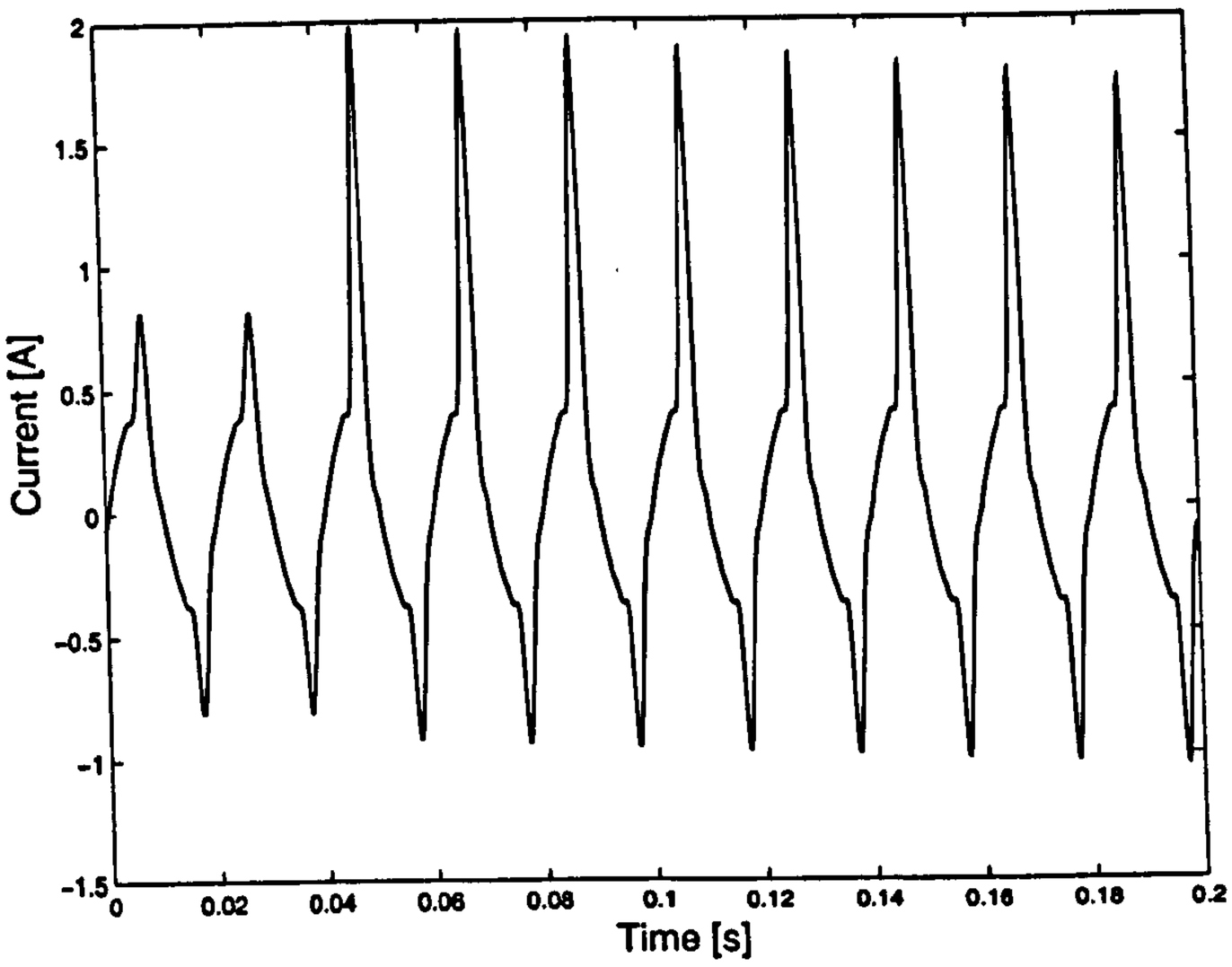

Figure 6.7.: Inrush current waveform

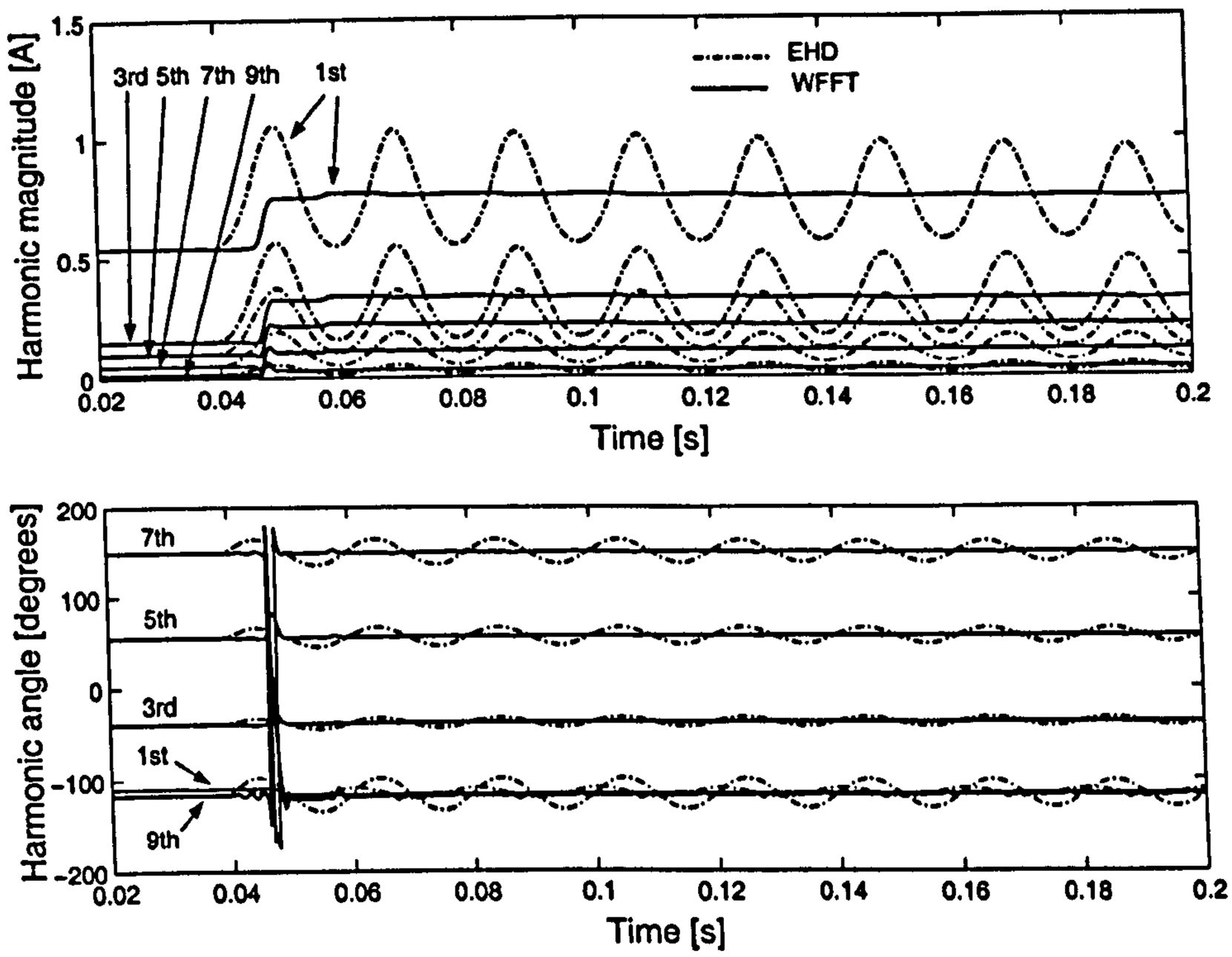

Figure 6.8.: Harmonic content of the inrush current

6.6. Dynamic Electrical Indices

Several electrical parameters are used to enable accurate power quality assessments of electrical installations and equipment. The most popular are given below. These parameters are normally expressed in terms of complex Fourier coefficients:

RMS voltage:

$$V_{\text{rms}} = \left(\sum_{n=-h}^{h} V_n V_{-n} \right)^{1/2}$$

RMS current:

$$I_{\text{rms}} = \left(\sum_{n=-h}^{h} I_n I_{-n} \right)^{1/2}$$

Apparent power:

$$\mathrm{S} = V_{\text{rms}} I_{\text{rms}}$$

Active power:

$$\mathrm{P} = \sum_{n=-h}^{h} V_n I_{-n}$$

Reactive power at fundamental frequency:

$$\mathrm{Q_1} = \frac{V_1 I_1}{2} \sin\theta$$

Distortion power:

$$\mathrm{D} = \left(\mathrm{S}^2 - \mathrm{P}^2 - \mathrm{Q}_1^2 \right)^{1/2}$$

Power factor:

$$\mathrm{PF} = \frac{\mathrm{P}}{\mathrm{S}}$$

Total harmonic distortion:

$$\mathrm{THD}_V = \frac{\sqrt{\sum_{n=2}^{h} |V_n|^2}}{|V_1|} \times 100\%$$

In principle, the Fourier transform only applies to voltage and current waveforms that exhibit a periodic behaviour. In practice, windowing FFTs have been used for quite some time to derive harmonic information under transient conditions. So far, no electrical parameters for power quality assessment under dynamic conditions have been put forward. One possible explanation is that the use of simple windowing FFT techniques do not always yield accurate harmonic

information and, hence, meaningful electric parameters could not be obtained. In this chapter, the accurate assessment of the dynamic evolution of harmonics allows for the extension of such definitions to be applied under transient conditions, at every time step. Accordingly, it is possible to talk about dynamic power quantities such as powers $S(t)$, $P(t)$, $Q(t)$ and $D(t)$; RMS values $V_{rms}(t)$ and $I_{rms}(t)$ as well as power factor $PF(t)$. For completeness the distortion factors: $THD_V(t)$ and $THD_I(t)$ can also be derived. These transient harmonic indices may find applications in the design of more robust protection and control schemes than those based on positive sequence, fundamental frequency parameters.

Also, the dynamic currents in the sequence domain can be obtained. The zero, positive and negative currents are derived from the phase domain quantities as follows

$$\begin{bmatrix} I_{(0)_h}(t) \\ I_{(+)_h}(t) \\ I_{(-)_h}(t) \end{bmatrix} = \frac{1}{3} \begin{bmatrix} 1 & 1 & 1 \\ 1 & a^2 & a \\ 1 & a & a^2 \end{bmatrix} \begin{bmatrix} I_{a_h}(t) \\ I_{b_h}(t) \\ I_{c_h}(t) \end{bmatrix}$$

where $a = 1\angle 120°$.

The inverse relationship also exist. Voltage quantities also obey the same transformation matrix.

6.7. Conclusions

The extended harmonic domain methodology has been presented in this chapter for the first time. It is based on the use of dynamic harmonics, orthogonal series expansions and their operational properties. The method is suitable for steady-state analysis as well as large signal dynamic analysis of electric networks with embedded power electronics controllers and non-linear loads. The EHD method is an extension of the well known HD method used in power systems harmonic analysis. This has the advantage that a wide range of models developed for the HD can be used for transient analysis with few or no modifications. Moreover, HD can also be used for EHD initialisation. This method yields accurate information of the time evolution of harmonic coefficients, and allows for an extension of power quality indices to the dynamic range. The EHD is an alternative linear, time-invariant, state-space equation for which all the powerful tools developed in linear control design can be applied.

7. Dynamic Harmonic Response of Power Electronics Controllers

7.1. Introduction

In the previous chapter the EHD was presented. It was shown that this domain gives the dynamic and periodic steady-state responses of linear and non-linear systems. In this chapter, the EHD is applied to the solution of time-varying systems. An important characteristic of time-varying systems is that when represented in EHD these systems are transformed into linear time-invariant systems. This is an important transformation since the full theory of linear time-invariant system can then be applied.

In the first chapters of this thesis it was shown that power electronics controllers can be represented by time-varying systems, and transformed into equivalent impedances using HD. In this chapter, space-state models for power electronics controllers such as the STATCOM and HVDC-VSC stations are obtained and transformed into linear time-invariant system using EHD.

It should be mentioned that the dynamic phasors technique, which is base in generalized averaging method, has been used to derive phasor-based models for AC power elements and FACTS controllers used for fault and stability studies [53][54]. In [110] a harmonic transfer function model based on complex Fourier series was used for control analysis of an inverter. Nevertheless, the EHD is a more complete approach used for harmonic modelling, suitable for harmonic propagation, resonance analysis and also for stability and control design.

7.2. Static Synchronous Compensator

Figure 7.1 represents a STATCOM connected to an AC system. The equations that describe the STATCOM are

$$\mathbf{v}_{abc_1}(t) = \mathbf{p}_s(t) v_{dc}(t) \tag{7.1}$$

and the current $i_1(t)$, is given by

$$i_1(t) = \mathbf{q}_s(t)\mathbf{i}_{abc}(t) \tag{7.2}$$

Also, the voltage in the capacitor is given by

$$\frac{dv_{dc}(t)}{dt} = \frac{1}{C} i_1(t) \tag{7.3}$$

The voltage drop across the three-phase impedance of the STATCOM circuit in Figure 7.1 is

$$\mathbf{v}_{abc}(t) - \mathbf{v}_{abc_1}(t) = R_e \mathbf{i}_{abc}(t) + L_e \frac{d\mathbf{i}_{abc}(t)}{dt} \tag{7.4}$$

A suitable combination of equations (7.1)–(7.4) yields a time state-space equation that describes the dynamics of the STATCOM,

$$\begin{bmatrix} \dot{\mathbf{i}}_{abc}(t) \\ \dot{v}_{dc}(t) \end{bmatrix} = \begin{bmatrix} -\frac{R_e}{L_e} & -\frac{1}{L_e}\mathbf{p}_s(t) \\ \frac{1}{C}\mathbf{q}_s(t) & 0 \end{bmatrix} \begin{bmatrix} \mathbf{i}_{abc}(t) \\ v_{dc}(t) \end{bmatrix} + \frac{1}{L_e} \begin{bmatrix} \mathbf{v}_{abc}(t) \\ 0 \end{bmatrix} \tag{7.5}$$

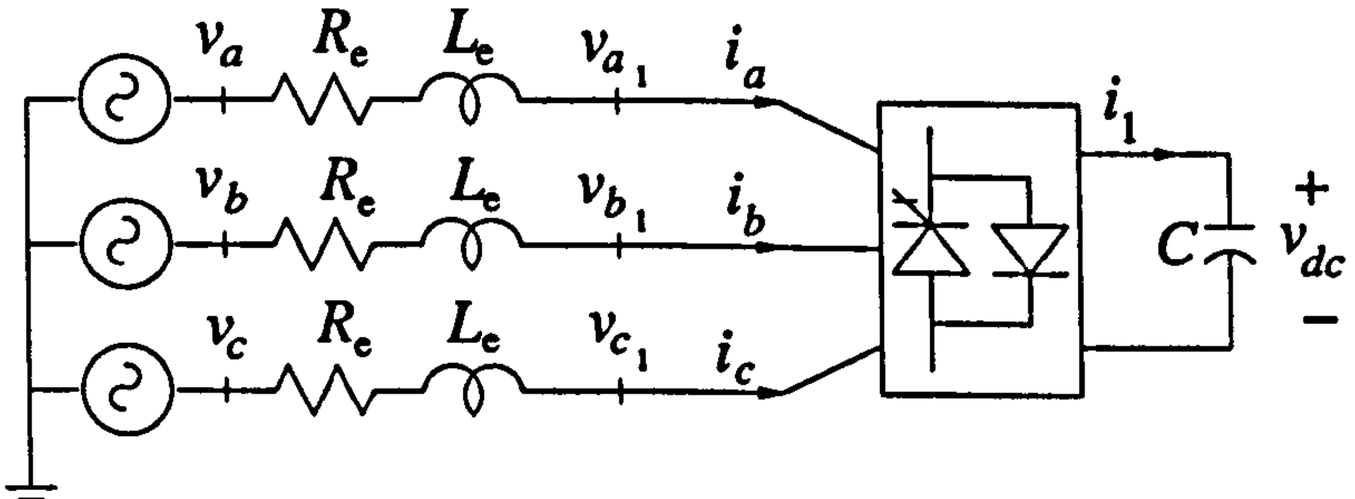

Figure 7.1.: STATCOM equivalent

Moreover, this equation can be transformed into a LTI system using the EHD method, given by

$$\begin{bmatrix} \dot{\mathbf{I}}_{abc}(t) \\ \dot{\mathbf{V}}_{dc}(t) \end{bmatrix} = \begin{bmatrix} -\frac{R_e}{L_e}\mathbf{U}_I - \mathbf{D}(j h\omega_0) & -\frac{1}{L_e}\mathbf{P}_s \\ \frac{1}{C}\mathbf{Q}_s & -\mathbf{D}(j h\omega_0) \end{bmatrix} \begin{bmatrix} \mathbf{I}_{abc}(t) \\ \mathbf{V}_{dc}(t) \end{bmatrix} + \frac{1}{L_e} \begin{bmatrix} \mathbf{V}_{abc} \\ 0 \end{bmatrix} \tag{7.6}$$

Where $\mathbf{p}_s(t)$, $\mathbf{q}_s(t)$, $\mathbf{P}_s$ and $\mathbf{Q}_s$ are as defined in Chapter 2.

7.2.1. Case study: Power quality disturbances

Power quality (PQ) is an umbrella term that embraces all aspects associated with amplitude, phase and frequency of voltage and current waveforms existing in a power circuit. A large number of PQ disturbances have been reported in the open literature, with some of them being transient in nature and other being related to periodic, steady-state operation. So far PQ has gained worldwide interest in both industry and academic level due to the problems which produce mainly in sensitive loads[3][36][49][55][104][105].

In this section two of the most important PQ disturbances are used to show the response of the STATCOM under such conditions, these PQ disturbances are a voltage impulse and a voltage sag. This case study involves a three-phase, PWM-controlled STATCOM where the PWM strategy has been selected to eliminate the 5th, 7th, 11th, 13th and 17th harmonics with a phase shift angle $\delta = 5°$. This value is used in order to set the conditions for active and reactive power exchange with the system. The parameters of the network are $R_e = 0.051\,\Omega$, $L_e = 0.27$ mH, $C = 4950\,\mu$F. The system voltage source is unbalanced, with the following values $v_a(t) = \sin\omega_0 t$ V, $v_b(t) = 0.9\sin(\omega_0 t - 118°)$ V and $v_c(t) = 1.02\sin(\omega_0 t + 121°)$ V. The system frequency is 50 Hz.

Accurate initial conditions for $\mathbf{I}_{abc}(t)$ and $\mathbf{V}_{dc}(t)$ were obtained by solving (7.6) with $\dot{\mathbf{I}}_{abc}(t)$ and $\dot{\mathbf{V}}_{dc}(t)$ set to zero; i.e. steady-state solution.

Two disturbance are applied to this system in order to analyse the dynamic harmonic response of the STATCOM. The disturbances correspond to a voltage impulse and to a voltage sag.

Voltage Impulse: In this study it is assumed a very sharp voltage impulse take place. The impulse is of three times the magnitude of the phase *a* with a duration of 0.1 ms. It occurs after 25 ms of simulation time, as shown in Figure 7.2. This disturbance is represented in EHD by using $3\mathbf{V}_a$ during 0.1 ms.

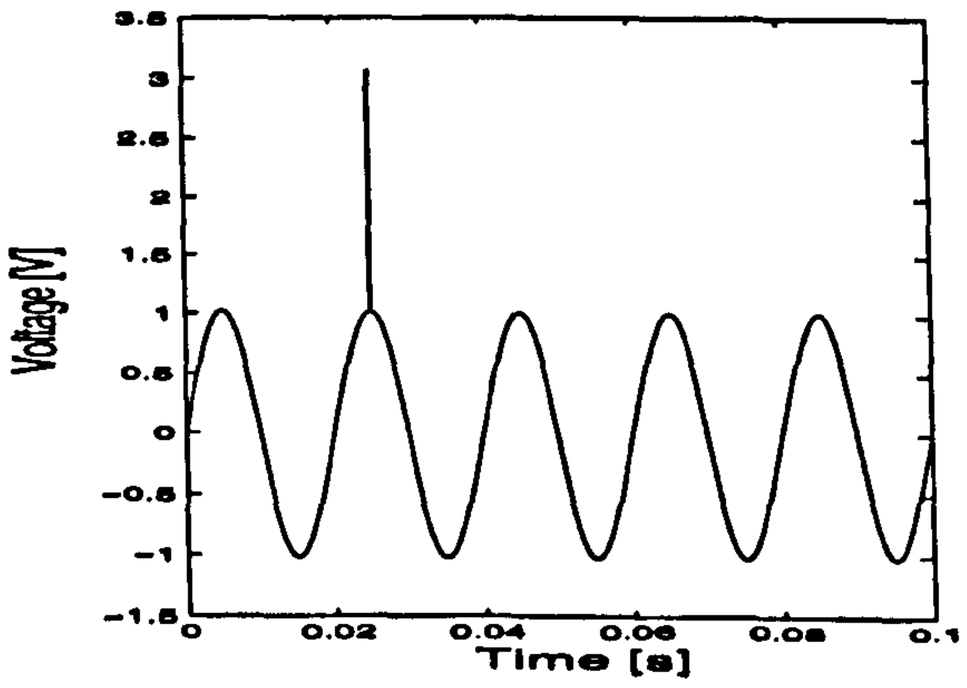

Figure 7.2.: Impulse imposed on the voltage source

Figure 7.3(a) shows the EHD solution, where the voltage $v_{a_1}(t)$, current $i_a(t)$ and voltage in the DC side $v_{dc}(t)$ are shown. Fifty harmonic terms were used in the simulation. The time representation of these variables is given in Figure 7.3(b). The results show that the impulse is quite difficult to appreciate in the voltage and current waveforms. However, the dynamic response of the harmonics is very sensitive to this very sharp voltage impulse, as shown in Figure 7.3(a). Such a sensitive characteristic of harmonics during disturbances could be used to good effect to explain several power quality disturbances.

Figure 7.4 shows the electrical parameters associated with this disturbance. These parameters were calculated as explained in Section 6.6. The results show that as expected, these pa-

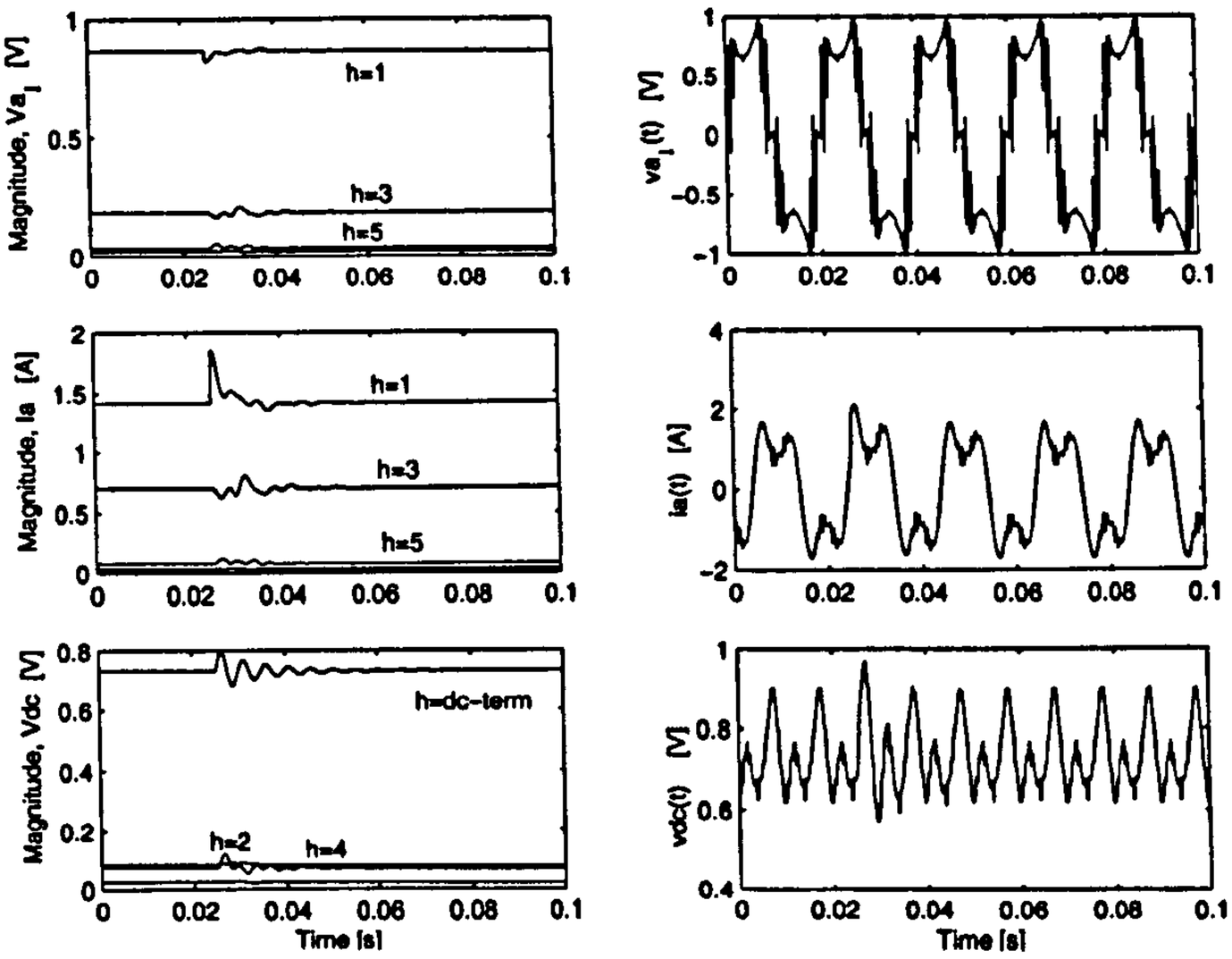

(a) Harmonic dynamic response (b) Time domain representation

Figure 7.3.: STATCOM voltages and currents using EHD

rameters are constant for periodic, steady-state operation but register significant changes during transient conditions due to the dynamic behaviour of the harmonics.

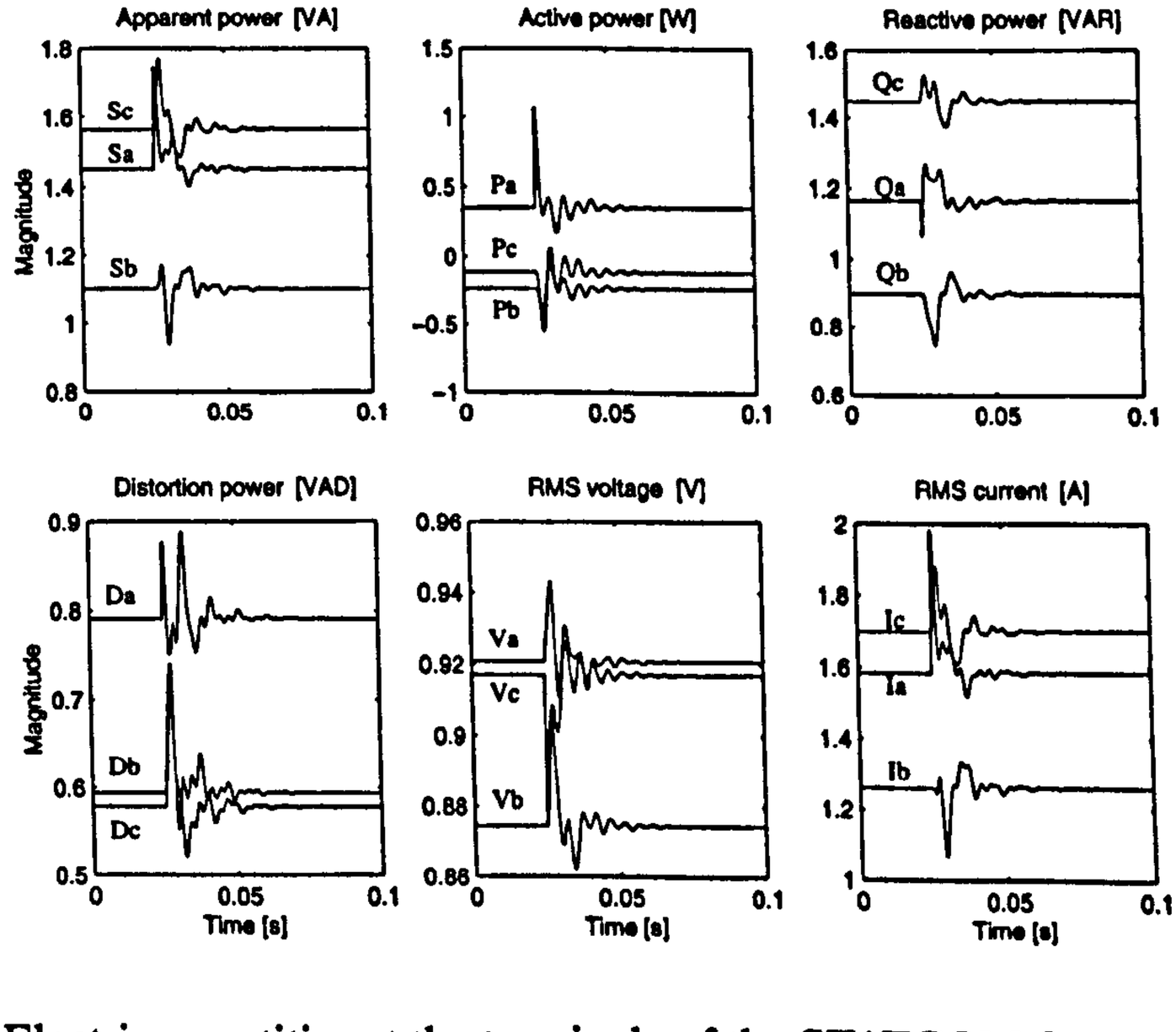

Figure 7.4.: Electric quantities at the terminals of the STATCOM for a voltage impulse

Voltage sag: This study also makes use of the system used in the previous case study. But, it is now assumed that the disturbance is a voltage sag lasting 0.115 s and taking place after a simulation time of 0.035 s. During the disturbance the voltage $v_a(t)$ reduces to half its pre-fault value, as shown in Figure 7.5. This disturbance is represented in EHD by using $\frac{1}{2}\mathrm{V}_a$ during

0.115 s.

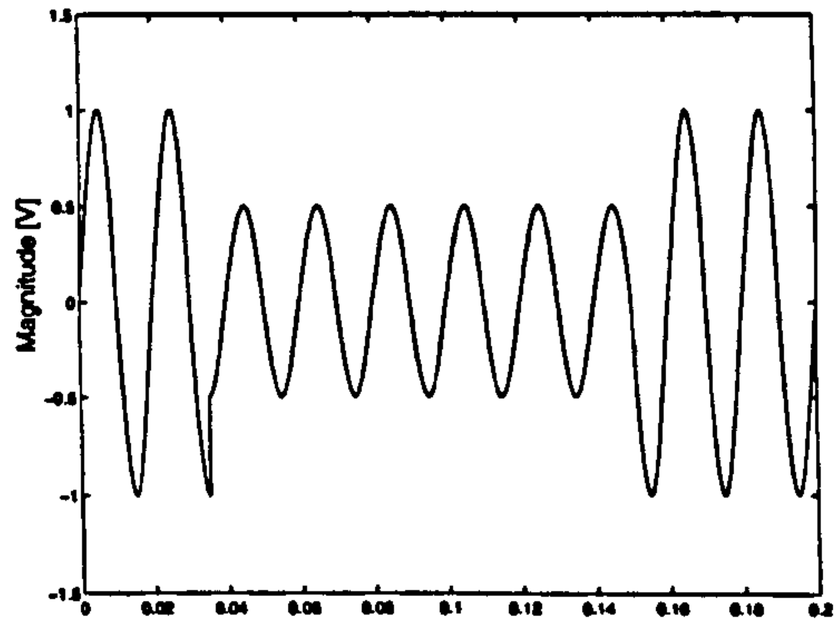

Figure 7.5.: Voltage sag disturbance

Figure 7.6(a) shows the EHD solution, where the voltage $v_{a_1}(t)$, current $i_a(t)$ and voltage in the DC side $v_{dc}(t)$ are shown. Fifty harmonic terms were used in the simulation. The time representation of these variables is given in Figure 7.6(b). This result shows that harmonics give very accurate information of the instant when the disturbance starts and when it finishes. Also, during the sag the harmonics reach a steady-state.

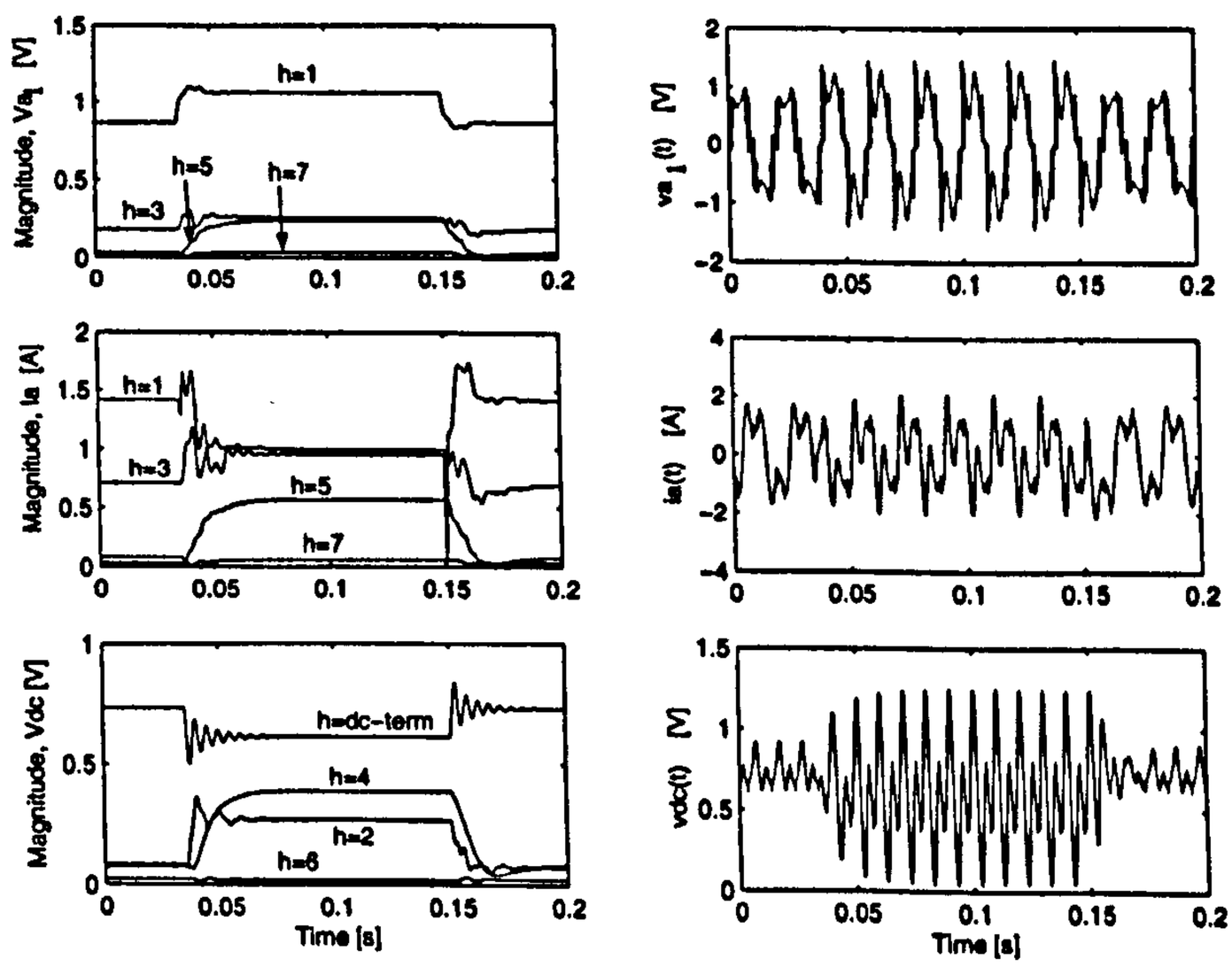

(a) Harmonics dynamic response (b) Time domain representation

Figure 7.6.: STATCOM voltages and currents using EHD

Figure 7.7 shows the dynamic behaviour of the main electrical parameters at the terminals of the STATCOM. These results show that as expected, these parameters are constant, for periodic, steady-state operation but register significant changes during transient conditions due to the dynamic behaviour of the harmonics. Figure 7.8 shows the THD for the voltage and current in the three phases.

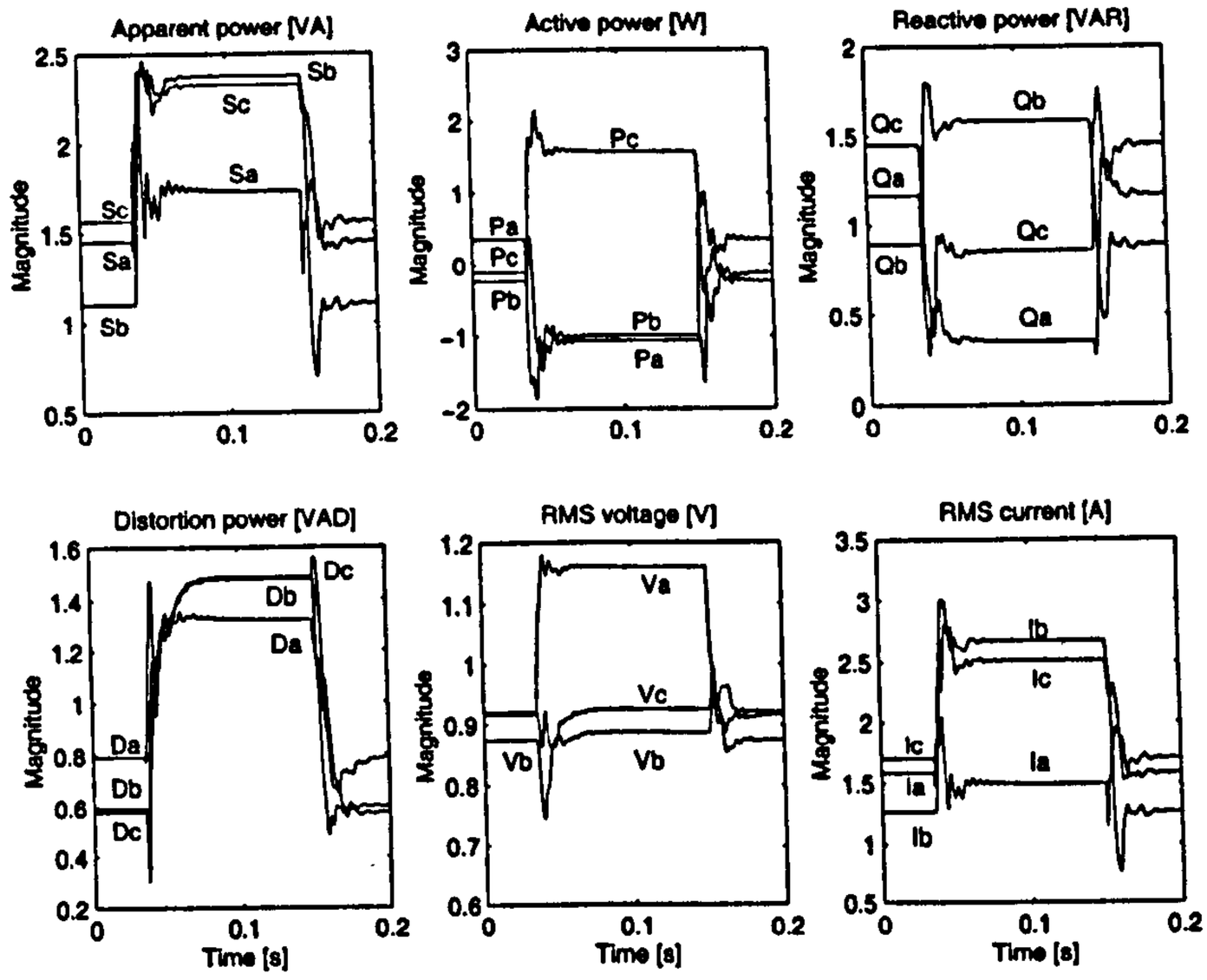

Figure 7.7.: Electric quantities at the terminals of the STATCOM for a voltage sag

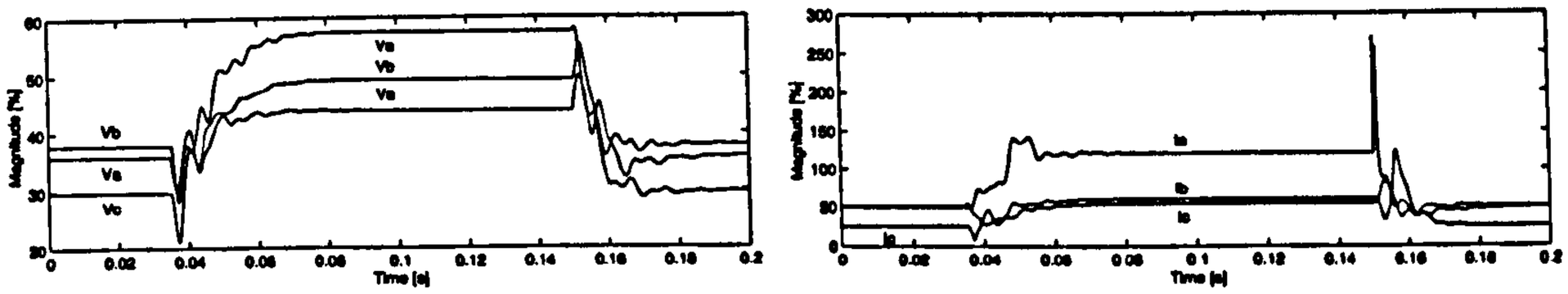

(a) THD in $v_{abc_1}(t)$ (b) THD in $i_{abc}(t)$

Figure 7.8.: THD voltage and current

7.2.2. Averaging results

To assess the number of harmonic terms required in a typical EHD solution Figure 7.9 compares results given by a standard numeric integration method to solve equation (7.5) and the EHD solution, expressed in the time domain. Both results compare very well with each other when 50 harmonics are used. The accuracy of the EHD solution decreases when the number of harmonic coefficients reduces, e.g. 5 harmonics. Figure 7.9 shows this comparison. It should be noted that using a reduced number of harmonics lead in an averaging result.

It is important to remark that if only the fundamental and the dc-term were to be used in the EHD method, it would yield, with suitable similarity transformations, a model that is compatible with those used in small signal stability analysis [94].

7.3. HVDC-VSC Back-to-back

The state-space model for the HVDC-VSC back-to-back configuration may be derived from the differential equations that describe the equivalent circuit of Figure 4.2.

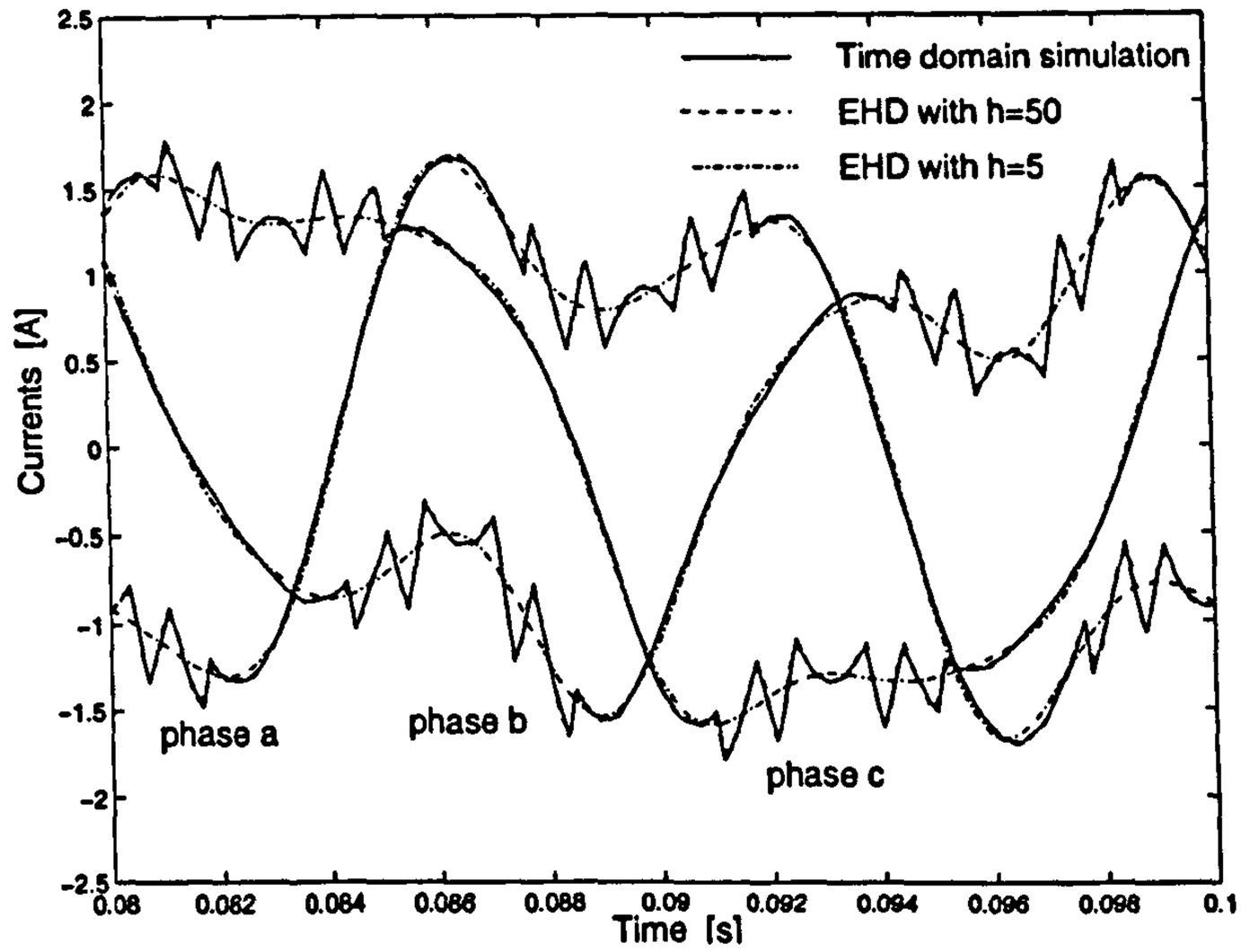

Figure 7.9.: Comparison of time domain simulations and EHD

The voltages at the output of the VSCs are given by the equations

$$\mathbf{v}_{abc_1}(t) = \mathbf{p}_{s_1}(t)v_{dc}(t) \tag{7.7}$$

$$\mathbf{v}_{ABC_1}(t) = \mathbf{p}_{s_2}(t)v_{dc}(t) \tag{7.8}$$

The current in the DC side of the VSCs are given by

$$i_1(t) = \mathbf{q}_{s_1}(t)\mathbf{i}_{abc}(t) \tag{7.9}$$

$$i_2(t) = \mathbf{q}_{s_2}(t)\mathbf{i}_{ABC}(t) \tag{7.10}$$

Also, the voltage in the capacitor is

$$\frac{\mathrm{d}v_{dc}(t)}{\mathrm{d}t} = \frac{1}{C}(i_1(t) + i_2(t)) \tag{7.11}$$

The voltage drops across the three-phase impedance of the HVDC-VSC back-to-back tie are

$$\mathbf{v}_{abc}(t) - \mathbf{v}_{abc_1}(t) = R_e\mathbf{i}_{abc}(t) + L_e\frac{\mathrm{d}\mathbf{i}_{abc}(t)}{\mathrm{d}t} \tag{7.12}$$

$$\mathbf{v}_{ABC}(t) - \mathbf{v}_{ABC_1}(t) = R_e\mathbf{i}_{ABC}(t) + L_e\frac{\mathrm{d}\mathbf{i}_{ABC}(t)}{\mathrm{d}t} \tag{7.13}$$

Suitable combination of equations (7.11)–(7.13) yields a time state-space equation that describes the dynamics of the HVDC-VSC back-to-back station,

$$\begin{bmatrix} \dot{\mathbf{i}}_{abc}(t) \\ \dot{\mathbf{i}}_{ABC}(t) \\ \dot{v}_{dc}(t) \end{bmatrix} = \begin{bmatrix} -\frac{R_e}{L_e} & 0 & -\frac{1}{L_e}\mathbf{p}_{s_1}(t) \\ 0 & -\frac{R_e}{L_e} & -\frac{1}{L_e}\mathbf{p}_{s_2}(t) \\ \frac{1}{C}\mathbf{q}_{s_1}(t) & \frac{1}{C}\mathbf{q}_{s_2}(t) & 0 \end{bmatrix} \begin{bmatrix} \mathbf{i}_{abc}(t) \\ \mathbf{i}_{ABC}(t) \\ v_{dc}(t) \end{bmatrix} + \frac{1}{L_e} \begin{bmatrix} \mathbf{v}_{abc}(t) \\ \mathbf{v}_{ABC}(t) \\ 0 \end{bmatrix} \tag{7.14}$$

Moreover, this equation can be transformed into a LTI system using the EHD method,

$$\begin{bmatrix} \dot{\mathbf{I}}_{abc}(t) \\ \dot{\mathbf{I}}_{ABC}(t) \\ \dot{\mathbf{V}}_{dc}(t) \end{bmatrix} = \begin{bmatrix} -\frac{R_e}{L_e}\mathbf{U}_\mathbf{I} - \mathbf{D}(\mathrm{j}h\omega_0) & 0 & -\frac{1}{L_e}\mathbf{P}_{s_1} \\ 0 & -\frac{R_e}{L_e}\mathbf{U}_\mathbf{I} - \mathbf{D}(\mathrm{j}h\omega_0) & -\frac{1}{L_e}\mathbf{P}_{s_2} \\ \frac{1}{C}\mathbf{Q}_{s_1} & \frac{1}{C}\mathbf{Q}_{s_2} & -\mathbf{D}(\mathrm{j}h\omega_0) \end{bmatrix} \begin{bmatrix} \mathbf{I}_{abc}(t) \\ \mathbf{I}_{ABC}(t) \\ \mathbf{V}_{dc}(t) \end{bmatrix} + \frac{1}{L_e} \begin{bmatrix} \mathbf{V}_{abc} \\ \mathbf{V}_{ABC} \\ 0 \end{bmatrix} \tag{7.15}$$

7.3.1. Case study

This study corresponds to an HVDC-VSC back-to-back with the following parameters: $R_e = 0.051\,\Omega$, $L_e = 0.27$ mH and $C = 4950\,\mu$F. The sources at both ends of the HVDC-VSC back-to-back station are three-phase and balanced, with value of 1 p.u. The VSCs use a harmonic cancellation elimination technique set to cancel out the 5th, 7th, 11th, 13th and 17th harmonics. Also, the HVDC-VSC back-to-back station uses a control system (see Appendix C) to maintain the DC side voltage at 1 p.u. Two cases were used for this system to analyse the dynamic response of the harmonics generated by the HVDC-VSC back-to-back station.

Case 1: An unbalanced disturbance was applied at 0.03 s of simulation. Phase a in the voltage source was reduced by half during a quarter of a cycle.

Figure 7.10 shows the harmonic magnitudes of currents $i_a(t)$, $i_b(t)$ and $i_c(t)$. The results show the harmonic response of the system to the voltage unbalance.

Using sequence quantities, as explained in Section 6.6, it can be seen from Figure 7.10 that during the transient period the zero sequence current contains a fundamental frequency term. This term is due to the unbalanced nature of the disturbance; the third harmonic term appears even during steady-state since it behaves like a zero sequence component [13]. For the positive and negative sequences a similar analysis can be carried out.

Figure 7.11 shows the DC side voltage and the injected powers into the HVDC-VSC back-to-back station. The harmonic content of the DC voltage during the disturbance reveals its

unbalanced nature since non-characteristic harmonics appear in the spectrum, i.e. 2nd and 4th harmonic. For completeness this figure also shows the powers response.

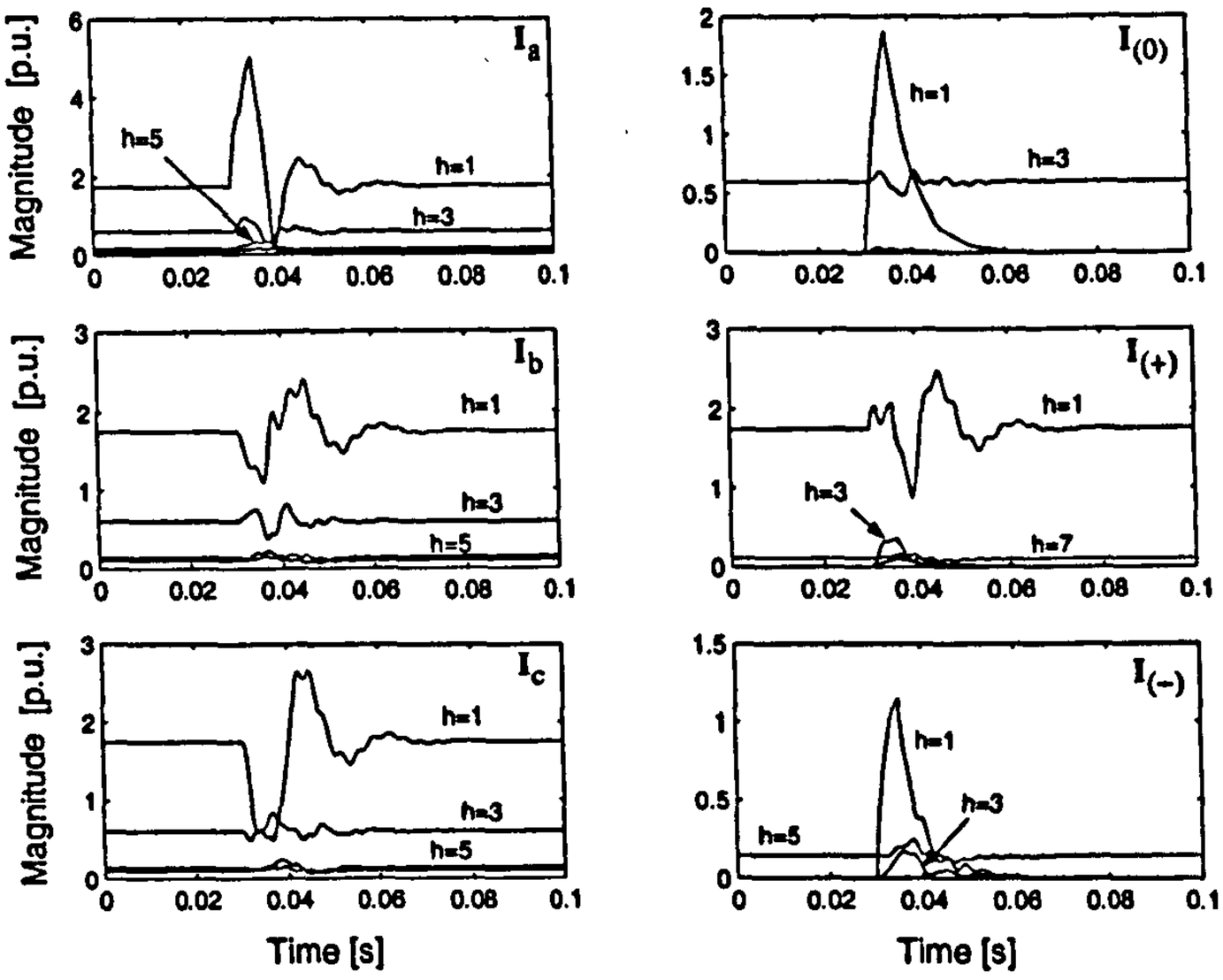

Figure 7.10.: Harmonic current response for the Case 1

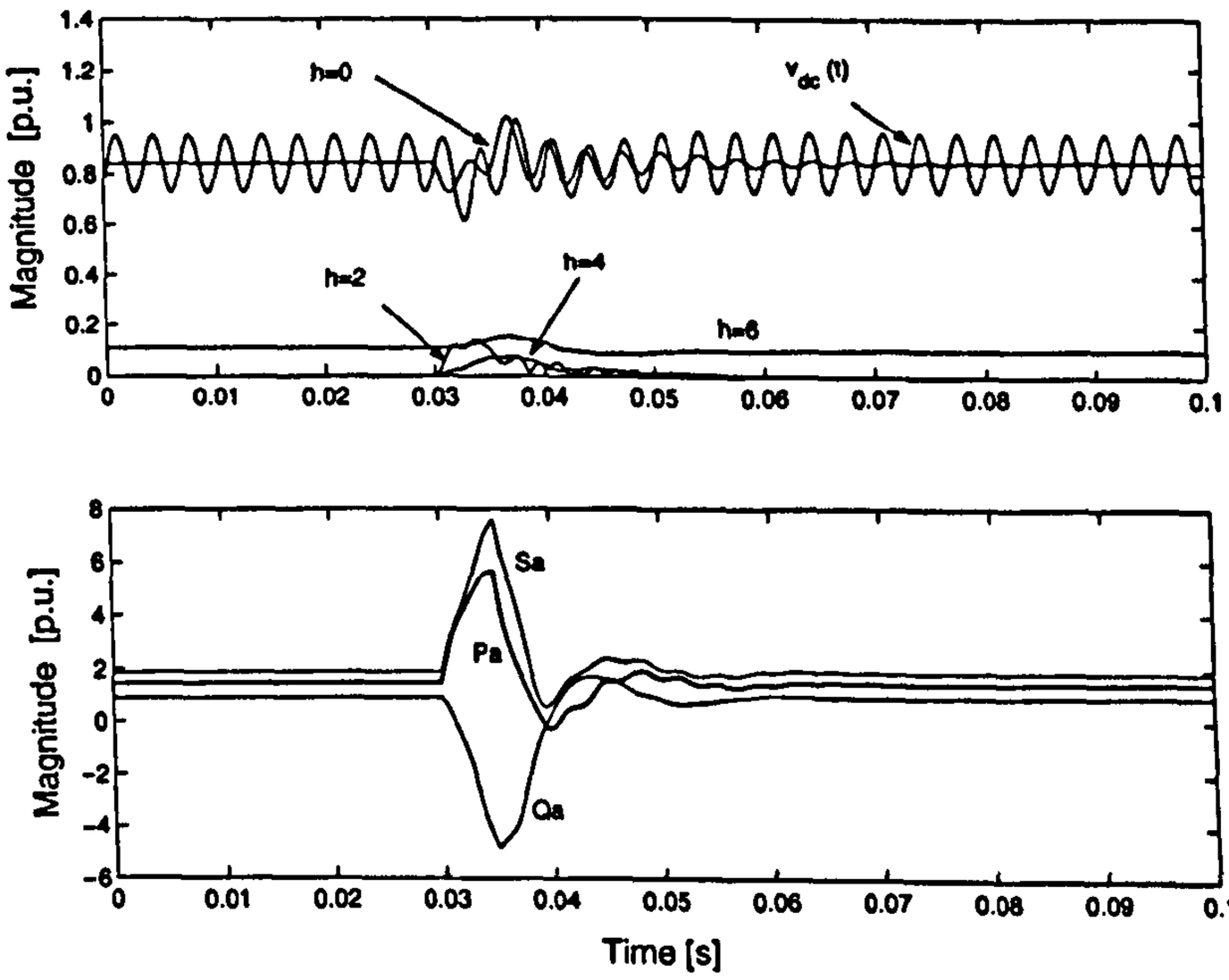

Figure 7.11.: DC side voltage and power flowing into the HVDC-VSC back-to-back for the Case 1

Case 2: A balanced disturbance is now applied at 0.03 s of simulation. The phase angle of the power dispatcher was changed to enable an increased power transfer through the HVDC-VSC back-to-back station.

Figure 7.12 shows the current response of the HVDC-VSC back-to-back station. It can be seen that the zero sequence current does not contain fundamental frequency term, since the disturbance is a balanced one. For the positive sequence only the fundamental frequency and the 7th harmonic appear during the transient and steady-state periods. For the negative sequence only the 5th harmonic appears. These results show that even under transient conditions, as long as the disturbance is balanced, the harmonics maintain their sequence natural behaviour.

Figure 7.13 shows the voltage in the DC side and the injected powers into the HVDC-VSC back-to-back station. In this case only the characteristic harmonics are present in the DC voltage. It should be noted that the power transfer changes from the initial operating state into new a one but maintaining the DC voltage at 1 p.u.

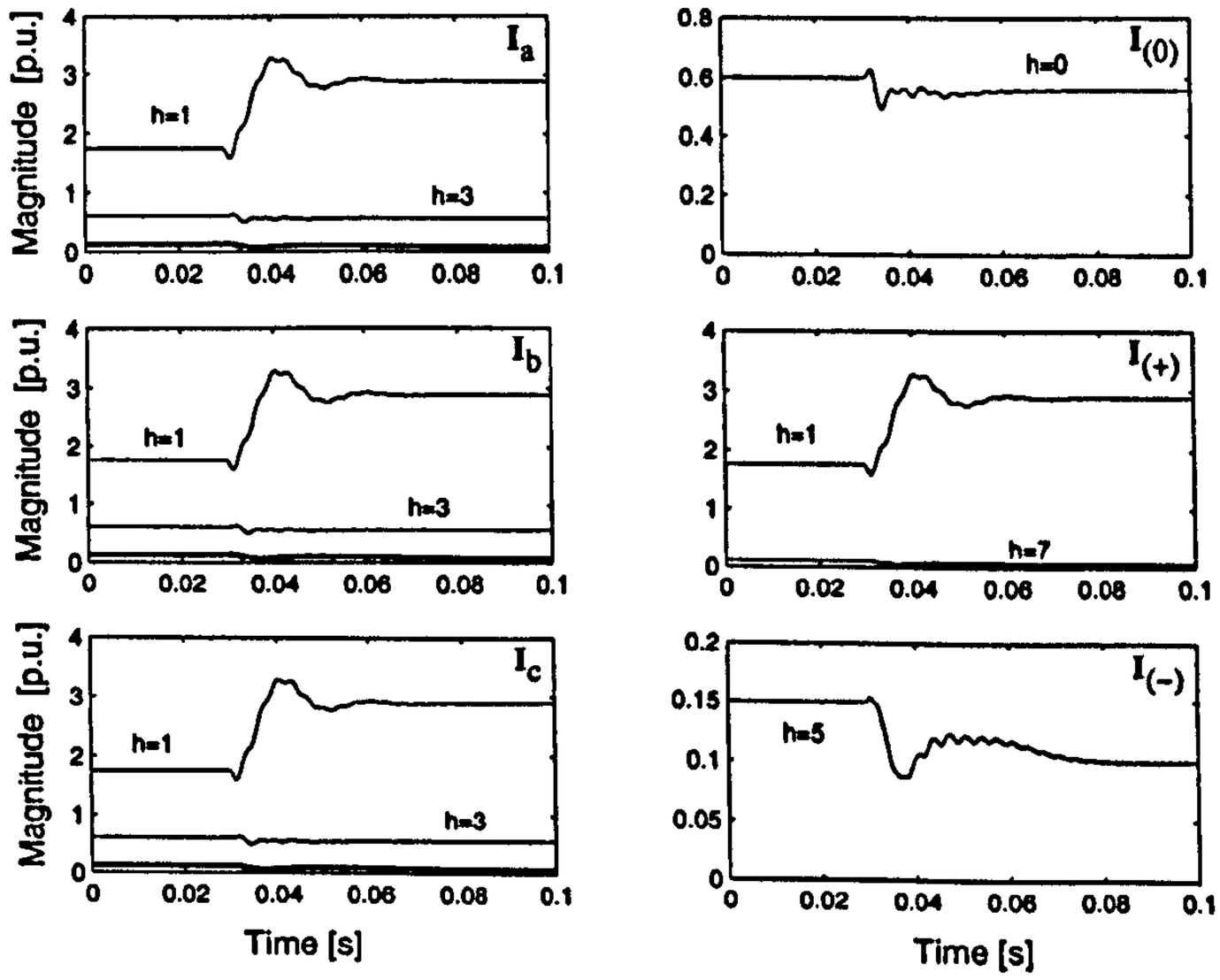

Figure 7.12.: Harmonic current response for Case 2

The results obtained from the dynamic response of the harmonic currents in the sequences (0,+ and −) give additional information which may be used to identify and characterise network imbalances.

7.4. HVDC-VSC Transmission System

The differential equations that describe the HVDC-VSC transmission system of Figure 4.7 are obtained as follows.

The voltages at the output of the VSCs are given by

$$\mathbf{v}_{abc_1}(t) = \mathbf{p}_{s_1}(t)v_{dc_1}(t) \tag{7.16}$$

$$\mathbf{v}_{ABC_1}(t) = \mathbf{p}_{s_2}(t)v_{dc_2}(t) \tag{7.17}$$

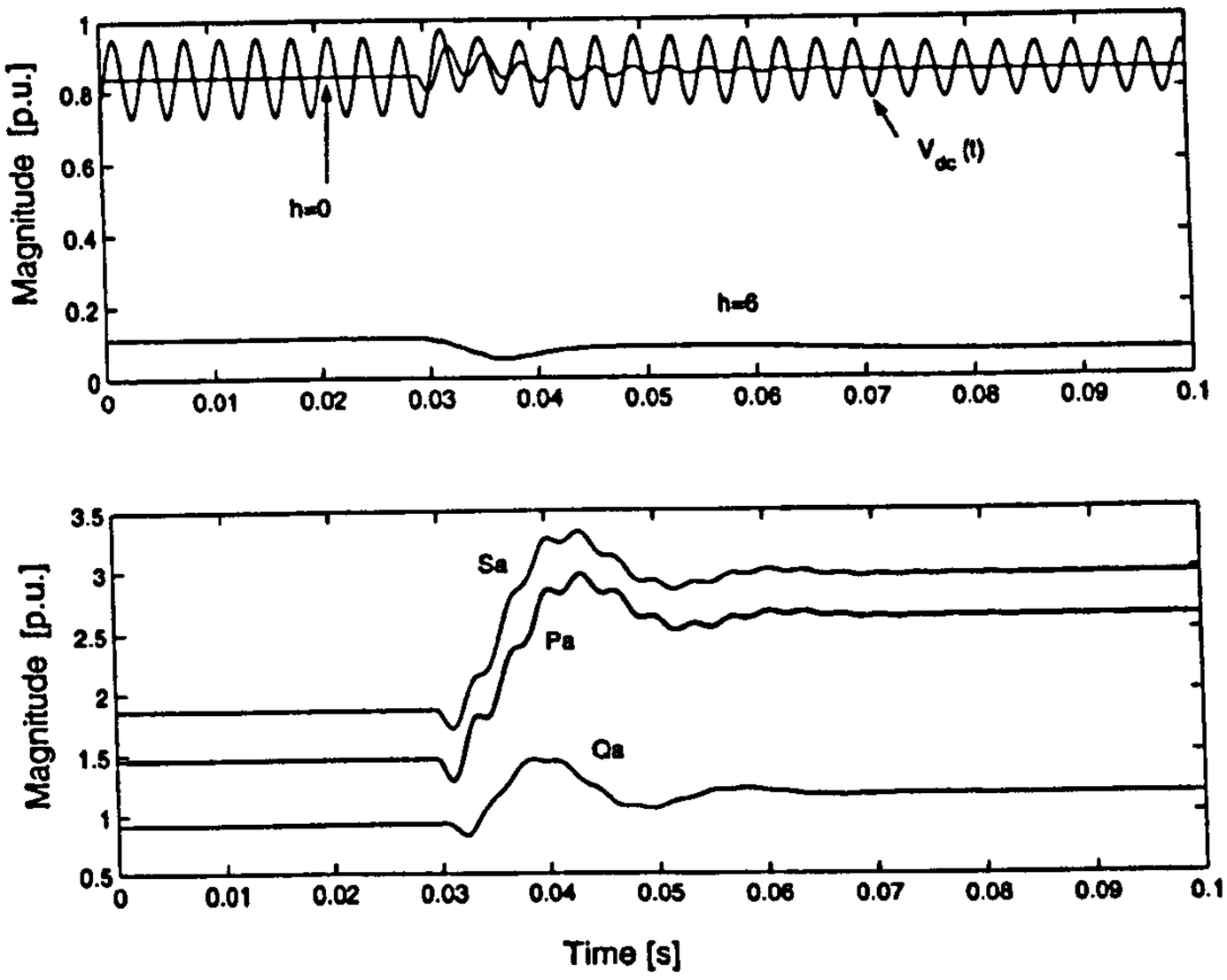

Figure 7.13.: DC side voltage and powers flowing into the HVDC-VSC back-to-back for Case 2

and the current in the DC side of the VSCs are

$$i_1(t) = \mathbf{q}_{s_1}(t)\mathbf{i}_{abc}(t) \tag{7.18}$$

$$i_2(t) = \mathbf{q}_{s_2}(t)\mathbf{i}_{ABC}(t) \tag{7.19}$$

Also, the voltage in the capacitors are given by

$$\frac{\mathrm{d}v_{dc_1}(t)}{\mathrm{d}t} = \frac{1}{C}(i_1(t) - i_1^c(t)) \tag{7.20}$$

$$\frac{\mathrm{d}v_{dc_2}(t)}{\mathrm{d}t} = \frac{1}{C}(i_2(t) - i_N^c(t)) \tag{7.21}$$

where $i_1^c(t)$ and $i_N^c(t)$ are the input and output currents of the cable. Since the cable model must cater for transient and steady-state analyses, a circuit representation similar to the one shown in Figure 7.14 should be used to represent the HVDC-VSC transmission system.

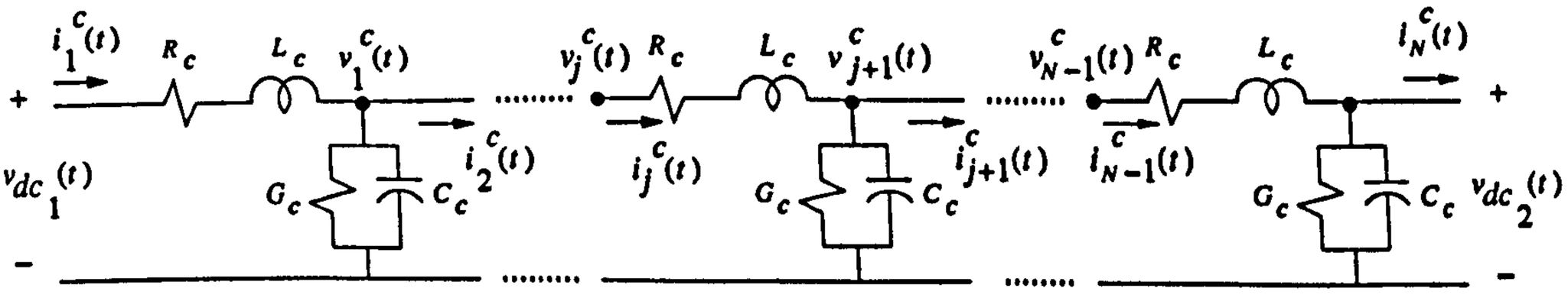

Figure 7.14.: Distributed parameter equivalent circuit of the $N-$section discretised cable

Using differential equations, the voltage drops across the three-phase impedance of the HVDC-VSC transmission system are,

$$\mathbf{v}_{abc}(t) - \mathbf{v}_{abc_1}(t) = R_e \mathbf{i}_{abc}(t) + L_e \frac{\mathrm{d}\mathbf{i}_{abc}(t)}{\mathrm{d}t} \tag{7.22}$$

$$\mathbf{v}_{ABC}(t) - \mathbf{v}_{ABC_1}(t) = R_e \mathbf{i}_{ABC}(t) + L_e \frac{\mathrm{d}\mathbf{i}_{ABC}(t)}{\mathrm{d}t} \tag{7.23}$$

For the cable shown in Figure 7.14, the differential equations which represent the cable are [106]:

$$\frac{\mathrm{d}i_1^c(t)}{\mathrm{d}t} = -\frac{R_c}{L_c} i_1^c(t) + \frac{1}{L_c}\left(v_{dc_1}(t) - v_2^c(t)\right) \tag{7.24}$$

$$\frac{\mathrm{d}v_2^c(t)}{\mathrm{d}t} = -\frac{G_c}{C_c} v_2^c(t) + \frac{1}{C_c}\left(i_1^c(t) - i_2^c(t)\right) \tag{7.25}$$

$$\vdots$$

$$\frac{\mathrm{d}i_j^c(t)}{\mathrm{d}t} = -\frac{R_c}{L_c} i_j^c(t) + \frac{1}{L_c}\left(v_j^c(t) - v_{j+1}^c(t)\right) \tag{7.26}$$

$$\frac{\mathrm{d}v_{j+1}^c(t)}{\mathrm{d}t} = -\frac{G_c}{C_c} v_{j+1}^c(t) + \frac{1}{C_c}\left(i_j^c(t) - i_{j+1}^c(t)\right) \tag{7.27}$$

$$\vdots$$

$$\frac{\mathrm{d}i_{N-1}^c(t)}{\mathrm{d}t} = -\frac{R_c}{L_c} i_{N-1}^c(t) + \frac{1}{L_c}\left(v_{N-1}^c(t) - v_{dc_2}(t)\right) \tag{7.28}$$

$$i_N^c(t) = i_{N-1}^c(t) - G_c v_{dc_2}(t) - C_c \frac{\mathrm{d}v_{dc_2}(t)}{\mathrm{d}t} \tag{7.29}$$

where N is the number of sections of the cable. $R_c = R'\Delta l$, $L_c = L'\Delta l$, $C_c = C'\Delta l$ and $G_c = G'\Delta l$. $\Delta l = l/N$ and l the cable length in km. R', L', C' and G' are the characteristic parameters of the cable in Ω/km, H/km, F/km and S/km, respectively.

From equations (7.21) and (7.29) the following equation is obtained,

$$\frac{\mathrm{d}v_{dc_2}(t)}{\mathrm{d}t} = -\frac{G_c}{C + C_c} v_{dc_2}(t) + \frac{1}{C + C_c}\left(i_2(t) - i_{N-1}^c(t)\right) \tag{7.30}$$

Suitable combinations of the previous equations yields a time state-space equation that describes the dynamics of the HVDC-VSC transmission system given by

$$\dot{\mathbf{x}}(t) = \mathbf{A}(t)\mathbf{x}(t) + \frac{1}{L_e}\mathbf{u}(t) \tag{7.31}$$

where

$$\mathbf{x}(t)=\begin{bmatrix} \mathbf{i}_{abc}(t) \\ \mathbf{i}_{ABC}(t) \\ v_{dc_1}(t) \\ v_{dc_2}(t) \\ i_1^c(t) \\ v_2^c(t) \\ i_2^c(t) \\ \vdots \\ v_{N-1}^c(t) \\ i_{N-1}^c(t) \end{bmatrix} \quad \mathbf{u}(t)=\begin{bmatrix} \mathbf{v}_{abc}(t) \\ \mathbf{v}_{ABC}(t) \\ 0 \\ 0 \\ 0 \\ 0 \\ 0 \\ \vdots \\ 0 \\ 0 \end{bmatrix}$$

$$\mathbf{A}(t)=\begin{bmatrix}
-\frac{R_e}{L_e} & 0 & -\frac{1}{L_e}\mathbf{p}_{s_1}(t) & 0 & 0 & 0 & 0 & 0 & 0 & 0 \\
0 & -\frac{R_e}{L_e} & 0 & -\frac{1}{L_e}\mathbf{p}_{s_2}(t) & 0 & 0 & 0 & 0 & 0 & 0 \\
\frac{1}{C}\mathbf{q}_{s_1}(t) & 0 & 0 & 0 & -\frac{1}{C} & 0 & 0 & 0 & 0 & 0 \\
0 & \frac{1}{C+C_c}\mathbf{q}_{s_2}(t) & 0 & -\frac{G_c}{C+C_c} & 0 & 0 & 0 & 0 & 0 & \frac{1}{C+C_c} \\
0 & 0 & \frac{1}{L_c} & 0 & -\frac{R_c}{L_c} & -\frac{1}{L_c} & 0 & 0 & 0 & 0 \\
0 & 0 & 0 & 0 & \frac{1}{C_c} & -\frac{G_c}{C_c} & -\frac{1}{C_c} & 0 & 0 & 0 \\
0 & 0 & 0 & 0 & 0 & \frac{1}{L_c} & -\frac{R_c}{L_c} & \ddots & 0 & 0 \\
0 & 0 & 0 & 0 & 0 & 0 & \ddots & \ddots & -\frac{1}{L_c} & 0 \\
0 & 0 & 0 & 0 & 0 & 0 & 0 & \frac{1}{C_c} & -\frac{G_c}{C_c} & -\frac{1}{C_c} \\
0 & 0 & 0 & -\frac{1}{L_c} & 0 & 0 & 0 & 0 & \frac{1}{L_c} & \frac{R_c}{L_c}
\end{bmatrix}$$

Moreover, this equation can be transformed into a LTI system using the EHD method, resulting in the general form of

$$\dot{\mathbf{X}}(t)=(\mathbf{A}-\mathbf{D}_d(\mathrm{j}h\omega_0))\mathbf{X}(t)+\frac{1}{L_e}\mathbf{U} \tag{7.32}$$

The state-space equation (7.32) is similar in form to (7.15) but it is larger due to the increased number of sections considered to represent the cable.

7.5. Conclusions

The EHD has been applied to obtain space-state models for the STATCOM, HVDC-VSC back-to-back tie and HVDC-VSC transmission system. This new state-space gives the dynamic response of the harmonics produced by these power electronics controllers. It was shown that

the harmonics have a very sensitive response to power quality disturbances, even for very sharp impulses. Such a sensitive characteristic may be used for control purposes, where observators may be used to reproduce the dynamic harmonic response of real systems.

These harmonics can be analysed from the sequences viewpoint giving additional information with which to analyse balanced and unbalanced conditions under transient and steady-state conditions. Moreover, the initial conditions for the STATCOM and HVDC-VSC configurations may be obtained from the HD steady-state models since the HD is a particular case of the EHD. State-space models for the UPFC and DVR may also be obtained. The state-space models may be used for stability analysis and control design.

8. Instantaneous Power Flow

8.1. Introduction

An instantaneous power flow (IPF) solution method for analysing the harmonic power flow problem is proposed in this chapter. The IPF uses the instantaneous power balance concept to formulate the problem. The methodology uses both the HD as a frame-of-reference and the Newton–Raphson method as numerical technique. The method is formulated exclusively in the frequency domain and applicable to systems which may also contain non-linear elements and power electronics controllers. The method offers a flexible and modular formulation which shows very strong convergence properties. The IPF is formulated, implemented in a computer program and tested for cases of linear and non-linear concentrated loads and the thyristor-controlled reactor (TCR) as an example of a power electronic controller.

The work on harmonic power flow analysis solution techniques was pioneered by D. Xia and G.T. Heydt [56][57] where the conventional Newton–Raphson power flow method was reformulated to include the harmonic current flows and to solve fundamental frequency parameters and harmonics simultaneously using Newton's method. In [58], the previous method was extended to include unbalanced systems and in [59] a converter model was included in the algorithm. A difficult task associated with this method is that each non-linear load type must be represented by its analytical expressions and included in the Jacobian. Also, it is reported that this method takes around 20 iterations to reach convergence in the presence of non-linear loads [55].

In [60] a different harmonic power flow approach is proposed. The method consists of two main parts; the first part is the construction of a harmonic Norton equivalent for the non-linearities using FFTs, and the second part performs the network solutions at the fundamental and one harmonic frequency at a time. The method requires the use of time domain solutions which interact with frequency domain solution through the use of FFTs.

In [61] a sequential method to solve the harmonic propagation problem is proposed, the emphasis of which is on the modelling of non-linear elements using the harmonic domain. A power flow solution is carried out at the fundamental frequency and then combined with a harmonic propagation solution. A modular approach for three-phase harmonic power flows is given in [62]. This modular concept consists in solving the system at fundamental frequency and the solution being used to initialise the full harmonic solution. This approach facilitates the devel-

opment of new non-linear models by including them only in the harmonic solution. The overall solution requires three iterative processes: The first is for the fundamental positive sequence power flow solution, the second is for the fundamental three-phase power flow solution, and the last one for the full harmonic solution. A hybrid methodology is described in [63] to solve the harmonic propagation problem. This method uses the frequency domain to represent linear components and the time domain for non-linear and time-varying components. The steady-state operating point is achieved using Poincaré's acceleration.

Several techniques have been put forward to solve the harmonic power flow problem. In all these methods the linear concentrated loads –for which their active and reactive powers are assumed to be known– are represented by an equivalent admittance at harmonic frequencies. The disadvantage of this representation is that many types of equivalent circuits exist, with their very different responses at high harmonic frequencies [107][43][13]. For the case of an unknown non-linear load an injected current or harmonic voltage source is normally used. A further characteristic of most of these methods is that the addition of a new electronic-based controller requires its analytical representation, and an ensuing non-straightforward reformulation of the Jacobian.

In this chapter, the most popular power electronic-based controllers are included in the nodal admittance matrix of the electric network by means of an equivalent harmonic admittance. The control equations such as active and reactive power, and variables such as harmonic voltages and firing angles are included in the Jacobian. The concentrated linear and non-linear loads are represented by their power and no admittance representation elsewhere is required.

The instantaneous power balance and the Newton–Raphson method are used to formulate the IPF method proposed in this chapter. This method follows the principle of conservation of energy as applied to electric circuits, where the instantaneous power and the average (active) power are the only powers which possess the conservation property under harmonic distortion. In the proposed methodology the HD is used as the frame-of-reference, where the fundamental frequency, harmonics and cross-coupling between harmonic frequencies are all involved in the solution at the same time.

In order to keep the explanation of the method simple, a single-phase system, linear and non-linear concentrated loads, and a TCR used for reactive power control are considered in this chapter. However, the methodology is general and it could be extended to encompass three-phase unbalanced networks and other non-linearities.

8.2. Power System Modelling in the Harmonic Domain

If all the network elements are represented by a harmonic admittance matrix, the nodal equations of the entire network is obtained with ease, i.e.

$$\begin{bmatrix} \mathbf{I}^1 \\ \mathbf{I}^2 \\ \vdots \\ \mathbf{I}^N \end{bmatrix} = \begin{bmatrix} \mathbf{Y}^{1,1} & \mathbf{Y}^{1,2} & \cdots & \mathbf{Y}^{1,N} \\ \mathbf{Y}^{2,1} & \mathbf{Y}^{2,2} & \cdots & \mathbf{Y}^{2,N} \\ \vdots & \vdots & \ddots & \vdots \\ \mathbf{Y}^{N,1} & \mathbf{Y}^{N,2} & \cdots & \mathbf{Y}^{N,N} \end{bmatrix} \begin{bmatrix} \mathbf{V}^1 \\ \mathbf{V}^2 \\ \vdots \\ \mathbf{V}^N \end{bmatrix} \tag{8.1}$$

where N is the number of nodes of the network, and the element $\mathbf{Y}^{i,j}$ is a $(2h+1) \times (2h+1)$ equivalent harmonic admittance matrix between nodes i and j, which has the form

$$\mathbf{Y}^{i,j} = \begin{bmatrix} Y^{i,j}_{-h,-h} & \cdots & Y^{i,j}_{-h,0} & \cdots & Y^{i,j}_{-h,h} \\ \vdots & \ddots & & & \vdots \\ Y^{i,j}_{0,-h} & \cdots & Y^{i,j}_{0,0} & \cdots & Y^{i,j}_{0,h} \\ \vdots & & & \ddots & \vdots \\ Y^{i,j}_{h,-h} & \cdots & Y^{i,j}_{h,0} & \cdots & Y^{i,j}_{h,h} \end{bmatrix}$$

Equation (8.1) can be written in a more compact form as

$$\mathbf{I}^{\text{nodal}} = \mathbf{Y}^{\text{nodal}} \mathbf{V}^{\text{nodal}} \tag{8.2}$$

where $\mathbf{Y}^{\text{nodal}}$ includes all the transmission elements such as transmission lines, transformers, capacitor banks, magnetic non-linearities and power electronics controllers.

The power flow problem consists in solving (8.2) for the nodal voltages $\mathbf{V}^{\text{nodal}}$ corresponding to an operating point of the electrical network. Since the known variables are the demanded powers and not the nodal current $\mathbf{I}^{\text{nodal}}$, then equations for the nodal currents based on the yet unknown nodal voltages and specified powers are required; this is the fundamental constraint of the power flow method.

8.3. Instantaneous Power Calculation

In conventional power flow methods, the balance of active and reactive power at the fundamental frequency is used to solve the classic power flow problem. In existing harmonic power flow methods, the balance of harmonic currents is also included in the formulation. Alternatively, in the IPF method proposed in this chapter, only the instantaneous power balance is used.

From equation (8.1) an arbitrary injection current, $\mathbf{I}^i$, is given by

$$\mathbf{I}^i = \sum_{j=1}^{N} \mathbf{Y}^{i,j} \mathbf{V}^j \tag{8.3}$$

and the calculated instantaneous power injected into node i is given by the convolution between the voltage and current, i.e.

$$\mathbf{P}^i_{\text{calc}} = \mathbf{V}^i \otimes \mathbf{I}^i \tag{8.4}$$

The vector $\mathbf{P}^i_{\text{calc}}$ represents the harmonics of the instantaneous power injected into node i.

An arbitrary harmonic element of $\mathbf{I}^i$, say I^i_y, from (8.3) is given by

$$I^i_y = \sum_{j=1}^{N} \sum_{n=-h}^{h} Y^{i,j}_{y,n} V^j_n \tag{8.5}$$

An arbitrary harmonic element of the instantaneous power, e.g. $P^i_{\text{calc}_x}$, is obtained from (8.4) as

$$P^i_{\text{calc}_x} = \sum_{n=-h}^{h} V^i_{x-n} I^i_n \tag{8.6}$$

Using (8.5) in (8.6),

$$P^i_{\text{calc}_x} = \sum_{n=-h}^{h} V^i_{x-n} \sum_{j=1}^{N} \sum_{m=-h}^{h} Y^{i,j}_{n,m} V^j_m \tag{8.7}$$

Equation (8.7) gives the x-th harmonic of the instantaneous power injected into node i. The instantaneous powers injected in all the nodes of the network are given by $i = 1,\ldots,N$ with $x = -h,\ldots,h$.

From the power flow problem viewpoint, the calculated instantaneous power, equation (8.7), must satisfy the instantaneous power demanded by the load. Hence, an instantaneous power representation of concentrated loads is required.

8.3.1. Concentrated linear load

Assuming that the specified (spd) active and reactive power loads at the fundamental frequency at node i are P^i_{f} and Q^i_{f}, respectively; where the load voltage is $v(t) = V^i_{\text{peak}} \sin(\omega_0 t - \theta^i_0)$ and the current response is $i(t) = I^i_{\text{peak}} \sin(\omega_0 t - \theta^i_0 + \phi^i)$. The angle θ^i_0 is the shift angle with respect to the reference node (slack node) and ϕ^i is the load angle. It follows that the instantaneous power, $p(t) = v(t)i(t)$, is given by

$$p(t) = V^i_{\text{peak}} I^i_{\text{peak}} \sin(\omega_0 t - \theta^i_0) \sin(\omega_0 t - \theta^i_0 + \phi^i) \tag{8.8}$$

Expanding (8.8) using Euler's identities, the following expression is obtained,

$$p(t) = P^i_{\text{spd}_{-2}} e^{j2\theta^i_0} e^{-j2\omega_0 t} + P^i_{\text{spd}_0} + P^i_{\text{spd}_2} e^{-j2\theta^i_0} e^{j2\omega_0 t} \tag{8.9}$$

where

$$P^i_{\text{spd}_{-2}} = \frac{1}{2}\left(P^i_{\text{f}} - jQ^i_{\text{f}}\right)$$

$$P^i_{\mathrm{spd}_0} = P^i_{\mathrm{f}} \qquad (8.10)$$
$$P^i_{\mathrm{spd}_2} = \frac{1}{2}\left(P^i_{\mathrm{f}} + \mathrm{j}Q^i_{\mathrm{f}}\right)$$

From the HD viewpoint, equation (8.9) is represented by the scheduled (scd) harmonic instantaneous power vector,

$$\mathbf{P}^i_{\mathrm{scd}} = \begin{bmatrix} \mathrm{e}^{\mathrm{j}2\theta^i_0} P^i_{\mathrm{spd}_{-2}} \\ 0 \\ P^i_{\mathrm{spd}_0} \\ 0 \\ \mathrm{e}^{-\mathrm{j}2\theta^i_0} P^i_{\mathrm{spd}_2} \end{bmatrix} \qquad (8.11)$$

which gives the representation of concentrated linear loads.

8.3.2. Concentrated non-linear loads

Equation (8.11) represents the scheduled instantaneous power for linear concentrated loads under sinusoidal conditions. The general representation of (8.11) may be given by

$$\mathbf{P}^i_{\mathrm{scd}} = \begin{bmatrix} \mathrm{e}^{\mathrm{j}h\theta^i_0} P^i_{\mathrm{spd}_{-h}} \\ \vdots \\ \mathrm{e}^{\mathrm{j}\theta^i_0} P^i_{\mathrm{spd}_{-1}} \\ P^i_{\mathrm{spd}_0} \\ \mathrm{e}^{-\mathrm{j}\theta^i_0} P^i_{\mathrm{spd}_1} \\ \vdots \\ \mathrm{e}^{-\mathrm{j}h\theta^i_0} P^i_{\mathrm{spd}_h} \end{bmatrix} \qquad (8.12)$$

which would encompass both linear and non-linear concentrated loads. The complex values, P^i_{spd}, are obtained for (8.10) if the load is linear, and from the convolution between the harmonic voltages and harmonic currents measured at the load point if it is non-linear. The angle θ^i_0 is an unknown variable which is the shift angle between the voltage zero-crossing in node *i* with respect to the system reference voltage zero-crossing (slack node).

8.4. Newton–Raphson Method Applied to Instantaneous Power Balance

Using the scheduled instantaneous power given by (8.12) and the calculated instantaneous power (8.7), the set of mismatch equations is

$$\begin{bmatrix} \Delta\mathbf{P}^1 \\ \vdots \\ \Delta\mathbf{P}^i \\ \vdots \\ \Delta\mathbf{P}^N \end{bmatrix} = \begin{bmatrix} \mathbf{P}^1_{\text{scd}} \\ \vdots \\ \mathbf{P}^i_{\text{scd}} \\ \vdots \\ \mathbf{P}^N_{\text{scd}} \end{bmatrix} - \begin{bmatrix} \mathbf{P}^1_{\text{calc}} \\ \vdots \\ \mathbf{P}^i_{\text{calc}} \\ \vdots \\ \mathbf{P}^N_{\text{calc}} \end{bmatrix} = \begin{bmatrix} 0 \\ \vdots \\ 0 \\ \vdots \\ 0 \end{bmatrix} \tag{8.13}$$

or in compact form,

$$\Delta\mathbf{P} = \mathbf{P}_{\text{scd}} - \mathbf{P}_{\text{calc}} = 0 \tag{8.14}$$

which form a set of $N \times (2h+1)$ equations. The variables are the harmonics of $\mathbf{V}^i$ and the voltage zero-crossing angle θ^i_0 per node, giving a set of $N \times (2h+1) + N$ unknown variables. The other N equations are obtained from the voltage zero-crossing at all the nodes, e.g. for node i the voltage zero-crossing (VZC) is given by

$$\text{VZC}^i = \sum_{n=-h}^{h} V^i_n e^{jn\theta^i_0} = 0 \tag{8.15}$$

With (8.14) and (8.15) for $i = 1,\ldots,N$ the complete set of mismatch equations is

$$\begin{bmatrix} \Delta\mathbf{P} \\ \mathbf{VZC} \end{bmatrix} = \begin{bmatrix} 0 \\ 0 \end{bmatrix} \tag{8.16}$$

Since (8.16) is a set of non-linear equations, they may be solved with the Newton–Raphson method using the following iterative equation,

$$\begin{bmatrix} \Delta\mathbf{V} \\ \Delta\theta_0 \end{bmatrix} = -\begin{bmatrix} \dfrac{\partial\Delta\mathbf{P}}{\partial\mathbf{V}} & \dfrac{\partial\Delta\mathbf{P}}{\partial\theta_0} \\ \dfrac{\partial\mathbf{VZC}}{\partial\mathbf{V}} & \dfrac{\partial\mathbf{VZC}}{\partial\theta_0} \end{bmatrix}^{-1} \begin{bmatrix} \Delta\mathbf{P} \\ \mathbf{VZC} \end{bmatrix}^{(k)} \tag{8.17}$$

where:

$$\Delta\mathbf{V} = \mathbf{V}^{(k+1)} - \mathbf{V}^{(k)}$$

$$\Delta\theta_0 = \Delta\theta_0^{(k+1)} - \theta_0^{(k)}$$

and 'k' an iteration counter.

It should be noted that the elements of the Jacobian (per node) are given by

$$\mathbf{J}^{i,k} = \begin{bmatrix} \frac{\partial \Delta P^i_{-h}}{\partial V^k_{-h}} & \cdots & \frac{\partial \Delta P^i_{-h}}{\partial V^k_0} & \cdots & \frac{\partial \Delta P^i_{-h}}{\partial V^k_h} & \frac{\partial \Delta P^i_{-h}}{\partial \theta^k_0} \\ \vdots & \ddots & & & \vdots & \vdots \\ \frac{\partial \Delta P^i_0}{\partial V^k_{-h}} & \cdots & \frac{\partial \Delta P^i_0}{\partial V^k_0} & \cdots & \frac{\partial \Delta P^i_0}{\partial V^k_h} & \frac{\partial \Delta P^i_0}{\partial \theta^k_0} \\ \vdots & & & \ddots & \vdots & \vdots \\ \frac{\partial \Delta P^i_h}{\partial V^k_{-h}} & \cdots & \frac{\partial \Delta P^i_h}{\partial V^k_0} & \cdots & \frac{\partial \Delta P^i_h}{\partial V^k_h} & \frac{\partial \Delta P^i_h}{\partial \theta^k_0} \\ \frac{\partial \mathrm{VZC}^i}{\partial V^k_{-h}} & \cdots & \frac{\partial \mathrm{VZC}^i}{\partial V^k_0} & \cdots & \frac{\partial \mathrm{VZC}^i}{\partial V^k_h} & \frac{\partial \mathrm{VZC}^i}{\partial \theta^k_0} \end{bmatrix}$$

for $i,k = 1,\ldots,N$.

8.4.1. Analytical form of the Jacobian

In the first instance, in order to obtain the analytical expression for the Jacobian, the partial derivative of (8.14) with respect to the nodal voltages is

$$\frac{\partial \Delta \mathbf{P}}{\partial \mathbf{V}} = \frac{\partial (\mathbf{P}_{\mathrm{scd}} - \mathbf{P}_{\mathrm{calc}})}{\partial \mathbf{V}} = -\frac{\partial \mathbf{P}_{\mathrm{calc}}}{\partial \mathbf{V}} \tag{8.18}$$

The partial derivative of the element $P^i_{\mathrm{calc}_x}$ of $\mathbf{P}_{\mathrm{calc}}$, with respect to an arbitrary element of the nodal voltage V^k_y of $\mathbf{V}^k$, using (8.7) for $i = k$ and $i \neq k$, are

$$\begin{aligned} \frac{\partial P^k_{\mathrm{calc}_x}}{\partial V^k_y} &= \sum_{n=-h,\neq x-y}^{h} V^k_{x-n} Y^{k,k}_{n,y} + \sum_{j=1,\neq k}^{N} \sum_{m=-h}^{h} Y^{k,j}_{x-y,m} V^j_m \\ &\quad + \sum_{m=-h,\neq y}^{h} Y^{k,k}_{x-y,m} V^k_m + 2 V^k_y Y^{k,k}_{x-y,y} \end{aligned} \tag{8.19}$$

$$\frac{\partial P^i_{\mathrm{calc}_x}}{\partial V^k_y} = \sum_{n=-h,\neq x-y}^{h} V^i_{x-n} Y^{i,k}_{n,y} + V^i_y Y^{i,k}_{x-y,y} \tag{8.20}$$

for $i,k = 1,\ldots,N$ and $x,y = -h,\ldots,h$.

Now the partial derivative of (8.14) with respect to the nodal voltages zero-crossing angles θ_0 is,

$$\frac{\partial \Delta \mathbf{P}}{\partial \theta_0} = \frac{\partial (\mathbf{P}_{\mathrm{scd}} - \mathbf{P}_{\mathrm{calc}})}{\partial \theta_0} = \frac{\partial \mathbf{P}_{\mathrm{scd}}}{\partial \theta_0} \tag{8.21}$$

and the partial derivative of the element $P^i_{\mathrm{scd}_x}$ with respect to an arbitrary nodal voltage zero-crossing angle θ^k_0, using (8.12) for $i = k$ and $i \neq k$, are

$$\frac{\partial P^k_{\mathrm{scd}_x}}{\partial \theta^k_0} = -\mathrm{j}x\mathrm{e}^{-\mathrm{j}x\theta^k_0} P^k_{\mathrm{spd}_x} \tag{8.22}$$

$$\frac{\partial P^i_{\mathrm{scd}_x}}{\partial \theta^k_0} = 0 \tag{8.23}$$

for $i,k = 1,\ldots,N$ and $x = -h,\ldots,h$.

The partial derivative of equation (8.15) with respect to the harmonic voltage V^k_y, for $i = k$ and $i \neq k$, are

$$\frac{\partial \mathrm{VZC}^k}{\partial V^k_y} = \mathrm{e}^{\mathrm{j}y\theta^k_0} \tag{8.24}$$

$$\frac{\partial \mathrm{VZC}^i}{\partial V^k_y} = 0 \tag{8.25}$$

for $i,k = 1,\ldots,N$ and $y = -h,\ldots,h$.

Finally, the partial derivative with respect to the voltage zero-crossing angle θ^k_0, for $i = k$ and $i \neq k$, are

$$\frac{\partial \mathrm{VZC}^k}{\partial \theta^k_0} = \sum_{n=-h}^{h} \mathrm{j}nV^k_n \mathrm{e}^{\mathrm{j}n\theta^k_0} \tag{8.26}$$

$$\frac{\partial \mathrm{VZC}^i}{\partial \theta^k_0} = 0 \tag{8.27}$$

for $i,k = 1,\ldots,N$.

With the use of equations (8.19), (8.20) and (8.22)–(8.27) the Jacobian matrix is calculated. Additional mismatch equations can be included in the main system represented by (8.17).

8.5. Active and Reactive Power Control using FACTS Controllers

FACTS controllers are used on transmission systems mainly to control active and reactive power at the fundamental frequency, where the active and reactive equations of these controllers are used as part of the Jacobian.

8.5.1. Reactive power control via TCR

For the case of a TCR connected at the node i, the fundamental frequency reactive power absorbed by the TCR is given by

$$Q_{\mathrm{f}}^{i} = \frac{2(\pi-\alpha)-\sin 2(\pi-\alpha)}{\pi X_L}|V_{\mathrm{f}}^{i}|^2$$

Where α is the firing angle of the thyristors, X_L the rated reactance of the reactor and V_{f} the RMS voltage at the terminals of the TCR [12].

In the harmonic domain, it is easy to show that if $|V_{\mathrm{f}}^{i}|^2 = 2V_{-1}^{i}V_{1}^{i}$, then the reactive power absorbed by the TCR is given by

$$Q_{\mathrm{f}}^{i} = \frac{2(\pi-\alpha)-\sin 2(\pi-\alpha)}{\pi X_L}2V_{-1}^{i}V_{1}^{i} \tag{8.28}$$

where the control variable is the thyristor's firing angle α.

The mismatch equation is then given by

$$\Delta Q_{\mathrm{f}}^{i} = Q_{\mathrm{scd}}^{i} - Q_{\mathrm{f}}^{i} \tag{8.29}$$

where Q_{scd}^{i} is the scheduled reactive power to be absorbed by the TCR at the fundamental frequency. Including this new mismatch equation into (8.17) results in additional elements appearing in the Jacobian, i.e.

$$\begin{bmatrix} \Delta \mathbf{V} \\ \Delta\theta_0 \\ \Delta\alpha \end{bmatrix} = -\begin{bmatrix} \frac{\partial \Delta \mathbf{P}}{\partial \mathbf{V}} & \frac{\partial \Delta \mathbf{P}}{\partial \theta_0} & 0 \\ \frac{\partial \mathbf{VZC}}{\partial \mathbf{V}} & \frac{\partial \mathbf{VZC}}{\partial \theta_0} & 0 \\ \frac{\partial \Delta Q_{\mathrm{f}}}{\partial V_{\pm 1}} & 0 & \frac{\partial \Delta Q_{\mathrm{f}}}{\partial \alpha} \end{bmatrix}^{-1} \begin{bmatrix} \Delta \mathbf{P} \\ \mathbf{VZC} \\ \Delta Q_{\mathrm{f}} \end{bmatrix}^{(k)} \tag{8.30}$$

where the new non-zero expressions in the Jacobian are

$$\frac{\partial \Delta Q_{\mathrm{f}}^{i}}{\partial V_{-1}^{i}} = -\frac{2(\pi-\alpha)-\sin 2(\pi-\alpha)}{\pi X_L}2V_{1}^{i} \tag{8.31}$$

$$\frac{\partial \Delta Q_{\mathrm{f}}^{i}}{\partial V_{1}^{i}} = -\frac{2(\pi-\alpha)-\sin 2(\pi-\alpha)}{\pi X_L}2V_{-1}^{i} \tag{8.32}$$

$$\frac{\partial \Delta Q_{\mathrm{f}}^{i}}{\partial \alpha} = -\frac{-2+2\cos 2(\pi-\alpha)}{\pi X_L}2V_{-1}^{i}V_{1}^{i} \tag{8.33}$$

On the other hand, the effect of the TCR is included in the nodal admittance matrix $\mathbf{Y}^{\mathrm{nodal}}$ as

follows

$$\mathbf{Y}^{\text{nodal}^{i,i}} = \mathbf{Y}^{\text{nodal}^{i,i}} + \mathbf{Y}_{\text{TCR}} \tag{8.34}$$

where the harmonic equivalent admittance of the TCR is given by

$$\mathbf{Y}_{\text{TCR}} = \frac{1}{L}\mathbf{D}^{-1}(\mathrm{j}h\omega_0)\mathbf{S}$$

where L is the inductance of the reactor, $\mathbf{D}(\mathrm{j}h\omega_0)$ is a diagonal matrix with entries $\mathrm{j}h\omega_0$ and $\mathbf{S}$ is a Toeplitz matrix which represents the operations of the thyristors, governed by the firing angle α and the current zero-crossing in the reactor, see Appendix D.

8.5.2. Reactive power control via TCSC

The thyristor-controlled series compensator (TCSC) may be used in the control of the fundamental reactive power flow between nodes i and j. This power is calculated by the expression

$$Q_{\text{f}}^{ij} = \frac{|V^i|^2}{X_{\text{TCSC}}(\alpha)} - \frac{|V^i||V^j|}{X_{\text{TCSC}}(\alpha)}\cos\left(\theta_0^i - \theta_0^j\right)$$

where $X_{\text{TCSC}}(\alpha)$ is the equivalent impedance of the TCSC at the fundamental frequency as a function of the thyristors firing angle α, given by [18]:

$$\begin{aligned} X_{\text{TCSC}}(\alpha) \;=\; & -X_C + (X_C + X_{LC})\frac{2(\pi-\alpha)+\sin 2(\pi-\alpha)}{\pi} \\ & -\frac{4X_{LC}^2\cos^2(\pi-\alpha)}{X_L}\frac{k\tan k(\pi-\alpha)-\tan(\pi-\alpha)}{\pi} \end{aligned} \tag{8.35}$$

where $k = \frac{1}{\sqrt{LC}\omega_0}$, $X_{LC} = \frac{X_C X_L}{X_C - X_L}$, and X_L and X_C are the rated impedance of the reactor and the capacitor, respectively.

The power expression may be re-written to enable a more appropriate expression for the IPF,

$$Q_{\text{f}}^{ij} = \frac{2V_{-1}^i V_1^i}{X_{\text{TCSC}}(\alpha)} - \frac{2\left(V_{-1}^i V_1^i V_{-1}^j V_1^j\right)^{1/2}}{X_{\text{TCSC}}(\alpha)}\cos\left(\theta_0^i - \theta_0^j\right) \tag{8.36}$$

where the mismatch equation to be included in the base system is

$$\Delta Q_{\text{f}}^{ij} = Q_{\text{scd}}^{ij} - Q_{\text{f}}^{ij} \tag{8.37}$$

and the unknown variable is the firing angle α.

The new elements in the Jacobian are

$$\frac{\partial \Delta Q_f^{ij}}{\partial V_{-1}^i} = -\frac{2V_1^i}{X_{TCSC}(\alpha)} + \frac{\left(V_{-1}^i V_1^i V_{-1}^j V_1^j\right)^{-1/2}\left(V_1^i V_{-1}^j V_1^j\right)}{X_{TCSC}(\alpha)} \cos\left(\theta_0^i - \theta_0^j\right) \quad (8.38)$$

$$\frac{\partial \Delta Q_f^{ij}}{\partial V_1^i} = -\frac{2V_{-1}^i}{X_{TCSC}(\alpha)} + \frac{\left(V_{-1}^i V_1^i V_{-1}^j V_1^j\right)^{-1/2}\left(V_{-1}^i V_{-1}^j V_1^j\right)}{X_{TCSC}(\alpha)} \cos\left(\theta_0^i - \theta_0^j\right) \quad (8.39)$$

$$\frac{\partial \Delta Q_f^{ij}}{\partial V_{-1}^j} = \frac{\left(V_{-1}^i V_1^i V_{-1}^j V_1^j\right)^{-1/2}\left(V_{-1}^i V_1^i V_1^j\right)}{X_{TCSC}(\alpha)} \cos\left(\theta_0^i - \theta_0^j\right) \quad (8.40)$$

$$\frac{\partial \Delta Q_f^{ij}}{\partial V_1^j} = \frac{\left(V_{-1}^i V_1^i V_{-1}^j V_1^j\right)^{-1/2}\left(V_{-1}^i V_1^i V_{-1}^j\right)}{X_{TCSC}(\alpha)} \cos\left(\theta_0^i - \theta_0^j\right) \quad (8.41)$$

$$\frac{\partial \Delta Q_f^{ij}}{\partial \theta_0^i} = -\frac{2\left(V_{-1}^i V_1^i V_{-1}^j V_1^j\right)^{1/2}}{X_{TCSC}(\alpha)} \sin\left(\theta_0^i - \theta_0^j\right) \quad (8.42)$$

$$\frac{\partial \Delta Q_f^{ij}}{\partial \theta_0^j} = \frac{2\left(V_{-1}^i V_1^i V_{-1}^j V_1^j\right)^{1/2}}{X_{TCSC}(\alpha)} \sin\left(\theta_0^i - \theta_0^j\right) \quad (8.43)$$

$$\frac{\partial \Delta Q_f^{ij}}{\partial \alpha} = \frac{V_{-1}^i V_1^i}{X_{TCSC}^2(\alpha)} \frac{\partial X_{TCSC}(\alpha)}{\partial \alpha} - \frac{2\left(V_{-1}^i V_1^i V_{-1}^j V_1^j\right)^{1/2}\left(V_{-1}^i V_1^i V_{-1}^j\right)}{X_{TCSC}^2(\alpha)} \frac{\partial X_{TCSC}(\alpha)}{\partial \alpha} \cos\left(\theta_0^i - \theta_0^j\right) \quad (8.44)$$

where

$$\begin{aligned}\frac{\partial X_{TCSC}(\alpha)}{\partial \alpha} = {} & -A_2 - A_5 - 2A_3 \cos 2(\pi - \alpha) \\ & -2A_4 \cos(\pi - \alpha) \sin(\pi - \alpha) \tan k(\pi - \alpha) \\ & +kA_4 \cos^2(\pi - \alpha) \sec^2 k(\pi - \alpha) \\ & +2A_5 \cos(\pi - \alpha) \sin(\pi - \alpha) \tan(\pi - \alpha)\end{aligned} \quad (8.45)$$

and

$$\begin{aligned}A_1 &= X_C \\ A_2 &= \frac{2(X_C + X_{LC})}{\pi} \\ A_3 &= \frac{X_C + X_{LC}}{\pi}\end{aligned}$$

$$A_4 = \frac{4kX_{LC}^2}{\pi X_L}$$
$$A_5 = \frac{4X_{LC}^2}{\pi X_L}$$

Once the new mismatch equation is included, the admittance of the TCSC, $\mathbf{Y}_{\text{TCSC}}$, is added to $\mathbf{Y}^{\text{nodal}}$ affecting the entries (i,i), (i,j), (j,i) and (j,j). The admittance $\mathbf{Y}_{\text{TCSC}}$ is obtained as shown in Appendix D.

8.5.3. Reactive power control via STATCOM

The STATCOM may be used to provide voltage support at node i by controlling the injection of reactive power at the fundamental frequency. The reactive power governing the operation of the STATCOM is given by

$$Q_{\text{f}}^i = \frac{|V^j|^2}{X_{\text{e}}} - \frac{|V^j||V^i|}{X_{\text{e}}}\cos\left(\theta_0^j - \theta_0^i\right)$$

X_{e} is the equivalent reactance of the coupling transformer; j is the secondary node side of the coupling transformer where the inverter is connected to; $|V^j| = \frac{mE_{\text{dc}}}{\sqrt{2}}$ where m is the modulation factor; and the angle θ^j is the shift angle ϕ_m of the modulation signal used in the firing control for the IGBTs of the converter. E_{dc} is the DC voltage of the converter. This expression may be re-written to make it more amenable to IPF,

$$Q_{\text{f}}^i = \frac{m^2E_{\text{dc}}^2}{2X_{\text{e}}} - \frac{mE_{\text{dc}}\left(V_{-1}^iV_1^i\right)^{1/2}}{X_{\text{e}}}\cos\left(\phi_m - \theta_0^i\right) \tag{8.46}$$

where the mismatch equation to be included in the base system is

$$\Delta Q_{\text{f}}^i = Q_{\text{scd}}^i - Q_{\text{f}}^i \tag{8.47}$$

and the unknown variables are the modulation factor m and the modulation shift angle ϕ_m.

The new elements in the Jacobian are:

$$\frac{\partial \Delta Q_{\text{f}}^i}{\partial V_{-1}^i} = \frac{2mE_{\text{dc}}\left(V_{-1}^iV_1^i\right)^{1/2}V_1^i}{X_{\text{e}}}\cos\left(\phi_m - \theta_0^i\right) \tag{8.48}$$

$$\frac{\partial \Delta Q_{\text{f}}^i}{\partial V_1^i} = \frac{2mE_{\text{dc}}\left(V_{-1}^iV_1^i\right)^{1/2}V_{-1}^i}{X_{\text{e}}}\cos\left(\phi_m - \theta_0^i\right) \tag{8.49}$$

$$\frac{\partial \Delta Q_{\text{f}}^i}{\partial \theta_0^i} = \frac{mE_{\text{dc}}\left(V_{-1}^iV_1^i\right)^{1/2}}{X_{\text{e}}}\sin\left(\phi_m - \theta_0^i\right) \tag{8.50}$$

$$\frac{\partial \Delta Q_{\text{f}}^i}{\partial m} = -\frac{mE_{\text{dc}}^2}{X_{\text{e}}} + \frac{E_{\text{dc}}\left(V_{-1}^iV_1^i\right)^{1/2}}{X_{\text{e}}}\cos\left(\phi_m - \theta_0^i\right) \tag{8.51}$$

$$\frac{\partial \Delta Q_{\mathrm{f}}^{i}}{\partial \phi_{m}} = -\frac{m E_{\mathrm{dc}} \left(V_{-1}^{i} V_{1}^{i}\right)^{1/2}}{X_{\mathrm{e}}} \sin\left(\phi_{m} - \theta_{0}^{i}\right) \tag{8.52}$$

At node j a harmonic voltage source $\mathbf{E}_{\mathrm{Th}}$ (similar to equation (3.4)) is connected to, which is treated like a PV node where the voltage magnitude is fixed, and phase angle governed by ϕ_m.

8.5.4. Active power control via TCSC

The TCSC may be used to control fundamental active power flow between nodes i and j. The power flow through this branch is calculated by the expression

$$P_{\mathrm{f}}^{ij} = \frac{|V^{i}||V^{j}|}{X_{\mathrm{TCSC}}(\alpha)} \sin\left(\theta_{0}^{i} - \theta_{0}^{j}\right)$$

which may be re-written to make it more amenable to IPF analysis

$$P_{\mathrm{f}}^{ij} = \frac{2\left(V_{-1}^{i} V_{1}^{i} V_{-1}^{j} V_{1}^{j}\right)^{1/2}}{X_{\mathrm{TCSC}}(\alpha)} \sin\left(\theta_{0}^{i} - \theta_{0}^{j}\right) \tag{8.53}$$

where the mismatch equation to be included in the base system is,

$$\Delta P_{\mathrm{f}}^{ij} = P_{\mathrm{scd}}^{ij} - P_{\mathrm{f}}^{ij} \tag{8.54}$$

and the unknown variable is the firing angle α.

The elements in the Jacobian are:

$$\frac{\partial \Delta P_{\mathrm{f}}^{ij}}{\partial V_{-1}^{i}} = -\frac{\left(V_{-1}^{i} V_{1}^{i} V_{-1}^{j} V_{1}^{j}\right)^{-1/2} \left(V_{1}^{i} V_{-1}^{j} V_{1}^{j}\right)}{X_{\mathrm{TCSC}}(\alpha)} \sin\left(\theta_{0}^{i} - \theta_{0}^{j}\right) \tag{8.55}$$

$$\frac{\partial \Delta P_{\mathrm{f}}^{ij}}{\partial V_{1}^{i}} = -\frac{\left(V_{-1}^{i} V_{1}^{i} V_{-1}^{j} V_{1}^{j}\right)^{-1/2} \left(V_{-1}^{i} V_{-1}^{j} V_{1}^{j}\right)}{X_{\mathrm{TCSC}}(\alpha)} \sin\left(\theta_{0}^{i} - \theta_{0}^{j}\right) \tag{8.56}$$

$$\frac{\partial \Delta P_{\mathrm{f}}^{ij}}{\partial V_{-1}^{j}} = -\frac{\left(V_{-1}^{i} V_{1}^{i} V_{-1}^{j} V_{1}^{j}\right)^{-1/2} \left(V_{-1}^{i} V_{1}^{i} V_{1}^{j}\right)}{X_{\mathrm{TCSC}}(\alpha)} \sin\left(\theta_{0}^{i} - \theta_{0}^{j}\right) \tag{8.57}$$

$$\frac{\partial \Delta P_{\mathrm{f}}^{ij}}{\partial V_{1}^{j}} = -\frac{\left(V_{-1}^{i} V_{1}^{i} V_{-1}^{j} V_{1}^{j}\right)^{-1/2} \left(V_{-1}^{i} V_{1}^{i} V_{-1}^{j}\right)}{X_{\mathrm{TCSC}}(\alpha)} \sin\left(\theta_{0}^{i} - \theta_{0}^{j}\right) \tag{8.58}$$

$$\frac{\partial \Delta P_{\mathrm{f}}^{ij}}{\partial \theta_{0}^{i}} = -\frac{2\left(V_{-1}^{i} V_{1}^{i} V_{-1}^{j} V_{1}^{j}\right)^{1/2}}{X_{\mathrm{TCSC}}(\alpha)} \cos\left(\theta_{0}^{i} - \theta_{0}^{j}\right) \tag{8.59}$$

$$\frac{\partial \Delta P_{\mathrm{f}}^{ij}}{\partial \theta_{0}^{j}} = \frac{2\left(V_{-1}^{i} V_{1}^{i} V_{-1}^{j} V_{1}^{j}\right)^{1/2}}{X_{\mathrm{TCSC}}(\alpha)} \cos\left(\theta_{0}^{i} - \theta_{0}^{j}\right) \tag{8.60}$$

$$\frac{\partial \Delta P_{\mathrm{f}}^{ij}}{\partial \alpha} = \frac{2\left(V_{-1}^{i} V_{1}^{i} V_{-1}^{j} V_{1}^{j}\right)^{1/2}}{X_{\mathrm{TCSC}}^{2}(\alpha)} \frac{\partial X_{\mathrm{TCSC}}(\alpha)}{\partial \alpha} \sin\left(\theta_{0}^{i} - \theta_{0}^{j}\right) \tag{8.61}$$

8.5.5. Active power control via STATCOM

The STATCOM may not have the capability to supply active power for long periods of time. Instead, the injection of active power at the fundamental frequency may be used for the control of voltage support. This STATCOM function may be well described by

$$P_{\mathrm{f}}^{i} = \frac{|V^{j}||V^{i}|}{X_{\mathrm{e}}} \sin\left(\theta_{0}^{j} - \theta_{0}^{i}\right)$$

or by an alternative expression which is more appropiate to IPF analysis,

$$P_{\mathrm{f}}^{i} = \frac{mE_{\mathrm{dc}}\left(V_{-1}^{i} V_{1}^{i}\right)^{1/2}}{X_{\mathrm{e}}} \sin\left(\phi_{m} - \theta_{0}^{i}\right) \tag{8.62}$$

where the mismatch equation to be included in the base system is

$$\Delta P_{\mathrm{f}}^{i} = P_{\mathrm{scd}}^{i} - P_{\mathrm{f}}^{i} \tag{8.63}$$

and the unknown variables are the modulation factor m and the modulation shift angle ϕ_m.

The elements in the Jacobian are:

$$\frac{\partial \Delta P_{\mathrm{f}}^{i}}{\partial V_{-1}^{i}} = -\frac{2mE_{\mathrm{dc}}\left(V_{-1}^{i} V_{1}^{i}\right)^{1/2} V_{1}^{i}}{X_{\mathrm{e}}} \sin\left(\phi_{m} - \theta_{0}^{i}\right) \tag{8.64}$$

$$\frac{\partial \Delta P_{\mathrm{f}}^{i}}{\partial V_{1}^{i}} = -\frac{2mE_{\mathrm{dc}}\left(V_{-1}^{i} V_{1}^{i}\right)^{1/2} V_{-1}^{i}}{X_{\mathrm{e}}} \sin\left(\phi_{m} - \theta_{0}^{i}\right) \tag{8.65}$$

$$\frac{\partial \Delta P_{\mathrm{f}}^{i}}{\partial \theta_{0}^{i}} = \frac{mE_{\mathrm{dc}}\left(V_{-1}^{i} V_{1}^{i}\right)^{1/2}}{X_{\mathrm{e}}} \cos\left(\phi_{m} - \theta_{0}^{i}\right) \tag{8.66}$$

$$\frac{\partial \Delta P_{\mathrm{f}}^{i}}{\partial m} = -\frac{E_{\mathrm{dc}}\left(V_{-1}^{i} V_{1}^{i}\right)^{1/2}}{X_{\mathrm{e}}} \sin\left(\phi_{m} - \theta_{0}^{i}\right) \tag{8.67}$$

$$\frac{\partial \Delta P_{\mathrm{f}}^{i}}{\partial \phi_{m}} = -\frac{mE_{\mathrm{dc}}\left(V_{-1}^{i} V_{1}^{i}\right)^{1/2}}{X_{\mathrm{e}}} \cos\left(\phi_{m} - \theta_{0}^{i}\right) \tag{8.68}$$

8.6. Algorithm Implementation

The generic form of the IPF algorithm is shown in Figure 8.1, and its more salient points are summarised below.

1) Select suitable initial values for the nodal voltages, e.g. $1\angle 0°$ at the fundamental

frequency and 0 for harmonics, and for FACTS controllers to provide initial values for **V**, θ_0 and α.

2) Build up the system harmonic admittance matrix $\mathbf{Y}^{linear}$ for the various linear elements such as transmission lines, capacitor banks, transformers, and and include them in the network admittance matrix $\mathbf{Y}^{nodal}$.

3) Use the initial conditions given in 1) to obtain the models of non-linear elements and FACTS controllers, such as the TCR, and include them in the harmonic admittance matrix $\mathbf{Y}^{nodal}$.

4) Use initial conditions to calculate the mismatch equations for the network $\Delta\mathbf{P}$ and **VZC** and for FACTS controllers $\Delta\mathbf{Q}_f$ and/or $\Delta\mathbf{P}_f$.

5) Calculate the Jacobian matrix.

6) Solve for $\Delta\mathbf{V}$, $\Delta\theta_0$ and $\Delta\alpha$ and update the variables **V**, θ_0, and α. Go to point 7) if error $\leq \varepsilon$, else to point 3) and use the newly updated variables in all the relevant calculations.

7) Once the nodal harmonic voltages have been obtained, the following information can be obtained: harmonic content, RMS values, power factors, active power, apparent power, reactive and distortion powers, THD values, and voltage and current waveforms.

Some remarks:

- The voltage in the slack node is fixed. However, harmonic voltages different from zero may be specified in this node.

- In a voltage controlled node, the magnitude of the voltage at the fundamental frequency is specified in the same way as in the conventional rectangular power flow methodology.

- Good initial conditions are mandatory in any iterative process, where 1 p.u. voltage magnitude and zero voltage angle at fundamental frequency provide suitable initial conditions in this case. For harmonic voltages a magnitude of 0.01 p.u. has been recommended in [57], but in the proposed method a harmonic voltage magnitude of zero was the best initial condition for the lowest THD voltages. The initial condition for the TCR's firing angles can be used as those obtained from a conventional power flow study.

- The calculated instantaneous power given in (8.7) may be obtained with ease from the convolution $\mathbf{P}_{calc} = \mathbf{V}^{nodal} \otimes \mathbf{I}^{nodal}$, where $\mathbf{I}^{nodal}$ is obtained from (8.2).

- Point 3) may be seen as a subroutine inside the main loop, a fact which helps the method to be treated in modular fashion from the modelling viewpoint. Convergence is not greatly affected since the equivalent harmonic admittance of the non-linear element and power electronics controllers, enhance the convergence characteristics of the overall system [108].

- The method is modular since non-linear and electronics-based controllers can be modelled separately and included independently in the formulation.

- The size of the overall system of equations to be solved is very large when many harmonics are considered in the solution, but the Jacobian is very sparse and factorisation can be used. The admittance matrix $\mathbf{Y}^{\text{nodal}}$ has dimensions of $N(2h+1) \times N(2h+1)$ but it remains very sparse even though the equivalent admittance matrices of non-linear elements and electronic controllers may have very wide band diagonals.

- The voltage and current in electrical systems will not normally contain even harmonics, but the instantaneous power will only contain the dc-term and even harmonics. This fact introduces complications in the IPF and further research work is required in order to reduce the requirement for storage, calculation and simulation time.

8.6.1. Case Study: System with linear and non-linear loads

System with concentrated linear loads: The three-node linear network [55] of Figure 8.2 was used to test the IPF method. The linear load is represented by equation (8.11), with $h = 2$. The data given for the electrical system is re-written in a way that is suitable for the IPF method.
Nodal voltages:

$$\mathbf{V}^1 = \sqrt{2}\begin{bmatrix} 0 \\ 1.05/2 \\ 0 \\ 1.05/2 \\ 0 \end{bmatrix}, \mathbf{V}^{2(0)} = \mathbf{V}^{3(0)} = \sqrt{2}\begin{bmatrix} 0 \\ 1.0/2 \\ 0 \\ 1.0/2 \\ 0 \end{bmatrix}$$

Voltages zero-crossings:

$$\theta_0^1 = 0 \text{ rad and } \theta_0^{2(0)} = \theta_0^{3(0)} = 0 \text{ rad}$$

Scheduled instantaneous powers:

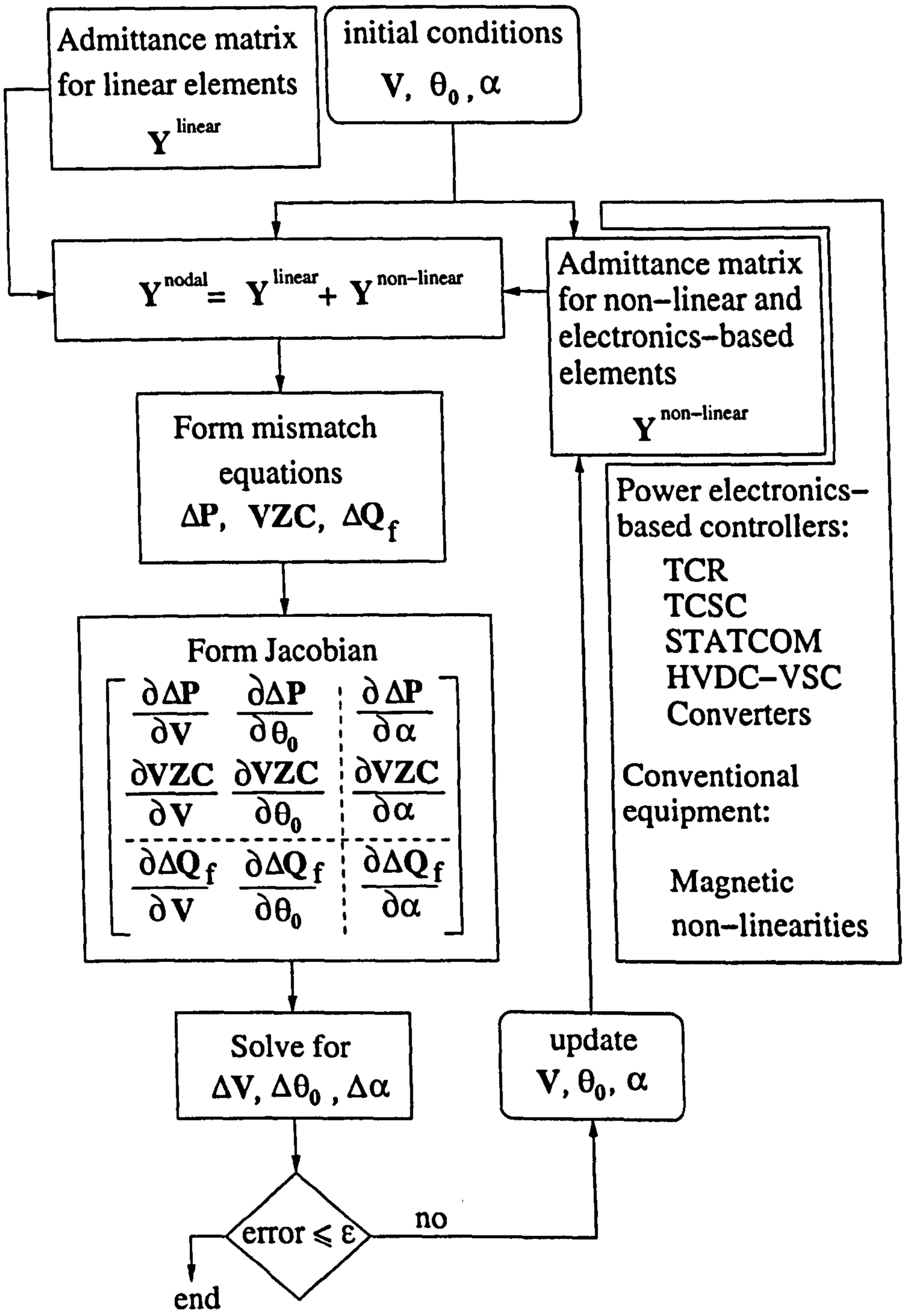

Figure 8.1.: Instantaneous power flow algorithm

$$\mathbf{P}^{2}_{scd} = \begin{bmatrix} \frac{1}{2}(0.96 - j2.07)e^{j\theta_0^2} \\ 0 \\ 0.96 \\ 0 \\ \frac{1}{2}(0.96 + j2.07)e^{-j\theta_0^2} \end{bmatrix}, \mathbf{P}^{3}_{scd} = \begin{bmatrix} \frac{1}{2}(3.15 + j2.85)e^{j\theta_0^3} \\ 0 \\ 3.15 \\ 0 \\ \frac{1}{2}(3.15 - j2.85)e^{-j\theta_0^3} \end{bmatrix}$$

Impedance of lines, e.g. line 1-2:

$$\mathbf{Z}^{1,2} = \begin{bmatrix} 0.01 - j0.02 & & & & & \\ & 0.01 - j0.01 & & & & \\ & & 0.01 & & & \\ & & & 0.01 + j0.01 & & \\ & & & & 0.01 + j0.02 & \end{bmatrix}$$

The IPF method converged to the solution in 5 iterations with an error of 1×10^{-12}, and the results are shown in Table 8.1. The error was calculated as the 2-norm of the variables, i.e. $\varepsilon = \left\| [\Delta V \; \Delta\theta_0 \; \Delta\alpha]^T \right\|$. It should be mentioned that with a conventional power flow using the Newton–Raphson method, also required 5 iterations to converge to the same error.

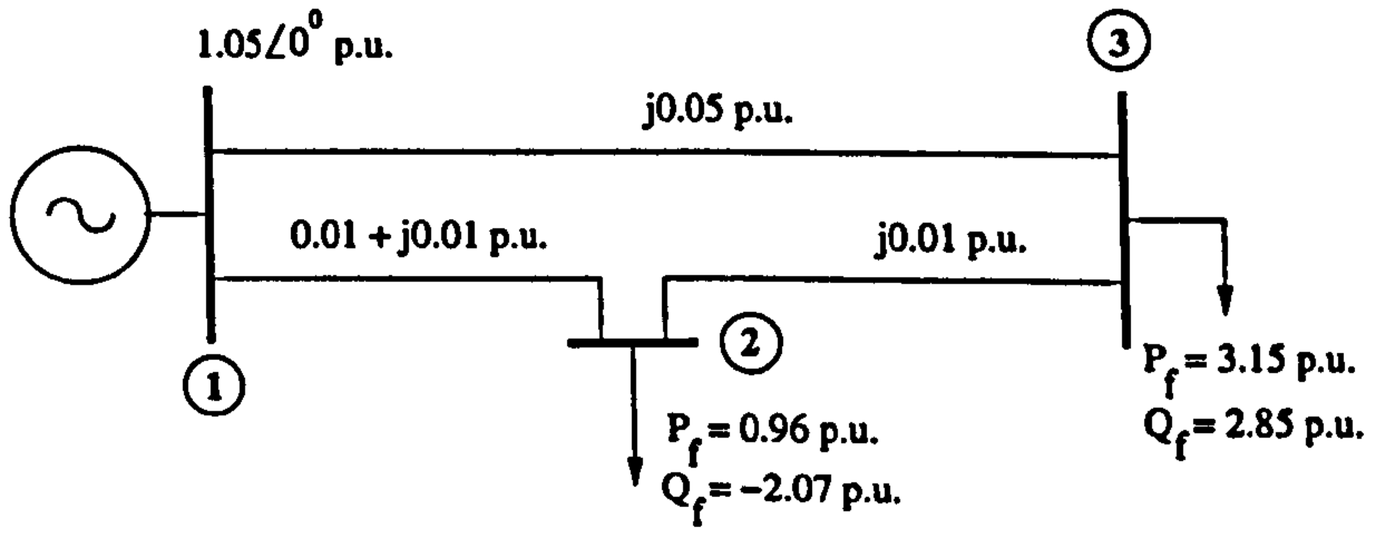

Figure 8.2.: Electrical network

Table 8.1.: Power flow solution using IPF, linear load

node	node	V_{rms}	θ_0	P	S
	1	1.05	0°	4.2	4.3293
	2	1.0204	−1.6847°	−0.96	2.2818
	3	1.0012	−2.8624°	−3.15	4.2479
a	*b*	P_{ab}	P_{ba}	S_{ab}	S_{ba}
1	2	3.15	−3.06	3.5	3.0613
2	3	2.10	−2.10	2.8862	2.8320
3	1	−1.05	1.05	1.4160	1.4849

System with concentrated non-linear load: The load connected at node 2 in the system of Figure 8.2 is changed from linear to a concentrated non-linear, specified by the harmonics $P_{\text{spd}_4} = -0.07 + j0.605$, $P_{\text{spd}_2} = 0.42 + j1.570$, $P_{\text{spd}_0} = 0.90$, and their complex conjugate for

the negative sequence harmonics. Using the IPF and 5 harmonics, the results shown in Table 8.2 were obtained. The solution was reached in 5 iterations to an error of 1×10^{-12}.

An important observation is that in the linear load (node 3) a harmonic voltage and current distortion appear, meaning that all the harmonics contribute to the active power of 3.15 p.u. and not only the fundamental frequency. Also the voltage zero-crossing angle θ_0 does not necessarily correspond to the phase angle of the voltage at the fundamental frequency. The losses (active power) in line 2-3 and line 3-1 are zero since the resistance in those lines is neglected. It is also interesting to see that the minimum distorted current is flowing in line 2-3.

Table 8.2.: Power flow solution using IPF, non-linear load

node	V_{rms}	θ_0	P	S	THD_V	THD_I
1	1.05	0°	4.1493	4.5056	0	29.8571
2	1.0202	−1.1542°	−0.90	2.5437	3.2362	51.7590
3	0.9999	−2.6180°	−3.15	4.3439	2.9209	2.3049
a	*b*	P_{ab}	P_{ba}	S_{ab}	S_{ba}	THD_I
1	2	3.1211	−3.0218	3.3081	3.2142	34.9433
2	3	2.1218	−2.1218	2.9810	2.9216	4.9301
3	1	−1.0282	1.0282	1.4378	1.5099	13.5943

8.6.2. Case study: System with TCR

A TCR is included in the test system as shown in Figure 8.3. The TCR is used to absorb 0.5 p.u. of reactive power at the fundamental frequency at node 2. Two cases are analysed below.

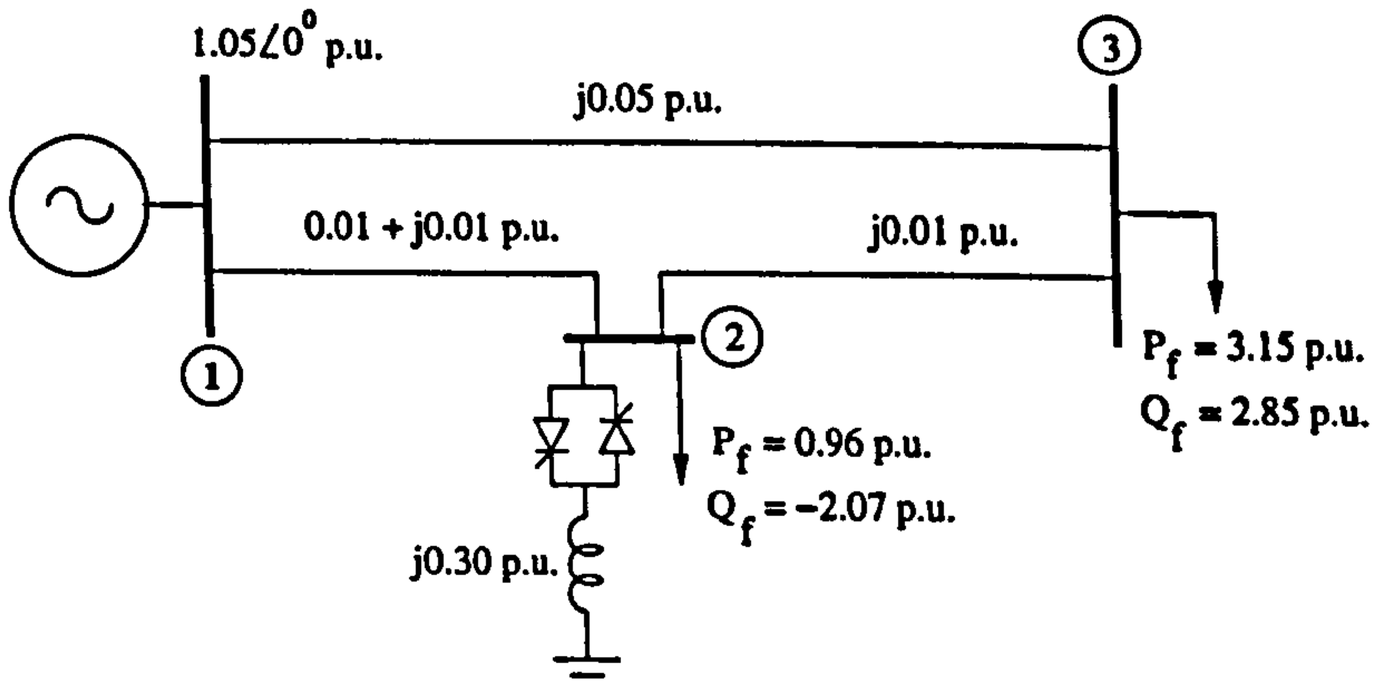

Figure 8.3.: Electrical network with TCR

At fundamental frequency: This case corresponds to a fundamental frequency study, i.e. $h = 2$. The solution required 4 iterations with an error of 1×10^{-6}. The results are shown in Table 8.3, where the initial firing angle was selected as $\alpha = 140°$ and the solution was $\alpha = 138.48°$. The same results were obtained using a conventional power flow where a reactive load of 0.5 p.u. was used instead of the TCR.

Table 8.3.: Power flow result using IPF, TCR with $h = 2$

node	node	V_{rms}	θ_0	P	S
	1	1.05	0°	4.2052	4.4847
	2	1.0157	−1.4971°	−0.96	1.8402
	3	0.9972	−2.7175°	−3.15	4.2479
a	*b*	P_{ab}	P_{ba}	S_{ab}	S_{ba}
1	2	3.2124	−3.1171	3.2405	3.1346
2	3	2.1571	−2.1571	2.8751	2.8228
3	1	−0.9929	0.9929	1.4302	1.5059

At harmonic frequencies: Corresponds to the same circuit as case 1, but the study now includes $h = 15$ harmonics. The solution required 7 iterations to converge to the same error. The results are shown in Table 8.4. The final firing angle was $\alpha = 138.55°$. More iterations were required in comparison to case 1 since more harmonics were used.

Table 8.4.: Power flow result using IPF, TCR with $h = 15$

node	V_{rms}	θ_0	P	S	THD_V	THD_I
1	1.05	0°	4.2038	4.4222	0	12.1122
2	1.0182	−0.2892°	−0.96	1.9372	1.4806	17.2986
3	1.0013	0.3490°	−3.15	4.1352	2.7180	9.5374
a	*b*	P_{ab}	P_{ba}	S_{ab}	S_{ba}	THD_I
1	2	3.1814	−3.0877	3.2149	3.1175	12.9196
2	3	2.1276	−2.1276	2.7783	2.7323	10.0655
3	1	−1.0224	1.0224	1.4067	1.4751	9.1298

The results show that the voltages, at the fundamental frequency, were affected by the harmonics generated by the TCR. For this case the voltages at the fundamental frequency are $V_2 = 1.0181\angle -1.5924°$ and $V_3 = 1.001\angle -2.7879°$, which when compared with those from Table 8.3, have a significant difference. On the other hand, comparing the voltage zero-crossing of Tables 8.4 and 8.3 it can be seen that they are very different due to the voltage distortion. The comparison of voltage waveforms for both cases are given in Figure 8.4.

From Table 8.3 the losses in line 1-2 are 0.0953 p.u., and from Table 8.4 the losses are 0.0937 p.u. This reduction in the losses is due to the difference in voltage profile, since at the fundamental frequency the voltage profile was better in case 2. Considering only the fundamental voltages, for case 2, the calculated losses in line 1-2 are 0.0922 p.u. meaning that the losses due to the harmonics are 0.0015 p.u.

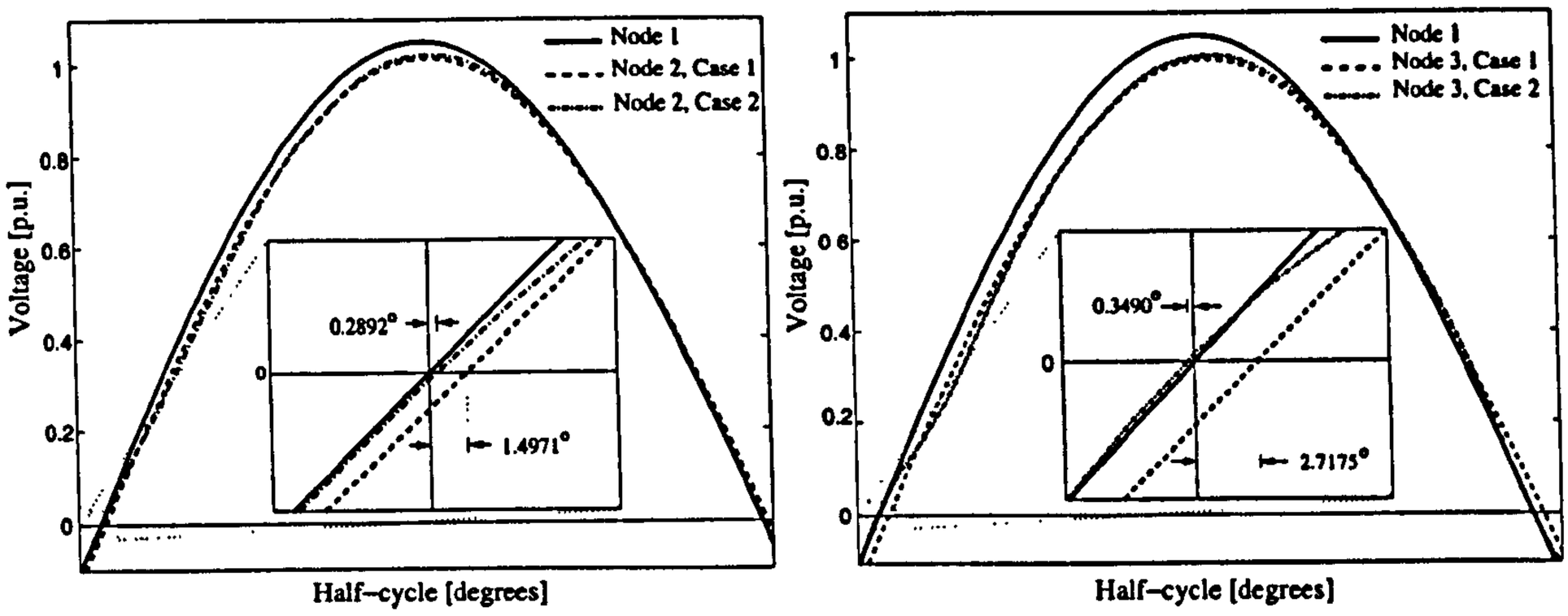

(a) Node 2 (b) Node 3

Figure 8.4.: Voltage waveforms

8.7. Concentrated Load Equivalent Admittance Matrix

In IPF we have that the solution is reached when the power mismatches are equal to zero, giving the harmonic voltages in the whole electrical network. Using the nodal admittance of the network and the nodal harmonic voltages, it is possible to obtain an equivalent admittance matrix of the concentrated loads.

From the network viewpoint, the instantaneous power injected into the network is given by

$$\mathbf{P}^{\text{nodal}} = \mathbf{V}^{\text{nodal}} \otimes \left\{ \mathbf{Y}^{\text{nodal}} \mathbf{V}^{\text{nodal}} \right\} \tag{8.69}$$

where at a particular node k, the instantaneous power is given by

$$\mathbf{P}^{k} = \mathbf{V}^{k} \otimes \left\{ \sum_{j=1}^{N} \mathbf{Y}^{k,j} \mathbf{V}^{j} \right\} \tag{8.70}$$

After some matrix manipulation, it is not difficult to show that equation (8.70) may be represented by

$$\mathbf{P}^{k} = \mathbf{V}^{k} \otimes \left\{ \left(\frac{1}{2h+1} \sum_{j=1}^{N} \mathbf{Y}^{k,j} \mathbf{V}^{j} \mathbf{V}^{k-\mathrm{T}} \right) \mathbf{V}^{k} \right\} \tag{8.71}$$

where $(-\mathrm{T})$ means the transpose of the vector inverse element by element, i.e.

$$\mathbf{V}^{-\mathrm{T}} = \left[\begin{array}{cccccc} \frac{1}{V_{-h}} & \cdots & \frac{1}{V_{-1}} & \frac{1}{V_0} & \frac{1}{V_1} & \cdots & \frac{1}{V_h} \end{array} \right]$$

Assuming that the concentrated load is connected at node k, and given by the admittance matrix $\mathbf{Y}^{k}_{\text{load}}$, then the instantaneous power injected by the load into the network is given by

$$\mathbf{P}^{k} = -\mathbf{V}^{k} \otimes \left\{ \mathbf{Y}^{k}_{\text{load}} \mathbf{V}^{k} \right\} \tag{8.72}$$

Comparing (8.71) with (8.72) the load for that particular nodal voltage condition can be obtained and is given by the admittance matrix

$$\mathbf{Y}_{\text{load}}^{k} = -\frac{1}{2h+1}\sum_{j=1}^{N}\mathbf{Y}^{k,j}\mathbf{V}^{j}\mathbf{V}^{k-\mathrm{T}} \tag{8.73}$$

It is interesting to notice that the admittance $\mathbf{Y}_{\text{load}}^{k}$ may have cross-coupling between harmonics if the nodal voltage contains harmonics. Special attention should be given to the way the matrices $\mathbf{V}^{j}\mathbf{V}^{k-\mathrm{T}}$ are obtained, where operations only need to be cared out for harmonics of $\mathbf{V}^{k}$ different from zero, giving

$$\mathbf{V}^{j}\mathbf{V}^{k-\mathrm{T}} = \begin{bmatrix} \frac{V_{-h}^{j}}{V_{-h}^{k}} & \cdots & \frac{V_{-h}^{j}}{V_{0}^{k}} & \cdots & \frac{V_{-h}^{j}}{V_{h}^{k}} \\ \vdots & \ddots & \vdots & \ddots & \vdots \\ \frac{V_{0}^{j}}{V_{-h}^{k}} & \cdots & \frac{V_{0}^{j}}{V_{0}^{k}} & \cdots & \frac{V_{0}^{j}}{V_{h}^{k}} \\ \vdots & \ddots & \vdots & \ddots & \vdots \\ \frac{V_{h}^{j}}{V_{-h}^{k}} & \cdots & \frac{V_{h}^{j}}{V_{0}^{k}} & \cdots & \frac{V_{h}^{j}}{V_{h}^{k}} \end{bmatrix}$$

This matrix can be interpreted as a sensitivity voltage matrix.

8.8. Conclusions

The new IPF methodology involves the fundamental frequency, harmonic frequencies and cross-coupling between harmonics in the same frame-of-reference, making the IPF a closed-form method. The IPF uses the Newton–Raphson method to solve the mismatch equations. The inclusion of non-linearities into the system, by means of an equivalent harmonic admittance matrix or by an instantaneous power load, is straightforward and does not affect the convergence of the method. The examples considered in this chapter require only 4–7 iterations to reach convergence. This strong convergence characteristic is not exhibited by previous harmonic power flow methodologies which take around 20 iterations to converge when non-linearities are included. The use of the harmonic domain makes the IPF a modular methodology. Additional FACTS or other power electronics controllers can be included with little difficulty in both parts of the formulation. In the first part a mismatch equation similar to that of the TCR is added and in the second part an equivalent harmonic admittance $\mathbf{Y}_{\text{FACTS}}$ is added into the equivalent system $\mathbf{Y}^{\text{nodal}}$. Further work is required in order to optimise the storage and calculation requirements of the method.

9. Conclusions

9.1. Summary of the Research Work

Simple harmonic models for most of the conventional power system equipment have been available in the open literature for quite some time. However, many of these models are linear in nature and cannot be used to study harmonic interactions between harmonic generating equipment, nor can they be used to study harmonic instabilities or harmonic propagation in weak systems.

Contemporary research on power systems harmonic modelling and analysis is firmly on the area of FACTS and Custom Power, with emphasis on the harmonic interaction of such power electronics controllers with the rest of the network. At present, the practice of conducting such studies using time domain simulations is widespread, but the information generated by them will only yield the aggregated response. More fundamental analysis concerning harmonic behaviour, resonance and stability characteristics of each equipment may not be assessed with time domain simulations.

It is shown in the open literature that the harmonic domain (HD) has characteristics and properties which may be used to carry out harmonic interactions and harmonic stability studies. However, most of the models presented in this domain are for conventional non-linear power plant components such as transmission lines, power transformers, synchronous generator and electric arc furnaces. Models also exist for FACTS devices such as the TCR and the TCSC, which are based on thyristor technology. In this thesis, the emphasis has been on the harmonic modelling of the new generation of power electronics controllers which use either GTOs or IGBTs and PWM control, i.e. VSC-based equipment.

The HD has its basis on operational matrices, a mathematical tool which offers a more general and systematic approach for the solution of linear, non-linear and time-varying systems, compared with conventional frequency and time domain methods. The concept of operational matrices refers to the manipulation of the series coefficients that describe the function $x(t)$ rather than working with $x(t)$ itself. Operational matrix methods take the approach of transforming the differential equations that describe the system into algebraic equations. This method is applied in this research for the first time to the modelling of VSC equipment based on PWM control which from the mathematical viewpoint, behave like a time-varying system due to the self-

commutation capabilities of the GTOs or IGBTs. The models obtained were for the STATCOM, UPFC, HVDC-VSC back-to-back tie, and HVDC-VSC transmission system.

These models may find useful applications on harmonic prediction and resonance analysis. They are in the form of electric equivalent circuits which may be made to interconnect easily with the models of conventional power plant equipment such as transmission lines, transformers, generators and other FACTS controllers. Hence, harmonic propagation studies in power networks and harmonic interactions between power components can be carried out in a unified frame-of-reference.

A research issue of great importance in this thesis, is that the operational matrix method based on complex Fourier series, the state-space representation and the averaging method were suitably combined to obtain a new state-space for dynamic harmonic modelling and analysis of linear, non-linear and time-varying systems. The new state-space has been termed extended harmonic domain (EHD) to reflect the fact that the HD is a particular case of the EHD. In the frame-of-reference afforded by EHD, it becomes quite a natural process to obtain the dynamic and steady-state responses of the harmonics in a single study. Moreover, the circuits may contain linear, non-linear and time-varying components.

This is a significant fact since the dynamic evolutions of the harmonics can be obtained with no need to resort to time domain simulations followed by WFFT analysis. Since exact harmonic variables are obtained in EHD, then it becomes plausible to derive exact dynamic electric indices. Some of these indices are the dynamic powers $S(t)$, $P(t)$, $Q(t)$ and $D(t)$; the RMS values $V_{\text{rms}}(t)$ and $I_{\text{rms}}(t)$; the power factor $PF(t)$; the distortion factors $THD_V(t)$ and $THD_I(t)$; and the dynamic sequences $I_{(0)}(t)$, $I_{(+)}(t)$ and $I_{(-)}(t)$.

The EHD was used to study the response of linear and non-linear circuit under dynamic conditions. The results show a very interesting dynamic behaviour of the harmonics, which show to be very sensitive to disturbances, even for very fast and sharp disturbances. Also, the HD was used to obtain the exact steady-state initial condition of circuits which contain very large time constants, such as inrush currents present during transformer energisations.

The EHD was used to obtain dynamic models for the STATCOM, HVDC-VSC back-to-back tie, and HVDC-VSC transmission system. The models are given in the form of state-space equations. A key property of EHD is the fact that time-varying systems are transformed into time-invariant systems when represented into this frame-of-reference. The models obtained were used to analyse the dynamic harmonic response of these power electronics controllers when subjected to power quality disturbances and system imbalances.

The other key contribution emanating from this research work is a harmonic power flow method which is based on the instantaneous power balance concept. This method is termed instantaneous power flow (IPF). The IPF supports all the power plant models which are already represented in HD. The instantaneous power flow problem is solved using the Newton–Raphson method, with its very strong convergence characteristics. It offers a new and more general alternative to solve harmonic power flow problem.

9.2. Future Research Work

HD models for the STATCOM, UPFC and HVDC-VSC stations should be used more extensively in harmonic propagation analysis, resonance analysis, harmonic stability studies and sensitivity analysis to gain further experience with the network-wide use of these controllers. Also, driving point impedance expressions for the UPFC and HVDC-VSC stations should be obtained following a similar procedure to that used to obtain the driving point impedance of the STATCOM. These types of equivalents should aid planning and operation engineers to gain a better understanding of critical operating points in large electric power networks.

The IPF method should be implemented in a way that is suitable for the harmonic solution of large-scale power systems, where sparsity techniques and object oriented programming should be used in order to achieve realistic computing times and storage requirements, together with code maintainability. The implementation should consider the fact that even harmonics are present in instantaneous powers, and that odd harmonics are present in voltages and currents. In this thesis, it was shown that the IPF has strong convergence properties, however, much more work should be done in this direction to test the IPF more fully, including larger systems, a large number of power electronics controllers and their interaction with other non-linearities in the system.

In control systems design, qualitative analysis such as stability, controllability, and observability may benefit from the state-space equation of the form $\dot{\mathbf{X}}(t) = \{\mathbf{A} - \mathbf{D}(\mathrm{j}h\omega_0)\}\mathbf{X}(t) + \mathbf{BU}$ being represented in EHD. This may be, in fact, an open area of research where power electronics controllers can be analysed from the system harmonic viewpoint. Of special interest should be the eigenanalysis results obtained for these kinds of systems, where the modes might be associated with physical properties of the system. Harmonic stability studies and design of control systems for the mitigation of harmonics could be another challenging area of study where EHD might find application.

An issue of great importance is the application of operational matrices to the study of power quality disturbances such as flicker, sags, impulses and electric noise, with possible extensions to chaotic signals. Preliminary research indicates that operational methods have a key role to play in such studies, but there are yet many issues to be resolved. Also, the use of alternative domains such as real Fourier, Hartley, Walsh, and Wavelets should be thoroughly evaluated with a view to select the most suitable transform according to the application at hand.

Bibliography

[1] G.C. Baker, "The Wave of Deregulation: Operation & Design Challenges", *IEEE Power Engineering Review*, Vol. 19, No. 11, November 1999, pp. 15–16.

[2] J. Shawarz, K. Staschus, T. Knop, "Overview of the EU Electricity Directive", *IEEE Power Engineering Review*, Vol. 20, No. 4, April 2000, pp. 4–7.

[3] G.T. Heydt, "Power Quality Engineering", *IEEE Power Engineering Review*, Vol. 21, No. 9, September 2001, pp. 5–7.

[4] J. Watson, "Climate Change, Technology and Realpolitik", *IEE Review*, Vol. 47, No. 2, March 2001, pp. 25–30.

[5] T.J. Hammons, D. Woodford, J. Loughtan, M. Chamia, J. Donahoe, D. Povh, B. Bisewski, W. Long, "Role of HVDC Transmission in Future Energy Development", *IEEE Power Engineering Review*, Vol. 20, No. 2, February 2000, pp. 10–25.

[6] N.G. Hingorani, "High Power Electronics and Flexible AC Transmission Systems", *IEEE Power Engineering Review*, Vol. 8, No. 7, July 1988, pp. 3–4.

[7] N.G. Hingorani, "Introducing Custom Power", *IEEE Spectrum*, June 1995, pp. 41–48.

[8] N.G. Hingorani, L. Gyugyi, *Understanding FACTS: Concepts and Technology of Flexible AC Transmission Systems*, The Institute of Electrical and Electronics Engineering, Inc., New York, 2000.

[9] Y.H. Song, A.T. Johns, *Flexible AC Transmission Systems (FACTS)*, The Institution of Electrical Engineers, England, 1999.

[10] B. Andersen, C. Barker, "A New Era of HVDC?", *IEE Review*, March 2000, pp. 33–39.

[11] S. Nilsson, "Special Application Considerations for Custom Power Systems", 1999 *IEEE-PES Winter Meeting Proceedings*, pp. 1127–1131.

[12] T.J.E. Miller, *Reactive Power Control in Electric Systems*, John Wiley & Sons, New York, 1982.

[13] E. Acha, M. Madrigal, *Power Systems Harmonics: Computer Modelling and Analysis*, John Wiley & Sons, Chichester, 2001.

[14] E. Larsen, C. Bowler, B. Damsky, S. Nilsson, "Benefits of Thyristor Controller Series Compensator", *International Conference on Large High Voltage Electric Systems (CIGRE)*, paper 14/37/38-04, Paris, 1992.

[15] X. Zhou, J. Liang, "Overview of Control for TCSC to Enhance the Stability of Power Systems", *IEE Proceedings Generation, Transmission and Distribution*, Vol. 146, No. 2, March 1999, pp. 125–130.

[16] S.G. Helbing, G.G. Karady, "Investigations of an Advanced Form of Series Compensator", *IEEE Transactions on Power Delivery*, Vol. 9, No. 2, April 1994, pp. 939–947.

[17] S.J. Kinney, M.A. Reynolds, J.F. Hauer, R.J. Piwko, B.L. Damsky, J.D. Eden, "Slatt Thyristor Controlled Series Capacitor System Test Results", *International Conference on Large High Voltage Electric Systems (CIGRE)*, paper 530-02, Tokyo, 1995.

[18] N. Christl, R. Hedin, K. Sadek, P. Lutzelberger, P.E. Krause, S.M. McKenna, A.H. Montoya, D. Togerson, "Advanced Series Compensator (ASC) with Thyristor Controlled Impedance", *International Conference on Large High Voltage Electric Systems (CIGRE)*, paper 14/37/38-05, Paris, September 1992.

[19] S.G. Jalali, R.H. Lasseter, I. Dobson, "Dynamic Response of a Thyristor Controlled Switched Capacitor", *IEEE Transactions on Power Delivery*, Vol. 9, No. 3, July 1994, pp. 1609–1615.

[20] B.M. Han, G.G. Karady, J.K. Park, "Interaction Analysis Model for Transmission Static Compensator with EMTP", *IEEE Transactions on Power Delivery*, Vol. 13, No. 4, October 1998, pp. 1297–1302.

[21] G. Joós, L. Moran, P. Ziogas, "Performance Analysis of a PWM Inverter VAR Compensator", *IEEE Transactions on Power Electronics*, Vol. 6, No. 3, July 1991, pp. 380–391.

[22] J.E. Hill, W.T. Norris, "Exact Analysis of a Multipulse Shunt Converter Compensator or Statcon. Part 1: Performance", *IEE Proceedings Generation, Transmission and Distribution*, Vol. 144, No. 2, March 1997, pp. 213–218.

[23] J.E. Hill, W.T. Norris, "Exact Analysis of a Multipulse Shunt Converter Compensator or Statcon. Part 2: Analysis", *IEE Proceedings Generation, Transmission and Distribution*, Vol. 144, No. 2, March 1997, pp. 219–224.

[24] L. Gyugyi, C.D. Schauder, S.L. Williams, T.R. Rietman, D.R. Torgerson, A. Edris, "The Unified Power Flow Controller: A New Approach to Power Transmission Control", *IEEE Transactions on Power Delivery*, Vol. 10, No. 2, April 1995, pp. 1085–1093.

[25] K.K. Sen, E.J. Stacey, "UPFC- Unified Power Flow Controller: Theory, Modeling, and Applications", *IEEE Transactions on Power Delivery*, Vol. 13, No. 4, October 1998, pp. 1453–1460.

[26] M. Aredes, K. Huesmann, E.H. Watanabe, "An Universal Active Power Line Conditioner", *IEEE Transactions on Power Delivery*, Vol. 13, No. 2, April 1998, pp. 545–551.

[27] K.R. Padiyar, A.M. Kulkarni, "Control Design and Simulation of Unified Power Flow Controller", *IEEE Transactions on Power Delivery*, Vol. 13, No. 4, October 1998, pp. 1348–1354.

[28] R. Mihalic, P. Zunko, D. Povh, "Improvement of Transient Stability Using Unified Power Flow Controller", *IEEE Transactions on Power Delivery*, Vol. 11, No. 1, January 1996, pp. 485–491.

[29] C. Fuerte-Esquivel, Steady State Modelling and Analysis of Flexible AC Transmission Systems, *PhD Thesis*, University of Glasgow, Glasgow, Scotland, 1997.

[30] H. Ambriz-Pérez, Flexible AC Transmission Systems Modelling in Optimal Power Flows Using Newton's Method, *PhD Thesis*, University of Glasgow, Glasgow, Scotland, 1999.

[31] E.W. Kimbark, *Direct Current Transmission*, Wiley-Interscience, New York, 1971.

[32] J. Arrillaga, *High Voltage Direct Current Transmission, IEE Power Engineering Series* 6, Peter Peregrinus, Stevenage, 1983.

[33] B.T. Ooi, X. Wang, "Boost Type PWM HVDC Transmission System", *IEEE Transactions on Power Delivery*, Vol. 6, No. 4, October 1991, pp. 1557–1563.

[34] R. Rudervall, J.P. Charpentier, R. Sharma, "High Voltage Direct Current (HVDC) Transmission Systems Technology Review Paper", *Presented at Energy Week 2000*, Washington, D.C., March 7–8, 2000.

[35] G. Asplund, "Application of HVDC Light to Power System Enhancement", *Proceedings of IEEE Power Engineering Society Winter Meeting*, Singapore, January 23–27, 2000, paper 0-7803-5938-0/00.

[36] J.A. Martínez, "Power Quality Analysis using Electromagnetic Transient Programs", *Proceedings of the ICHQP-98*, October 1998, Athens Greece, pp. 590–597.

[37] I.I. Lazaro, J.J. Rico, G.T. Heydt, "Analysis of Switching Loads in Networks using Operational Matrices", *IEEE Power Engineering Review*, Vol. 20, No. 3, March 2000, pp. 51–53.

[38] H.W. Dommel, *Electromagnetic Transient Program (EMTP Theory Book)*, Bonneville Power Administration, USA, 1986.

[39] Manitoba HVDC Research Centre, *PSCAD/EMTDC: Electromagnetic Transients Program Including DC Systems*, 1994.

[40] E. Acha, Modelling of Power Systems Transformers in the Complex Conjugate Harmonic Space, *PhD Thesis*, University of Canterbury, Christchurch, New Zealand, 1988.

[41] J.A. Medina, Power Systems Modelling in the Harmonic Domain, *PhD Thesis*, University of Canterbury, Christchurch, New Zealand, 1992.

[42] M.L. Lisboa, Three-Phase Three-Limb Transformer Models in the Harmonic Domain, *PhD Thesis*, University of Canterbury, Christchurch, New Zealand, 1996.

[43] J. Arrillaga, B.C. Smith, N.R. Watson, A.R. Wood, *Power System Harmonic Analysis*, John Wiley & Sons, Chichester, 1997.

[44] M. Madrigal, Power Systems Modelling in the Hartley Harmonic Domain, (in spanish) *MSc* Thesis, Universidad Autónoma de Nuevo León, Mexico, 1996.

[45] L.J. Bohmann, R.H. Lasseter, "Harmonic Interactions in Thyristor Controlled Reactor Circuits", *IEEE Transactions on Power Delivery*, Vol. 4, No. 3, July 1989, pp. 1919–1926.

[46] J.J. Rico, E. Acha, T.J.E. Miller, "Harmonic Domain Modelling of Three Phase Thyristor-Controlled Reactors by Means of Switching Vectors and Discrete Convolutions", *IEEE Transactions on Power Delivery*, Vol. 11, No. 3, July 1996, pp. 1678–1684.

[47] J.J. Rico, Steady State Modelling of Non-Linear Power Plant Components, *PhD Thesis*, University of Glasgow, 1997.

[48] G.T. Heydt, P.S. Fjeld, C.C. Liu, D. Pierce, L. Tu, G. Hensley, "Applications of the Windowed FFT to Electric Power Quality Assessment", *IEEE Transactions on Power Delivery*, Vol. 14, No. 4, October 1999, pp. 1411–1416.

[49] J. Arrillaga, N.R. Watson, S. Chen, *Power Quality Assessment*, John Wiley & Sons, Chichester, 2000.

[50] P.T. Krein, J. Bentsman, R.M. Bass, B.L. Lesieutre, "On the Use of Averaging for the Analysis of Power Electronic Systems", *IEEE Transactions on Power Electronics*, Vol. 5, No. 2, April 1990, pp. 182–190.

[51] S.R. Sanders, J.M. Noworolski, X.Z. Lui, G.C. Verghese, "Generalized Averaging Method for Power Conversion Circuits", *IEEE Transactions on Power Electronics*, Vol. 6, No. 2, April 1991, pp. 251–259.

[52] N.M. Wereley, S.R. Hall, "Linear Time Periodic Systems: Transfer Functions, Poles, Transmission Zeroes and Directional Properties", *Proceedings of the 1991 American Control Conference*, Boston, MA., June 26–28, 1991, pp. 1179–1184.

[53] A.M. Stanković, T. Aydin, "Analysis of Asymmetrical Faults in Power Systems Using Dynamic Phasors", *IEEE Transactions on Power Systems*, Vol. 15, No. 3, August 2000, pp. 1062–1086.

[54] A.M. Stanković, P. Mattavelli, V. Caliskan, G.C. Verghese, "Modeling and Analysis of FACTS Devices with Dynamic Phasors", *IEEE Power Engineering Society, Winter Meeting 2000*, 23–27 January, Singapore, Vol. 2, pp. 1440–1446.

[55] G.T. Heydt, *Electric Power Quality*, Stars in a Circle Publications, Scottsdale, 1991.

[56] D. Xia, G.T. Heydt, "Harmonic Power Flow Studies Part I - Formulation", *IEEE Transactions on Power Apparatus and Systems*, Vol. PAS-101, No. 6, June 1982, pp. 1257–1265.

[57] D. Xia, G.T. Heydt, "Harmonic Power Flow Studies - Part II Implementation and Practical Application", *IEEE Transactions on Power Apparatus and Systems*, Vol. PAS-101, No. 6, June 1982, pp. 1266–1270.

[58] M. Valcarcel, J.G. Mayordomo, "Harmonic Power Flow for Unbalanced Systems", *IEEE Transactions on Power Delivery*, Vol. 8, No. 4, October 1993, pp. 2052–2059.

[59] J.G. Mayordomo, L.F. Beites, R. Asensi, F. Orzaez, M. Izzeddine, L. Zabala, "A Contribution for Modeling Controlled and Uncontrolled AC/DC Converters in Harmonic Power Flows", *IEEE Transactions on Power Delivery*, Vol. 13, No. 4, October 1998, pp. 1501–1508.

[60] W. Xu, J.R. Marti, H.W. Dommel, "A Multiphase Harmonic Load Flow Solution Technique", *IEEE Transactions on Power Systems*, Vol. 6, No. 1, February 1991, pp. 174–182.

[61] J. Arrillaga, A. Medina, M.L.V. Lisboa, M.A. Cavia, P. Sánchez, "The Harmonic Domain. A Frame of Reference for Power System Harmonic Analysis", *IEEE Transactions on Power Delivery*, Vol. 10, No. 1, February 1995, pp. 433–440.

[62] G.N. Bathurst, B.C. Smith, N.R. Watson, J. Arrillaga, "A Modular Approach to the Solution of the Three-Phase Harmonic Power-Flow", *IEEE Transactions on Power Delivery*, Vol. 15, No. 3, July 2000, pp. 984–989.

[63] A. Semlyen, M. Shlash, "Principles of Modular Harmonic Power Flow Methodology", *IEE Proceedings Generation, Transmission and Distrib*ution, Vol. 147, No. 1, January 2000, pp. 1–6.

[64] M. Sakui, H. Fujita, M. Shioya, "A Method for Calculating Harmonic Current of a Three-Phase Bridge Uncontrolled Rectifier with DC Filter", *IEEE Transactions on Industry Electronics*, Vol. 36, No. 3, 1989, pp. 434–440.

[65] L. Hu, R. Yacamini, "Calculation of Harmonic Interference in HVDC Systems with Unbalance", *Proceedings of the International Conference on AC and DC Power Transmission*, 1991, pp. 390–394.

[66] J.M. Cano, G.A. Orcajo, J.G. Mayordomo, R. Asensi, M.F. Cabanas, M.G. Melero, "New Transfer Functions for an Accurate Estimation of Harmonic Distortion in AC/DC Converters Working Under Unbalanced Conditions", *IEEE Transactions on Industry Applications*, Vol. 37, No. 2, March/April 2001, pp. 642–649.

[67] L. Salazar, G. Joós, "PSPICE Simulation of Three-Phase Inverters by Means of Switching Functions", *IEEE Transactions on Power Electronics*, Vol. 9, No. 1, January 1994, pp. 35–42.

[68] A.D. Graham, "Non Characteristic Line Harmonics of PWM AC-DC Converters", *Proceedings of the 9th International Conference on Harmonics and Quality of Power*, Vol. III, October 1–4, 2000, Orlando Fl., pp. 955–960.

[69] B.K. Lee, M. Ehsani, "A Simplified Functional Simulation Model for Three-Phase Voltage-Source Inverter Using Switching Function Concept", *IEEE Transactions on Industrial Electronics*, Vol. 48, No. 2, April 2001, pp. 309–321.

[70] C. Schauder, M. Gernhardt, E. Stacey, T. Lemak, L. Gyugyi, T.W. Cease, A. Edris, "Development of a ±100 MVAR Static Condenser for Voltage Control and Transmission Systems", *IEEE Transactions on Power Delivery*, Vol. 10, No. 3, July 1995, pp. 1486–1496.

[71] C. Schauder, E. Stacey, M. Lund, A. Keri, A. Mehraban, A. Edris, "AEP UPFC Project: Installation, Commissioning and Operation of the ±160 MVA STATCOM (Phase I)", *IEEE Transactions on Power Delivery*, Vol. 13, No. 4, October 1998, pp. 1530–1535.

[72] N.H. Woodley, "DVR Field Experience– .6 to 6 MVA Systems", *IEEE T&D Conference & Exposition*, New Orleans, April 11–17, 1999.

[73] N. Mohan, T.M. Undeland, W.P. Robbins, *Power Electronics: Converters, Applications, and Design*, John Wiley & Sons, New York, 1989.

[74] P. Wood, *Switching Power Converters*, Van Nostrard Reinhold Company, New York, 1981.

[75] C. Shauder, M. Gernhardt, E. Stacey, T.W. Cease, A. Edris, "Development of a ±100 MVAR Static Condenser for Voltage Control of Transmission Systems", *IEEE Transactions on Power Delivery*, Vol. 10, No. 3, July 1995, pp. 1486–1496.

[76] M. Mohaddes, A.M. Gole, P.G. McLaren, "A Neutral Network Controlled Optimal Pulse-Width Modulated STATCOM", *IEEE Transactions on Power Delivery*, Vol. 14, No. 2, April 1999, pp. 481–488.

[77] B.T. Ooi, G. Joos, X. Huang, "Operating Principles of Shunt STATCOM based on 3-Level Diode-Clamped Converters", *IEEE Transactions on Power Delivery*, Vol. 14, No. 4, October 1999, pp. 1504–1510.

[78] W. Min, J. Min, J. Choi, "Control of STATCOM Using Cascade Multilevel Inverter for High Power Applications", *Proceedings of the 1999 IEEE International Conference on Power Electronics and Drive Systems*, PEDS-99, Hong Kong, July 1999, pp. 871–876.

[79] P.W. Lehn, M.R. Iravani, "Experimental Evaluation of STATCOM Closed Loop Dynamics", *IEEE Transactions on Power Delivery*, Vol. 13, No. 4, October 1998, pp. 1378–1384.

[80] D. Shen, X. Liang, Y. Han, "A Modified Per-unit STATCOM Model and Analysis of Open Loop Response Time", *IEEE* paper 0-7803-5938-0/00/2000.

[81] Y. Zhuang, R.W. Menzies, O.B. Nayak, H.M. Turanli, "Dynamic Performance of a STATCON at an HVDC Inverter Feeding a Very Weak AC System", *IEEE Transactions on Power Delivery*, Vol. 11, No. 2, April 1996, pp. 958–964.

[82] Y. Ni, L. Snider, "STATCOM Power Frequency Model with VSC Charging Dynamics and its Application in the Power System Stability Analysis", *Proceedings of the 4th International Conference on Advances in Power System Control, Operation and Management*, APSCOM-97, Hong Kong, November 1997, pp. 119–124.

[83] M. Mohaddes, A.M. Gole, S. Elez, "Steady State Frequency Response of STATCOM", *IEEE Transactions on Power Delivery*, Vol. 16, No. 1, January 2001, pp. 18–23.

[84] S. Dong, W. Zhonghong, J.Y. Chen, Y.H. Song, "Harmonic Resonance Phenomena in STATCOM and Relationship to Parameters Selection of Passive Components", *IEEE Transactions on Power Delivery*, Vol. 16, No. 1, January 2001, pp. 46–52.

[85] G. Joós, X. Huang, B.T. Ooi, "Direct-Coupled Multilevel Cascaded Series Var Compensators", *IEEE Transactions on Industry Applications*, Vol. 34, No. 5, September/October 1998, pp. 1156–1163.

[86] K. Chan, A. Kara, "Voltage Sags Mitigation with an Integrated Gate Commutated Thyristor based Dynamic Voltage Restorer", *Proceedings of the 8th ICHQP*, Athens Greece, October 1998, pp. 561–565.

[87] L. Gyugyi, "Dynamic Compensation of AC Transmission Lines by Solid-state Synchronous Voltage Sources", *IEEE Transactions on Power Delivery*, Vol. 9, No. 2, April 1994, pp. 904–911.

[88] ABB Company homepage, http://www.abb.com/powersystems

[89] SIEMENS Company homepage, http://www.ev.siemens.de/en/pages/hvdcinst.htm

[90] A. Lindberg, T. Larsson, "PWM and Control of Three Level Voltage Source Converters in an HVDC Back-to-back Station", *Proceedings of the AC and DC Power Transmission Conference*, 29 April–3 May 1996, pp. 297–302.

[91] Z. Zhang, J. Kuang, X. Wang, B.T. Ooi, "Force Commutated HVDC and VSC Based on Phase-Shifted Multi-Converter Modules", *IEEE Transactions on Power Delivery*, Vol. 8, No. 2, April 1993, pp. 712–718.

[92] J. Kuang, B.T. Ooi, "Series Connected Voltage-Source Converter Modules for Force-Commutated SVC and DC-Transmission", *IEEE Transactions on Power Delivery*, Vol. 9, No. 2, April 1994, pp. 977–983.

[93] D.E. Rice, "A Detailed Analysis of Six-Pulse Converter Harmonic Currents", *IEEE Transactions on Industry Applications*, Vol. 30, No. 2, March/April 1994, pp. 294–304.

[94] S. Banerjee, G.C. Verghese, *Nonlinear Phenomena in Power Electronics*, IEEE Press, New York, 2001.

[95] M.E. Amoli, T. Florence, "Voltage and Current Harmonic Content of a Utility System: A Summary of 1120 Test Measurements", *IEEE Transactions on Power Delivery*, Vol. 5, No. 3, July 1990, pp. 1552–1557.

[96] N.R. Raju, S.S. Venkata, V.V. Sastry, "The Use of Decoupled Converters to Optimize the Power Electronics of Shunt and Series AC System Controllers", *IEEE Transactions on Power Delivery*, Vol. 12, No. 2, April 1997, pp. 895–900.

[97] H.S. Patel, R.G. Hoft, "Generalized Techniques of Harmonic Elimination and Voltage Control in Thyristor Inverter: Part I-Harmonic Elimination", *IEEE Transactions on Industry Applications*, Vol. IA-9, Vol. 9, No. 3, May/June 1973, pp. 310–317.

[98] A. Vabae, I. Takahashi, H. Akagi, "A New Neutral-Point-Clamped PWM Inverter", *IEEE Transactions on Industry Applications*, Vol. IA-17, No. 5, September/October 1981, pp. 518–523.

[99] J.G. Mayordomo, M. López, A. Asensi, L.F. Beites, J.M. Rodriguez, "A General Treatment of Traction PWM Converters for Load Flow and Harmonic Penetration Studies", *Proceedings of the IEEE-ICHQP 1998*, Athens, Greece, 14–16 October, pp. 685–692.

[100] D. Shen, W. Liu, Z. Wang, "Study on the Operation Performance of STATCOM under Unbalanced and Distorted System Voltage", *Proceedings of 2000 IEEE Power Engineering Society Winter Meeting*, January 2000, Singapore, paper 0-7803-5938-0/00.

[101] L. Xu, O. Anaya, V.G. Agelidis, E. Acha, "Development of Prototype Custom Power Devices for Power Quality Enhancement", *Proceedings of IEEE-ICHQP 2000*, Orlando, USA, pp. 775–783.

[102] M. Madrigal, O. Anaya, E. Acha, J.G. Mayordomo, R. Asensi, "Single-Phase PWM Converters Array for Three-Phase Reactive Power Compensation. Part I: Time Domain Studies", *Proceedings of IEEE-ICHQP 2000*, Orlando, USA, pp. 451–547.

[103] M. Madrigal, E. Acha, J.G. Mayordomo, R. Asensi, A. Hernández, "Single-Phase PWM Converters Array for Three-Phase Reactive Power Compensation. Part II: Frequency Domain Studies", *Proceedings of IEEE-ICHQP 2000*, Orlando, USA, pp. 645–651.

[104] R.C. Dugan, M.F. McGranaghan, H.W. Beaty, *Electrical Power Systems Quality*, McGraw-Hill, 1996.

[105] M.H.J. Bollen, *Understanding Power Quality Problems: Voltage Sags and Interruptions*, IEEE Press, New York, 2000.

[106] M.S. Mamis, M. Köksal, "Solution of Eigenproblems for State-space Transient Analysis of Transmission Lines", *Electric Power System Research*, Vol. 55, 2000, pp. 7–14.

[107] Task Force on Harmonics Modeling and Simulation, "Modeling and Simulation of Power Propagation of Harmonics in Electric Power Networks, Part I: Concepts, Models, and Simulation Techniques", *IEEE Transactions on Power Delivery*, Vol 11, No. 1, January 1996, pp. 452–465.

[108] E. Acha, A. Semlyen, N. Rajakovic, "A Harmonic Domain Computational Package for Nonlinear Problems and its Application to Electric Arcs", *IEEE Transactions on Power Delivery*, Vol. 5, No. 3, July 1990, pp. 1390–1397.

[109] V.A. Caliskan, G.C. Verghese, A.M. Stankovic, "Multifrequency Averaging of DC/DC Converters", *IEEE Transactions on Power Electronics*, Vol. 14, No. 1, January 1999, pp. 124–133.

[110] E. Möllerstedt, B. Bernhardsson, "Out of Control Because of Harmonics: An Analysis of the Harmonic Response of an Inverter Locomotive", *IEEE Control Systems Magazine*, August 2000, pp. 70–81.

[111] Z. Yao, B.T. Ooi, "Utilization of Cable Capacitance in GTO-HVDC Transmission", *IEEE Transactions on Power Delivery*, Vol. 13, No. 3, July 1998, pp. 945–951.

[112] L. Gyugyi, "A Unified Power Flow Control Concept for Flexible AC Transmission Systems", *IEE Fifth International Conference on AC and DC Power Transmission*, London, Publication No. 345, pp. 19–26. Reprinted in *IEE Proceedings-C*, Vol. 139, No. 4, July 1992.

[113] H. Chen, Y. Wang, R. Zhou, "Transient and Voltage Stability Enhancement via Coordinated Excitation and UPFC Control", *IEE Proceedings Generation, Transmission and Distribution*, Vol. 148, No. 3, May 2001, pp. 201–208.

[114] S. Bruno, E. De Tuglie, M. La Scala, P. Scarpellini, "Dynamic Security Corrective Control by UPFCs", *IEEE Transactions on Power Systems*, Vol. 16, No. 3, August 2001, pp. 490–497.

[115] W.H. Feng, "A Unified Model for the Analysis of FACTS Devices in Damping Power System Oscillations. III. Unified Power Flow Controller", *IEEE Transactions on Power Delivery*, Vol. 15, No. 3, July 2000, pp. 978–983.

[116] H.F. Wang, M. Jazaeri, A.T. Johns, "Investigation into the Dynamic Interactions of Multiple Multifunctional Unified Power Flow Controllers", *IEEE Power Engineering Review*, Vol. 20, No. 7, July 2000, pp. 45–48.

[117] H.F. Wang, "Applications of Modelling UPFC into Multi-machine Power Systems", *IEE Proceedings Generation, Transmission and Distribution*, Vol. 146, No. 3 , May 1999, pp. 306–312.

[118] H.F. Wang, "Damping Function of Unified Power Flow Controller", *IEE Proceedings Generation, Transmission and Distribution*, Vol. 146, No. 1, January 1999, pp. 81–87.

[119] K.S. Smith, L. Ran, J. Penman, "Dynamic Modelling of a Unified Power Flow Controller", *IEE Proceedings Generation, Transmission and Distribution*, Vol. 144, No. 1, January 1997, pp. 7–12.

[120] C.R. Fuerte-Esquivel, E. Acha, "Unified Power Flow Controller: A Critical Comparison of Newton-Raphson UPFC Algorithms in Power Flow Studies", *IEE Proceedings Generation, Transmission and Distribution*, Vol. 144, No. 5, September 1997, pp. 437–444.

[121] A. Nabavi-Niaki, M.R. Iravani, "Steady-state and Dynamic Models of Unified Power Flow Controller (UPFC) for Power System Studies", *IEEE Transactions on Power Systems*, Vol. 11, No 4, November 1996, pp. 1937–1943.

[122] H. Zhengyu, N. Yinxin, C.M. Shen, F.F. Wu, C. Shousun, B. Zhang, "Application of Unified Power Flow Controller in Interconnected Power Systems-modeling, Interface, Control Strategy, and Case Study", *IEEE Transactions on Power Systems*, Vol. 15, No. 2, May 2000, pp. 817–824.

[123] J.Y. Liu, Y.H. Song, P.A. Mehta, "Strategies for Handling UPFC Constraints in Steady-state Power Flow and Voltage Control", *IEEE Transactions on Power Systems*, Vol. 15, No. 2, May 2000, pp. 566–571.

[124] C.R. Fuerte-Esquivel, E. Acha, H. Ambriz-Pérez, "A Comprehensive Newton-Raphson UPFC Model for the Quadratic Power Flow Solution of Practical Power Networks", *IEEE Transactions on Power Systems*, Vol. 15, No. 1, February 2000, pp. 102–109.

[125] M. Noroozian, L. Angquist, M. Ghandhari, G. Andersson, "Use of UPFC for Optimal Power Flow Control", *IEEE Transactions on Power Delivery*, Vol. 12, No. 4, October 1997, pp. 1629–1634.

[126] S.Y. Ge, T.S. Chung, "Optimal Active Power Flow Incorporating Power Flow Control Needs in Flexible AC Transmission Systems", *IEEE Transactions on Power Systems*, Vol. 14, No. 2, May 1999, pp. 738–744.

[127] H. Ambriz-Pérez, E. Acha, C.R. Fuerte-Esquivel, A. De la Torre, "Incorporation of a UPFC Model in an Optimal Power Flow using Newton's Method", *IEE Proceedings Generation, Transmission and Distribution*, Vol. 145, No. 3, May 1998, pp. 336–344.

[128] B. Mwinyiwiwa, B.T. Ooi, Z. Wolanski, "UPFC Using Multiconverter Operated by Phase-shifted Triangle Carrier SPWM Strategy", *IEEE Transactions on Industry Applications*, Vol. 34, No. 3, May-June 1998, pp. 495–500.

[129] J.H.R. Enslin, J. Zhao, R. Spee, "Operation of the Unified Power Flow Controller as Harmonic Insulator", *IEEE Transactions on Power Electronics*, Vol. 11, No. 6, November 1996, pp. 776–784.

A. PWM Converters

A.1. PWM Converter used in the PSCAD/EMTDC STATCOM Model

A STATCOM based on a six–pulse VSC configuration and IGBTs was implemented in PSCAD/EMTDC, as shown in Figure E.1. This model uses the PWM scheme shown Figure A.1 to control the operation of the IGBTs. In this figure v_r is the carrier signal with frequency f_r, and v_s is the modulation signal with frequency f_s, e.g. 50 Hz. The functions g_1 to g_6 are the conduction stages of IGBTs 1 to 6 respectively. Where $g_1 = 1$ when $v_s > v_r$ and zero otherwise; g_3 and g_5 are 120° and $-120°$ phase shifted with respect to g_1, respectively. Similarly, $g_2 = 0$ when $v_s > v_r$ and 1 otherwise; g_6 and g_2 are 120° and $-120°$ phase shifted with respect to g_2, respectively. By examining the operation of the VSC it is not difficult to see that the switching functions per phase are given by $s_{ab} = g_1g_6 - g_4g_3$, $s_{bc} = g_3g_2 - g_6g_5$ and $s_{ca} = g_5g_4 - g_2g_1$. The switching functions s_{ab}, s_{bc} and s_{ca} are used in the harmonic domain models to represent the operation of the VSC.

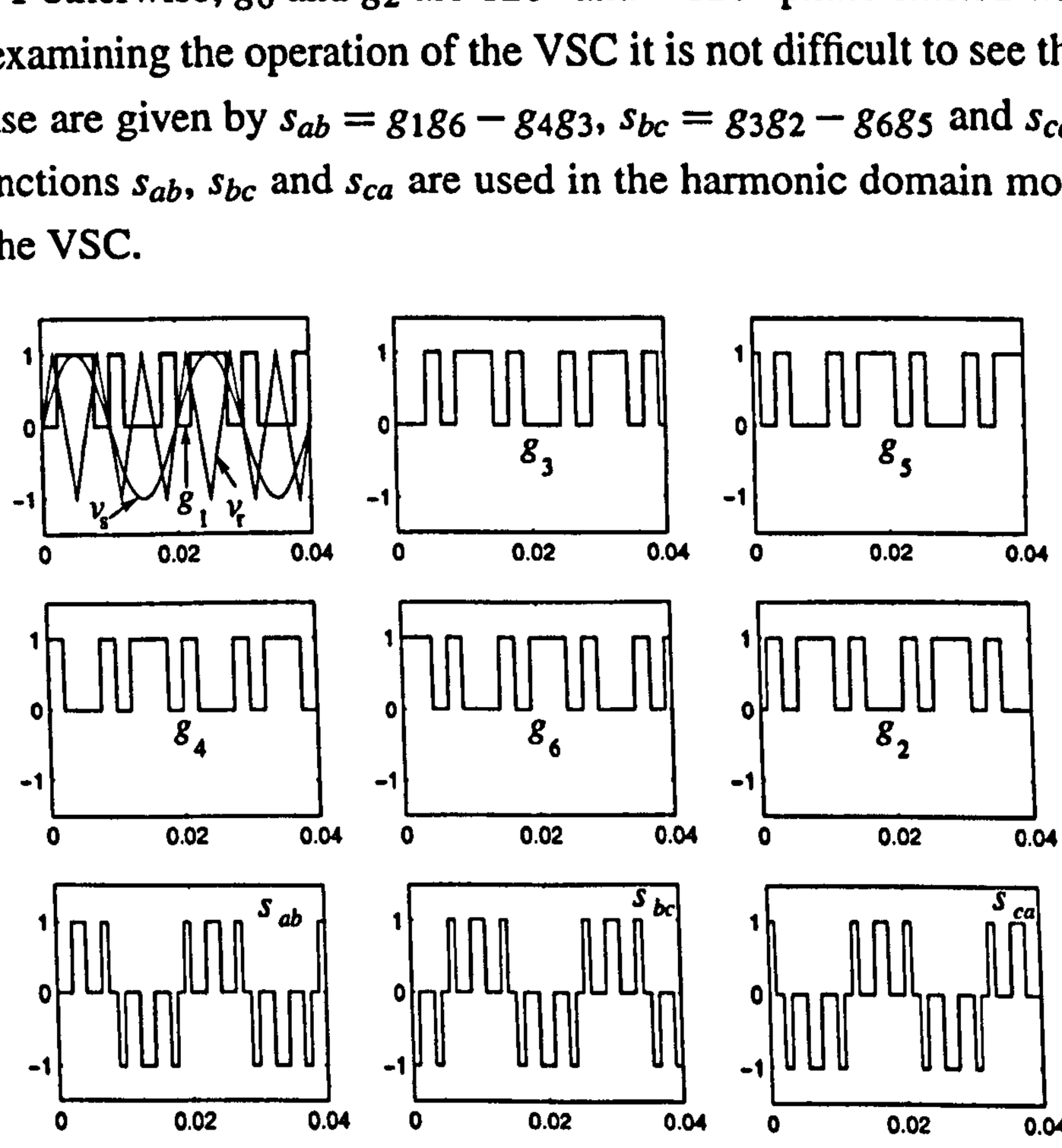

Figure A.1.: PWM technique used in the PSCAD/EMTDC model

A.2. Harmonics Generated by the Unipolar Voltage Switching

Assuming that the modulation signal is given by $v_{sa}(t) = m\cos(\omega_s t)$ and the carrier signal by $v_r(t) = f(\omega_r t)$. The switching function $s_{ab}(t)$ is giving by the following series [74]:

$$\begin{aligned} s_{ab}(t) &= m\cos(\omega_s t) \\ &-(4/\pi)\sum_{p=1}^{p=\infty}\cos(p\pi)\{J_1[m(2p-1)\pi/2]/(2p-1)\} \\ &\times\cos[(2p-1)\omega_r t] \\ &-(4/\pi)\sum_{p=1}^{p=\infty}\sum_{q=1}^{q=-\infty}\cos[(p+q)\pi]\{J_{2q}[m(2p-1)\pi/2]/(2p-1)\} \\ &\times\cos[(2p-1)\omega_r t \pm 2q\omega_s t] \\ &-(4/\pi)\sum_{p=1}^{p=\infty}\sum_{q=1}^{q=-\infty}\cos[(p+q)\pi][J_{2q-1}(mp\pi)/2p] \\ &\times\cos[2p\omega_r t \pm (2q-1)\omega_s t] \end{aligned} \tag{A.1}$$

where J is the Bessel function, i.e. $J_{2q-1}(mp\pi)$ is the Bessel function of the first kind of order $2q-1$ and argument $mp\pi$.

The wanted component in this series is $m\cos(\omega_s t)$, which has a peak amplitude value of 1, and is controllable by varying m, the *modulation factor*. The second term (summations) of the expression comprises the *carrier frequency* and its harmonics. It is note that as m is increased from 0 to 1, the amplitudes of these components decrease.

It is clear that if ω_r is not an integer multiple of ω_s, then some components will have lower frequency than the wanted output frequency, commonly refer to *subharmonics*. If $\omega_r = k\omega_s$ and k integer, the resulting angular frequencies are $[(2p-1)k \pm 2q]\omega_s$ and $[2pk \pm (2q-1)]\omega_s$. The second of these is an odd multiple of ω_s regardless of whether k is even or odd. The first is an even multiple if k is even, and odd if k is odd. Even order harmonics are very undesirable in the voltage, since the half-wave symmetry of the waveform is lost. Also, there will be a value of q for every p that yields a DC component in the voltage, which is even worst when this component interact with power transformers. Thus, it can be reduced that ω_r should always be an odd multiple of ω_s, and $\omega_s = \omega_0$ the angular frequency of the electric system as is the case of Figure 2.3.

Note that the degeneracy of the spectrum makes it difficult to calculate the amplitudes of individual components when ω_r/ω_s is an integer, these amplitudes are the sums of a number of contributions, each having a Bessel coefficient. There seem to be no closed-form solutions for such summations.

The benefits of PWM, apart from its giving the ability to control the fundamental frequency

component magnitude, are two: First, if k is large, then the amplitudes of the low order harmonics (sidebands) are very low, so that the higher distortion content is offset by the upward shifting in frequency of the high-amplitude components of the spectrum, making them easier to filter.

A practical insight, is that the amplitude of the fundamental frequency component varies linearly with m in the range of $m \leq 1$, to increase further the amplitude of the fundamental frequency component, m is increased beyond 1, resulting in what is called *overmodulation*. Overmodulation causes to contain more harmonics in the sidebands as compared with the linear range ($m \leq 1$). The harmonics with dominant amplitudes in the linear range may not be dominant during overmodulation. More significantly, with overmodulation, the amplitude of the fundamental frequency component does not vary linearly with the modulation factor [73].

A.3. Multi-module PWM Converter

Figure A.2 shows a multi-pulse configuration, which enables harmonic elimination at the electromagnetic interface level, without resorting to increased switching frequencies in the PWM control scheme. Here the object is to reduce the harmonic content of the output voltage by cascading the n_i PWM VSCs using a suitable magnetic circuit arrangement. In general, harmonic cancellation is achieved by phase shifting the harmonic components to be cancelled in such a way that when the output voltages of individual units are added together, the targeted harmonic components are cancelled out. This can be achieved by using phase shifting transformers. One simple way to represent this effect in harmonic domain calculations is to use a phase-shifted carrier signals, a technique which is explained below [85][99][103].

The single-phase PWM converter unit, n_i, uses unipolar voltage switching, as shown in Figure 2.3. The number of pulses per half-cycle of the switching function $s_{n_i}(t)$ is given by the frequency modulation ratio m_f,

$$m_f = \frac{\omega_r}{\omega_s} \tag{A.2}$$

where the harmonics generated by the voltage converter i are given by

$$h = 2jm_f \pm k \quad j,k = 1,2,3,\ldots \tag{A.3}$$

which are the harmonics of $s_{n_i}(t)$.

Harmonics cancellation at the AC side is possible by shifting the carrier signal of each individual PWM control scheme, say converter i, by δ_{r_i} rad, and using equal modulation signals, v_s, for all the PWM converters. The shifted angles for the n_i carrier signals are given by

$$\delta_{r_i} = 2\pi(i-1)/n_i \tag{A.4}$$

A. PWM Converters

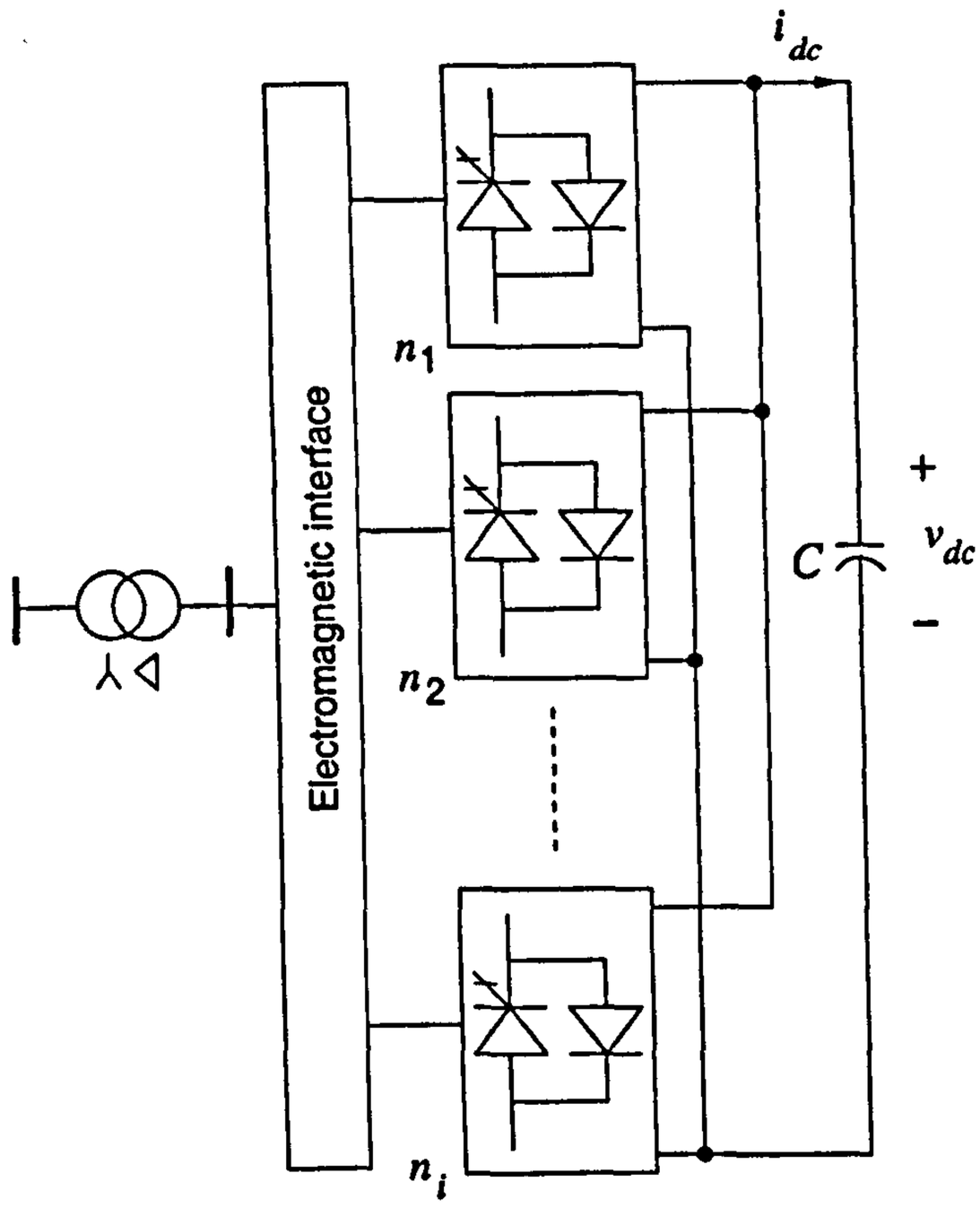

Figure A.2.: Multi-pulse VSC with n_i PWM converters

Using n_i PWM converters in parallel, the harmonics generated by the multi-pulse converter are given by the following sequence,

$$h = 2jn_i m_f \pm k \quad j,k = 1,2,3,\ldots \tag{A.5}$$

and the magnitude of the harmonics are given by

$$S_{\mathrm{VSC}_h} = \frac{S_{n1_h} + S_{n2_h} + \cdots + S_{ni_h}}{n_i} \tag{A.6}$$

Using this technique, the magnitude of the fundamental frequency component is equal to the modulation factor m.

In general, by using the three switching functions (one per line-to-line voltage), different switching functions can be obtained, as shown in Figure A.3. It should be remarked that only the two-level switching functions in Figure A.3(a) and (b) correspond to the VSC topology shown in Figure 2.2. The switching function in Figure A.3(c) corresponds to a six-level topology.

A.4. Neutral-point-clamped PWM Converter

The neutral-point-clamped PWM converter [98] shown in Figure A.4 is a converter which produces an AC line-to-line voltage with five levels. This converter uses unipolar voltage switching or selective harmonic elimination. This configuration can also be represented by means of

A. PWM Converters

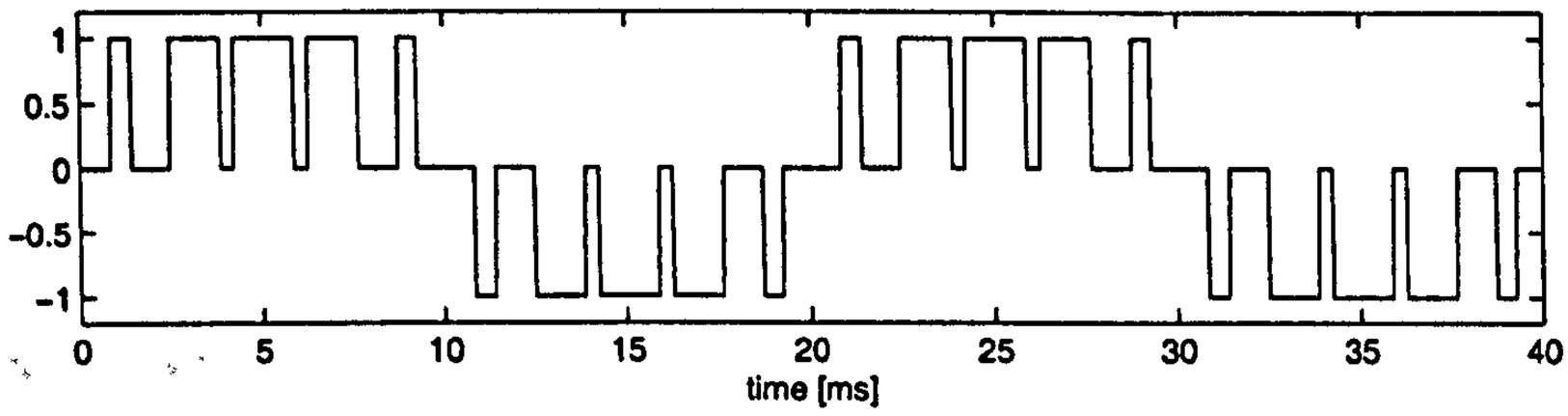

(a) Two–level VSC and switching frequency of 250 Hz

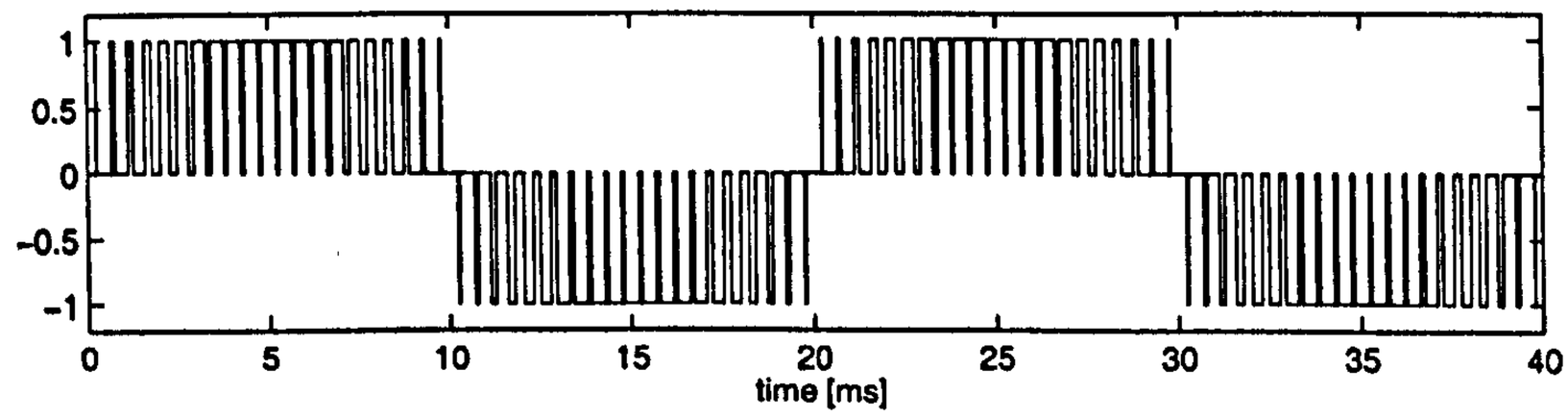

(b) Two–level VSC and switching frequency of 1050 Hz

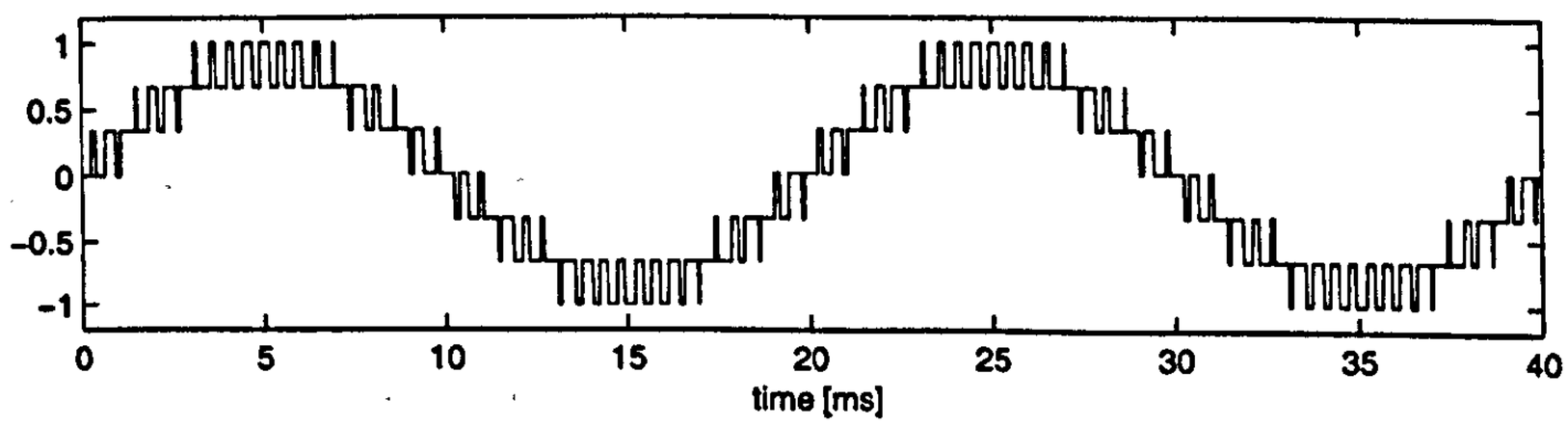

(c) Six–level VSC and switching frequency of 450 Hz

Figure A.3.: Switching functions of VSCs

switching functions.

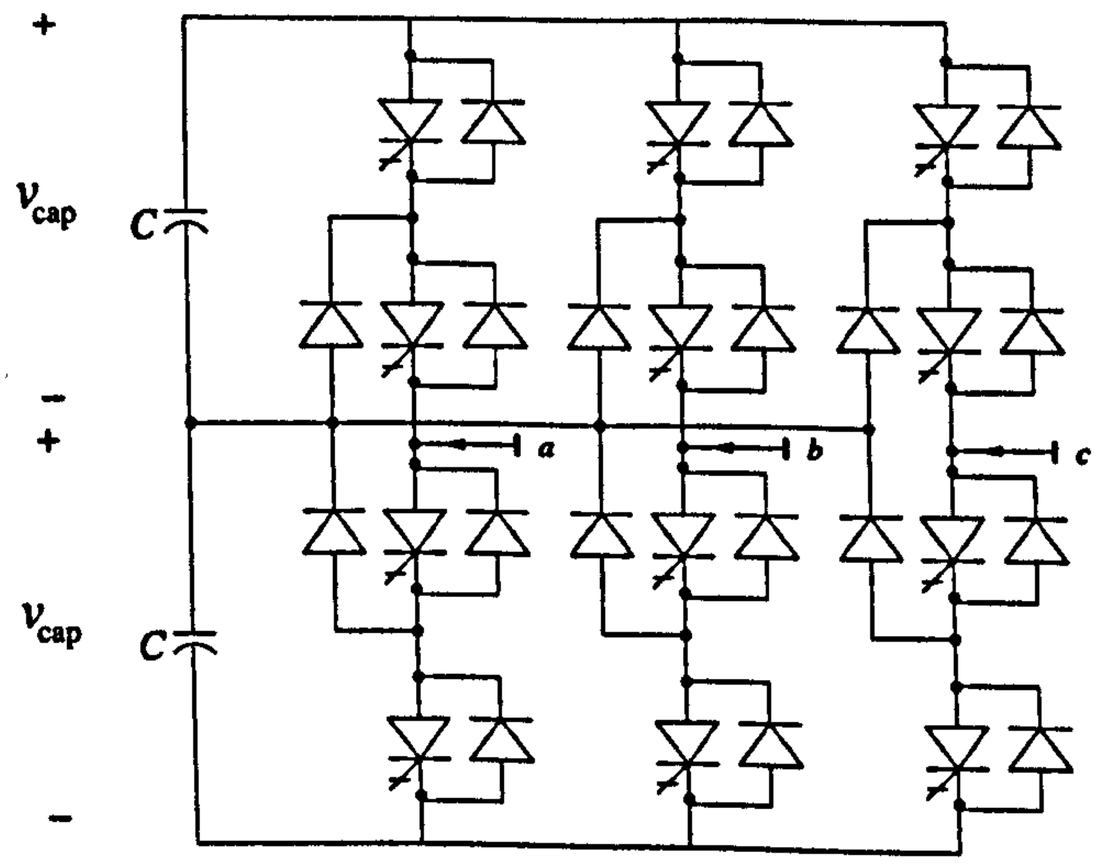

Figure A.4.: Neutral-point-clamped PWM converter

B. Steady-state Harmonic Domain

Steady-state harmonic domain has been used to model power systems elements such as magnetic non-linearities, electric arc, synchronous generators, transmission lines, power transformers, and some FACTS and Custom Power controllers [43][13]. In this appendix a review of the harmonic domain is given.

B.1. Harmonic Domain

The HD analysis may be based on the use of the complex Fourier series, where a periodical function $x(t)$ with period of T_0 is given by the series

$$x(t) = \sum_{n=-\infty}^{\infty} X_n e^{jn\omega_0 t} \tag{B.1}$$

where $\omega_0 = 2\pi/T_0$ is the angular frequency in rad/s and X_n is the n-th harmonic coefficient of the series, and given by

$$X_n = \frac{1}{T_0}\int_0^{T_0} x(t)e^{-jn\omega_0 t}dt \tag{B.2}$$

where $X_{-n} = X_n^*$.

A matrix representation of the series (B.1) may be expressed by

$$x(t) = \mathbf{G}^{\mathrm{T}}(t)\mathbf{X} \tag{B.3}$$

where using only h harmonics

$$\mathbf{G}(t) = \begin{bmatrix} e^{-jh\omega_0 t} \\ \vdots \\ e^{-j\omega_0 t} \\ 1 \\ e^{j\omega_0 t} \\ \vdots \\ e^{jh\omega_0 t} \end{bmatrix}; \quad \mathbf{X} = \begin{bmatrix} X_{-h} \\ \vdots \\ X_{-1} \\ X_0 \\ X_1 \\ \vdots \\ X_h \end{bmatrix} \tag{B.4}$$

The vector $\mathbf{G}(t)$ is the orthogonal base of the Fourier series and $\mathbf{X}$ a complex vector given by the coefficients of the series.

B.1.1. Multiplication of a periodical function by a constant

This operation is given by

$$y(t) = Kx(t) \tag{B.5}$$

where K is a constant value, and $y(t)$ and $x(t)$ are periodical functions. The matrix representation of (B.5) is given by

$$\mathbf{G}^{\mathrm{T}}(t)\mathbf{Y} = K\mathbf{G}^{\mathrm{T}}(t)\mathbf{X} \tag{B.6}$$

Since equation (B.6) has the term $\mathbf{G}^{\mathrm{T}}(t)$ in both sides, it follows that,

$$\mathbf{Y} = K\mathbf{X} \tag{B.7}$$

Equation (B.7) represents the relationship between the harmonics of $y(t)$ and $x(t)$ in equation (B.5).

B.1.2. Dynamic periodical functions

The dynamic operation is given by the expression

$$y(t) = \frac{\mathrm{d}x(t)}{\mathrm{d}t} \tag{B.8}$$

where the derivative of the series (B.3) yields,

$$\begin{aligned} \frac{\mathrm{d}x(t)}{\mathrm{d}t} &= \frac{\mathrm{d}\mathbf{G}^{\mathrm{T}}(t)}{\mathrm{d}t}\mathbf{X} + \mathbf{G}^{\mathrm{T}}(t)\frac{\mathrm{d}\mathbf{X}}{\mathrm{d}t} \\ &= \mathbf{G}^{\mathrm{T}}(t)\mathbf{D}(\mathrm{j}h\omega_0)\mathbf{X} \end{aligned} \tag{B.9}$$

where $\frac{\mathrm{d}\mathbf{X}}{\mathrm{d}t} = 0$ since $\mathbf{X}$ is not a function of time. So equation (B.8) in HD representation is given by

$$\mathbf{Y} = \mathbf{D}(\mathrm{j}h\omega_0)\mathbf{X} \tag{B.10}$$

where $\mathbf{D}(\mathrm{j}h\omega_0)$ is the operational matrix of differentiation given by

$$\mathbf{D}(\mathrm{j}h\omega_0) = \begin{bmatrix} -\mathrm{j}h\omega_0 & & & & & \\ & \ddots & & & & \\ & & -\mathrm{j}\omega_0 & & & \\ & & & 0 & & \\ & & & & \mathrm{j}\omega_0 & \\ & & & & & \ddots \\ & & & & & & \mathrm{j}h\omega_0 \end{bmatrix} \tag{B.11}$$

and the inverse of $\mathbf{D}(\mathrm{j}h\omega_0)$ represents the operation of integration.

B.1.3. Multiplication of periodical functions

The multiplication of two periodical functions, $z(t)$ and $x(t)$, yields a periodical response $y(t)$ given by

$$y(t) = z(t)x(t) \tag{B.12}$$

In matrix form is

$$\mathbf{G}^{\mathrm{T}}(t)\mathbf{Y} = \mathbf{G}^{\mathrm{T}}(t)\mathbf{Z}\mathbf{G}^{\mathrm{T}}(t)\mathbf{X} \tag{B.13}$$

and after some algebra it can be shown that

$$\mathbf{G}^{\mathrm{T}}(t)\mathbf{Y} = \mathbf{G}^{\mathrm{T}}(t)\mathbf{Z}\mathbf{X} \tag{B.14}$$

which can be represented by the following equation in HD,

$$\mathbf{Y} = \mathbf{Z}\mathbf{X} \tag{B.15}$$

where the matrix $\mathbf{Z}$ is a banded diagonal Toeplitz matrix,

$$\mathbf{Z} = \begin{bmatrix} Z_0 & Z_{-1} & \cdots & Z_{-h} & & & \\ Z_1 & \ddots & \ddots & \ddots & \ddots & & \\ \vdots & \ddots & Z_0 & Z_{-1} & \ddots & \ddots & \\ Z_h & \ddots & Z_1 & Z_0 & Z_{-1} & \ddots & Z_{-h} \\ & \ddots & \ddots & Z_1 & Z_0 & \ddots & \vdots \\ & & \ddots & \ddots & \ddots & \ddots & Z_{-1} \\ & & & Z_h & \cdots & Z_1 & Z_0 \end{bmatrix} \tag{B.16}$$

where the entries are the harmonic coefficients of $z(t)$. Matrices whose entries are constant along each diagonal are called Toeplitz matrices.

Also, equation (B.12) is given by the discrete convolution of $\mathbf{Z}$ with $\mathbf{X}$, i.e.

$$\mathbf{Y} = \mathbf{Z} \otimes \mathbf{X} \tag{B.17}$$

The HD presented in this appendix, is extended in Chapter 6 for the case when the coefficients of the series (B.1) have a dynamic behaviour, i.e. $X_n(t)$. This dynamic consideration yields a new and more general harmonic domain which compress the time evolution of the harmonics from the transient to the steady-state response.

B.2. Electric Circuit Representation

The electric circuit representation of electric elements in HD, is similar to the phasor representation of passive elements under sinusoidal steady-state conditions. For non-sinusoidal steady-state conditions the HD can be applied to linear, non-linear and switching elements. For the most common elements, their representation in the HD are given below.

The response of a resistance is given by the expression

$$v(t) = Ri(t) \Rightarrow \mathbf{V} = R\mathbf{I} \tag{B.18}$$

The response of an inductor is given by the dynamic expression

$$v(t) = L\frac{\mathrm{d}i(t)}{\mathrm{d}t} \Rightarrow \mathbf{V} = L\mathbf{D}(\mathrm{j}h\omega_0)\mathbf{I} \tag{B.19}$$

and the response of a capacitor is given by

$$v(t) = \frac{1}{C}\int i(t)\mathrm{d}t \Rightarrow \mathbf{V} = \frac{1}{C}\mathbf{D}^{-1}(\mathrm{j}h\omega_0)\mathbf{I} \tag{B.20}$$

The voltage in a switching device such as a GTO or IGBT is given by

$$v(t) = s(t)v_s(t) \Rightarrow \mathbf{V} = \mathbf{S}\mathbf{V}_s \tag{B.21}$$

where $s(t)$ represents the turn-on and turn-off of the device and $v_s(t)$ is the voltage source. $\mathbf{S}$ is a Toeplitz matrix.

C. Phase Angle Control for the VSC

The following controls considerations were used to obtain the steady-state and transient conditions of the various power electronics controllers addressed in this thesis:

Steady-state STATCOM model: In steady-state the STATCOM does not supply active power, and this characteristic leads to a constant $v_{cap}(0^+)$, and a dc-term in the current $\mathbf{I}_1$ equal to zero, i.e. $I_{1_0} = 0$. So, the control must be capable to give such a current condition by controlling the phase angle of the VSC voltage output.

Steady-state HVDC-VSC back-to-back model: The steady-state operation of the HVDC-VSC back-to-back involves the transfer of active power between VSCs, but with no active power supplied by the DC capacitor. Under these conditions, the dc-term of the current in the capacitor must be zero, i.e. $I_{1_0} + I_{2_0} = 0$, resulting in a dc-term current flowing from one VSC to the other. So, the control must be able to give the correct current condition by controlling the phase angle of the VSC voltage output selected to be the master DC voltage regulator.

Steady-state HVDC-VSC transmission system model: The steady-state operation of the HVDC-VSC transmission system also involves the transfer of active power between the VSCs through the DC cable, but with no active power supplied by the DC capacitors. Under these conditions the dc-term of the current in the capacitors must be zero, i.e. the dc-term current I_{1_0} must be the same as the dc-term current I_{dc_0}, and equal to I_{2_0} at the other end of the HVDC-VSC transmission system, giving the same conditions as in the HVDC-VSC back-to-back, i.e. $I_{1_0} + I_{2_0} = 0$. So, the control must be capable of giving the current condition by controlling the phase angle of the VSC voltage output selected to be the master DC voltage regulator.

Steady-state UPFC model: The control considerations required for the steady-state operation of the UPFC are similar to those of the HVDC-VSC back-to-back tie. The only major difference is that in this case the power dispatcher (VSC 2) is used to supply a controllable series voltage (magnitude and angle at fundamental frequency) with the transmission line.

C. *Phase Angle Control for the VSC*

Iterative process: With reference to the characteristic of Figure C.1, an iterative process is used to determine the current condition required by the previous three models. The iterative process is based on the capacitor's current-output voltage angle characteristic of the VSC, which is represented by the solid line. The iterative process is as follows:

1) The dashed line is an approximation given by the two initial points $(\delta_0,\Delta I_0)$-$(\delta_1,\Delta I_1)$ and represented by the equation

$$\delta = \frac{1}{M}(\Delta I - \Delta I_1) + \delta_1$$

where

$$M = \frac{\Delta I_1 - \Delta I_0}{\delta_1 - \delta_0}$$

and for $\Delta I = 0$ the new angle δ must be close to the solution.

2) Then $\delta_{new} = -\frac{1}{M}\Delta I_1 + \delta_1$ and the harmonic coefficients of the switching function are shifted as follows

$$S_{ab_h} = S_{ab_h} e^{-jh\delta_{new}}$$

3) The VSC model is updated with the new switching functions, and the electric system is solved to obtain a new dc-term current flowing in the capacitor ΔI_{new}.

4) Make $\Delta I_0 = \Delta I_1$, $\Delta I_1 = \Delta I_{new}$, $\delta_0 = \delta_1$ and $\delta_1 = \delta_{new}$ and go to step 2). The process is repeated until $\Delta I_{new} \leq \varepsilon$.

The initial condition for δ_0 may be taken as $\delta_0 = \delta_{VSC}$. Where δ_{VSC} is the phase angle of the VSC which is used as a power dispatcher in the HVDC-VSC stations, or the voltage system angle at the PCC for the STATCOM application. Experience indicates that since the angle δ_0 is close to the solution, $\delta_1 = \delta_0 + 0.1$ may be used. Using this iterative process, solutions have been arrived at within three iterations.

Transient analysis for the VSC: In all transient analysis of VSC applications, a control system must be used to maintain the DC voltage in the capacitor at a constant value. This is done by controlling the output phase voltage angle of the VSC in the STATCOM or the output phase voltage angle in the master DC voltage regulator in the HVDC-VSC stations.

Block control: The PI control system shown in Figure C.2 may be used for such a purpose. $V_{dc_{ref}}$ is the reference dc-term voltage obtained from a steady-state solution given by $\delta_1^{(0)}$. The state-space equation for the control is given by

C. Phase Angle Control for the VSC

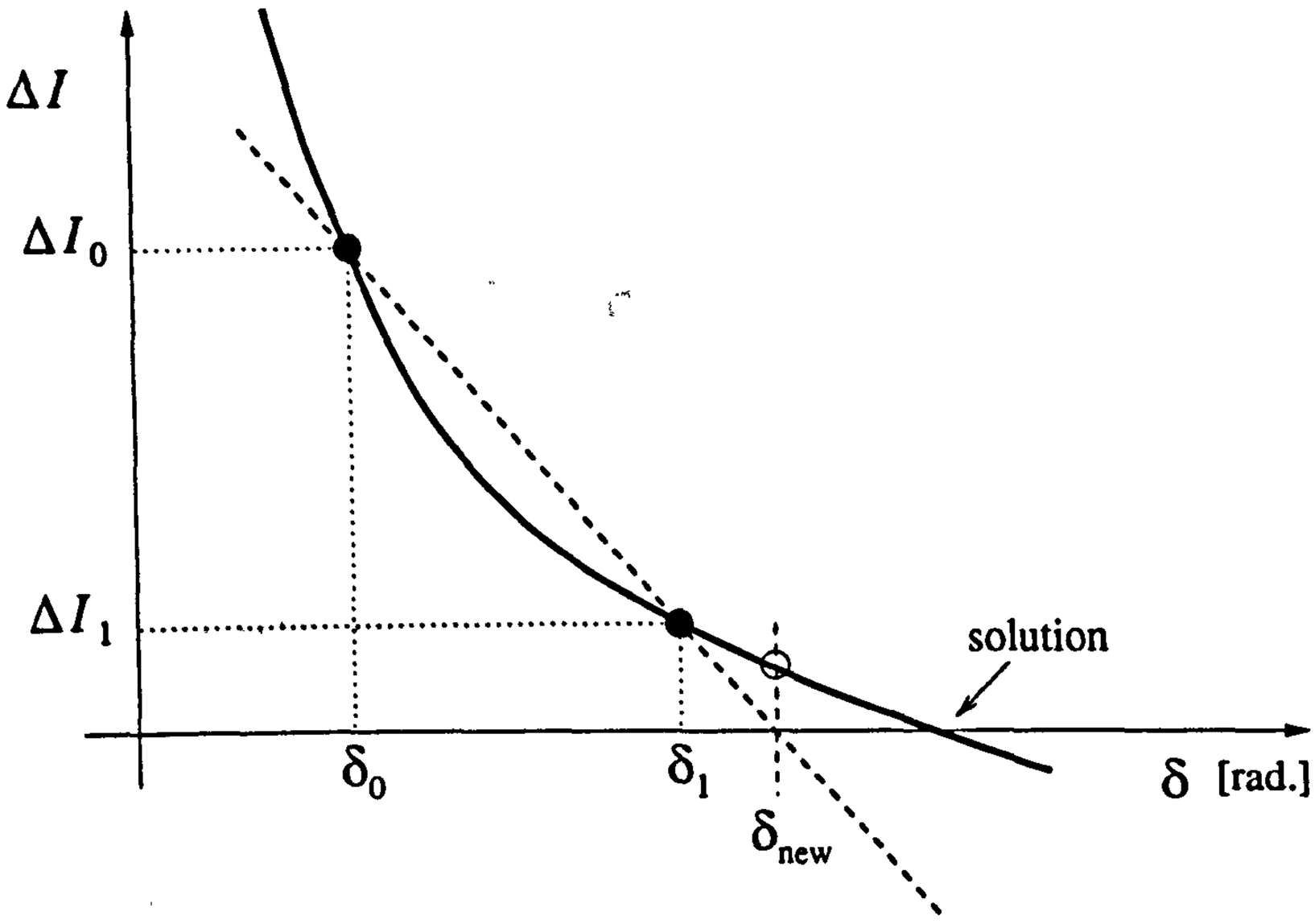

Figure C.1.: Current-phase voltage angle characteristic

$$\frac{d\Delta\delta_1}{dt} = -\frac{1}{T}\Delta\delta_1 + \frac{K}{T}\varepsilon$$
$$\varepsilon = V_{dc_{ref}} - V_{dc_{measure}}$$
$$\delta_1 = \Delta\delta_1 + \delta_1^{(0)}$$

where $V_{dc_{measure}}$ is the dc-term of V_{dc}. The state-space equation is used since time domain simulations are carried out in the dynamic harmonic domain used in this thesis.

Good results have been obtained in this thesis by using a gain $K = 10$ and a time constant $T = 0.01$ s.

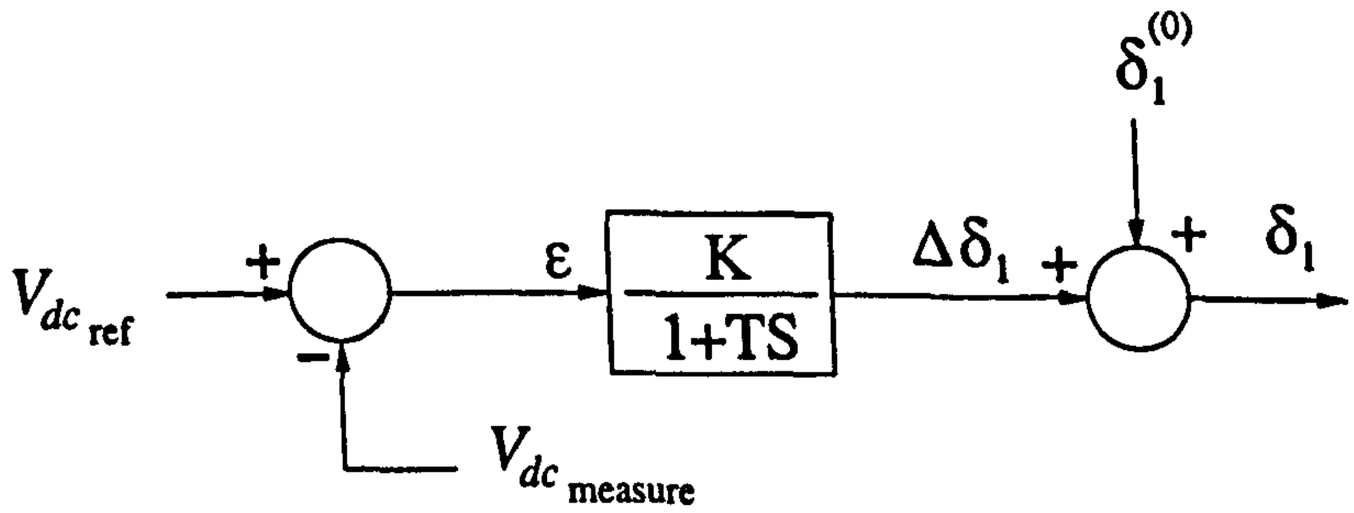

Figure C.2.: Control block diagram

D. TCR and TCSC Models

The TCSC comprises a TCR in parallel with a capacitor, as shown in Figure D.1. The TCSC has three basic modes of operation: blocked thyristors (zero conduction), bypassed thyristors (full conduction) and vernier mode operation (partial conduction). In vernier mode, and depending on the firing angle value, the fundamental frequency operating point lies on either the capacitive or the inductive regions.

The TCSC steady-state response may be calculated by using both time domain and frequency domain solution techniques. The latter approach, however, is only accurate if the solution incorporates the fundamental and harmonic phasors of the various quantities involved. In this appendix the TCSC and the TCR are analysed from the harmonic viewpoint and explained below.

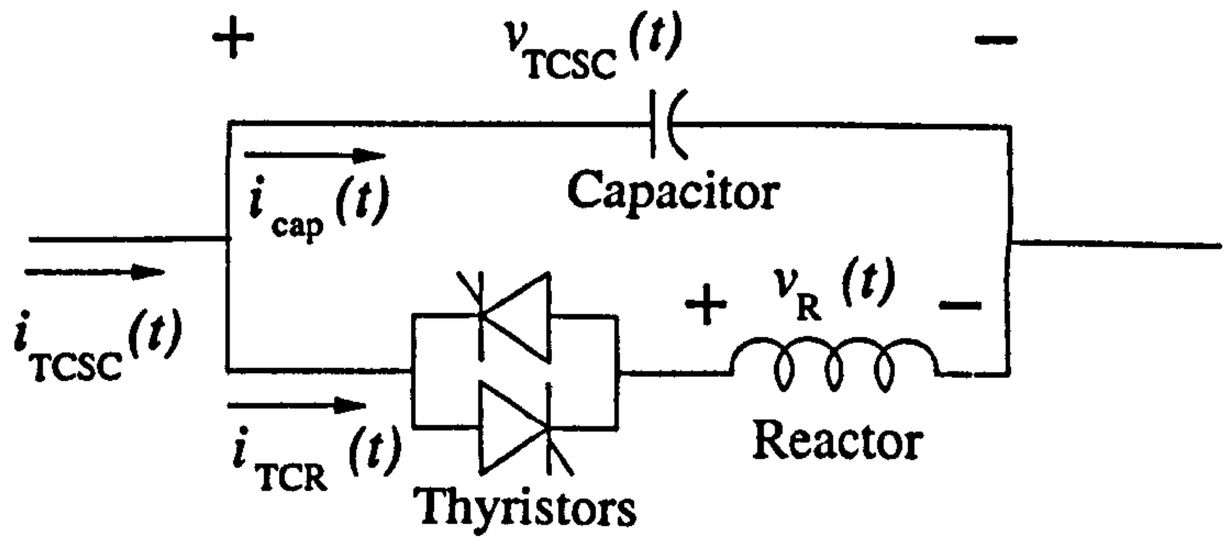

Figure D.1.: Thyristor-controlled series compensator scheme

D.1. Thyristors Turn-on and Turn-off

Since the thyristor does not have a turn-off capability unlike the GTO or IGBT, then it should be treated as a non-linear device in order to obtain the switching function that represents its operation. The method used to obtain the switching function is explained below.

Figure D.2 illustrates the basic operation of the TCR, which is governed by the thyristors turn-on and turn-off actions. The capacitor voltage zero-crossing is taken as the reference for issuing the firing signal α. If the first thyristor fires at a time θ_{a1}, the thyristor turns-on and conducts for a period σ_1. It turns-off with the thyristor current zero-crossing, at a time θ_{b1}. An

equidistant firing scheme is assumed, i.e. $\theta_{a2} - \theta_{a1} = \pi$. $s(\theta)$ is the switching function.

The analysis is started at the capacitor voltage zero-crossing θ_0; a zero voltage condition which may be expressed in terms of complex Fourier harmonic coefficients,

$$v_{TCR} = \sum_{n=-\infty}^{\infty} V_n e^{jn\theta} = 0, \quad \text{for } \theta = \theta_0 \tag{D.1}$$

It should be noted that the capacitor voltage in the TCSC and the TCR voltage have the same value.

The end of the conduction period, given by the zero-crossing of the thyristors current, occurs when the areas A_1 and A_2 are both zero, i.e.

$$\begin{aligned} A_1 &= \int_{\theta_{a1}}^{\theta_{b1}} v_{TCR} d\theta = \sum_{n=-\infty}^{\infty} \frac{V_n}{jn} \left(e^{jn\theta_{b1}} - e^{jn\theta_{a1}} \right) = 0 \\ A_2 &= \int_{\theta_{a2}}^{\theta_{b2}} v_{TCR} d\theta = \sum_{n=-\infty}^{\infty} \frac{V_n}{jn} \left(e^{jn\theta_{b2}} - e^{jn\theta_{a2}} \right) = 0 \end{aligned} \tag{D.2}$$

where

$$\theta_{a1} = \theta_0 - (\pi - \alpha) \tag{D.3}$$

$$\theta_{a2} = \theta_{a1} + \pi$$

Solving (D.1) and (D.2) for θ_0 , θ_{b1} and θ_{b2} using Newton-Raphson's method, the following equation is solved by iteration,

$$\begin{bmatrix} \theta_0 \\ \theta_{b1} \\ \theta_{b2} \end{bmatrix}^{(k+1)} = \begin{bmatrix} \theta_0 \\ \theta_{b1} \\ \theta_{b2} \end{bmatrix}^{(k)} - \begin{bmatrix} J_{11} & J_{12} & J_{13} \\ J_{21} & J_{22} & J_{23} \\ J_{31} & J_{32} & J_{33} \end{bmatrix}^{-1} \begin{bmatrix} v_{TCR} \\ A_1 \\ A_2 \end{bmatrix}^{(k)} \tag{D.4}$$

"k" is an iteration counter and the Jacobian elements are:

$$\begin{aligned} J_{11} = \frac{\partial v_{TCR}}{\partial \theta_0} &= \sum_{n=-\infty}^{\infty} jnV_n e^{jn\theta_0} \\ J_{12} = \frac{\partial v_{TCR}}{\partial \theta_{b1}} &= 0 \\ J_{13} = \frac{\partial v_{TCR}}{\partial \theta_{b2}} &= 0 \\ J_{21} = \frac{\partial A_1}{\partial \theta_0} &= -\sum_{n=-\infty}^{\infty} V_n e^{jn(\theta_0 - (\pi - \alpha))} \end{aligned}$$

$$
\begin{aligned}
J_{22} = \frac{\partial A_1}{\partial \theta_{b1}} &= \sum_{n=-\infty}^{\infty} V_n e^{jn\theta_{b1}} \\
J_{23} = \frac{\partial A_1}{\partial \theta_{b2}} &= 0 \\
J_{31} = \frac{\partial A_2}{\partial \theta_0} &= -\sum_{n=-\infty}^{\infty} V_n e^{jn(\theta_0+\alpha)} \\
J_{32} = \frac{\partial A_2}{\partial \theta_{b1}} &= 0 \\
J_{33} = \frac{\partial A_2}{\partial \theta_{b2}} &= \sum_{n=-\infty}^{\infty} V_n e^{jn\theta_{b2}}
\end{aligned}
$$

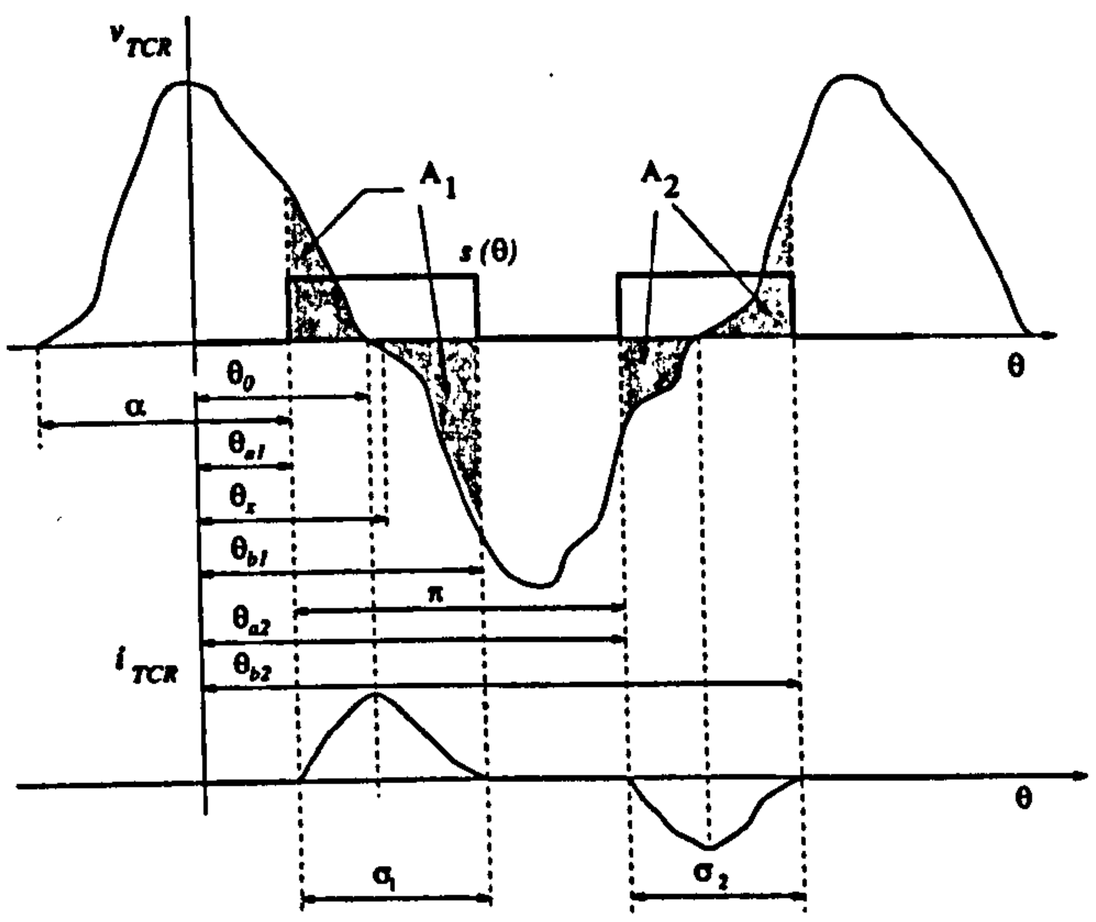

Figure D.2.: Thyristor-controlled reactor operation.

The initial conditions required for the solution of (D.4) may be taken to correspond to a sinusoidal waveform, which is given by the zero-crossing of the fundamental component of $v_{TCR}(\theta)$. The initial value for θ_0 is given by,

$$\theta_0^{(0)} = \frac{\pi}{2} - \arctan\left(\frac{\Im\{V_1\}}{\Re\{V_1\}}\right) \tag{D.5}$$

and the initial conditions for θ_{b1} and θ_{b2} can be taken by assuming quarter-wave symmetry,

$$
\begin{aligned}
\theta_{b1}^{(0)} &= \theta_0^{(0)} + \left(\theta_0^{(0)} - \theta_{a1}^{(0)}\right) \\
\theta_{b2}^{(0)} &= \theta_{b1}^{(0)} + \pi
\end{aligned} \tag{D.6}
$$

After achieving convergence for θ_0, $\theta_{b1}$and θ_{b2}, the centre of the switching function $s(\theta)$ is taken to be at

$$\theta_x = \theta_{a1} + \frac{\sigma_1}{2} \tag{D.7}$$

where the conduction angles are given as

$$\sigma_1 = \theta_{b1} - \theta_{a1}$$
$$\sigma_2 = \theta_{b2} - \theta_{a2}$$

Then θ_x , σ_1 and σ_2 are used to calculate the harmonic content of the switching function,

$$S_0 = \frac{\sigma_1 + \sigma_2}{2\pi} \tag{D.8}$$

$$S_n = \frac{2}{n\pi}\left(\sin\frac{n\sigma_2}{2}\cos n\pi + \sin\frac{n\sigma_1}{2}\right)e^{-jn\theta_x} \tag{D.9}$$

It should be noted that the formulation is general. It caters for the case when the conduction periods of thyristors 1 and 2 differ, due to a voltage waveform with loss of quarter-wave symmetry.

D.2. TCR Model

The voltage across the reactor can be described by the following equations,

$$v_R(t) = s(t)v_{TCR}(t) \tag{D.10}$$

$$v_R(t) = L\frac{di_{TCR}(t)}{dt} \tag{D.11}$$

where the TCR conduction period is governed by the switching function $s(t)$. L is the inductance of the linear reactor and $i_{TCR}(t)$ is the current flowing through the reactor. Equations (D.10) and (D.11) in the harmonic domain are given as

$$\mathbf{V}_R = \mathbf{S}\mathbf{V}_{TCR} \tag{D.12}$$

$$\mathbf{V}_R = L\mathbf{D}(jh\omega_0)\mathbf{I}_{TCR} \tag{D.13}$$

By combining (D.12) and (D.13),

$$\mathbf{I}_{TCR} = \frac{1}{L}\mathbf{D}^{-1}(jh\omega_0)\mathbf{S}\mathbf{V}_{TCR} = \mathbf{Y}_{TCR}\mathbf{V}_{TCR} \tag{D.14}$$

where

$$\mathbf{Y}_{TCR} = \frac{1}{L}\mathbf{D}^{-1}(jh\omega_0)\mathbf{S} \tag{D.15}$$

The admittance matrix (D.15) includes all the harmonics and cross-coupling between harmonics, giving a complete representation of the TCR in steady-state.

D.3. TCSC Model

The TCSC is well described by the parallel combination of the TCR and capacitor admittance,

$$\mathbf{Y}_{TCSC} = \mathbf{Y}_C + \mathbf{Y}_{TCR} \tag{D.16}$$

where $\mathbf{Y}_C = C\mathbf{D}(j h\omega_0)$ is the admittance matrix of the series capacitor and C is its capacitance.

The transfer admittance matrix $\mathbf{Y}_{TCSC}$ represents a complete model for the TCSC in steady-state, where all the harmonics and cross-coupling between harmonics are explicitly represented.

E. Diagrams in PSCAD/EMTDC

In order to compare the results generated with the harmonic domain models emanating from this research and those given by PSCAD/EMTDC the following important points should be noted:

1. The switching functions must be the same. In this case the switching functions presented in Appendix A for PSCAD/EMTDC models are used.

2. All the parameters in the HD models are refered to the star side of the transformer according to Figure 2.2.

3. All the parameters in the PSCAD/EMTDC models are refered to the delta side of the transformer, i.e. converter side, as shown in the diagrams in this appendix.

4. To represent the same system in both, the harmonic domain and PSCAD/EMTDC, the results must be interpreted as follows: 1) Phase voltage in the HD is the same as the line to line voltage in PSCAD/EMTDC. 2) DC voltage in the HD is the same as in the PSCAD/EMTDC. 3) Currents obtained in the HD are line currents, and those of PSCAD/EMTDC are phase currents, i.e. $i_a(t)$ and $i_{\text{conv}_a}(t)$, according to Figure 2.2. The following considerations should also be taken into account: 4) Impedance parameters must be affected by the star-delta connection, so, the impedance in the HD models is three times the impedance in PSCAD/EMTDC, i.e. $Z_{HD} = 3Z_{PSCAD}$, 5) The capacitor parameters is the same in both HD and PSCAD/EMTDC models.

E. Diagrams in PSCAD/EMTDC

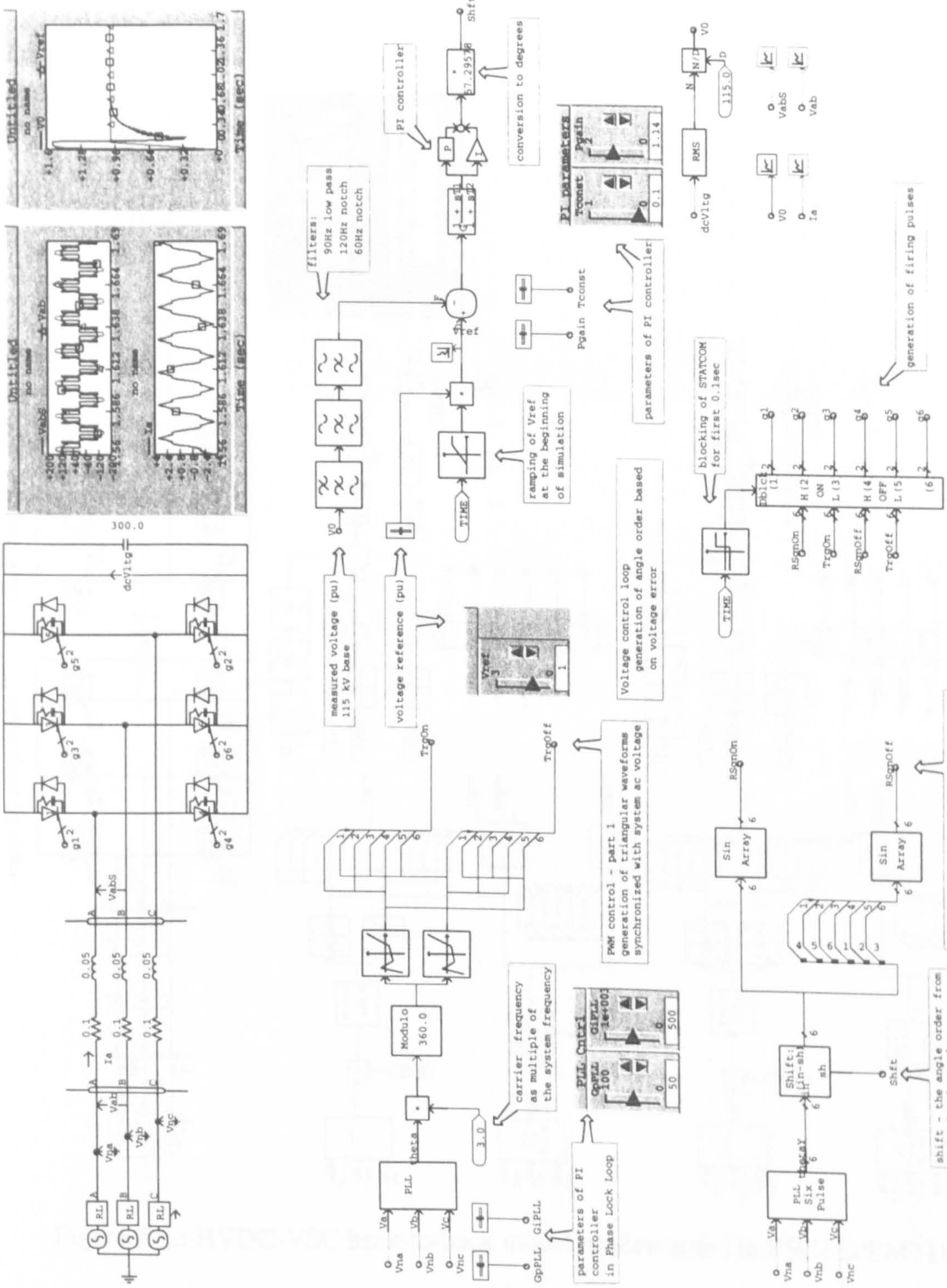

Figure E.1.: STATCOM diagram model implemented in PSCAD/EMTDC

E. Diagrams in PSCAD/EMTDC

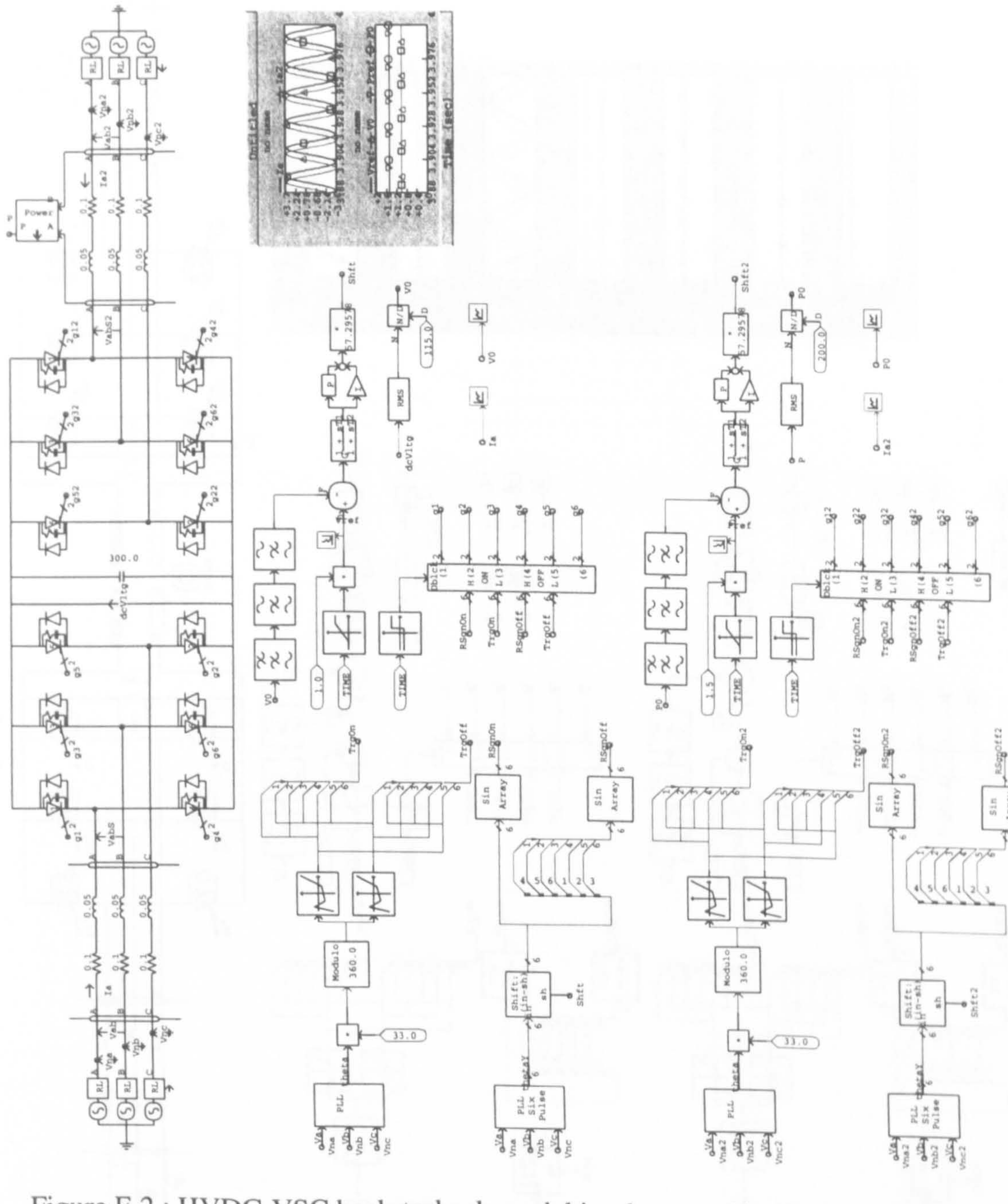

Figure E.2.: HVDC-VSC back-to-back model implemented in PSCAD/EMTDC

E. Diagrams in PSCAD/EMTDC

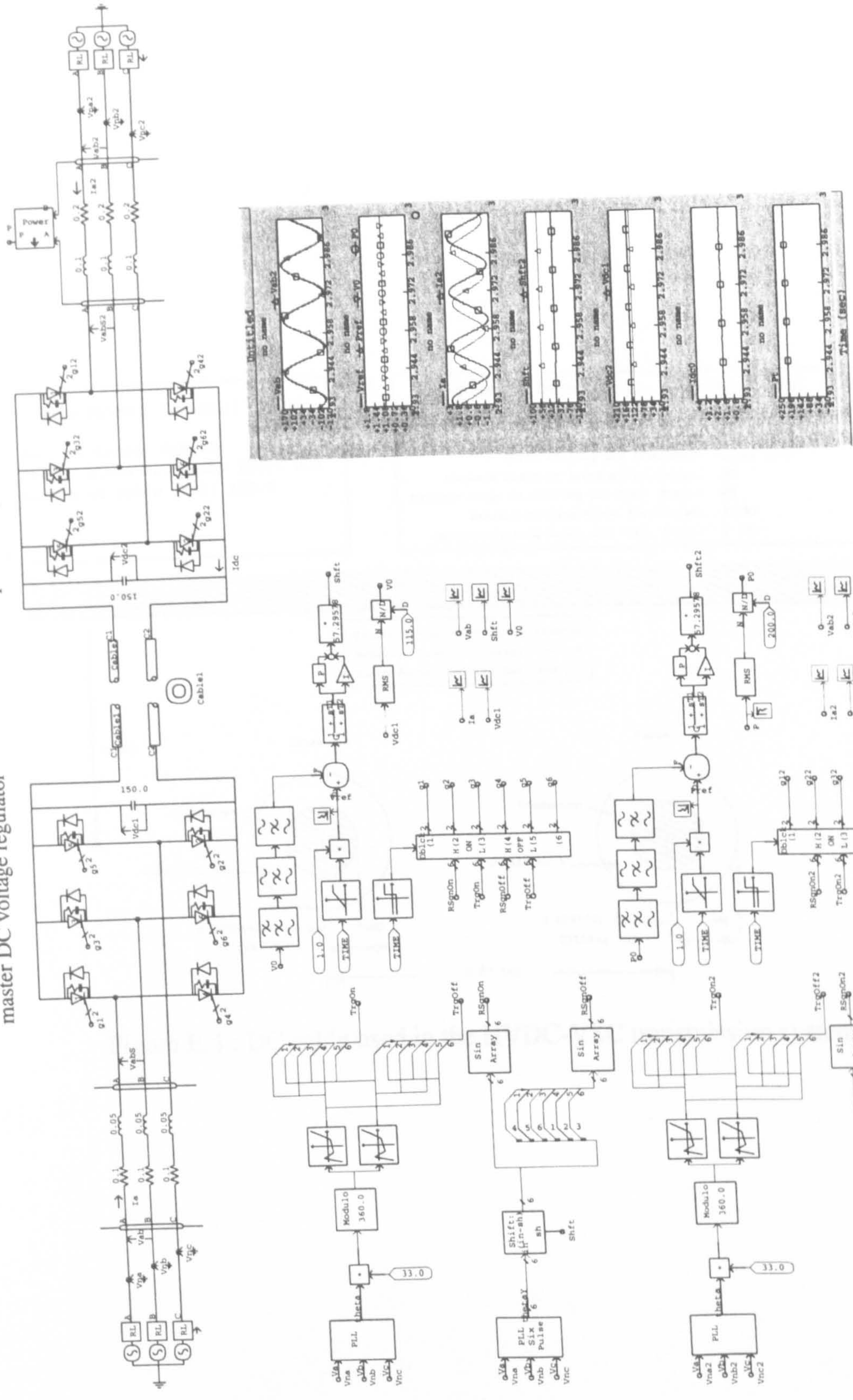

Figure E.3.: HVDC-VSC transmission system model implemented in PSCAD/EMTDC

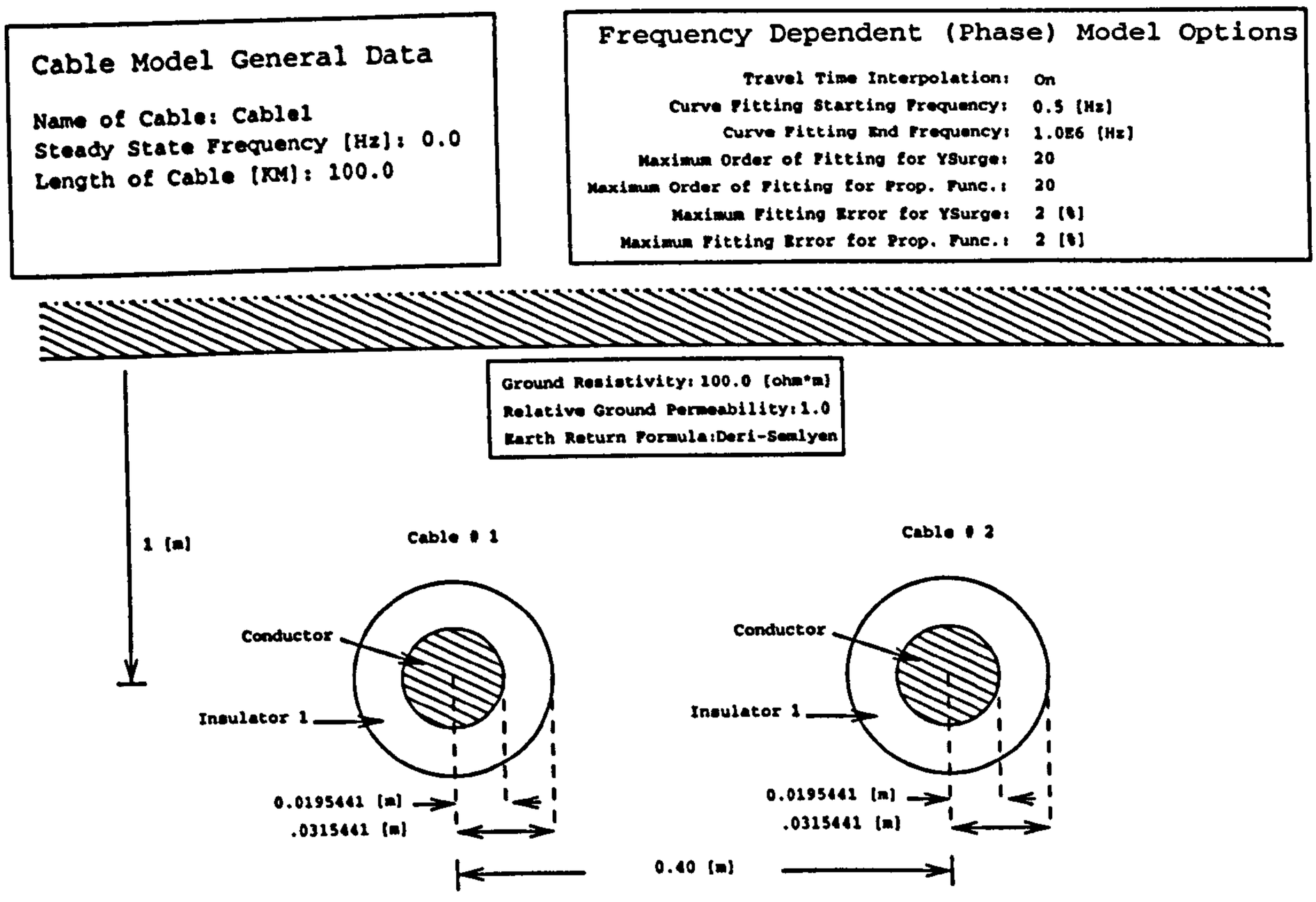

Figure E.4.: DC cable used in the HVDC-VSC transmission system